Prokaryotic dissolution of sulfide minerals

Prokaryotic Dissolution of Sulfide Minerals

Sarah Jones

Birkbeck, University of London

Thesis submitted for the degree of
Doctor of Philosophy

2022

Declaration of Originality

I, Sarah Jones, confirm that the work presented in this thesis is my own. Where data or information has included contributions of others, this has been outlined in the Statement of Contribution on the proceeding page.

Statement of Contribution

Chapter 2 – The EPMA and LA-ICP-MS machines and the I18 beamline at Diamond were calibrated prior to analyses carried out by me by Andrew Beard, Birkbeck, Iain McDonald, Cardiff University, and Konstantin Ignatyev, Diamond Lightsource, respectively. μXANES data collected by me was extracted by Karen Hudson-Edwards.

Chapter 3 – ICP-OES analysis runs were carried out by Gary Tarbuck and John McArthur, UCL, using samples prepared by me. Genes associated with carbon fixation and copper resistance were identified by Dr. Tom Osborne, University of Bedfordshire and used as a reference for expression analyses carried out by me in this chapter. The R Script used for Deseq2 normalisation was adapted from scripts written by Dr. Carlos Martinez Ruiz, UCL.

Chapter 4 - ICP-OES analysis runs were carried out by Gary Tarbuck and John McArthur, UCL, using samples prepared by me. Following the initial ICP-OES run, a subsequently required dilution of ICP-OES samples was carried out by Marco Crisci due to Coronavirus restrictions on laboratory use. R Scripts used for Deseq2 normalisation and differential expression were adapted from scripts written by Dr. Carlos Martinez Ruiz, UCL.

Sarah Jones

Prof. Andrew Carter (Supervisor)

Abstract

Sulfide minerals are a source of high-value metals such as copper, however, traditional methods of extracting metals from sulfide minerals are costly and energy intensive. Bioleaching offers a low-input method of metal extraction, which works by exploiting the sulfur and iron metabolisms of acidophilic prokaryotes to break down ore. In this thesis, properties of sulfide minerals were investigated, as well as the mechanisms underlying their breakdown in the presence of the naturally-occurring SC3 bioleaching consortium. SC3 is a group of acidophilic prokaryotes enriched from the Skouriotissa copper mine in Cyprus. The consortium includes bacteria (*Leptospirillum ferrodiazotrophum*, *Acidithiobacillus* spp., and one member of the Rhodospirillales) and archaea (*Ferroplasma* spp., and the Thermoplasmatales member "G-plasma").

Meta-omics techniques were used to explore metabolism genes expressed during bioleaching of chalcopyrite and a low-grade copper ore from SC3's native environment (Phoukassa ore). Geochemical analyses demonstrated significant differences in mineral breakdown in the presence of the consortium compared to abiotic conditions. In the presence of these sulfide minerals, SC3 expressed genes associated with iron and sulfur metabolism, potentially indicating a mechanism behind enhanced mineral breakdown. The results represent the first RNA-seq studies of iron and sulfur metabolism genes in a naturally occurring bioleaching consortium. Additionally, some species in the consortium possesed and were expressing putative sulfur metabolism genes previously unknown in their respective species. An updated model of the mechanisms behind chalcopyrite breakdown and a novel model of Phoukassa ore breakdown were produced. The consortium did not grow on the primary antimony mineral, stibnite. To improve the background understanding of this poorly studied mineral, the first comprehensive dataset of trace elements in stibnite was obtained using WDS-EPMA, LA-ICP-MS, μXRF, and μXANES analyses. By combining techniques from the fields of geochemistry, microbiology and molecular biology, this thesis creates an improved understanding of sulfide mineral breakdown.

Dedication

This thesis is dedicated to my parents, Tula and Tudor Jones,

the most extraordinary people I have ever met

Diolch i chi am bopeth

Acknowledgments

Firstly, I would like to express my thanks to the London NERC Doctoral Training Programme for funding this PhD project.

I would like to thank my supervisors, Professor Joanne Santini, Professor Karen Hudson-Edwards, and Professor Andrew Carter for their help and guidance throughout this project. A great deal of thanks is also due to all my Santini Lab colleagues, past and present, especially Dr. Tom Osborne, for additional support and guidance, Marco Crisci for moral support and helping with sample dilution, Simona Della Valle for being a fantastic lab co-worker and friend, and Dr. Cam Watson, for being a distraction. Thushyanthi Sivagnanam is warmly thanked for laboratory help and technical support. I would also like to thank the examiners Prof. Karen Olsson-Francis and Dr. Lena Ciric for feedback which has greatly improved the quality of this thesis.

Many people provided technical support for the analytical techniques used in this thesis, without whom completion of this research would have been impossible. My sincere gratitude therefore goes to Andrew Beard, Konstantin Ignatyev, Gary Tarbuck, Jim Davy, Iain McDonald, and Martin Vickers. Additionally, Paul Pohwat at the Smithsonian Museum and Robin Hansen at the Natural History Museum, who provided stibnite samples, and Phil Richardson, who provided stibnites from his personal collection.

A major thank you to Dr. Steve Cross, for not only being an exceptional mentor and friend, but also for saving me from homelessness during a global pandemic. Additional thanks to April and Ben Cross for being a welcome distraction and an all-round pair of delights.

I am extremely grateful for the love, support and proof-reading skills of the Science Showoff Talent Factory. In particular, Dr. Claire Price and Dr. Cerys Bradley for extremely useful feedback, Dr. Anna Ploszajski, and Dr. Oz Ismail for motivational

tea breaks, mind-clearing swims, therapeutic conversations and big laughs. A major thank you also goes to Hana Ayoob for being my virtual work colleague during the course of the highly unusual year of 2020. Your support and ability to keep me going during challenging moments and sharing victories with me has truly meant a lot. Additionally, Dr. Shalaka Kurup, thank you so much for cheering me on and generally being a phenomenal friend. The support of Kimberley Freeman and Cass Hugill has been immeasurable, your kindness and belief in me has meant so much.

To my excellent family, who have always believed in me and supported me in everything I do, I would like to say diolch yn fawr iawn – teulu gorau yn y byd! In particular, diolch i Bertie a Eira, for helping me to remain calm during trying times. I could never get through anything as monumental as the past years without the unwavering support of Kara Hills, Ruth Maloney-Cox and John Lee. Thank you so much for being there for me, always.

For inspiring and supporting me to pursue science with her kind encouragement and commitment to excellent research, I would like thank the late Dr. Petra Kidd, a much missed mentor and friend.

Lastly, my biggest thanks goes to Carlos, without the support of whom, completing this thesis would have been impossible. Your kindness, patience and intelligence makes you the most excellent person I know.

Contents

DECLARATION OF ORIGINALITY 2

STATEMENT OF CONTRIBUTION 3

ABSTRACT 4

ACKNOWLEDGMENTS 6

CONTENTS 8

FIGURES 15

TABLES 17

CH. 1 – GENERAL INTRODUCTION 18

1.1 PROJECT OVERVIEW 18

1.2 SULFIDE MINERALS 19

1.3 BIOLEACHING 21

1.4 ENVIRONMENTAL IMPACTS OF SULFIDE MINERAL DISSOLUTION 23

1.5 SULFIDE MINERAL DISSOLUTION 25

1.5.1 PATHWAYS OF SULFIDE MINERAL DISSOLUTION 25

1.5.2 DIRECT VS INDIRECT DISSOLUTION 26

1.6 SULFUR OXIDATION 27

1.6.1 Sulfur Oxidising Microbes 28
1.6.2 Mechanisms of Microbial Sulfur Oxidation 28

1.7 IRON OXIDATION 31

1.7.1 Iron Oxidising Microbes 31
1.7.2 Microbial iron oxidation at low pH 32

1.8 APPROACHES TO STUDYING MICROBIAL SULFIDE MINERAL DISSOLUTION 33

1.8.1 SC3 Consortium 33
1.8.1.1 The Skouriotissa Mine Site 34
1.8.1.2 Consortium Overview 35
1.8.1.3 SC3 Metabolisms Relevant to Sulfide Mineral Breakdown 39
1.8.1.3.1 Sulfur Metabolism Genes in Acidithiobacilli 40
1.8.1.3.2 Sulfur Metabolism Genes in Other SC3 Members 45
1.8.1.3.3 Iron Metabolism Mechanisms in the SC3 Consortium 46
1.8.2 Sulfide Mineral Selection 52
1.8.2.1 Chalcopyrite 52
1.8.2.2 Phoukassa ore 52
1.8.2.3 Stibnite 52
1.8.3 Meta-omics and the Application of Next Generation Sequencing to Studies of Bioleaching Communities 53
1.8.3.1 Metagenomics 53
1.8.3.1.1 16s rDNA Sequencing 54
1.8.3.1.2 Genome-resolved Metagenomics 54
1.8.3.2 Metatranscriptomics 57
1.8.3.2.1 RNA-seq 57

1.9 AIMS AND OBJECTIVES 59

CHAPTER 2 - META-OMIC ANALYSES OF CHALCOPYRITE BIOLEACHING WITH AN ACIDOPHILIC CONSORTIUM OF PROKARYOTES 61

2.1 INTRODUCTION 61

2.1.1 General Introduction 61
2.1.2 Chalcopyrite 62
2.1.2.1 Abiotic Chalcopyrite Dissolution 63
2.1.2.2 Chalcopyrite Bioleaching 64
2.1.3 Formation of Hypotheses 66
2.1.4 Aims and Objectives 67

2.2 MATERIALS AND METHODS 68

2.2.1 Experimental Design 68
2.2.2 Preliminary Metagenomic Study: Resolving the SC3 Consortium Genomes 73
2.2.3 Powder X-Ray Diffraction 77
2.2.4 Chalcopyrite Composition Analysis 77
2.2.5 Microbial Growth Conditions 78
2.2.6 Scanning Electron Microscopy 79
2.2.7 Geochemical Analyses of Supernatant 80
2.2.8 Gene Comparison Analyses 80
2.2.8.1 Unknown Species – Comparisons to Known Species 80
2.2.8.2 Identification of Genes of Interest 81
2.2.8.2.1 Identifying Genes Associated with Sulfur and Iron Metabolism 81
2.2.8.2.2 Identifying Genes Associated with Additional Metabolism Processes 82
2.2.9 16s rDNA Sequencing 83
2.2.9.1 DNA Isolation for 16s rDNA sequencing 83
2.2.9.2 16s rDNA Sequencing and Data Analysis of Obtained Sequences 84
2.2.10 Whole-Community RNA-seq of the SC3 Consortium during Chalcopyrite Bioleaching 85
2.2.10.1 RNA Isolation of the SC3 Consortium during Chalcopyrite Bioleaching for RNA-seq 85
2.2.10.2 RNA Sequencing and Data Analysis 86
2.2.11 Graphics and Statistical Analysis 87

2.3 RESULTS 88

2.3.1 Growth Substrate Mineral Composition Analyses 88
2.3.2 Scanning Electron Microscopy 90

2.3.3 Dissolution of Chalcopyrite in Biotic and Abiotic Conditions 93
2.3.4 Establishing the Species of the SC3 Consortium Present during Chalcopyrite Bioleaching 96
2.3.5 Genome Comparison of Unclassified SC3 Members to Known Genomes of Related Strains 98
2.3.6 Identification of Genes of Interest within the SC3 Consortium Genomes 100
2.3.6.1 Genes Associated with Iron and Sulfur Metabolism 100
2.3.6.2 Genes Associated with Nitrogen Fixation 104
2.3.7 RNA-seq Investigation of Gene Expression during SC3 Growth on Chalcopyrite 104
2.3.7.1 RISC Metabolism Associated Gene Expression 105
2.3.7.2 Iron Metabolism Associated Gene Expression 107
2.3.7.3 Expression of Genes Associated with Additional Metabolism Processes 109
2.3.7.3.1 Nitrogen Fixation Associated Gene Expression 109
2.3.7.3.2 Carbon Metabolism Associated Gene Expression 110
2.3.8 Model of Chalcopyrite Dissolution by SC3 Consortium 111
2.3.9 Results Summary 114

2.4 DISCUSSION 114

2.4.1 The Bioleaching Potential of the SC3 Consortium 114
2.4.2 The Bioleaching Mechanisms of the SC3 Consortium 115
2.4.3 Metatranscriptomic Insights in SC3 Community Functioning 118
2.4.4 Limitations 120
2.4.5 Conclusion 121

CHAPTER 3 - METATRANSCRIPTOMIC ANALYSIS OF LOW-GRADE COPPER ORE BIOLEACHING 123

3.1 INTRODUCTION 123

3.1.1 General Introduction 123
3.1.2 Low-Grade Copper Ore Mineralogy 124
3.1.3 Pyrite Dissolution 125

3.1.4 Formation of Hypotheses 126
3.1.5 Aims and Objectives 127

3.2 MATERIALS AND METHODS 128

3.2.1 Experimental Design 128
3.2.2 Phoukassa Ore 129
3.2.3 Phoukassa Ore Compositional Analysis 130
3.2.4 Microbial Growth 130
3.2.5 Scanning Electron Microscopy 131
3.2.6 Geochemical Analyses of Supernatant 131
3.2.7 RNA-seq 132
3.2.7.1 RNA Isolation and Sequencing 132
3.2.7.2 RNA-seq Data Analysis 133
3.2.8 Graphics and Statistical Analysis 133

3.3 RESULTS 135

3.3.1 Growth Substrate Mineral Composition Analyses 135
3.3.2 Scanning Electron Microscopy 137
3.3.3 Dissolution of Phoukassa Ore in Biotic and Abiotic Conditions 140
3.3.4 Metatranscriptomic Insights into Gene Expression during Growth of SC3 on Phoukassa Ore 144
3.3.4.1 Sulfur and Iron Metabolism Gene Expression during Growth of SC3 on Phoukassa Ore 150
3.3.4.2 Nitrogen Fixation 156
3.3.4.3 Carbon Fixation 157
3.3.4.4 Model of Phoukassa Ore Bioleaching by the SC3 Consortium 157

3.4 DISCUSSION 160

3.4.1 The Potential of the SC3 Consortium to Bioleach Low-Grade Ore 160
3.4.2 Mechanisms of Phoukassa Ore Bioleaching by the SC3 Consortium 162
3.4.3 Conclusion 165

CHAPTER 4 – CHARACTERISATION OF TRACE ELEMENTS AND EXPLORATION OF BIOLEACHING POTENTIAL IN STIBNITE 166

4.1 INTRODUCTION 166

4.1.1 GENERAL INTRODUCTION 166
4.1.2 STIBNITE 167
4.1.3 STIBNITE DISSOLUTION 169
4.1.4 BIOLEACHING POTENTIAL OF STIBNITE 169
4.1.5 THE PRESENCE OF TRACE ELEMENTS AS IMPURITIES IN STIBNITE 171
4.1.6 HYPOTHESES FORMATION 172
4.1.7 AIMS AND OBJECTIVES 173

4.2 MATERIALS AND METHODS 174

4.2.1 EXPERIMENTAL OVERVIEW 174
4.2.2 PRELIMINARY MICROBIAL GROWTH TRIALS ON STIBNITE 175
4.2.2.1 ACIDOPHILIC GROWTH TRIALS ON STIBNITE 175
4.2.2.2 NEUTROPHILIC GROWTH TRIALS ON STIBNITE 176
4.2.3 STIBNITE CHARACTERISATION STUDY 178
4.2.3.1 STIBNITE COLLECTION AND SAMPLE PREPARATION 179
4.2.3.2 POWDER X-RAY DIFFRACTION (PXRD) 182
4.2.3.3 ELECTRON PROBE MICRO ANALYSIS (EPMA) 182
4.2.3.4 LASER INDUCTIVELY COUPLED PLASMA MASS SPECTROMETRY (LA-ICP-MS) 183
4.2.3.5 μXRF AND X-RAY ABSORPTION NEAR EDGE STRUCTURE (XANES) 184
4.2.3.6 STATISTICAL ANALYSIS 185

4.3 RESULTS 186

4.3.1 BACTERIAL GROWTH TRIALS 186
4.3.1.1 ACIDOPHILE TRIALS 186
4.3.1.2 NEUTROPHILE TRIALS 186
4.3.2 CONFIRMATION OF MINERAL IDENTITY 187
4.3.3 QUANTIFICATION OF TRACE ELEMENTS VIA ELECTRON PROBE MICRO ANALYSIS - WAVELENGTH DISPERSIVE SPECTROSCOPY (EPMA-WDS) 188

4.3.4 Quantification of Trace Elements via Laser Inductively Coupled Plasma Mass Spectrometry (LA-ICP-MS) 191
4.3.5 Qualitative Assessment of Trace Element Presence and Zonation Spectroscopy 194
4.3.6 Speciation of Se in Stibnites 195

4.4 DISCUSSION 197

4.4.1 Trace Element Trends in Stibnite 197
4.4.2 The Effect of Host Rock and Deposit Type on Trace Elements in Stibnite 198
4.4.3 Selenium Speciation in Stibnite 200
4.4.4 Stibnite as a Substrate for Microbial Growth 201
4.4.5 Conclusion 203

CHAPTER 5 GENERAL DISCUSSION 205

5.1 THESIS OVERVIEW 205

5.2 METABOLISMS OF THE SC3 CONSORTIUM 207

5.3 SULFIDE MINERAL DISSOLUTION 209

5.4 CONTRIBUTIONS TO THE FIELD OF METATRANSCRIPTOMICS 210

5.5 PRACTICAL APPLICATIONS OF EXPERIMENTAL FINDINGS 211

5.6 LIMITATIONS OF LABORATORY STUDIES ON BIOLEACHING CONSORTIA 212

5.7 FUTURE DIRECTIONS FOR RESEARCH 213

5.8 CONCLUSION 216

REFERENCES 217

APPENDICES 277

APPENDIX I –CHAPTER 2 GROWTH IMAGES CHALCOPYRITE 277
APPENDIX II - NORMALITY TESTS AND SIGNIFICANCE TESTS OF CHAPTER 2 DATA 278
APPENDIX III – ICP-OES CHALCOPYRITE (PPM) 279
APPENDIX IV - GENE SIMILARITY SCORES BLAST 280
APPENDIX V - CHAPTER 3 GROWTH IMAGES PHOUKASSA ORE 293
APPENDIX VI - ADDITIONAL RNA-SEQ PLOT PHOUKASSA ORE 293
APPENDIX VII – STIBNITE BACKGROUND INFORMATION 294
APPENDIX VIII – PHOTOGRAPHS OF STIBNITE SAMPLES ANALYSED IN CHAPTER 2 304
APPENDIX IX – XAS SUMMARY OF BEAM ENERGIES AND SCANS CONDUCTED AND XANES STANDARDS 306
APPENDIX X– STIBNITE PXRD PATTERNS 308
APPENDIX XII - EPMA X-RAY VALUES 316

Figures

Figure 1.1 – Simplified overview of the bioleaching process 22
Figure 1.2. The steps of microbially mediated sulfur oxidation in aerobic conditions at low pH and the corresponding enzymes. 29
Figure 1.3. – Model of sulfur oxidation in a) At. ferrooxidans; b) At. thiooxidans and c) At. ferrivorans. 43
Figure 1.4 – At. ferrooxidans ferrous iron oxidation electron transfer model. 47
Figure 1.5 – Iron oxidation in L. ferrodiazotrophum. 50
Figure 1.6 – Iron oxidation in F. acidarmanus. 51
Figure 1.7 – Overview of the Genome-Resolved Metagenomic Process 56
Figure 1.8 – overview of stages in the RNA-seq analysis process. 58
Figure 2.1 – Structure of chalcopyrite 64
Figure 2.2 - Overview of Chapter 2 Experimental Work 69
Figure 2.3 - schematic of chalcopyrite dissolution experiment flasks (100ml flasks). 79
Figure 2.4 pXRD pattern for the laboratory grade chalcopyrite used in growth experiments. 89
Figure 2.5 - Mean element concentrations (ppm) of the chalcopyrite examined in this chapter 90
Figure 2.6 SEM images of SC3 consortium at 12 weeks' growth on chalcopyrite 92
Figure 2.7 - mean supernatant ICP-OES results showing percentage of total A) iron, B) copper, and C) sulfur leached from chalcopyrite 94
Figure 2.8 - mean pH values over time for biotic and abiotic $CuFeS_2$ samples 95
Figure 2.9 - Relative frequencies of microbial families in the SC3 consortium at 8 weeks' growth on chalcopyrite determined by 16s rRNA gene sequencing. 97
Figure 2.10 – violin plot of metatranscriptome RNA-seq counts per species. 98

Figure 2.11 – Tile graph of proteins implicated in sulfur metabolism and associated electron transport chains 100
Figure 2.12 – Tile graph of proteins implicated in iron metabolism and associated electron transport chains 103
Figure 2.13 – Expression of known sulfur metabolism and associated electron transport chain genes in bacteria and archaea within the SC3 consortium, grown on chalcopyrite for 8 weeks. 106
Figure 2.14 – Expression of putative iron oxidation genes and associated electron transport chain in the SC3 consortium, grown on chalcopyrite for 8 weeks. 108
Figure 2.15 - Expression of genes in the nitrogen-fixation associated nif gene clusters of At. ferrooxidans and L. ferrodiazotrophum at 8 weeks growth on chalcopyrite. 110
Figure 2.16 - Expression of genes associated with carbon fixation in SC3 consortium at 8 weeks' growth on chalcopyrite 111
Figure 2.17 – Model of the proposed mechanism of chalcopyrite dissolution by the SC3 consortium. 112
Figure 3.1 - Schematic of Phoukassa ore dissolution experiment flasks 131
Figure 3.2 - PXRD pattern for the Phoukassa ore used in growth experiments 136
Figure 3.3 - Mean element concentrations (ppm) of the Phoukassa ore dissolved in nitric acid, as measured by ICP-OES 137
Figure 3.4 – SEM images of SC3 on Phoukassa ore at 16 weeks' growth 139
Figure 3.5 - mean supernatant ICP-OES results showing percentage of A) iron, B) copper, and C) sulfur leached from Phoukassa ore 141
Figure 3.6 – mean supernatant ICP-OES results (ppm) for copper, iron and sulfur from Phoukassa ore 142
Figure 3.7 - mean pH values over time for biotic and abiotic Phoukassa samples. 143
Figure 3.8 – Principal components analyses (PCA) using metatranscriptomic data at the two time points. 145
Figure 3.9 – Expression differences of all genes by species. 147
Figure 3.10 - Expression of known iron oxidation, sulfur oxidation, nitrogen fixation, and carbon fixation genes 149
Figure 3.11 - Expression of known sulfur metabolism and associated electron transport chain genes in the bacteria of the SC3 consortium grown on Phoukassa ore for 8 and 16 weeks. 151
Figure 3.12 – Expression of known sulfur metabolism and associated electron transport chain genes in the archaea of the SC3 consortium grown on Phoukassa ore for 8 and 16 weeks 152
Figure 3.13 - Expression of iron oxidation and associated electron transport protein genes in the bacteria of the SC3 consortium grown on Phoukassa ore for 8 and 16 weeks. 154
Figure 3.14 - Expression of iron oxidation genes in the archaea of the SC3 consortium grown on Phoukassa ore for 8 and 16 weeks. 155
Figure 3.15 – Expression of nitrogen fixing nif genes in the SC3 consortium at week 8 and 16 of growth on Phoukassa ore. 156

Figure 3.16 - Expression of genes associated with carbon fixation in SC3 consortium at 8 and 16 weeks' growth on Phoukassa Ore. *157*
Figure 3.17 - Model of Phoukassa ore dissolution showing significant differences in gene expression between week 8 and week 16 *158*
Figure 4.1 – Structure of stibnite *168*
Figure 4.2 – WDS Mean and Standard Error of Sb and S percentages in stibnite samples *189*
Figure 4.3 - Mean concentration (%) of trace elements in stibnites split by host rock (a), and deposit type (b) as analysed by WDS. *190*
Figure 4.4 – Mean concentration (ppm) of trace elements in stibnites *192*
Figure 4.5 – Boxplot of scaled LA-ICP-MS data *193*
Figure 4.6 - Intensity of Se in Stb 1(A), 7(B), 14(C), 16(D) analysed with μXRF. *195*
Figure 4.7 – Selenium K-edge averaged, normalised XANES spectra for stibnite samples and standards *196*

Tables

Table 1.1 - Key Sulfide Minerals 20
Table 1.2 – Overview of the Microorganisms Present in SC3 Consortium 36
Table 2.1 – MAM Constituents 74
Table 2.2 – SC3 Consortium General Genome Information 76
Table 2.3 – Blast results of G plasma genome against available genomes of *Cuniculiplasma divulgatum* 99
Table 4.1 – Minimal Salts Medium 178
Table 4.2 – Stibnite Samples and Origins 179
Table 4.3 - pH values during growth on stibnite 187
Table 4.4 – ICP-OES data concentrations of S and Sb in biotic and abiotic samples after 4 weeks growth on stibnite 187
Table 4.5 – major phases in each of the stibnite samples 188

Chapter 1 – General Introduction

1.1 Project Overview

Worldwide, sulfide minerals are mined to extract valuable metals, such as copper (Wenk and Bulakh, 2005). However, traditional methods of metal extraction from sulfide minerals can be expensive, energy intensive and cause pollution (Zhao *et al.*, 2019). A cost-effective and low input solution to this problem could be bioleaching. Bioleaching consists of extracting metals by exploiting microbial metabolisms that break minerals down (Gilbertson, 2000). Determining what role different microbes in a bioleaching consortium are playing during the dissolution process of sulfide minerals could contribute to the optimisation of prokaryote selection for bioleaching (Rawlings and Johnson, 2007).

Bioleaching is based on microbially driven sulfur and iron cycling processes that naturally occur in the waters of former mine sites, causing highly acidic conditions (acid mine drainage, AMD). Therefore, a better understanding of the processes underlying sulfide mineral dissolution is essential not only in improving the bioleaching process, but also in helping to inform prevention strategies for the environmentally destructive formation of AMD. Consequently, there are economic and environmental benefits of understanding sulfide mineral breakdown. Despite this, many unknowns remain with regards to the multi-step sulfur and iron oxidation processes underlying this technique. For example, within the genomes of many common bioleaching microbes, some of the genes responsible for the production of key sulfur and iron-oxidising enzymes have not yet been identified.

Exploring the genomes of microbes in a bioleaching consortium can address this issue, helping to clarify each species' sulfur and iron oxidation pathways. However, genomic studies alone are insufficient to fully determine the function of bioleaching consortia (Cárdenas *et al.*, 2010). Transcriptome studies can determine which microorganisms are actively expressing sulfur and iron oxidation genes, as only actively transcribed genes are quantified. Consequently, transcriptome studies can

be used to identify whether sulfur and iron oxidation genes of interest are being expressed in a particular species during sulfide mineral breakdown. This can provide key information in the effort to resolve prokaryotic sulfur and iron oxidation pathways during bioleaching.

RNA sequencing (RNA-seq) is a next generation, high throughput sequencing technique that can be used for whole transcriptome profiling. To date, only two RNA-seq whole-community transcriptomic studies have been conducted on bioleaching consortia (Marín *et al.*, 2017; Ma *et al.*, 2019) and no studies in the literature have attempted to examine the expression of genes associated with sulfur and iron metabolism in a naturally occurring bioleaching consortium using RNA-seq.

This thesis aims to further our understanding of microbially driven sulfide mineral breakdown, with a particular focus on understanding the sulfur and iron oxidation pathways of bioleaching microbes. During the research described in this thesis, a naturally occurring bioleaching consortium was used to break down different sulfide minerals. Community-level genomic and RNA-seq transcriptomic studies were employed to identify the presence and expression of genes associated with sulfur and iron oxidation in the prokaryotes in the consortium during sulfide mineral breakdown.

This initial chapter will provide background information and context for the studies described in the following chapters, a background to the approaches employed in this research, an overview of the aims and objectives of the research, and a summary of the thesis' structure.

1.2 Sulfide Minerals

Minerals that combine a sulfide anion with a metal or metalloid belong to a class of minerals known as "sulfide minerals" (Vaughan and Corkhill, 2017). They are ubiquitous worldwide and are a very important group of ore minerals – they are often mined to extract metals (such as copper and zinc) present as major

components of the minerals (Vaughan and Coker, 2016). Additionally, economically important metals such as cadmium, zinc, lead, gold and silver can also occur in smaller quantities as impurities in these minerals or be associated with sulfide mineral deposits (Gribble and Hall, 1985). In this context, furthering the knowledge base associated with sulfide mineral breakdown could be significant in improving the practical and economic viability of precious metal extraction. Additionally, understanding the factors affecting the dissolution of these minerals is environmentally significant as their breakdown products can cause AMD and/or release potentially toxic elements, such as lead and arsenic (which can be present as impurities in sulfide minerals) into water courses (Johnson and Hallberg, 2005).

Pyrite is the most abundant member of this mineral class (Vaughan and Coker, 2016), however a wide variety (c. 500 total) of other sulfide minerals has been identified globally (Wenk and Bulakh, 2005). An overview of some of the key sulfide minerals is shown in Table 1.1, below.

Table 1.1 - Key Sulfide Minerals

Mineral Name	**Formula**	**Key Notes**	**Literature Demonstrating Enhanced Dissolution in the Presence of Microbes**
Arsenopyrite	FeAsS	Major source of environmental arsenic	(Jin *et al.*, 2012; Deng *et al.*, 2017; Borja *et al.*, 2019)
Chalcocite	Cu_2S	Additional copper ore mineral	(Hawkes, Franzmann and Plumb, 2006; Xingyu *et al.*, 2010; Lee *et al.*, 2011)
Chalcopyrite	$CuFeS_2$	Main ore of copper	(Dopson and Lindström, 2004; Vilcáez, Suto and Inoue, 2008; Zhou *et al.*, 2009; Feng *et al.*, 2013)
Cinnabar	HgS	Main mercury ore, historical use as pigment, toxic	(Limited Studies; Wang *et al.*, 2013)

Galena	PbS	Main ore of lead	(Garcia, Bigham and Tuovinen, 1995; Park, Kim and Kim, 2010; Baba *et al.*, 2011; Chaerun, Putri and Mubarok, 2020)
Molybdenite	MoS_2	Main ore of molybdenum	(Pistaccio *et al.*, 1994; Olson and Clark, 2008)
Orpiment	As_2S_3	Historical use as pigment, extremely toxic	(Limited Studies; Zhang *et al.*, 2015; Zhang, Yang and Yang, 2015)
Pyrite	FeS	Most abundant sulfide mineral	(Rodríguez *et al.*, 2003a; Dopson and Lindström, 2004; Okibe and Johnson, 2004; Gleisner, Herbert and Frogner Kockum, 2006)
Pyrrhotite	Fe (1-x) S, where x is 0-0.2	Non-stochiometric variant of rare troilite (FeS)	(Vegliò *et al.*, 2000; Ni *et al.*, 2014; Gu *et al.*, 2015; Zhao *et al.*, 2017; Kim, Koh and Kwon, 2021)
Realgar	As_4S_4	Historically used to colour fireworks, toxic	(Zhang *et al.*, 2007; Chen *et al.*, 2011)
Sphalerite	ZnS	Main ore of zinc	(Konishi, Nishimura and Asai, 1998; Haghshenas *et al.*, 2009; Schippers *et al.*, 2019)
Stibnite	Sb_2S_3	Main ore of antimony	(Torma and Gabra, 1977)

Sulfide minerals have been established in the literature to exhibit enhanced dissolution in the presence of particular microbes (Table 1.1). This is a naturally occurring process, however, the anthropogenic harnessing of microbial sulfide mineral dissolution may also occur – a process known as bioleaching.

1.3 Bioleaching

Bioleaching describes the exploitation of microbial metabolisms to extract metals from sulfide mineral ore, and is most commonly utilised to recover copper, nickel, cobalt, zinc and uranium (Gilbertson, 2000; Vera, Schippers and Sand, 2013).

Compared to traditional methods of sulfide mineral processing, such as pyrometallurgy, bioleaching has reduced costs and energy inputs (Gilbertson, 2000). Bioleaching can also have other environmental advantages by improving the economic viability of exploiting low-grade ore that would otherwise be discarded as waste.

Bioleaching as a metal extraction method is based on the naturally occurring sulfur and iron cycling processes that occur in AMD. As shown in Fig 1.1, the metabolisms of sulfur and iron oxidising bacteria can enhance the breakdown of sulfide minerals through the regeneration of protons (via sulfuric acid) and the oxidant Fe^{3+}, respectively.

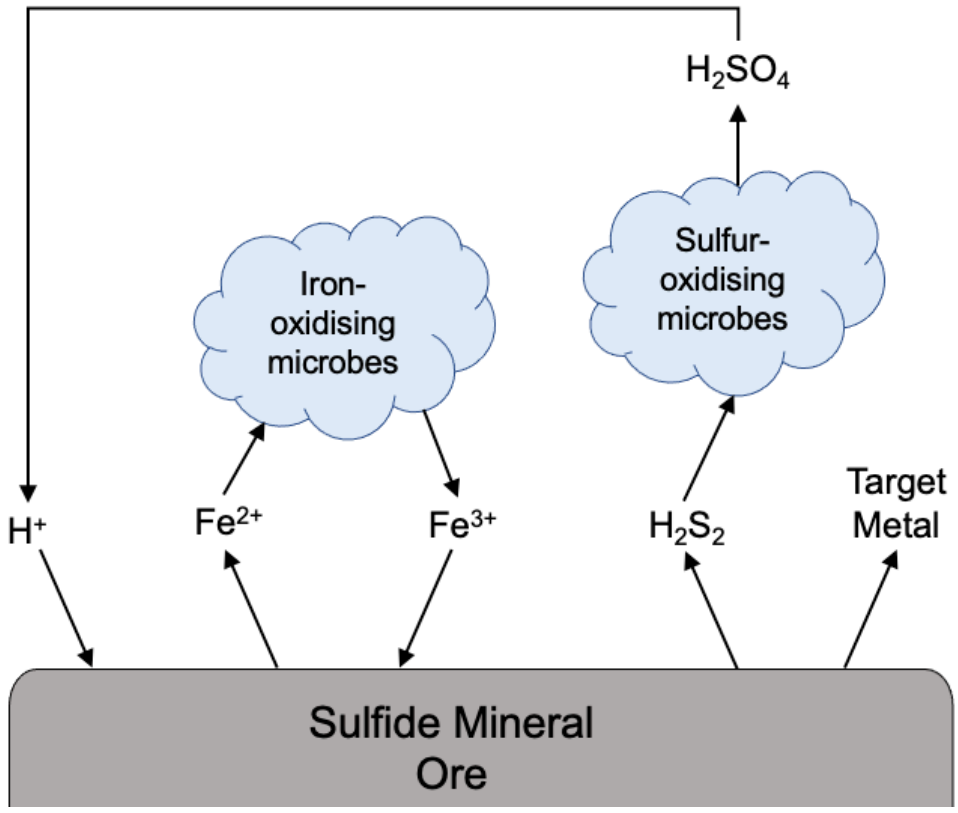

Figure 1.1 – Simplified overview of the bioleaching process showing the regeneration of oxidants by iron and sulfur oxidising microbes, resulting in the release of target metals.

There is an extremely diverse selection of microorganisms that have been successfully used in bioleaching applications (Rohwerder *et al.*, 2003a). However, due to the production of sulfuric acid resulting from sulfide mineral breakdown (Bini,

2010), and the low nutrient environment of “bare” mineral substrates (Valdés *et al.*, 2010), the organisms utilised for bioleaching are typically acidophilic chemolithoautotrophs. Limited evidence suggests heterotrophs could directly contribute to bioleaching via iron oxidation (Bacelar-Nicolau and Johnson, 1999). However, heterotrophs are typically regarded as playing a predominantly indirect role in mineral dissolution, at a community level, by metabolising organic compounds that may inhibit chemolithotrophic activity (Shiers, Collinson and Watling, 2016). Heterotrophs could also aid chemolithoautotrophic mineral dissolution through production of chelating agents, surfactants and vitamins (Johnson and Roberto, 1997).

As demand for metals intensifies, and high quality ores are depleted, reliance on lower quality ores is increasing (Crowson, 2012; Memary *et al.*, 2012). Use of bioleaching can make the exploitation of low grade ores economically viable, and the generally simple operating procedures make it accessible for a broad range of users (Watling, 2006). However, to date, uptake of this technology has remained relatively limited (Johnson, 2018). The possible reasons for this include the potential for failure. For example, Brierley and Kuhn (2009, 2010) describe failure of a commercial scale heap bioleaching system attributed to fluoride toxicity that was in turn attributed to prior laboratory investigations not being sufficiently comprehensive. An enhanced understanding of the community dynamics and processes occurring during bioleaching could improve the efficiency and reliability of this process, reducing the likelihood of failures.

1.4 Environmental Impacts of Sulfide Mineral Dissolution

Understanding the breakdown of sulfide minerals by microbes is not only important to enhancing bioleaching practices, but also in understanding the factors driving the environmentally damaging formation of AMD. AMD describes the acidic waters created near current or (more likely) historic mining sites as a result of the sulfuric acid released when sulfide minerals exposed to air (after being mined) undergo oxidative dissolution (Johnson, 2003). Whilst water levels may have been managed by pumping during the functional life of the mine, expensive water

removal and treatment activities are frequently abandoned following the termination of mining, leading natural water levels to return and increasing the potential for AMD (Johnson and Hallberg, 2005). As the metabolic activities of iron and sulfur oxidising microbes result in the breakdown of sulfide minerals, their presence in mine waste environments can accelerate the rate of AMD formation, potentially by several orders of magnitude (Singer and Stumm, 1970). As protons can act as oxidants in the dissolution sulfide minerals, a feedback loop is created by these sulfur metabolisms, causing the pH to fall to <2 (Baker & Banfield 2003). In some instances, the pH of waters at AMD sites has been recorded as reaching negative values (Nordstrom and Alpers, 1999a).

This environmental problem is exacerbated by the fact that sulfide minerals present in mine wastes commonly bear a wide range of potentially toxic elements (PTEs), either as a major element (*e.g.* arsenic in arsenopyrite), or as minor and trace elements present as impurities or inclusions. As the minerals breakdown, these PTEs are released into the environment (Wu *et al.*, 2009). Additionally, low pH increases the mobility of some metals (*e.g.* Cu, Sb, Pb, Zn, Ni) that would be immobile at neutral pH (Cravotta and Kirby, 2004; Akcil and Koldas, 2006; Król, Mizerna and Bożym, 2020). Consequently, AMD waters are usually contaminated with elevated levels of mobile PTEs, which can then be transported to watercourses and soils, posing a significant risk to the environment (Lu and Wang, 2012). Where AMD waters have been transported away from the origin mine, their acidity can contribute to the remobilisation of deposited metals in sediments further away from the mine site (Johnston *et al.*, 2017). The overall environmental impact of AMD is, therefore, notably detrimental, with acidity and PTE loads affecting aquatic life and contaminating water supplies (Nordstrom and Alpers, 1999b; Nordstrom, 2000), as well as acid levels increasing rates of soil erosion and destroying vegetation (Dhir, 2018).

The sulfur and iron oxidising processes and the microorganisms involved in AMD creation are highly comparable to those exploited beneficially in bioleaching. Consequently, clarifying sulfide mineral breakdown processes is important both to improve bioleaching practice and for informing strategies for the prevention of

AMD. In particular, there are currently notable gaps in our understanding of the metabolic pathways driving sulfide mineral dissolution processes. However, to understand these gaps, we must first look at what is currently known regarding sulfide mineral dissolution processes.

1.5 Sulfide Mineral Dissolution

Sulfide minerals are relatively insoluble, meaning that their breakdown requires oxidation followed by dissolution processes, compared to some other minerals that can simply dissolve (Moses *et al.*, 1987). Throughout this thesis, "dissolution" of sulfide minerals refers to the combined processes of oxidation and dissolution that result in mineral breakdown. In the following sub-sections, the broad pathways of sulfide mineral dissolution are discussed.

1.5.1 Pathways of Sulfide Mineral Dissolution

The mechanism by which sulfide minerals are oxidised by microbes varies depending on the mineral properties. The two pathways are the "polysulfide pathway" and the "thiosulfate pathway" named after the intermediate sulfur species generated during mineral dissolution. Acid-insoluble minerals, such as pyrite and tungstenite are oxidised via the thiosulfate pathway. Conversely, the polysulfide pathway is the mechanism by which acid-soluble minerals such as chalcopyrite, galena and arsenopyrite are oxidised (Schippers and Sand, 1999).

The thiosulfate pathway in pyrite proceeds via the oxidation of S_2 to a thiosulfate group by ferric iron hexahydrate and subsequent cleaving of the Fe-S_2 bond (Johnson, 2014):

$$FeS_2 + 6\ Fe^{3+} + 3\ H_2O \rightarrow S_2O_3^{2-} + 7\ Fe^{2+} + 6\ H^+ \qquad \text{Eq.1.1}$$

This thiosulfate is rapidly oxidised, either abiotically with ferric iron, or via sulfur-oxidising microbes. The oxidation of thiosulfate results in tetrathionate, which may then degrade to a number of compounds, including: trithionate, pentathionate,

sulfite and elemental sulfur. These species may then be oxidised to sulfate via biotic or abiotic reactions. The thiosulfate to sulfate stage of the process can be summarised via Eq 1.2. (Vera, Schippers and Sand, 2013):

$$S_2O_3^{2-} + 8\ Fe^{3+} + 5\ H_2O \rightarrow 2\ SO_4^{2-} + 8\ Fe^{2+} + 10\ H^+ \qquad \text{Eq. 1.2}$$

The polysulfide pathway, demonstrated by Schippers and Sand (1999), involves minerals whose metal-sulfur bonds can be broken apart prior to sulfur oxidation. Consequently, these minerals are susceptible to proton attack, which is the initial stage of mineral breakdown. In acidic conditions, protons facilitate the cleaving of metal from the sulfur moiety and the subsequent formation of hydrogen sulfide. However, in the presence of ferric iron, a sulfide cation (H_2S^+) is formed (in place of H_2S) which spontaneously dimerises, leaving H_2S_2. This is subsequently oxidised by ferric iron to elemental sulfur, via additional polysulfides (Eq. 1.3-4). Finally, elemental sulfur may be microbially oxidised to sulfate, then sulfuric acid (Eq. 1.5) (Schippers and Sand, 1999; Rawlings, 2002).

$$MS + Fe^{3+} + H^+ \rightarrow M^{2+} + 0.5\ H_2S_n + Fe^{2+} \text{ (where } n \geq 2) \qquad \text{Eq. 1.3}$$

$$0.5\ H_2S_n + Fe^{3+} \rightarrow 0.125\ S_8 + Fe^{2+} + H^+ \qquad \text{Eq. 1.4}$$

$$0.125\ S_8 + 1.5\ O_2 + H_2O \rightarrow SO_4^{2-} + 2\ H^+ \qquad \text{Eq. 1.5}$$

The formation of thiosulfate and other polythionates may occur via side reactions (Schippers and Sand, 1999).

1.5.2 Direct vs Indirect Dissolution

Much of the early literature discussing sulfide mineral oxidation describes the potential existence of a “direct” mechanism of sulfide mineral oxidation whereby microbes attach to the mineral surface and directly oxidise sulfide without ferric iron as an oxidant (*e.g.* Sand *et al.*, 1995; Bosecker, 1997). It has now been broadly

recognised that this mechanism is unlikely to exist (Rawlings, 2011; Vera, Schippers and Sand, 2013; Tao and Dongwei, 2014).

Although evidence has suggested that no direct oxidation takes place within the mineral structure, it has been proposed that there may be contact and non-contact bioleaching. The former describes leaching that occurs via cells attached to the mineral surface (within an EPS matrix) generating ferric iron, and the latter defined as bioleaching facilitated by planktonic microorganisms oxidising iron which then oxidises sulfur when it comes into contact with mineral surfaces (Rawlings, 2002). An additional process of "cooperative leaching" has also been described, whereby some free-living bacteria oxidise sulfur species released by contact leaching bacteria (Tributsch, 2001).

1.6 Sulfur Oxidation

In the preceding sections, the overall pathways of sulfide mineral dissolution were discussed. In order for these pathways to proceed, oxidation of sulfur must take place. Jones *et al.* (2014) suggest the following equations for both this complete oxidation (Eq. 1.6) and the partial oxidation of sulfide to elemental sulfur (Eq. 1.7):

$H_2S + 2O_2 \rightarrow 2H^+ + SO_4^{2-}$ (Eq. 1.6)

$2H_2S + O_2 \rightarrow 2S^0 + H_2O$ (Eq. 1.7)

The overall oxidation of sulfur from its most reduced form, sulfide, to its most oxidised state, sulfate, involves $8e^-$ transfers. The oxidation of sulfide to sulfate has many potential intermediate steps, including: polysulfides, elemental sulfur, sulfite, thiosulfate, and tetrathionate. Sulfide (2-) may exist in the form of metal sulfides or as hydrosulfide (Rohwerder and Sand, 2007). Many of the steps in the sulfur oxidation pathway can proceed either abiotically, or be facilitated by microbes. However, elemental sulfur (S^0) is thermodynamically stable at low pH, meaning abiotic oxidation will not occur. Consequently, in acidic environments, the only oxidation of elemental sulfur is that mediated by microbes (Rohwerder *et al.*, 2003a).

1.6.1 Sulfur Oxidising Microbes

The reduced forms of sulfur (RISCs) can be utilised for energy generation by a very ecologically, physiologically and phylogenetically diverse range of prokaryotes (Friedrich *et al.*, 2005; Karavaiko, Dubinina and Kondrat'eva, 2006; Rohwerder and Sand, 2007; Frigaard and Dahl, 2008; Johnson and Hallberg, 2008; Ghosh and Dam, 2009; Dopson and Johnson, 2012). These microbes can be categorised based on their optimum growth pH (neutrophiles or acidophiles) and energy sources (phototrophs or chemotrophs) (Truper and Fischer, 1982; Brune, 1989; Friedrich *et al.*, 2005; Konhauser, 2007; Fenchel, King and Blackburn, 2012). However, most bioleaching microbes are acidophilic chemolithoautotrophs, *i.e.* prokaryotes that thrive in low-pH environments, capable of exploiting inorganic electron sources (*e.g.* RISCs) for energy generation and CO_2 fixation. The genomes of sulfur oxidising prokaryotes possess a range of sulfur oxidation associated genes, capable of producing different enzymes that catalyse the numerous steps in the sulfur oxidation pathway. These enzymes and their role in the sulfur oxidation pathway are discussed in more detail in the following section.

1.6.2 Mechanisms of Microbial Sulfur Oxidation

In the 135 years since the discovery of the first sulfur oxidising microbe, *Beggiatoa* (Winogradsky, 1887), a great deal of knowledge has been acquired regarding the biochemical mechanisms of sulfur oxidation processes. Nonetheless, due to the complexity of the biochemistry involved and the diversity of species capable of sulfur oxidation, much also remains unknown.

There are a large number of enzymes and proteins that have the potential to catalyse the oxidation of RISCs (Liu, 2008). There is often more than one catalyst for each RISC, and the number of sulfur oxidation pathways is almost as great as the diversity of microbes capable of oxidative sulfur metabolism.

Fig. 1.2, below provides a simplified overview of the enzymes and pathways involved in dissimilatory oxidation of RISCs.

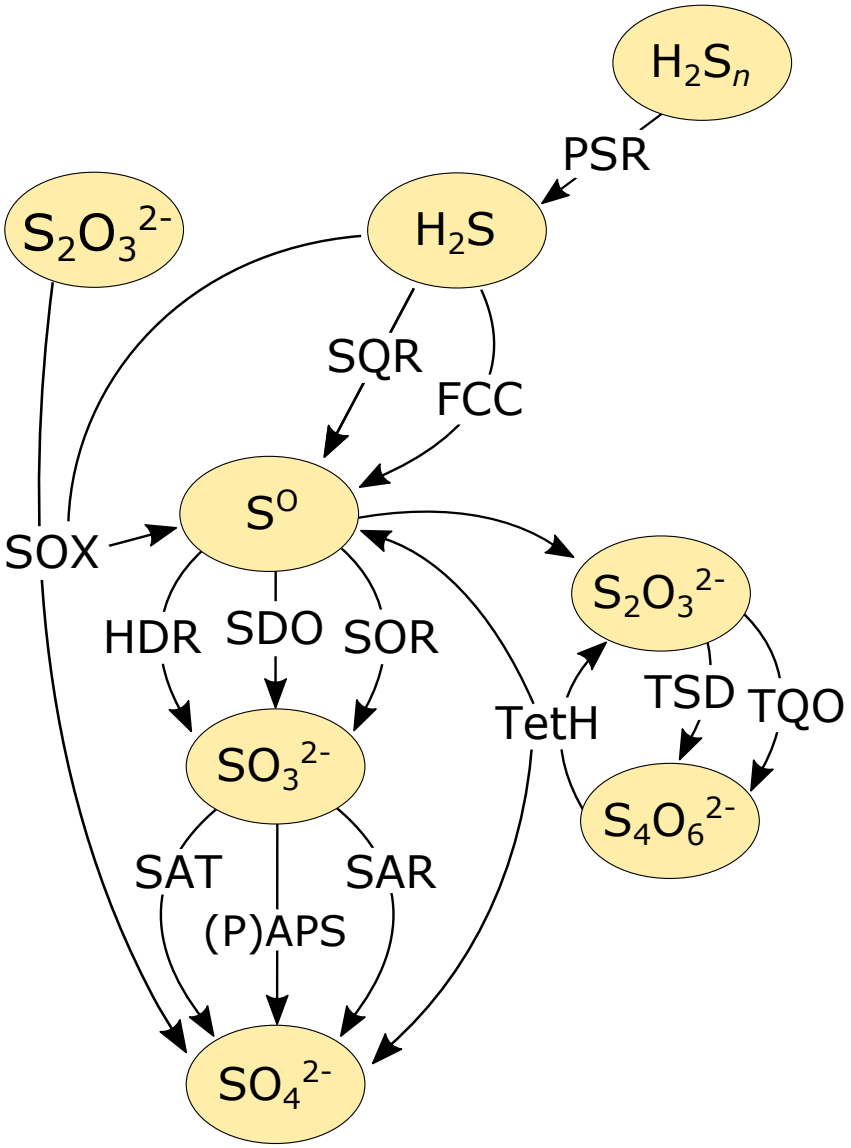

Figure 1.2. The steps of microbially mediated sulfur oxidation in aerobic conditions at low pH and the corresponding enzymes. PSR: polysulfide reductase, SQR: sulfide-quinone reductase, FCC: flavocytochrome c sulfide dehydrogenase, HDR: heterodisulfide reductase, SOR: sulfur oxygenase reductase, SDO: sulfur dioxygenase, SAT: sulfate adenylyltransferase, SAR: sulfite:acceptor oxidoreductase, (P)APS: phosphoadenosine phosphosulfate reductase and adenylylsulfate kinase, SOX: sulfur oxidation pathway, TQO: thiosulfate-quinone oxidoreductase, TSD: thiosulfate dehydrogenase, TETH: tetrathionate hydrolase.

Hydrogen disulfide generated during the initial stages of sulfide mineral breakdown is transformed to sulfide by polysulfide reductase (PSR, Krafft, Gross and Kröger, 1995). Oxidation of sulfide is a two-electron reaction that takes place via the cytoplasmic membrane bound sulfide-quinone reductase (SQR, EC 1.8.5.4). SQR shuttles electrons to a membrane quinone pool, where ubiquinone is reduced. Alternately, this oxidation can be facilitated by flavocytochrome *c* sulfide dehydrogenase (FCC, EC 1.8.2.3). The elemental sulfur resulting from this reaction can then be oxidised via a number of enzymes: a periplasmic, glutathionate-dependent sulfur dioxygenase (SDO, EC 1.13.11.18); sulfur oxygenase reductase (SOR, EC 1.13.11.55) (Urich *et al.*, 2004); or heterodisulfide reductase (HDR, EC 1.8.7.3). SOR can generate sulfite, thiosulfate and sulfide (Ghosh and Dam, 2009). Sulfite is then oxidised to sulfate via sulfate adenylyltransferase (SAT, EC 2.7.7.4), or a sulfite:acceptor oxidoreductase (SAR). It is probable that an intermediary step occurs in the SAT pathway, wherein sulfite is first oxidised to APS via an unknown enzyme. There is a third pathway proposed by Yin *et al.* (2014), whereby sulfite sequentially oxidised to sulfate by phosphoadenosine phosphosulfate reductase (PAPS, EC 1.8.4.8), then subsequently by adenylylsulfate kinase (APS, EC 2.7.1.25).

In the S_4I pathway, tetrathionate is generated as an intermediate species; thiosulfate is oxidised to tetrathionate via thiosulfate-quinone oxidoreductase (TQO, EC 1.8.5.2). Janiczek *et al.* (2007) described a thiosulfate dehydrogenase (TSD) purified from *Acidithiobacillus ferrooxidans,* an enzyme comprised of four identical subunits, which also forms tetrathionate. Subsequently, tetrathionate hydrolase (TetH, EC 3.12.1.B1) hydrolyses tetrathionate to thiosulfate and sulfate (Tano *et al.*, 1996; Kanao *et al.*, 2013). Elemental sulfur may also be a product of this reaction (Yin *et al.*, 2014).

The Sox pathway is a multi-enzyme system found in the periplasm, first described in *Paracoccus pantotrophus* (Friedrich *et al.*, 2000, 2001). This system is capable of oxidising sulfide, elemental sulfur, sulfite, and thiosulfate, producing a final product of sulfate. The Sox system is reportedly widely distributed amongst

prokaryotes possessing sulfur oxidising capabilities (Ghosh and Dam, 2009; Rameez *et al.*, 2020). It has not yet been found in any archaeal species.

Although overall the steps involved in sulfur oxidation have been established, within individual species the exact mechanism for certain steps remains unknown. This is the case for many common bioleaching microbes, and exploring their genomes would enable the creation of updated models of sulfur oxidising enzymes in different species, and consequently lead to an improved understanding of the role of bioleaching prokaryotes in sulfide mineral breakdown.

1.7 Iron Oxidation

While sulfur oxidation is essential, it is not the only microbial process facilitating sulfide mineral oxidation. Iron oxidation is also a very important process, as ferric iron is a chemical oxidant that breaks the covalent bonds holding sulfide minerals together (Sand *et al.*, 1995; Christel *et al.*, 2018). At low pH, ferrous iron is relatively stable and abiotic oxidation is very slow (Johnson, Kanao and Hedrich, 2012). Thus, microbes are vital to the iron oxidation process in acidic environments.

1.7.1 Iron Oxidising Microbes

The iron oxidisers most relevant to bioleaching are the acidophiles, as sulfide mineral dissolution primarily occurs at low pH. Acidophilic iron oxidisers are phylogenetically diverse, and include members of both the Bacteria and Archaea. Although chemolithoautotrophs are the microbes most commonly associated with bioleaching; autotrophs, mixotrophs and heterotrophs have all been shown to oxidise ferrous iron (Kappler *et al.*, 2015). Consequently, any member of a metabolically mixed bioleaching community could potentially contribute to iron oxidation.

1.7.2 Microbial iron oxidation at low pH

As sulfide mineral breakdown predominantly occurs at low pH, the iron oxidation process of interest is that of the acidophiles. Acidophilic iron oxidising microbes generate energy by reducing oxygen via electrons donated from Fe^{2+} (Hedrich, Schlömann and Barrie Johnson, 2011). Oxygen is the only electron acceptor that can be used in this reaction, due to the high redox potential of the Fe(II)/Fe(III) couple (+0.77 at pH2) under acidic conditions (Roger *et al.*, 2012). As oxygen is the only freely available molecule that has a higher redox potential at low pH(+1.12V) (Ilbert and Bonnefoy, 2013), all iron oxidation mechanisms in acidophiles are aerobic.

The nature of the acidic environment is reflected in the iron oxidation mechanism of acidophilic iron oxidisers. The high concentration of protons outside the cell combined with the neutral pH environment inside the cell membrane creates the opportunity for a trans-membrane gradient which can be exploited by acidophilic microorganisms (Bonnefoy and Holmes, 2011). Protons can move across the cell membrane, allowing ATP to be produced with the help of membrane-bound ATP synthase. However, if this process were to continue in an unmitigated manner, the cytoplasm would become acidified, causing the cell to die. A counterbalance is required for the protons, in the form of negatively charged particles (Johnson, Kanao and Hedrich, 2012). Ferrous iron oxidation can provide these counterbalancing electrons whilst reducing oxygen (the “downhill pathway”).

Alongside the downhill pathway, reducing equivalents such as NADH are also produced by exploiting the electrons generated from ferrous iron oxidation. However, this process requires energy, as the NAD+/NADH couple has a significantly lower redox potential (-0.32V) than the iron couple, meaning that if electrons are going to be moved from Fe to NAD+, they have to be pushed “uphill” against the electron potential gradient. This “uphill pathway” is thought to be powered by the ATP generated by the proton motive force. The downhill and uphill pathways run concurrently in iron oxidising chemoautotrophs (Johnson, Kanao and Hedrich, 2012), however the uphill pathway is not required in heterotrophic iron

oxidisers, as organic carbon oxidation can be used to produce reducing equivalents (Bird, Bonnefoy and Newman, 2011). Although all acidophilic chemolithoautotrophs rely on both the downhill and uphill pathways working in parallel, the complexes mediating the processes notably vary between genera. These iron oxidising mechanisms are discussed for specific species in Section 1.8.1.3.3, below.

A number of gaps remain in our knowledge with regards to the mechanisms involved in prokaryotic iron oxidation; the pathways and associated genes involved in iron oxidation have thus far only been identified in a handful of species. This means for many common bioleaching organisms, the mechanism of iron oxidation is not yet fully elucidated. Exploring the genomes and transcriptomes of bioleaching microbes could help increase our understanding of iron oxidation mechanisms and thus, improve our overall understanding of the microbially driven sulfide mineral dissolution.

1.8 Approaches to Studying Microbial Sulfide Mineral Dissolution

This thesis details experimental work conducted to address the gaps in knowledge surrounding sulfide mineral dissolution processes. The experimental work focussed primarily on a bioleaching consortium grown on various sulfide minerals. Metagenomic and metatranscriptomic techniques were used to identify the presence of sulfur and iron oxidising genes within the consortium, and whether these genes were expressed during mineral breakdown. In the following sections, a background is provided to some of the key methods employed.

1.8.1 SC3 Consortium

To study the sulfide mineral dissolution processes responsible for bioleaching, study organisms needed to be selected. It is well established that mixed consortia are more effective at bioleaching than pure cultures (Qiu *et al.*, 2005; Zhang *et al.*, 2008; Liu, Gu and Xu, 2011). Additionally, in AMD environments where sulfide dissolution occurs naturally, mineral breakdown is facilitated by mixed microbial

communities. Therefore, a naturally occurring bioleaching consortium was selected, named “SC3”. SC3 was enriched from a bioleaching trial column in a working copper mine in Skouriotissa, Cyprus (Hellenic Cu Mines Ltd).

1.8.1.1 The Skouriotissa Mine Site

The Skouriotissa mine is located within the Nicosia district of Cyprus. It is one of the oldest working mines in the world, with exploitation of the site dating back multiple millennia (Naden *et al.*, 2006; Cyprus Geological Survey, 2017). Following rediscovery of the site in 1914, modern mining began in the 1920s and has continued ever since (Cyprus Geological Survey, 2017). Original ore reserves at the Skouriotissa mine site were estimated at more than 5.4Mt, with a Cu percentage of 2.3 (Naden *et al.*, 2006). In more recent years, microbes have been employed to improve copper extraction at the site; heap bioleaching has occurred at Skouriotissa since 1996, with copper cathode production via this method averaging 8,000 t yr^{-1} (Brierley and Brierley, 2013).

Located on the northern part of the Troodos ophiolite, within the metamorphosed very low grade Upper Pillow Lava suite, the Phoukassa deposit is a volcanogenic massive sulfide ore deposit of the Cyprus type (Taylor *et al.*, 1986; European Planetary Science Congress, 2013). Formation temperatures comparable to modern day black-smokers provide evidence that the genesis of the Skouriotissa sulfide deposits was exhalative (Adamides, 2010). The host rock for the sulfide deposits is predominantly basalt, and pyrite is the most abundant sulfide mineral within the Skouriotissa ore deposits, followed by chalcopyrite (Constantinou and Govett, 1973; Adamides, 2010). Other copper minerals present are: covellite, bornite, digenite, idaite and minor amounts of chalcocite (Constantinou and Govett, 1973). In terms of non-copper sulfide minerals, different areas of the site have varying abundances of sphalerite, with very rare mackinawite, extremely rare marcasite and trace pyrrhotite (Constantinou and Govett, 1973; Constantinou, 1975).

1.8.1.2 Consortium Overview

Bacterial species present within the SC3 consortium include: *Leptospirillum ferrodiazotrophum*, several *Acidithiobacillus* species, and one member of the order *Rhodospirillales*. There are also archaeal species present: *Ferroplasma acidarmanus, Ferroplasma* type II and the *Thermoplasmatales* member dubbed "G plasma". Additionally, there are three as yet unnamed strains in the consortium that are related to, but distinct from, three of the above named species. The SC3 consortium has been derived from an acidic bioleaching environment and concordantly all of the microbes present in the group are acidophiles, with members deriving energy via a variety of metabolic pathways. Table 1.2., below provides a representative overview of the species present, based on published literature. However, it should be noted that some features such as optimum pH and temperature vary depending on both strain and environmental factors.

Table 1.2 – Overview of the Microorganisms Present in SC3 Consortium, and what is known regarding published strains of these species in literature *indicates that there is a distinct, related species also present in the consortium which is yet to be named.

Species	Phylum	Metabolism	(An)aerobe?	Optimum pH (growth range)	Optimum ºC (growth range)	References for published strains
*Acidithiobacillus ferrooxidans**	Proteobacteria	Chemolithoautotroph	Facultative anaerobe	~2 (1 - 6)	~30 (10-42)	Quatrini & Johnson 2019; Quatrini et al. 2009; Valdes et al. 2008; Kai et al. 2007; Kelly & Wood 2000; Leduc & Ferroni 1994; Drobner et al. 1990; Temple & Colmer 1951 (Kappler *et al.*, 2015)
*Acidithiobacillus ferrivorans**	Proteobacteria	Chemolithoautotroph	Facultative anaerobe	~2.5 (1.9-3.4)	~25 (4-37)	(Guerra-Bieberach *et al.*, 2017) Christel et al. 2016; Talla et al. 2014;

						Liljeqvist et al. 2013; Liljeqvist et al. 2011; Hallberg et al. 2010; Hallberg et al. 2009
Acidithiobacillus thiooxidans	Proteobacteria	Chemolithoautotroph	Obligate aerobe	~2.5 (0.5-5)	~28 (10-37)	Quatrini et al. 2017; Fazzini et al. 2013; Valdes *et al.*, 2011 Suzuki et al. 1999 Konishi, Asai and Yoshida, 1995
Rhodospirillales (Acidisphaera species?)	Proteobacteria	Chemoorgano-heterotrophs, Factultative photoorgano-heterotrophs?	Aerobe (*Ac* spp.)	(2.9-6)	unknown	Kay, Haanela and Johnson, 2014; Hiraishi, 2015
Leptospirillum ferrodiazotrophum (*L.* group III)	Nitrospirae	Chemolithoautotroph	Aerobe, possible facultative anaerobe	(0.7-1.45)	Recorded at 36, 37, 42	Chen et al. (2015a) Aliaga Goltsman et al. 2013 Aliaga Goltsman et al. 2009 Tyson et al. 2005

*'*G plasma'/ *Cuniculiplasma divulgatum*	Euryarchaeota	Organoheterotroph	Facultative anaerobe	1-1.2 (0.5-4)	37-40 (0-48)	Golyshina et al. 2019 Golyshina et al. 2016 a,b; Jones et al. 2014; Comoli & Banfield 2014 Yelton et al. 2013
*Ferroplasma acidarmanus**	Euryarchaeota	Chemomixotroph	Facultative anaerobe	1.2 (0.2-2.5)	45 42-45	(Dopson, Baker-Austin and Bond, 2007) Edwards et al. 2000) Dopson et al. 2004
Ferroplasma Type II	Euryarchaeota	Heterotroph	Facultative anerobe(?)	unknown	unknown	Yelton et al. 2013 (Tyson *et al.*, 2004)

The SC3 consortium was selected as a naturally occurring community that is representative of typical bioleaching consortia. Indeed, the SC3 consortium was initially enriched from a working bioleaching trial column at the Skouriotissa copper mine site. The species within the consortia are all known to be found in AMD environments (Baker and Banfield, 2003) and many of the species (*e.g. Acidithiobacillus, Leptospirillium, Ferroplasma)* are commonly employed bioleaching organisms (Garcia, Bigham and Tuovinen, 1995; Dopson *et al.*, 2004; Corkhill *et al.*, 2008; Halinen *et al.*, 2012; Zhang *et al.*, 2017). In line with this, the species present in the SC3 consortium are known to possess the sulfur and iron oxidation capabilities required to facilitate sulfide mineral breakdown. The sulfur and iron metabolisms of the species found in SC3 are discussed in greater detail in the following Section (1.8.1.3).

1.8.1.3 SC3 Metabolisms Relevant to Sulfide Mineral Breakdown

As previously established in this chapter, sulfur and iron oxidation by microbes is the driving factor behind sulfide mineral dissolution. The genomes of sulfur and iron oxidising microbes contain genes that encode various enzymes that catalyse the oxidation of RISCs and iron. This thesis looks at the presence and expression of these genes within the members of the SC3 consortium, as although it is established that some species in the consortium can oxidise sulfide fully to sulfate, some genes corresponding to vital steps in the pathway are currently unknown. In other species, the relevant genes are known to be present in the SC3 genomes, but have not yet been shown to be expressed. The following sections outline what is currently known with regards to sulfur and iron metabolism genes in the SC3 consortium species.

1.8.1.3.1 Sulfur Metabolism Genes in Acidithiobacilli

As the best studied genus of acidophiles, it is unsurprising that *Acidithiobacillus* presents some of the most complete models of sulfur oxidation. Acidithiobacilli can facilitate the complete aerobic oxidation of sulfide to sulfate, following a series of oxidation steps mediated by an array of enzymes and proteins, as outlined in Figures 1.3 A-C.

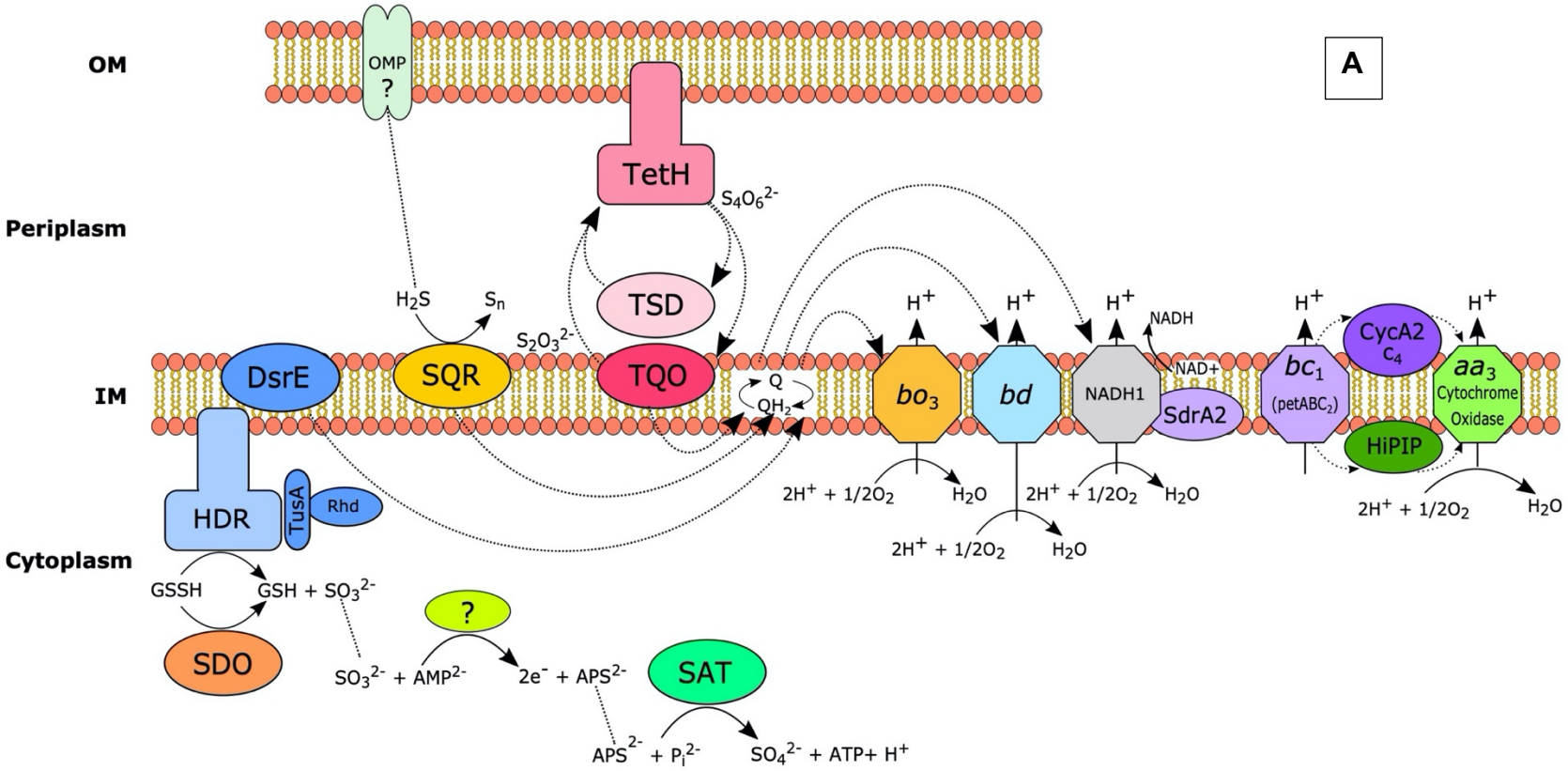
A
OM
Periplasm
IM
Cytoplasm
OMP
?
TetH
$S_4O_6^{2-}$
TSD
H_2S
S_n
$S_2O_3^{2-}$
TQO
DsrE
SQR
Q
QH_2
HDR
TusA
Rhd
GSSH
GSH + SO_3^{2-}
SDO
?
SO_3^{2-} + AMP^{2-}
$2e^-$ + APS^{2-}
SAT
APS^{2-} + P_i^{2-}
SO_4^{2-} + ATP+ H^+
H^+
bo_3
bd
NADH1
NADH
NAD+
SdrA2
bc_1
(petABC$_2$)
CycA2
c_4
aa_3
Cytochrome
Oxidase
HiPIP
$2H^+ + 1/2O_2$
H_2O

B

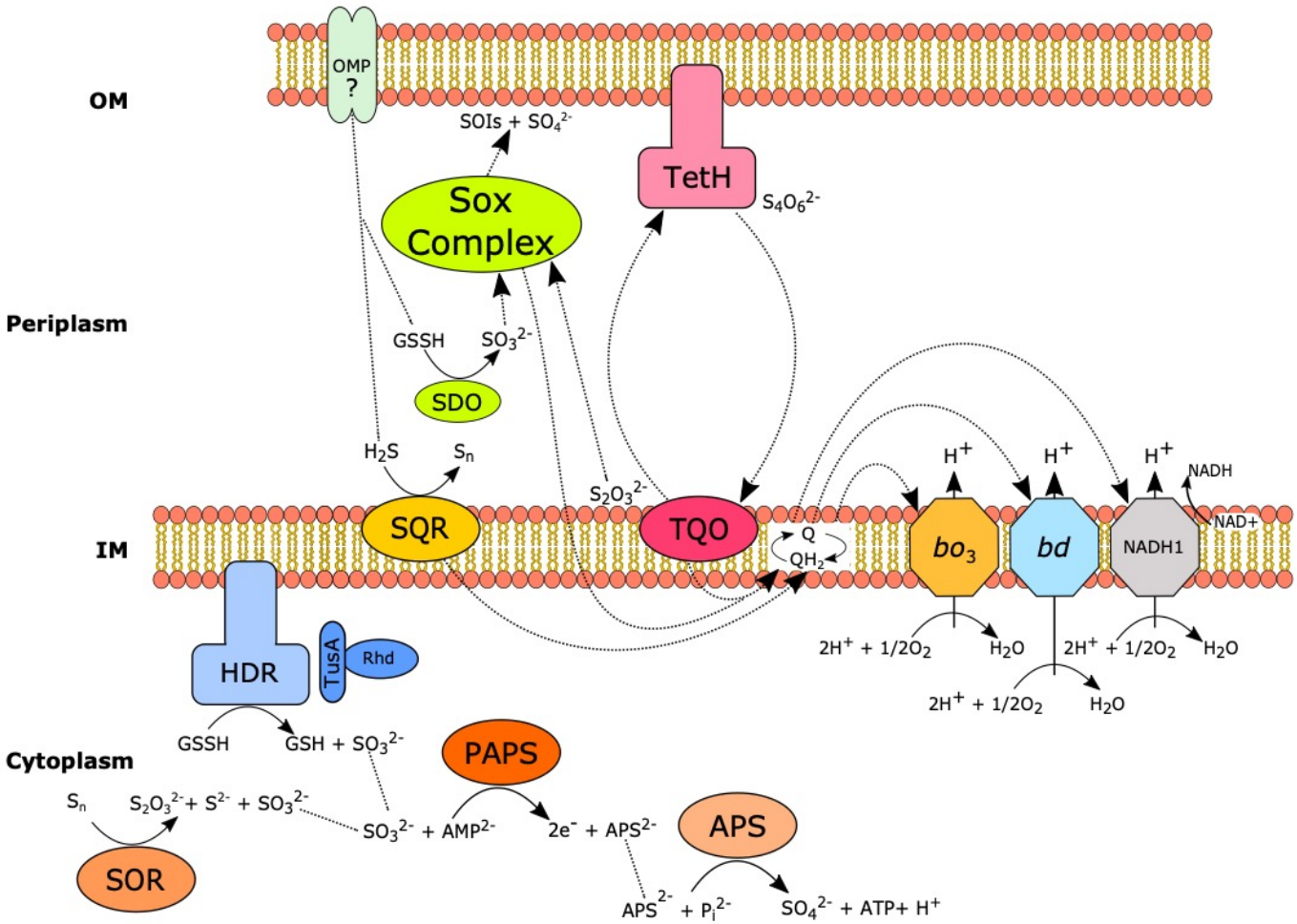
OM
Periplasm
IM
Cytoplasm
OMP ?
SOIs + SO_4^{2-}
Sox Complex
TetH
$S_4O_6^{2-}$
GSSH
SO_3^{2-}
SDO
H_2S
S_n
SQR
$S_2O_3^{2-}$
TQO
Q
QH_2
H^+
H^+
H^+
NADH
NAD+
bo_3
bd
NADH1
$2H^+ + 1/2O_2$
H_2O
$2H^+ + 1/2O_2$
H_2O
$2H^+ + 1/2O_2$
H_2O
HDR
TusA
Rhd
GSSH
GSH + SO_3^{2-}
PAPS
S_n
$S_2O_3^{2-}$ + S^{2-} + SO_3^{2-}
SOR
SO_3^{2-} + AMP^{2-}
$2e^-$ + APS^{2-}
APS
APS^{2-} + P_i^{2-}
SO_4^{2-} + ATP + H^+

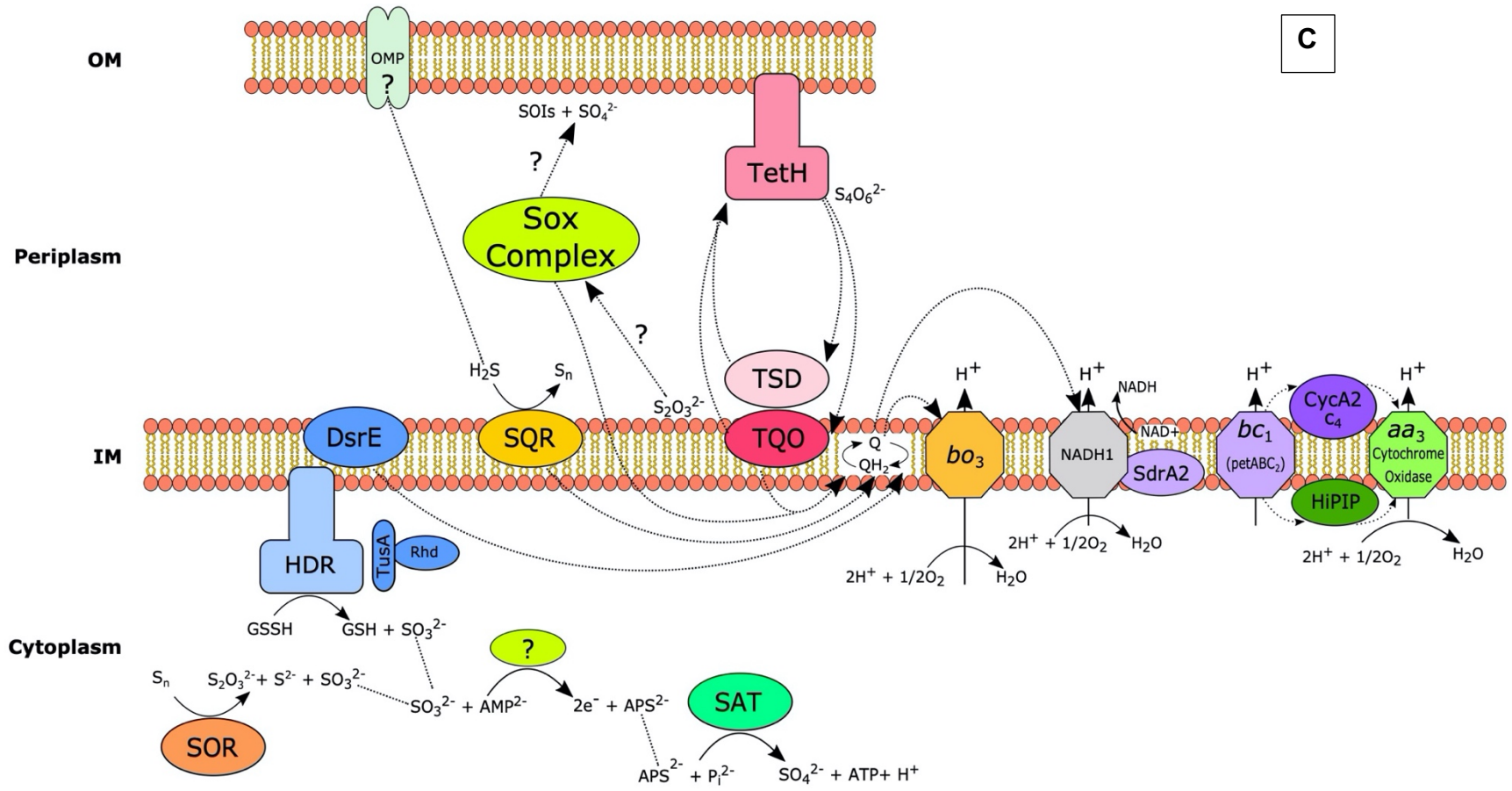

Figure 1.3. – Model of sulfur oxidation in a) At. ferrooxidans; b) At. thiooxidans and c) At. ferrivorans.

Sulfide oxidation proceeds via the inner membrane-bound sulfide-quinone reductase (SQR), which facilitates the oxidation of hydrogen sulfide to elemental sulfur. Insoluble elemental sulfur in the periplasm is most likely converted to glutathionate persulfide (GSSH) by membrane bound thiols prior to oxidation. This GSSH is conveyed via transferases (DsrE, TusA and Rhd) to a heterodisulfide reductase (HDR) complex which catalyses its oxidation to sulfite and

GSH. Alternatively, elemental sulfur may be oxidised by sulfur oxygenase reductase (SOR) or sulfur dioxygenase (SDO). It is predicted that sulfite oxidation in At. ferrooxidans and At. ferrivorans is catalysed by an as-yet unknown enzyme, generating adenosine-5'-phosphosulfate (APS), which is then further oxidised to sulfate, with concomitant ATP and proton generation by sulfate adenylyltransferase (SAT). In At. thiooxidans, sulfite oxidation is via phosphoadenosine phosphosulfate (PAPS) reductase, wherein sulfite is first oxidised to PAPS by the PAPS reductase, then oxidised to APS, and sulfate by APS kinase. In all three species, the oxidation of thiosulfate to tetrathionate is mediated by thiosulfate quinone oxidoreductase (TQO) or thiosulfate dehydrogenase (TSD), while an outer membrane-bound, homodimeric tetrathionate hydrolase (TetH) hydrolyses tetrathionate to thiosulfate. At. thiooxidans and At. ferrivorans both possess the alternate sulfur oxidation pathway - SOX. Across the Acidithiobacilli, electrons produced by RISC oxidation are thought to be transferred to the quinone pool (Q/QH2), from which they are transported to the membrane bound terminal oxidases bo3 and/or bd. Alternately, the electrons generated in RISC oxidation can be transferred indirectly to an aa_3 oxidase for O_2 reduction (via high potential iron-sulfur protein (HiPIP)), or to a NADH1 complex, via which NADH can be generated. These figures were created based on information collected from Rohwerder and Sand, 2003; Valdés *et al.*, 2008; Quatrini *et al.*, 2009; Valdes *et al.*, 2011; Kikumoto *et al.*, 2013; Talla *et al.*, 2014; Yin *et al.*, 2014; Christel *et al.*, 2016; Zhang *et al.*, 2016; Wang *et al.*, 2019; Camacho *et al.*, 2020)

Although the sulfur oxidation pathways of the *Acidithiobacilli* are more complete than for many other sulfur oxidisers, there are still notable gaps. For example, the catalyst responsible for sulfite oxidation in *At. ferrooxidans* and *At. ferrivorans* remains unknown. Additionally, as of yet there has been no identification in the *Acidithiobacilli* (or indeed the other SC3 members) of an enzyme such as polysulfide reductase (PSR) that would mediate the conversion of hydrogen disulfide to sulfide. Therefore, it is currently unclear how this key step in the initial stages of sulfide mineral breakdown is being facilitated by the SC3 consortium.

1.8.1.3.2 Sulfur Metabolism Genes in Other SC3 Members

The evidence for sulfur oxidation genes in the other SC3 members is more limited than in the Acidithiobacilli. An SQR homologue is, to date, the only RISC oxidising enzyme found in the *L. ferrodiazotrophum* genome (Aliaga Goltsman *et al.*, 2009; Chen *et al.*, 2015). Research has indicated the presence of a SQR homologue in G plasma/*Cuniculiplasma* suggesting these organisms could have the potential to oxidise sulfide. However, to date no studies have found evidence of expression of any RISC oxidising genes in this species (Jones, Schaperdoth and Macalady, 2014).

F. acidarmanus and other strains of *Ferroplasma* have been shown to possess the RISC oxidising genes *sor* and *sqr* (Chen *et al.*, 2007; Jones, Schaperdoth and Macalady, 2014), but it is unclear whether these genes are active. There are no current reports for growth using RISCs as electron donors in the *Ferroplasma* species present in the SC3 consortium.

The Rhodospirillales in the consortium is thought to be related to *Acidisphaera.* None of the available *Acidisphaera* sequenced thus far have been found to have RISC oxidising capabilities, and the family

Acetobacteraceae are not associated with sulfur oxidation. Therefore, ascertaining the presence of any RISC oxidation genes in this strain would be novel.

This thesis looks to improve our understanding of RISC oxidation in the SC3 consortium by identifying RISC oxidising genes previously undocumented in their respective species, and determining whether these genes are expressed. This can help us fill the gaps in understanding with regards to RISC oxidation pathways in the SC3 consortium. In turn, this helps to determine the role each consortium member is playing during sulfur oxidation, and consequently, enhances our understanding of sulfide breakdown pathways.

1.8.1.3.3 Iron Metabolism Mechanisms in the SC3 Consortium

Alongside the ability to oxidise RISCs, many members of the SC3 consortium possess iron oxidation capabilities. Iron redox cycling is significantly less complex than that of sulfur, as it predominantly exists in one of two oxidation states - either as ferrous (Fe^{2+}) or ferric (Fe^{3+}) iron (Taylor and Konhauser, 2011). The mechanisms of iron oxidation for energy generation by microbes are, nonetheless, somewhat complex.

At. ferroxidans was the first iron oxidiser to be discovered (Colmer et al., 1940) and has since then been prolifically studied. Consequently, *At. ferrooxidans* provides the most well-understood model of iron oxidation in acidophilic prokaryotes (Ingledew, 1982; Castelle *et al.*, 2008; Quatrini *et al.*, 2009; Ishii *et al.*, 2015). Fig 1.4, below, shows the oxidation pathway for iron in *At. ferrooxidans.*

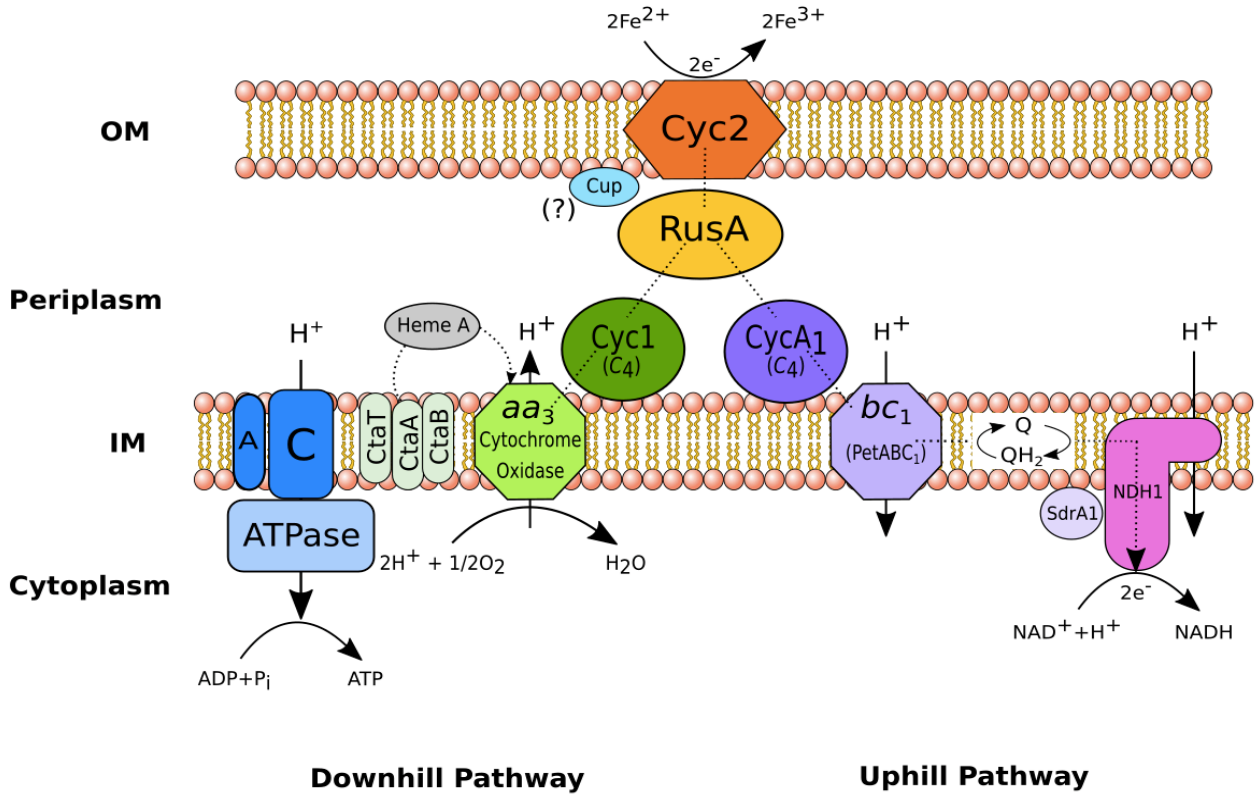

Figure 1.4 – At. ferrooxidans ferrous iron oxidation electron transfer model. The electron transport chain in At. ferroxidans spans the inner (IM) and outer membranes (OM), forming a super-complex that begins with a high molecular-weight outer membrane bound cytochrome c (CycC). Iron remains outside the cell as it is oxidised via this CycC. Electrons flow from CycC to the periplasmic rusticyanin (RusA) and are thereafter directed to either the downhill pathway or the uphill pathway. In the downhill pathway, electrons move from RusA to the

membrane-bound periplasmic cytochrome c, Cyc1, finally reducing oxygen via aa3-type terminal cytochrome oxidase. In the uphill pathway, electrons move from RusA to the alternate membrane-bound periplasmic cytochrome c, CycA1. From CycA1, electrons pass to a reverse-functioning bc1 complex positioned within the inner cell membrane and then via the membrane-associated ubiquinone pool to the NADH-1 oxidoreductase complex (NDH1), where NAD+ is reduced. (Figure based on information and diagrams in: Elbehti, Brasseur and Lemesle-Meunier, 2000; Quatrini et al., 2006; Castelle et al. 2008; Quatrini et al., 2009; Ilbert & Bonnefoy, 2013; Ishii et al., 2015)

Pathways of iron oxidation have also been elucidated in some of the other SC3 species. *At. ferrivorans,* although closely related to *At. ferrooxidans,* has notable differences in its iron oxidation complexes. In *At. ferrivorans*, two different iron oxidation pathways exist. At least two strains of *ferrivorans* have been shown to possess both the *rus* and *petI* operons (Talla *et al.*, 2014; Liljeqvist et al., 2013), with studies showing that *ferrivorans* may possess more than one gene coding for rusticyanin: *rusA* (as found in *At. ferrooxidans* type strain), as well as *rusB* (as found in other strains of ferrooxidans) (Liljeqvist *et al.*, 2011; Talla *et al.*, 2014). A second putative pathway in *At. ferrivorans* is via an iron oxidase (HIPIP) encoding gene, *iro.* Of the *Acidithiobacillus* genus, only *At. ferrivorans* and *ferriphilus* have been shown to possess *iro,* (Tran *et al.*, 2017).

Iron oxidation in *Leptospirillum spp.* has been demonstrated to involve two cytochromes – Cyt_{572}, located in the outer membrane and proposed to be the direct oxidant of iron; and Cyt_{579}, found in the periplasm, through which electrons are passed via cytochrome *c* to a cbb_3 type cytochrome oxidase (Jeans *et al.*, 2008; Blake, 2012; Aliaga Goltsman *et al.*, 2013; L. X. Chen *et al.*, 2015a). Fig. 1.5, below, shows an overview of the potential mechanism of iron oxidation in *L. ferrodiazotrophum.*

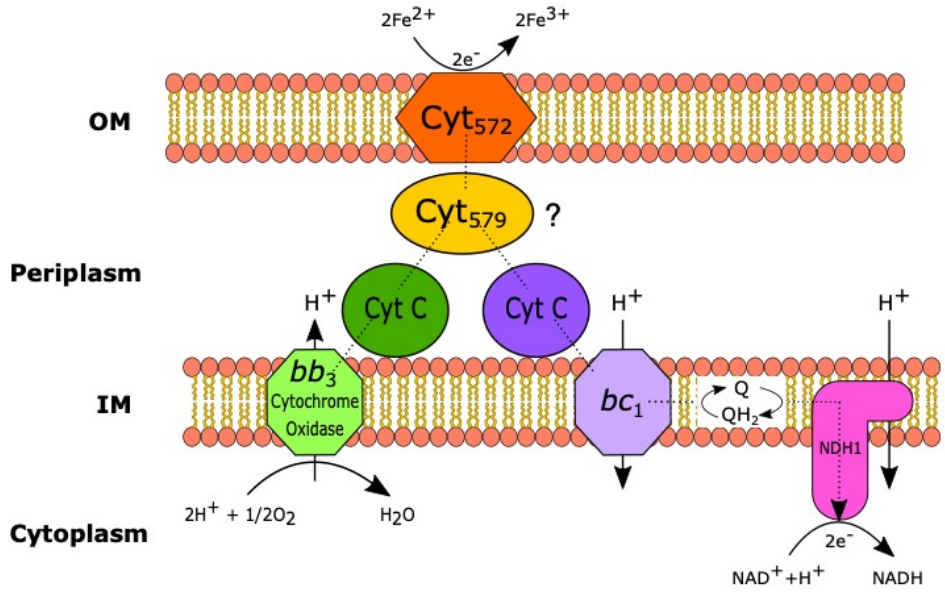

Figure 1.5 – Iron oxidation in L. ferrodiazotrophum. Direct oxidation occurs via the outer membrane Cyt$_{572}$, with electrons passing through a potential periplasmic Cyt$_{579}$ to Cyt c to inner membrane bound terminal oxidases. Based on images and information in (Aliaga Goltsman *et al.*, 2009; Ilbert and Bonnefoy, 2013)

Ferroplasma acidarmanus is proposed to oxidise iron via a blue-copper protein which shares similarities with sulfocyanins and rusticyanins (Dopson, Baker-Austin and Bond, 2005; Castelle *et al.*, 2015), as shown in Fig. 1.6, below. It has been speculated that both *F. acidarmanus* and *F.* Type II contain a SoxM-like super complex, which consists of a Rieske-cytochrome *bc$_1$* complex and terminal oxidases (Castelle *et al.*, 2015). SoxM super complexes are typically found in non-iron oxidising *Sulfolobus species* (Ibid).

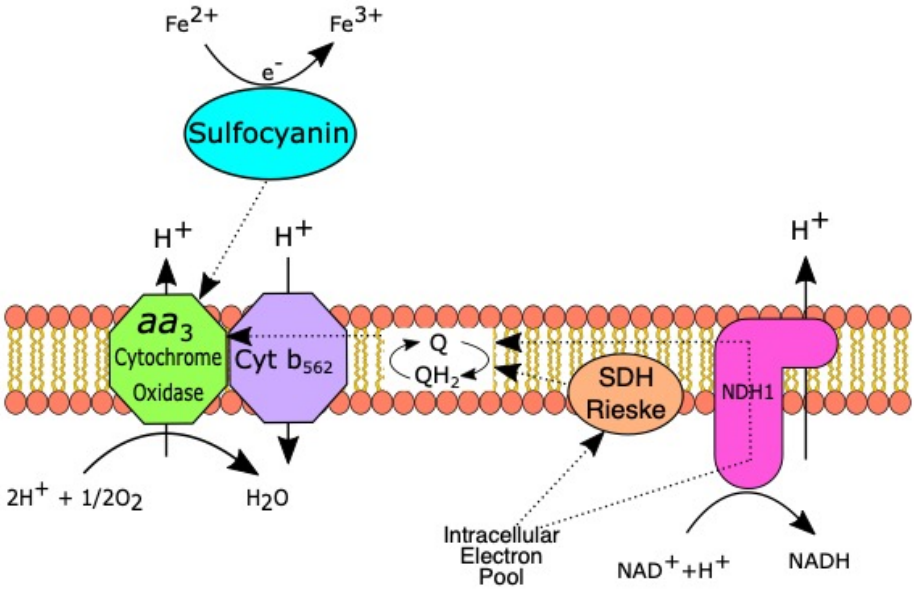

Figure 1.6 – Iron oxidation in F. acidarmanus. Oxidation of iron is via a sulfocyanin-type blue-copper protein. SDH: succinate dehydrogenase. Based on images and information in (Dopson, Baker-Austin and Bond, 2005; Ilbert and Bonnefoy, 2013; Castelle et al., 2015).

Finally, although G plasma was shown by Yelton *et al.* (2013) to contain rusticyanin homologues, no iron oxidation abilities were found in the strain isolated by Golyshina *et al.* (2016b).

1.8.2 Sulfide Mineral Selection

To explore the processes involved in sulfide mineral breakdown, relevant minerals needed to be selected. Three sulfide mineral ores are studied in this thesis: chalcopyrite, Phoukassa ore (low-grade copper ore) and stibnite. These ores were selected due to their importance in metal provision and potential for environmental pollution.

1.8.2.1 Chalcopyrite

Chalcopyrite ($CuFeS_2$) is a copper-bearing sulfide mineral and globally the most important ore of copper (Pradhan *et al.*, 2008). Copper is typically extracted from chalcopyrite via pyrometallurgy, but this is both expensive and has potential environmental impacts, such as increased ambient air pollution (Dimitrijević *et al.*, 2009). In addition, an ever increasing demand for copper combined with ever depleted ore reserves means that over time, there is an increasing reliance on lower grade ores and methods for efficiently extracting copper from these will become more essential (Watling, 2006; Brierley and Brierley, 2013).

1.8.2.2 Phoukassa ore

Phoukassa ore is a low-grade copper bearing ore derived from the Phoukassa deposit at the Skouriotissa mine site (as described in Section 1.8.1.1). There are a variety of Cu-bearing phases present in the ores derived from this deposit, alongside pyrite. As lower grade ores at the site have been subject to processing via bioleaching, it is important to gain a better understanding of the bioleaching process by native microbes.

1.8.2.3 Stibnite

Stibnite represents the most economically important source of antimony, however, relatively little is known about this mineral, including the processes

involved in its dissolution. This is significant, as antimony is a contaminant of growing concern with regards to its potential environmental impact (Herath, Vithanage and Bundschuh, 2017). Additionally, very limited work has been conducted exploring the relationship between microbes and stibnite. As a result, it is not clear whether stibnite is a good candidate for bioleaching, and similarly, factors affecting the release of Sb into the environment remain poorly understood.

1.8.3 Meta-omics and the Application of Next Generation Sequencing to Studies of Bioleaching Communities

In order to harness microbial community processes for industrial uses, such as for bioleaching, the characteristics of these community interactions must be elucidated – a task that can be accomplished with the aid of meta-omics. Meta-omics describes the application of multiple complimentary "-omics" analyses (*e.g.* genomics, transcriptomics) to the study of microbial communities. The benefits of a "meta-" approach include the absence of the requirement to obtain a pure culture of one species, as well as the ability to study the abundance and gene expression of all community members *in situ* during a process of interest, as understanding the interactions during the target usage is key to developing biotechnological applications of a microbial community (Dugat-Bony *et al.*, 2015; Ghosh, Mehta and Khan, 2018). Herein, techniques in metagenomics and metatranscriptomics are discussed, with a focus on their application to bioleaching consortia.

1.8.3.1 Metagenomics

While genomics provides an insight into the DNA sequence of a singular organism, metagenomics involves sequencing of a mixed community at the same time (Tyson *et al.*, 2004). Depending on the technique employed, metagenomics can be used to both identify the types of organisms present in a microbial community, as well as exploring the functional genes present within individual species. Approaches to metagenomics can include genome

resolved metagenomics and 16s rRNA marker gene sequencing (Ghosh, Mehta and Khan, 2018).

1.8.3.1.1 16s rDNA Sequencing

Establishing which species are present in a naturally-occurring bioleaching consortium is an essential first step in determining the functionality of the consortium. One approach to this is 16s rRNA gene sequencing, which uses the 16s rRNA gene to identify the species of prokaryptes present in a sample (Woese and Fox, 1977). The 16s rRNA (part of the small 30s rRNA subunit) gene is highly conserved between prokaryotes, even between distantly related species. Differential identification of prokaryotic species using 16s rRNA gene sequencing is possible as some regions of the gene are "hypervariable". Primers used in the PCR amplification of the rRNA gene are designed to bind to the conserved regions typically found on either side of these hypervariable regions, thereby amplifying the hypervariable regions (Han *et al.*, 2002). The process of 16s rRNA gene sequencing involves: extraction of DNA, amplification of the 16S rRNA amplicon using PCR universal primers, and preparation of a library before sequencing via a platform such as short-read Illumina sequencing (D'Amore *et al.*, 2016).

Previous studies have successfully used 16S rDNA sequencing to assess the types of species capable of growth on sulfide minerals. For example, Dopson & Lindström (2004) examined species present in a bioleaching consortium grown on pyrite, arsenical pyrite and chalcopyrite, while Ma *et al.* (2018) used 16s rDNA sequencing to compare changes in bioleaching community dynamics in differently enriched groups. This approach is therefore well established as a method of identifying species in a bioleaching consortia.

1.8.3.1.2 Genome-resolved Metagenomics

Exploring the genomes of the SC3 consortium can help us to understand the roles different members of the consortium are playing during bioleaching. In

order to achieve this, the full genomes of the present members of the consortium need to be assembled. This can be achieved via genome-resolved metagenomics.

Genome-resolved metagenomics involves the assembly of species' individual genomes from the sequencing data of a mixed community. The major benefit of this technique is that it can be used for the recovery of whole genomes for species that have not been or cannot be isolated as a pure culture (Malmstrom and Eloe-Fadrosh, 2019). This could be extremely important for the study of bioleaching communities, where it may be difficult to culture isolates due to reliance on inter-species interactions for metabolic substrates. Additionally, unlike marker-gene studies, which can only provide insight into the phylogenetic nature of the metagenome, genome-resolved metagenomics also delivers information about the metabolic capabilities of the community (Narasingarao *et al.*, 2012), a key tool in establishing bioleaching community function. The typical procedure followed is outlined in Fig 1.7, below.

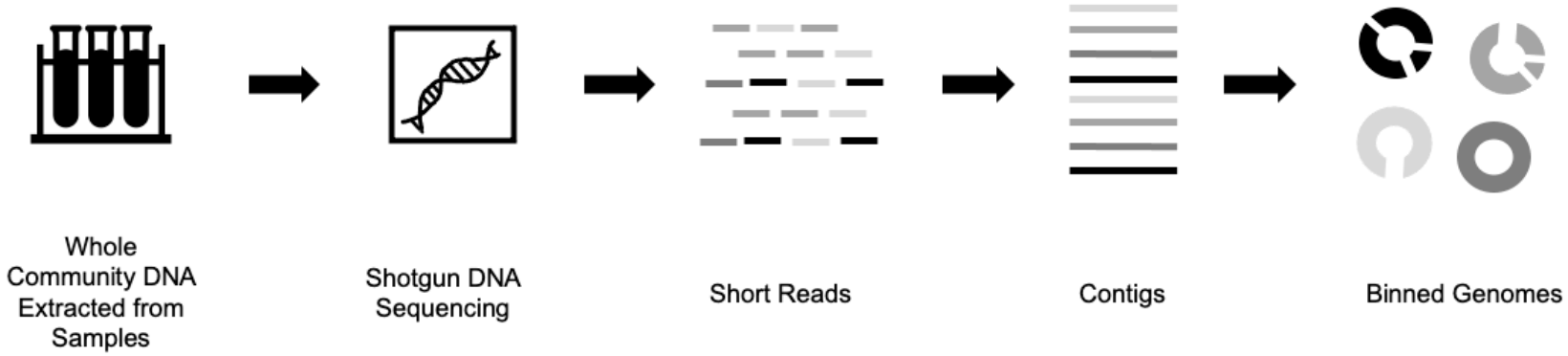

Figure 1.7 – Overview of the Genome-Resolved Metagenomic Process. DNA is extracted from a heterogenous microbial sample. This DNA is shotgun sequenced. This sequence data generates short reads which are combined and organised into longer stretches of sequence, known as contigs and then scaffolds (orientated fragments of gene sequences) (Tyson et al., 2004; Ayling, Clark and Leggett, 2019; Luo et al., 2019). These contigs/scaffolds then undergo "binning", where they are categorised into groups of fragments originating from the same genome (Uritskiy and Di Ruggiero, 2019).

The initial metagenome-assembled genomes were published in 2004 (Tyson *et al.*, 2004), and since then this technology has been used to establish the structure and diversity of microbial communities from a wide range of ecosystems, such as microbial mats (Fullerton *et al.*, 2017; Wong *et al.*, 2018), wastewater bioreactors (Kantor *et al.*, 2015), sugarcane waste (Cassman *et al.*, 2018), and human and animal microbiomes (Lee *et al.*, 2017; Stewart *et al.*, 2018; Olm *et al.*, 2019).

1.8.3.2 Metatranscriptomics

While DNA sequencing can be used to identify the species present in a sample, and even the genes those species possess, it does not tell us how the community is functioning. For example, it is possible to obtain intact DNA from inactive cells (Remonsellez *et al.* 2009). To know which genes are being actively transcribed and therefore expressed by a particular species, it is necessary to look to the transcriptome (Milanese *et al.*, 2019). The metatranscriptome of a community of bacteria provides a snapshot in time of which genes are being transcribed into RNA and consequently can provide important information on which genes are up-regulated under particular circumstances. This can provide key information on how the community is functioning. Until very recently, little work had been conducted examining the metatranscriptome of bioleaching communities. One of the few early instances in the literature focussing on this topic was Galleguillos *et al.* (2008) who studied gene expression in a bioleaching community using random arbitrary primed PCR. More recent studies of bioleaching community transcriptomes have utilised next generation sequencing, although these studies are also very scant.

1.8.3.2.1 RNA-seq

The most holistic method available for metatranscriptomic sequencing is RNA sequencing (RNA-seq). This ultra-high throughput technology is method of transcriptome sequencing that, unlike earlier methods such as

random arbitrary primed PCR, provides a complete picture of the metatranscriptome. RNA-seq analysis generally follows the process outlined in Figure 1.8.

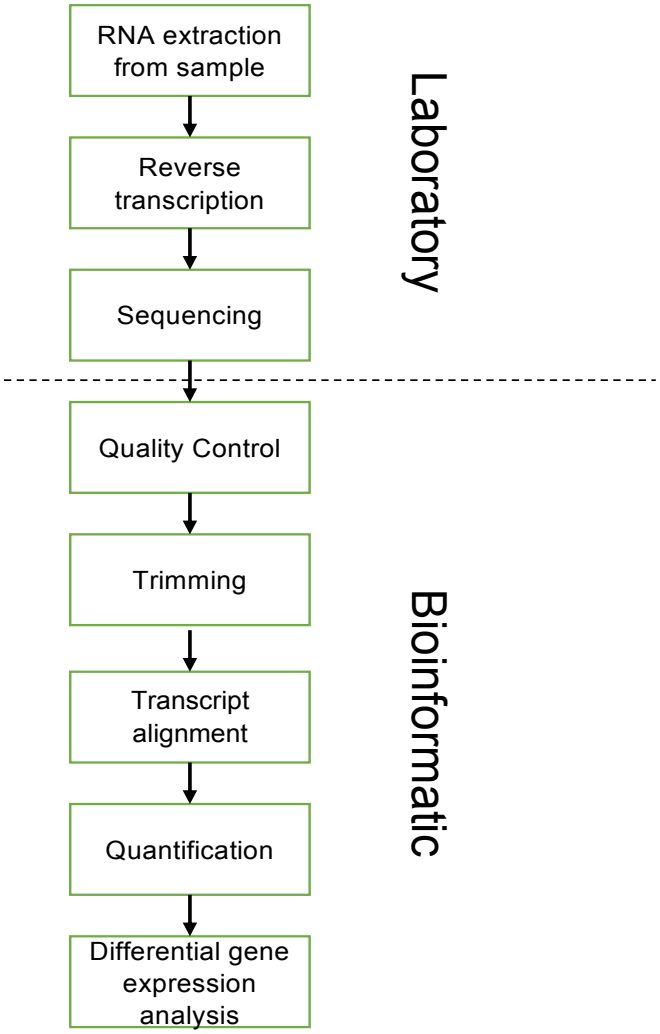

Figure 1.8 – overview of stages in the RNA-seq analysis process. RNA is isolated from the samples and extracted RNA is then reverse transcribed to cDNA and adapters are added to one or both ends of cDNA fragments. Fragments may be optionally amplified via PCR, or alternately may be directly sequenced via a high-throughput sequencing platform such as Illumina or Roche 454. The resulting reads are then processed through quality control, adapters and low quality reads are trimmed. The output from this can be aligned either to a known reference genome or de novo assembly can be conducted. Following this, statistical analysis of the data can allow for the determination of differential expression between groups.

A small number of authors have used RNA-seq to explore gene expression in a bioleaching community. For example, Marín *et al.* (2017) used RNA-seq to examine the expression of genes associated with carbon fixation metabolisms in a bioleaching consortium grown on chalcopyrite. Ma *et al.* (2019) researched constructed bioleaching consortia with a focus on adaptations for resistance to the extreme low-pH environment. However, to date, there have been extremely few other metatranscriptomic studies of acidophiles and no RNA-seq studies examining iron and sulfur metabolism gene expression in naturally occurring bioleaching consortia. Using RNA-seq to explore the SC3 consortium would therefore not only offer an opportunity to study the therefore contribute to the scant number of metatranscriptomic studies of acidophiles. Additionally, RNA-seq offers an opportunity to study metabolism genes of all SC3 members at once. This is highly important to this study, as observing gene expression of a whole community provides a closer analogue to “in practice” bioleaching processes, compared to collecting data from individual species.

1.9 Aims and Objectives

The aim of the experimental work detailed in this thesis was to add to the knowledge base regarding sulfide minerals and the processes involved in their dissolution, specifically copper ores and stibnite. In particular, this work aimed to identify the presence and expression of sulfur and iron oxidising genes in a naturally occuring bioleaching consortium during sulfide mineral breakdown.

The key objectives of this project were as follows:

1. To collect geochemical information about sulfide mineral breakdown using a naturally occurring bioleaching consortium and compare this to an abiotic control. This objective is addressed in all results chapters.
2. To identify genes associated with metabolic processes in the bioleaching consortium with regards to chalcopyrite dissolution, and

examine whether these genes are expressed after 8 weeks' growth on this mineral. This objective is addressed in Chapter 2 of this thesis.

3. To establish whether metabolism genes are differentially expressed over time during dissolution of an environmental copper sulfide ore (Phoukassa ore). This objective is addressed in Chapter 3 of this thesis.

4. To produce models of chalcopyrite and Phoukassa ore breakdown using metatranscriptomic data mapped to geochemical data over time. This objective is addressed in Chapters 2 and 3 of this thesis.

5. To determine the types and quantities of impurities in different stibnites from around the world and from different types of ore deposit, as this knowledge could help further what is known regarding factors affecting rates of stibnite dissolution in the environment. This objective is addressed in Chapter 4 of this thesis.

Chapter 2 - Meta-omic Analyses of Chalcopyrite Bioleaching with an Acidophilic Consortium of Prokaryotes

2.1 Introduction

2.1.1 General Introduction

Demand for copper steadily increases each year (Kulczycka *et al.*, 2016). Chalcopyrite ($CuFeS_2$) is the primary mineral used for the production of copper worldwide (Pradhan *et al.*, 2008). At present, the majority of copper extraction from chalcopyrite is achieved through pyrometallurgy (thermal ore treatment), a process that is both energy and water intensive (Bobadilla-Fazzini *et al.*, 2017). The pyrometallurgical process also contributes to air pollution as a source of particulates and sulfur dioxide (Serbula *et al.*, 2017; European Environment Agency, 2019). Therefore, as water scarcity and concerns over environmental pollution grow, meeting the increasing demand for copper presents a significant challenge. Finding alternative methods of copper extraction is key to a sustained and sustainable copper supply.

Bioleaching offers a potential solution and is increasingly being explored as a low-input, low-emission method of copper extraction (Wang *et al.*, 2020; Brar *et al.*, 2021). There are, however, significant gaps in our understanding of the mechanisms involved in the bioleaching of chalcopyrite. For example, we are yet to identify all the metabolic genes that catalyse chalcopyrite breakdown by bioleaching organisms, and data on the expression of these metabolic genes during bioleaching remains scant. The reason for this lack of data may lie in the significant challenges associated with isolating acidophiles and cultivating them in vitro (Johnson and Quatrini, 2020). Consequently, until recently, molecular data on some bioleaching acidophiles could not be easily obtained.

Recent advances in whole-community DNA and RNA sequencing (metagenomics and metatranscriptomics) offer opportunities to resolve some of these knowledge gaps, by eliminating the need for isolation of individual species. Instead, during meta-omic sequencing, the genome and transcriptome of all species in a community can be sequenced together. This can provide key information on the presence and expression of relevant metabolic genes during community chalcopyrite bioleaching. Nonetheless, metagenomic and metatranscriptomic studies of bioleaching, and indeed acid mine communities themselves, have thus far been very limited (Quatrini and Johnson, 2018). Indeed, previous metatranscriptomic studies of chalcopyrite bioleaching have been limited to studies of microbial adaptations to acidic environments (Ma *et al.*, 2019), and carbon fixation pathways (Marín *et al.*, 2017). There have been no previous metatranscriptomics studies of sulfur and iron oxidising genes during chalcopyrite bioleaching.

In order to address the gaps in knowledge regarding chalcopyrite bioleaching, the dissolution of this mineral under abiotic and biotic conditions is examined in this chapter. Gene comparison techniques are employed to establish which species are present in a naturally occurring (derived from a mine environment) consortium (SC3, described in Section 1.8.1); and which sulfur and iron metabolism genes these species possess. Metatranscriptomics is then used to examine whether genes predicted to be involved in sulfur and iron metabolism are expressed when the consortium is grown on chalcopyrite. The results of this chapter's work are then applied to create an updated model of chalcopyrite dissolution.

2.1.2 Chalcopyrite

The opaque, rock forming mineral chalcopyrite is the most abundant copper containing sulfide mineral and holds roughly 70% of global copper reserves (Panda *et al.*, 2015). Occurring predominantly in hydrothermal deposits, it is globally distributed, meaning the impacts and potential

benefits of chalcopyrite breakdown are a global concern (Wenk and Bulakh, 2005).

Although various pathways of chalcopyrite dissolution have been proposed, the detailed mechanisms of chalcopyrite dissolution are still debated. The following sections will outline what is currently known about chalcopyrite dissolution and bioleaching.

2.1.2.1 Abiotic Chalcopyrite Dissolution

Chalcopyrite is a notably recalcitrant mineral, as a result of its high lattice energy, semiconductor properties and the purported tendency for the formation of a passivating layer (Ahmadi *et al.*, 2010; Wang *et al.*, 2012, 2016; Crundwell, 2015; Tanne and Schippers, 2019). Consequently, abiotic breakdown of chalcopyrite to extract copper is energy intensive, usually involving the application of high temperatures (pyrometallurgy).

Without heat, abiotic chalcopyrite dissolution in strong acid can proceed via Eq. 2.1, however the rate of reaction is very slow (Shiers, Collinson and Watling, 2016).

$$CuFeS_2 + O_2 + 4H^+ \rightarrow Cu^{2+} + Fe^{2+} + 2S^0 + 2H_2O \quad \text{(Eq. 2.1)}$$

In sulfuric acid, a non-oxidative process may also contribute to chalcopyrite leaching (Li *et al.*, 2013):

$$CuFeS_2 + 4H^+ \rightarrow Cu^{2+} + Fe^{2+} + 2H_2S \quad \text{(Eq. 2.2)}$$

Alternatively, where ferric iron is present as an oxidant, the reaction is suggested to proceed via (Pradhan *et al.*, 2008):

$$CuFeS_2 + 4Fe^{3+} \rightarrow Cu^{2+} + 2S + 5Fe^{2+} \quad \text{(Eq. 2.3)}$$

There has been some suggestion that these leaching mechanisms may be common to both biotic and abiotic breakdown (Watling, 2006), with Li and

Huang (2011) reporting that the redox mechanisms occurring do not change in microbial presence or absence, but rather that chalcopyrite oxidation is accelerated in biotic conditions. Abiotic rates are notably slower because in the absence of microbes, sulfur oxidation stalls at the elemental sulfur stage, causing pH to increase and dissolution rates to slow (Schippers and Sand, 1999).

2.1.2.2 Chalcopyrite Bioleaching

Chalcopyrite bioleaching involves the application of microbes to facilitate mineral dissolution. Several factors influence the mechanism by which microbial breakdown occurs, including, notably, the structure of chalcopyrite (Fig 2.1, below) (Kocaman, Cemek and Edwards, 2016).

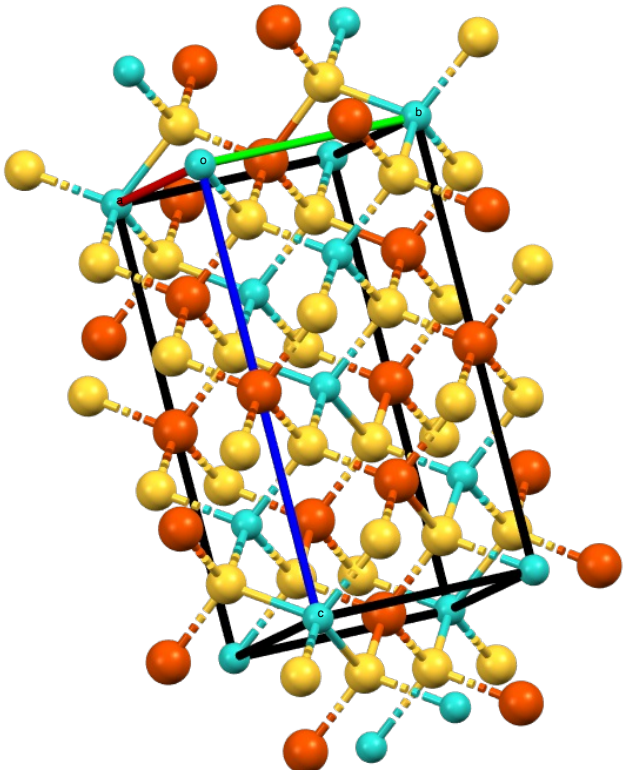

Figure 2.1 – Structure of chalcopyrite created in Mercury (Macrae et al., 2020) based on structural data from Knight, Marshall and Zochowski (2011). Orange atoms represent Fe; Yellow S; Blue Cu. Blue line shows the c parameter. The structure of chalcopyrite is very comparable to the parent structure of sphalerite (ZnS) (Deer, Howie and Zussman, 1986), with the exception of the double length c parameter (edge).

The chalcopyrite structure allows for initial attack by both protons and ferric iron, and as a result, microbial chalcopyrite breakdown follows the polysulfide pathway, as detailed in Section 1.5.1. The following equations represent overall chalcopyrite breakdown by this mechanism (Schippers and Sand, 1999):

$$CuFeS_2 + Fe^{3+} + H^+ \rightarrow Cu^{2+} + 0.5H_2S_n + Fe^{2+} \quad \text{(Eq. 2.4)}$$

$$0.5H_2S_n + Fe^{3+} \rightarrow 0.125\ S_8 + Fe^{2+} + H^+ \quad \text{(Eq. 2.5)}$$

$$0.125\ S_8 + 1.5\ O_2 + H_2O \rightarrow SO_4^{2-} + 2H^+ \quad \text{(Eq. 2.6)}$$

As demonstrated by the above equations, Fe^{3+} and H^+ are key oxidants that initiate and perpetuate chalcopyrite breakdown. Consequently, by regenerating these oxidants, iron and sulfur oxidising microbes have a clear role in the bioleaching process. Indeed, the link between iron and sulfur oxidising microbes and chalcopyrite breakdown is well established, as highlighted by numerous studies (D'Hugues *et al.*, 2002; Behrad Vakylabad, 2011; Zhao *et al.*, 2013; Marín *et al.*, 2017).

Previous studies of chalcopyrite bioleaching have also established that mixed cultures enhance bioleaching efficacy compared to isolated strains (Akcil, Ciftci and Deveci, 2007; Tao *et al.*, 2021). It is therefore evident that defining the iron and sulfur oxidation capabilities of the entire microbial community is key to understanding chalcopyrite bioleaching mechanisms. Despite this, little attention has been paid to the specific roles played by each strain during chalcopyrite bioleaching, and to date, there are no gene expression studies examining how the sulfur and iron metabolism genes of a microbial community fit together and function during chalcopyrite bioleaching. The work described in this chapter looks to address this gap.

2.1.3 Formation of Hypotheses

Based on the information discussed in this introduction, the following hypotheses were formed and tested in this chapter:

H_1 - Chalcopyrite breakdown will be greater in the presence of a typical bioleaching consortium than in the abiotic samples
H_2 - Species in the naturally occurring SC3 bioleaching consortium that possess iron and/or sulfur metabolisms would have additional iron and sulfur genes previously unknown in their respective species
H_3 - Genes predicted to be involved in sulfur and iron metabolism will be expressed when the consortium is grown on chalcopyrite

To summarise how these hypotheses were reached:
H_1 - It has been extensively demonstrated in the literature that chalcopyrite dissolution is enhanced in the presence of iron and sulfur oxidising microbes. The SC3 bioleaching consortium studied in this chapter contains several species that have been demonstrated to oxidise sulfur and/or iron (Section 1.8.1.3). Therefore, it is theorised that this consortium would increase total chalcopyrite breakdown. No previous research has been conducted regarding the bioleaching potential of the SC3 bioleaching consortium as a whole, so confirming this hypothesis is an essential first step in resolving chalcopyrite breakdown mechanisms.

H_2 – Members of the consortium are known to possess the ability to oxidise sulfur and iron, however, for most of the strains the oxidation mechanisms have not yet been fully elucidated or the pathway has incomplete steps. Thus, it is likely that there are as yet unidentified iron and sulfur oxidising genes within the genomes of the SC3 consortium members.

H_3 - As iron and sulfur oxidising genes facilitate chalcopyrite breakdown, it is expected that these genes will be expressed during bioleaching. Previous research shows that iron and sulfur oxidising microbes express

the genes associated with these processes when iron and sulfur are available (Holmes and Bonnefoy, 2007; Liljeqvist, Rzhepishevska and Dopson, 2013; Ai *et al.*, 2019; Feng *et al.*, 2020).

Testing these hypotheses will add to the knowledge base regarding sulfur and iron oxidation genes in bioleaching acidophiles; and will help to establish how the SC3 consortium functions as a whole, including the different roles played by consortium members during bioleaching.

2.1.4 Aims and Objectives

As shown in this introduction, sulfur and iron oxidation by microbes is the driving force behind chalcopyrite bioleaching, offering a sustainable alternative to traditional copper extraction. However, the iron and sulfur oxidising genes that drive this process are not fully documented in many common bioleaching organisms. Additionally, despite the insights gene expression data could bring to understanding bioleaching mechanisms, metatranscriptomic studies of bioleaching consortia are extremely limited. A model of chalcopyrite breakdown by the SC3 bioleaching consortium, integrating gene expression information with geochemical data, would provide a clearer picture of how the sulfur and iron oxidation genes of the different SC3 consortium members fit together to facilitate bioleaching. Meta-omics data can also be used to look at other genes, such as nitrogen and carbon fixation. This supporting information can help us to build a picture of how the community is functioning.

With these points in mind, the aims of the experimental work detailed in this chapter were to improve the understanding of chalcopyrite breakdown mechanisms, and to examine the roles played by different members of a typical bioleaching consortium during biotic dissolution of chalcopyrite. To achieve these aims, the following objectives were outlined:

1. To collect geochemical information about chalcopyrite breakdown by a naturally occurring bioleaching consortium and compare this to an abiotic control.
2. To identify genes in the bioleaching consortium associated with sulfur and iron oxidation processes that facilitate chalcopyrite dissolution
3. To examine whether these genes are expressed after 8 weeks' growth on chalcopyrite.
4. To examine the expression of additional metabolism genes that may be relevant to community functioning, including nitrogen and carbon fixation.
5. To create a model of chalcopyrite dissolution by the SC3 consortium using genomic and metatranscriptomic data.

2.2 Materials and Methods

2.2.1 Experimental Design

Numerous studies have looked at the geochemistry of chalcopyrite bioleaching. Similarly, a large number of individual acidophiles have been examined for their bioleaching potential. What is lacking, to date, is a comprehensive approach, integrating geochemistry, community genomics and community transcriptomics to build a multi-dimensional picture of chalcopyrite breakdown. An experimental plan was designed that would use this integrated approach to test the hypotheses and meet the outlined aims and objectives of this chapter. Figure 2.2, below provides a visual summary of the experimental steps taken.

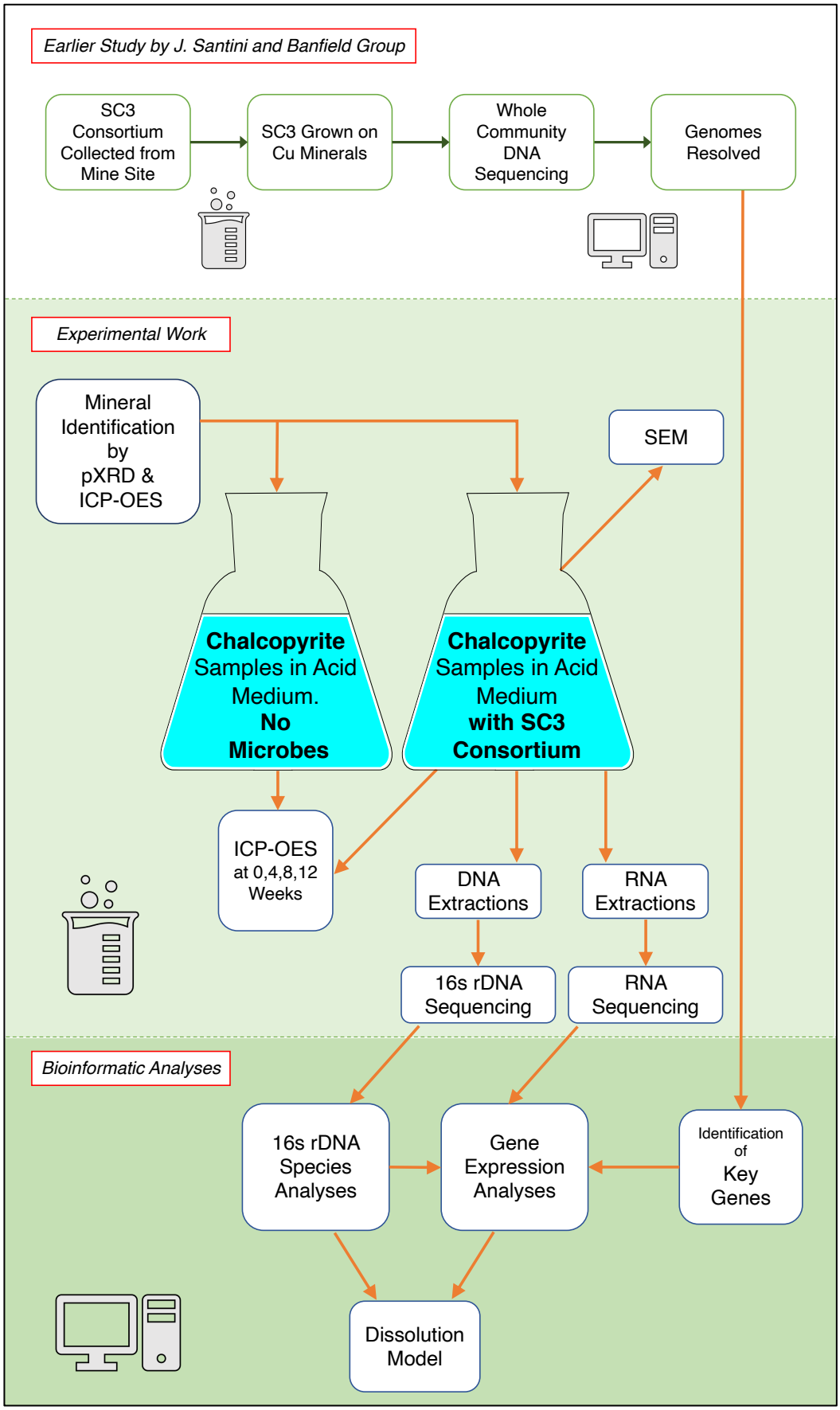

Figure 2.2 - Overview of Chapter 2 Experimental Work

In order to carry out this comprehensive chalcopyrite bioleaching study, a group of relevant microbes needed to be selected. The group selected for experimental work was a naturally occurring bioleaching consortium, as it was representative of microbes naturally found at sulfide mineral mining sites. The species make-up of this group (dubbed SC3, detailed in Section 1.8.1) was already known due to a metagenomic study conducted prior to this thesis by J. Santini and the Banfield Lab (described in Section 2.2.2).

The SC3 consortium was chosen for this chapter's experimental work as it was predominantly comprised of species known to possess the iron and sulfur metabolisms necessary for bioleaching. The consortium is known to grow on copper sulfide minerals, due to being derived from a native copper mine site, where it was already in industrial use as part of a bioleaching trial. Therefore, studying this consortium offered the opportunity to fulfil the aim of examining the roles played by a typical consortium during chalcopyrite bioleaching.

To commence experimental work for this chapter, the mineral used in the bioleaching study was confirmed as chalcopyrite by both pXRD and a strong acid dissolution, followed by ICP-OES analysis. This multi-technique approach to characterising substrates is commonly used in bioleaching studies (*e.g.* Olubambi *et al.*, 2007; Martins, Patto and Leão, 2019). It was essential to establish this baseline in order to create an accurate model of mineral dissolution.

Next, the bioleaching study was set up; the SC3 consortium was grown on chalcopyrite samples in an acidic medium, alongside abiotic controls. The dissolution of the mineral was tracked over time using ICP-OES, in line with numerous previous bioleaching studies (Hedrich *et al.*, 2018; Ma *et al.*, 2019). SEM observations of microbial samples were used to explore whether microbes were attached to the mineral surface, providing contextual information on the breakdown process.

As the genomes had been resolved 2 years prior to the experimental work described in this chapter, the consortium had been subject to a great number of subcultures. 16s rDNA sequencing was therefore used to confirm that the expected species were still present and contamination had not occurred. Re-establishing which microbes were present in the consortium was essential to the accurate alignment of RNA-seq data. 16s rDNA was therefore sequenced at the same time point as RNA-seq. Two of the strains in the consortium had not been assigned to known species. Therefore, comparative genomic techniques were used in combination with the 16s rDNA in an attempt to classify these strains.

Comparative genomic analyses were used to identify key genes in the genomes of the consortium members. These were genes associated with sulfur and iron metabolism that can demonstrate the mechanism of chalcopyrite breakdown in the consortium. Additional genes that may be relevant to community functioning were also identified (carbon and nitrogen fixation). These additional genes provide supporting information that can help us further understand the roles played by the SC3 consortium members during chalcopyrite dissolution.

Total cell numbers were not necessary to achieve the aims and objectives of this work. This is in line with the only metatranscriptomic study of bioleaching carried out prior to the commencement of the work described in this thesis (Marín *et al.*, 2017). In addition, conducting cell counts would potentially compromise the primary aim of the research, as to conduct accurate cell counts using a counting chamber or similar would require significant dislodgement of cells from the mineral surface. Continued adhesion and subsequent biofilm formation is key to chalcopyrite bioleaching efficiency (Rodríguez *et al.*, 2003b; Q. Li *et al.*, 2018). Repeated removal of cells to monitor cell counts would therefore interrupt chalcopyrite breakdown processes. Therefore, preliminary growth trials were instead used to establish a time frame for RNA extraction. Preliminary growth trials and RNA extractions were carried out under the same

conditions as this chapter's experimental work; these trials showed that sufficient RNA for sequencing was only obtained beyond 8 weeks, making t0 RNA extractions impossible. Similarly, in other metatranscriptomics studies of acidophiles, the first RNA extractions are significantly later than t0 (Marín *et al.*, 2017; Ma *et al.*, 2019). This is likely attributable to the well-established challenges involved in nucleic acid extraction from acidophilic communities (Zammit *et al.*, 2011; Hedrich *et al.*, 2016).

To accomplish the aims of this study, only one time point was required for RNA-seq. Indeed, metatranscriptomic studies are often used to elucidate ecological processes by profiling an environment at one moment in time (Cooper *et al.*, 2014). However, due to the aforementioned difficulties associated with RNA extraction from acidic environments, two time points were included to provide a higher chance of sufficient RNA retrieval for sequencing. Whole community RNA was therefore extracted from the biotic samples at both 8 and 12 weeks' growth. Sufficient RNA for sequencing was only obtained at 8 weeks' growth.

Due to the cost prohibitive nature of large replicate numbers in RNA sequencing, replicate numbers in most metatranscriptomics studies are typically low. Indeed, some high profile acidophile metatranscriptomics studies have only one sample per condition (L. Chen *et al.*, 2015). However, three replicates is regarded by the European Bioinformatics Institute (EMBL-EBI) as the minimum number of RNA-seq samples required for inferential analyses (Huerta and Burke, 2020). Three replicates are used in a vast number of metatranscriptomics studies (Edlund *et al.*, 2018; Wang *et al.*, 2021), including the only two existing metatranscriptomics chalcopyrite bioleaching papers (Marín *et al.*, 2017; Ma *et al.*, 2019). Three replicates were therefore created for each time point of RNA and DNA extraction. A novel bioinformatics pipeline was developed to process the RNA-seq data.

Finally, a model of chalcopyrite dissolution was proposed, incorporating the collected metagenomic and metatranscriptomic data to provide a novel and comprehensive picture of chalcopyrite bioleaching by a naturally occurring bioleaching consortium.

The following sections provide further detail on the methods used to achieve this experimental plan.

2.2.2 Preliminary Metagenomic Study: Resolving the SC3 Consortium Genomes

This work was carried out prior to the commencement of the rest of the work described in this thesis. All the work described in this Section (2.2.2.1 only) was conducted by Prof. J. Santini (field and laboratory work) and the Banfield Lab in UC Berkley, California (genomics). This is the only work described in this thesis carried out by Prof. Santini and/or the Banfield Lab.

The SC3 consortium was collected by Santini in 2013; samples were taken from a leaching column (designated short column 3, SC3), operating at ambient temperature and acidic pH (temperature range 16-26 ºC; pH 1.5-2.1. Santini, unpublished data) at the Skouriotissa copper mine in Cyprus. The leaching column had previously been established at the site to improve bioleaching processes, and contained ore and indigenous microbes. Cu-bearing minerals in the ore comprised chalcopyrite, chalcocite, bornite and pyrite (Kossoff, Hudson-Edwards and Santini, unpublished data). Further information on Skouriotissa, including the overall geology of this site is described in Section 1.8.1.1 and in Constantinou and Govett (1973); Constantinou, (1975).

Approximately 0.5 g of ore from the bioleaching test column designated SC3 was used as the initial inoculum for enrichments in a minimal acid medium (MAM), made up as listed in Table 2.1, below.

Table 2.1 – MAM, made up to 1 litre in purified deionised water, adjusted to pH 1.5 with H_2SO_4

Reagent	**Concentration**
$(NH_4)_2SO_4$	0.4 g L^{-1}
KH_2PO_4	0.4 g L^{-1}
$MgSO_4.7H_2O$	0.4 g L^{-1}
Trace elements SL8 containing W & Se (Atlas, 2004)	1ml L^{-1}

Enrichments were incubated at 28ºC with no shaking and the samples sub-cultured using a 5% inoculum. Subculturing occurred every 8 weeks and involved 0.5ml inoculum being pipetted from the previous culture into a 28ml McCartney bottle containing 0.25g laboratory grade chalcopyrite (sieved to <50 µm; Alfa Aesar, CAS Number : 1308-56-1) and 10ml of MAM. After >5 transfers, 3 replicate samples of the SC3 consortium grown on chalcopyrite or chalcocite in MAM were used for extraction and sequencing of their DNA. DNA extractions from cultures occurred at 4 and 8 weeks using the PowerSoil DNA isolation kit (MoBio), following the manufacturer's instructions. Sequencing was conducted by RTL Genomics (Lubbock, Texas, USA). Libraries were prepared according to manufacturer's instructions using the KAPA HyperPrep Library kit (KAPA Biosystems, Inc., Wilmington MA). The Illumina HiSeq 2500 platform was used to sequence the metagenome, using the 2x250 Rapid mode (averaging 24 million reads per sample, maximum 50 million, minimum 10 million). Average coverage was 400 (minimum 190, maximum 740).

The genomes of the SC3 consortium were resolved by the Banfield Lab using genome-resolved metagenomic techniques (Tyson *et al.*, 2004). The dereplicated draft genomes and annotations were privately obtained from ggKbase (http://ggkbase.berkeley.edu/). An overview of the genomes is shown in Table 2.2, below. Gene annotation included both automatic gene annotation and manual curation. The genomes are, as yet, unpublished. The SC3 consortium was established to be made up of 11 bacterial and

archaeal strains. The bacterial strains are: 5 *Acidithiobacilli spp.,* a strain of the species *Leptospirillum ferrodiazotrophum,* and a member of the order Rhodospirillales. The archaea present in the consortium are: 3 *Ferroplasma spp.* and an archaeon dubbed “G plasma”, potentially a strain of the species *Cuniculiplasma divulgatum.*

Table 2.2 – SC3 Consortium General Genome Information (data from the GGKbase database)

Species	Size (Mbp)	Completeness	Number of Contigs	Longest contig (kbp)	Number of Genes	GC Content (%)
Acidithiobacillus ferrooxidans	3.07	near complete	146	186.35	3310	58.51
Acidithiobacillus ferrooxidans related	3.49	near complete	782	85.88	4394	57.5
Acidithiobacillus thiooxidans	2.83	near complete	126	232.22	2996	52.83
Acidithiobacillus ferrivorans	2.48	near complete	92	174.45	2560	57.15
Acidithiobacillus ferrivorans related	2.16	near complete	262	52.36	2366	57.29
Leptospirillum ferrodiaz-otrophum	2.51	partial	106	150.83	2425	58.99
Ferroplasma acidarmanus	1.94	near complete	238	55.91	2190	36.36
Ferroplasma acidarmanus related	1.77	near complete	232	50.46	2039	36.61
Ferroplasma Type II	1.61	near complete	250	58.53	1876	37.26
Rhodospirillales	3.15	near complete	39	423.88	2997	65.95
G plasma	1.77	near complete	179	259.68	1974	37.26

Following this study, the SC3 consortium was sub-cultured in MAM onto chalcopyrite >20 times (*i.e.* a 5% inoculum pipetted from the previous culture into fresh medium and mineral). This ensured none of the original ore was present in the SC3 consortium culture and that the consortium was adapted to growth on chalcopyrite. These cultures were then used as the inoculum for this chapter's bioleaching study (Section 2.2.5).

2.2.3 Powder X-Ray Diffraction

In order to fulfil the aims of this research (to improve the understanding of chalcopyrite breakdown) the identity of the mineral used in the bioleaching study needed to be confirmed as chalcopyrite. The phase identity of the chalcopyrite used was confirmed using powder X-ray diffraction (PXRD) analysis. X-ray diffraction has been used to establish phase identity of bioleaching substrates in numerous papers (Rodríguez *et al.*, 2003a; Fantauzzi *et al.*, 2011; Liu *et al.*, 2015). To conduct this analysis, a sample of the mineral was ground and sieved to < 200 μm. PXRD was carried out using a Stoe Stadi-P Mo diffractometer (Stoe & Cie GmbH, Darmstadt, Germany), with operating conditions of 2θ=2°-40°, 0.5 step, 5 s count time per step. The resulting diffraction patterns were analysed using DIFFRAC.SUITE EVA v3.1 (Bruker, Germany), and phase identification was achieved using the International Centre for Diffraction Data PDF database (Gates-Rector and Blanton, 2019).

2.2.4 Chalcopyrite Composition Analysis

To assess the bulk composition of the chalcopyrite used in the bioleaching experiment, 3 samples (10mg) of mineral were dissolved in nitric acid and concentration of Cu, Fe and S was analysed using ICP-OES at the Wolfson Laboratory for Environmental Geochemistry, UCL. This analysis established the baseline quantities of Cu, Fe and S in the mineral substrate and, in combination with ICP-OES analyses (Section 2.2.7), allowed for the calculation of the percentage of Cu, Fe and S leached out by the SC3

consortium. Bulk composition of bioleaching substrates has been established using ICP-OES in a number of previous studies (Nguyen *et al.*, 2015; Huang *et al.*, 2018).

2.2.5 Microbial Growth Conditions

In this section, the growth conditions for samples used in geochemical testing, 16s rDNA sequencing and RNA-seq are described.

Samples were created by adding 0.75g laboratory grade chalcopyrite (sieved to <50 μm; Alfa Aesar, CAS Number : 1308-56-1) and 50ml Minimal Acid Medium (MAM, Table 2.1, Section 2.2.2) to 100ml conical flasks (Fig 2.3). This substrate to medium ratio is in line with other chalcopyrite bioleaching studies where the mineral is typically added at between 1-3% wt/vol (He *et al.*, 2010; Yu *et al.*, 2011; Buetti-Dinh *et al.*, 2020). A 5% inoculum of the SC3 consortium was transferred to all biotic samples which were then incubated alongside abiotic controls at 28°C without shaking for up to 12 weeks. It has been demonstrated that initial inoculum does not have a significant bearing on overall bioleaching (Wang *et al.*, 2008), nonetheless, a 5% inoculum was used to keep transfers in line with the earlier SC3 study conducted by Prof. Santini and the Banfield Lab, and the protocols of other bioleaching studies (*e.g.* Donati *et al.*, 1996; Das and Ghosh, 2018). Sterile conditions were maintained throughout experimental set-up to ensure contamination with non-target species did not occur, and to ensure the control samples remained abiotic. Further, sub-samples (20μl) were examined at 400x magnification under a Leica DM 2500 LED optical microscope (Leica Microsystems GmbH, Wetzlar, Germany) at 4 week intervals to confirm the presence or absence of microbes in biotic and abiotic samples, respectively.

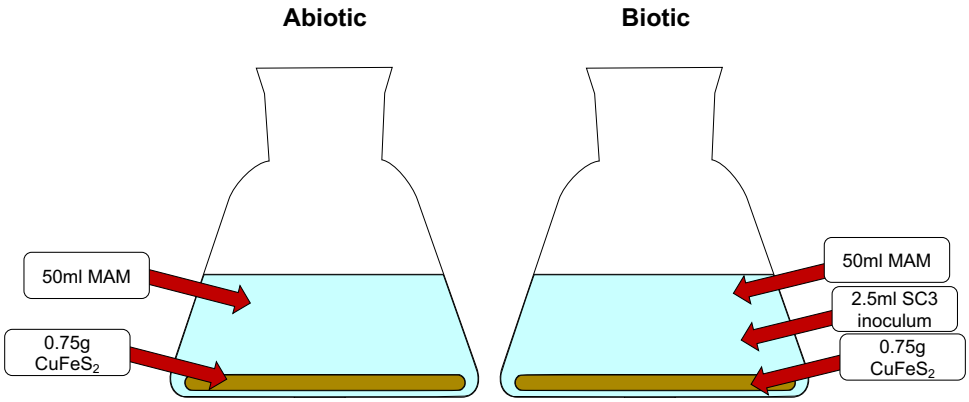

Figure 2.3 - schematic of chalcopyrite dissolution experiment flasks (100ml flasks). Images of growth can be seen in Appendix I.

The minimal acid medium used in this study is a modified version of 9K medium (Silverman and Lundgren, 1959), which is the standard medium for growth of numerous chemoautotrophic acidophiles, including *Acidithiobacillius spp.* (Mackintosh, 1978; He *et al.*, 2010). Ferrous sulfate is usually provided in the 9K liquid medium as a source of electrons. This was not included in the MAM, to allow the Fe and S from the chalcopyrite mineral to serve as electron donors instead. A modified 9K has been used in numerous studies of acidophilic microorganisms (*e.g.* Zammit *et al.*, 2011).

2.2.6 Scanning Electron Microscopy

To examine whether microbes were present on mineral surfaces, mineral samples from 50ml biotic samples cultures at 12 weeks' growth were adhered to stubs, freeze dried (Mondulyo freeze-drier, Edwards, UK) and gold coated using an Agar Sputter Coater (Agar Scientific Ltd., UK), prior to imaging via scanning electron microscopy (SEM) at Earth Sciences, UCL. SEM imaging was carried out using a JEOL JSM-6480LV SEM (JEOL Ltd., Japan).

2.2.7 Geochemical Analyses of Supernatant

To establish the breakdown of chalcopyrite over time in the biotic and abiotic samples, ICP-OES and pH testing analyses were employed. At 0, 4, 8 and 12 weeks, supernatant (10ml per sample) was collected from 3 biotic and 3 abiotic samples at 0 time, 4 weeks, 8 weeks, and 12 weeks. Samples were filtered through 0.22 µm syringe filters and stored at -20ºC prior to ICP-OES analysis. Samples were acidified prior to analysis with 1% HNO_3 (an acidification strength established as suitable for inorganic analyses (Pappas, 2012). ICP-OES analysis was carried out using a Varian 720 ICP-OES (Varian Inc., CA, USA). Standards and blanks were matrix matched to the samples. Percentage of total Cu, Fe and S leached were calculated by dividing concentrations of Cu, Fe and S in the supernatant by total values for Cu, Fe and S in the mineral, as established in Section 2.2.5 and multiplying by 100. The pH values of sample supernatant were assessed using MilliporeSigma MColorpHast pH indicator strips (pH 0-2.5, Merck KGaA, Darmstadt, Germany).

2.2.8 Gene Comparison Analyses

2.2.8.1 Unknown Species – Comparisons to Known Species

Although the genome sequences of each SC3 consortium had been resolved prior to this research, further analyses of the genomes were required. In order to establish whether sulfur and iron oxidising genes in the SC3 consortium strains were novel in their respective species, it was necessary to first establish whether the consortium's unidentified strains – G plasma and Rhodospirillales were representatives of a known species.

As 16s rDNA sequencing had shown the presence of Thermoplasmatales, and previous studies have shown G plasma to be a representative of this group, the G plasma gene sequence was compared to previously sequenced Thermoplasmatales species. The sequence identity of both

the whole genome and the 16s rRNA gene was compared to sequences from *Cuniculiplasma divulgatum* strains S5 (Accession number: NR_144620.1) and PM4 (Accession number: NZ_LT671858.1). This was achieved using "BLAST 2 sequences" (Zhang *et al.*, 2000) via BLASTN (Altschul *et al.*, 1990), on the NCBI website.

16s rDNA sequencing had also shown the presence of a member of the Acetobacteraeceae family – a family within the Rhodospirillales order. Therefore, the same method was attempted to establish the similarity between the genome of the SC3's Rhodospirillales member and previously sequenced species in the Acetobacteraeceae family: *Acidisphaera rubrifaciens* HS-SP3, (Accession number: GCA_000964365.1), *Acidisphaera sp.* L21 (Accession number: GCA_009765685.1), and *Acidisphaera sp.* S103 (Accession number: GCA_009765975.1).

2.2.8.2 Identification of Genes of Interest

The objectives laid out for this project included identifying the genes that facilitate chalcopyrite dissolution and those that help establish how the community is functioning. To this end, "genes of interest" were identified within the genomes of the SC3 species.

2.2.8.2.1 Identifying Genes Associated with Sulfur and Iron Metabolism

Firstly, an exhaustive literature review was conducted, which collated an extensive list of gene sequences associated with sulfur and iron metabolism. Next, sequence comparisons were made to establish what iron and sulfur genes were present in each SC3 species.

The sequence comparisons were as follows: protein sequences of genes associated with sulfur and iron metabolism known from literature were compared to the genomes using "BLAST 2 sequences" (Zhang *et al.*,

2000) and BLASTP (Altschul *et al.*, 1990). Where the gene had not been previously annotated by automatic or manual curation of the genome, only shared sequences with identity values of above 95% and coverage of over 95% were accepted. Where the gene had previously been comparably automatically annotated via KEGG, UNIPROT or UNIREF on GGKbase, identity values of over 70% and coverage of over 90% were accepted. With the exception of *sqr* in Rhodospirillales (74% identity), all protein sequences of genes were over 85% identical to the query sequences. These are stringent values, and represent a more conservative approach than previous literature, where identity values as low as 30% have been accepted as homologous (Pearson, 2013; Barco *et al.*, 2015). A maximum E value of <0.0001 was assigned to ensure a high level of identity across the length of the gene. The results of this analysis showed that all gene comparison E values were several orders of magnitude lower than this. The identified “key genes” were used in downstream RNA-seq data analyses.

2.2.8.2.2 Identifying Genes Associated with Additional Metabolism Processes

To provide information about additional metabolism functions that could be contributing essential inputs to the microbial community, N fixation and C fixation genes were identified in the SC3 consortium.

Potential nitrogen fixing gene sequences were identified via a literature search. Protein sequences of nitrogen fixation genes from the literature were then compared to the SC3 genomes in the same method outlined in 2.2.8.2.1.

Preliminary work conducted by Dr Tom Osborne identified genes predicted to be involved in carbon fixation (unpublished data). This is the only work described in this thesis conducted by Dr Osborne. This work was confirmed, built upon and expanded by me using BLAST 2 sequences as

described in 2.2.8.2.1 above. These genes, alongside the N fixation genes identified above, were used in downstream RNA-seq data analyses.

2.2.9 16s rDNA Sequencing

As the genome assemblies had been conducted a number of years prior to the experimental work described in this chapter, it was necessary to re-establish the species make-up of the SC3 consortium. To this end, 16s rDNA sequencing was used, ensuring expected species were present and contamination with unexpected strains had not occurred. This process consisted of extracting DNA at 8 weeks' growth, sequencing and bioinformatic data processing (described in Sections 2.2.9.1-2, below).

2.2.9.1 DNA Isolation for 16s rDNA sequencing

For the 16S rDNA sequencing, DNA was extracted from 3 samples at 8 weeks' growth using a MoBio PowerSoil DNA isolation kit (MoBio Laboratories, CA, USA). This kit was selected as it has been demonstrated to recover high quality community DNA from a wide range of growth substrates (Mahmoudi, Slater and Fulthorpe, 2011; Wu *et al.*, 2011; Evans, López-Legentil and Erwin, 2018; Shaffer *et al.*, 2022). Use of this kit is regarded as the standardised protocol of community DNA extraction for major microbiome projects, such as the Earth Microbiome Project (Marotz *et al.*, 2018). Prior to extraction samples were examined at 400x magnification under a Leica DM 2500 LED optical microscope (Leica Microsystems GmbH, Wetzlar, Germany). Entire cultures (50ml) were centrifuged for 20 mins at 30,910 x *g* in a Beckman coulter Avanti J-26 centrifuge (JA 25.50 rotor, Beckman Coulter Inc., CA, USA) at 4ºC before the supernatant was removed. Liquid from PowerBead tubes was removed and used to resuspend the microbial pellet before being reapplied to the tubes. Following this, MoBio PowerSoil DNA isolation kit was used in accordance with the manufacturer's instructions, with the following modification: elution was carried out with 50 µl not 100 µl of the sterile

elution buffer. DNA quantities were assessed using a NanoDrop 2000 spectrophotometer (Thermo Scientific, UK). Samples were then immediately transferred to a -80ºC freezer for storage prior to sequencing.

2.2.9.2 16s rDNA Sequencing and Data Analysis of Obtained Sequences

The three DNA samples isolated at week 8 were sequenced by RTL Genomics (Lubbock, Texas, USA) via paired-end Illumina MiSeq (Min reads per sample: 10,216, Max: 13,885, Median: 11,234). The V4 region of the 16s rRNA gene was targeted using the primers:

Forward	515F GTGCCAGCMGCCGCGGTAA
Reverse	806R GGACTACHVGGGTWTCTAAT

A number of bioinformatic pipelines have been developed by which 16s rDNA sequence data can be analysed, such as Mothur (Schloss *et al.*, 2009), UPARSE (Edgar, 2013) and QIIME (1 and 2) (Caporaso *et al.*, 2010; Bolyen *et al.*, 2018), of which, the QIIME packages are the most frequently recommended by comparison papers (Nilakanta *et al.*, 2014; Almeida *et al.*, 2018; Straub *et al.*, 2019).

The data received from RTL Genomics had been formatted as FASTA files to be used by QIIME 1. Consequently, it was not possible to use QIIME2 for the initial steps in data processing, where files are required to be in the FASTQ format. A combination of the QIIME (Caporaso *et al.*, 2010) and QIIME2 (Bolyen *et al.*, 2019) platforms were therefore employed to analyse the 16s rDNA data.

Firstly, raw 16s rDNA sequencing data was demultiplexed into sample-specific libraries using the QIIME split_libraries.py command, with a mapping file containing sample barcodes and primers. During this step, sequences shorter than 200 bp and with a quality score below 25 were

removed. At the recommendation of RTL Genomics, maximum homopolymer length was set at 1000 and primers were ignored. The output of this script was imported as an “artifact” into QIIME2, and thereafter, the vsearch dereplicate-sequences (Rognes *et al.*, 2016) and feature-table functions were used to dereplicate the sequence data and create a feature table. Closed reference clustering into OTUs with 97% identity was conducted using the Silva 132 97% OTUs reference database (Quast, 2013). Taxonomy was assigned using a Naïve Bayes pre-trained classifier trained on Silva 132 99% OTUs (Pedregosa *et al.*, 2011; Bokulich *et al.*, 2018).

2.2.10 Whole-Community RNA-seq of the SC3 Consortium during Chalcopyrite Bioleaching

In order to meet the objective of analysing whether, and which, genes relevant to bioleaching are expressed during chalcopyrite bioleaching, RNA sequencing of the SC3 consortium grown on chalcopyrite was carried out. This process consisted of extracting and sequencing whole-community RNA, and bioinformatic processing of the sequence data , as described in Sections 2.2.10.1-2, below.

2.2.10.1 RNA Isolation of the SC3 Consortium during Chalcopyrite Bioleaching for RNA-seq

RNA was extracted using an adapted protocol for the MoBio PowerMicrobiome RNA isolation kit (MoBio Laboratories, CA, USA). This kit was selected as it offers a robust method of whole-community RNA-extraction that has been successfully used for retrieving RNA from a number of environments (De Filippis *et al.*, 2016; Delforno *et al.*, 2019; Ogunade, Pech-Cervantes and Schweickart, 2019; Ayala-Muñoz *et al.*, 2020). It has been shown to retrieve high RNA yields and purity for metatranscriptomic studies (Reck *et al.*, 2015).

Briefly, prior to extraction samples were examined at 400x magnification under a Leica DM 2500 LED optical microscope (Leica Microsystems GmbH, Wetzlar, Germany). Entire cultures (50ml) were then centrifuged for 20 mins at 30,910 *x g* at 4ºC before the supernatant was poured off. RNA from the microbial pellet was then extracted using the MoBio PowerMicrobiome RNA isolation kit according to the manufacturer's instructions, with the following modification: elution was using 50µl rather that 100 µl of sterile elution buffer. Samples were kept on ice while RNA quantities were assessed using a NanoDrop 2000 spectrophotometer. Samples were then immediately transferred to a -80ºC freezer for storage prior to sequencing. Although RNA was extracted at weeks 8 and 12, NanoDrop analyses showed insufficient RNA was extracted from week 12 samples for the intended sequencing. Consequently, only 3 week 8 samples were sent for sequencing.

2.2.10.2 RNA Sequencing and Data Analysis

Ribosomal RNA was depleted, libraries were prepared and sequencing was conducted by RTL Genomics (Lubbock, Texas, USA). The Illumina NextSeq 550 platform was used to conduct 150bp, non-stranded, paired-end RNA-seq analysis (averaging 33 million reads per sample, maximum 46 million, minimum 20 million).

A dedicated workflow was created to analyse the metatranscriptomics data, incorporating a number of bioinformatic tools. The RNA-seq data analysis pipeline was initiated with the creation of a reference metatranscriptome, to which the RNA-seq data could be pseudo-aligned. The reference metatranscriptome was created by first concatenating all genomes from the SC3 consortium into a single reference. Next, this metagenome was run through Prodigal v2.6.3 (Hyatt *et al.*, 2010) to predict gene sequences, thus creating the reference metatranscriptome (MetaRef). A similar method was used by Stolze *et al.*, (2018) who

combined four previously established metagenome “bins” to create a reference metatranscriptome.

The quality of the sequenced metatranscriptomic data was checked using FastQC v0.11.7 (Andrews, 2010). Low quality reads and adapters were trimmed using CutAdapt v1.18 (Martin, 2011). Kallisto v0.44.0 (Bray *et al.*, 2016) was then used to extract estimated read counts from the trimmed reads using the MetaRef as a reference. Genes were considered expressed if counts aligned to that sequence were >5. Gene counts below this threshold were removed, as low gene expression is indistinguishable from noise. Read counts were normalised by sample using Deseq2 (Love, Huber and Anders, 2014). The expression level of gene sequences of interest (identified via BLAST in Section 2.2.8.2) were then established in R studio.

2.2.11 Graphics and Statistical Analysis

To ensure appropriate statistical tests were employed, datasets (pH, ICP-OES) were tested for normality first visually, via Q-Q plots and kernel density plot histograms, then using Shapiro-Wilk tests, and were found not to be normally distributed (Appendix II). Consequently, non-parametric statistical tests were employed to determine the significance of results. Linear mixed effects models for differences in elements between biotic and abiotic accounting for the effect of time point, Kruskal-Wallis analysis of variance testing and Mann-Whitney U testing were used to establish differences between treatments (Appendix II).

Statistical analyses, bioinformatic work and production of figures showing data were carried out in R version 3.4.3 (R Core Team, 2017), using R studio version 1.1.423 (RStudio Team, 2016), with packages: “ggplot2” (Wickham, 2016), “ggpubr” (Kassambara, 2018), “forcats” (Wickham, 2019), “dplyr” (Wickham *et al.*, 2019), “tximport” (Soneson, Love and Robinson, 2016), “readr” (Wickham, Hester and Francois, 2018),

"devtools" (Wickham, Hester and Chang, 2019), "ggbiplot" (Vincent Q Vu, 2011), "gridExtra" (Auguie and Antonov, 2017). Diagrams illustrating experiment schematics, metabolic pathways and biogeochemical cycles were produced using Inkscape (Inkscape, 2019).

2.3 Results

2.3.1 Growth Substrate Mineral Composition Analyses

In order to meet the research aim of improving the knowledge base surrounding microbial chalcopyrite breakdown, it was essential to confirm that the identity of mineral used in this chapter's experimental work was indeed chalcopyrite. The mineral was verified using pXRD and ICP-OES analyses.

Chalcopyrite was established by pXRD to be the major phase within the sample (Fig 2.4, below).

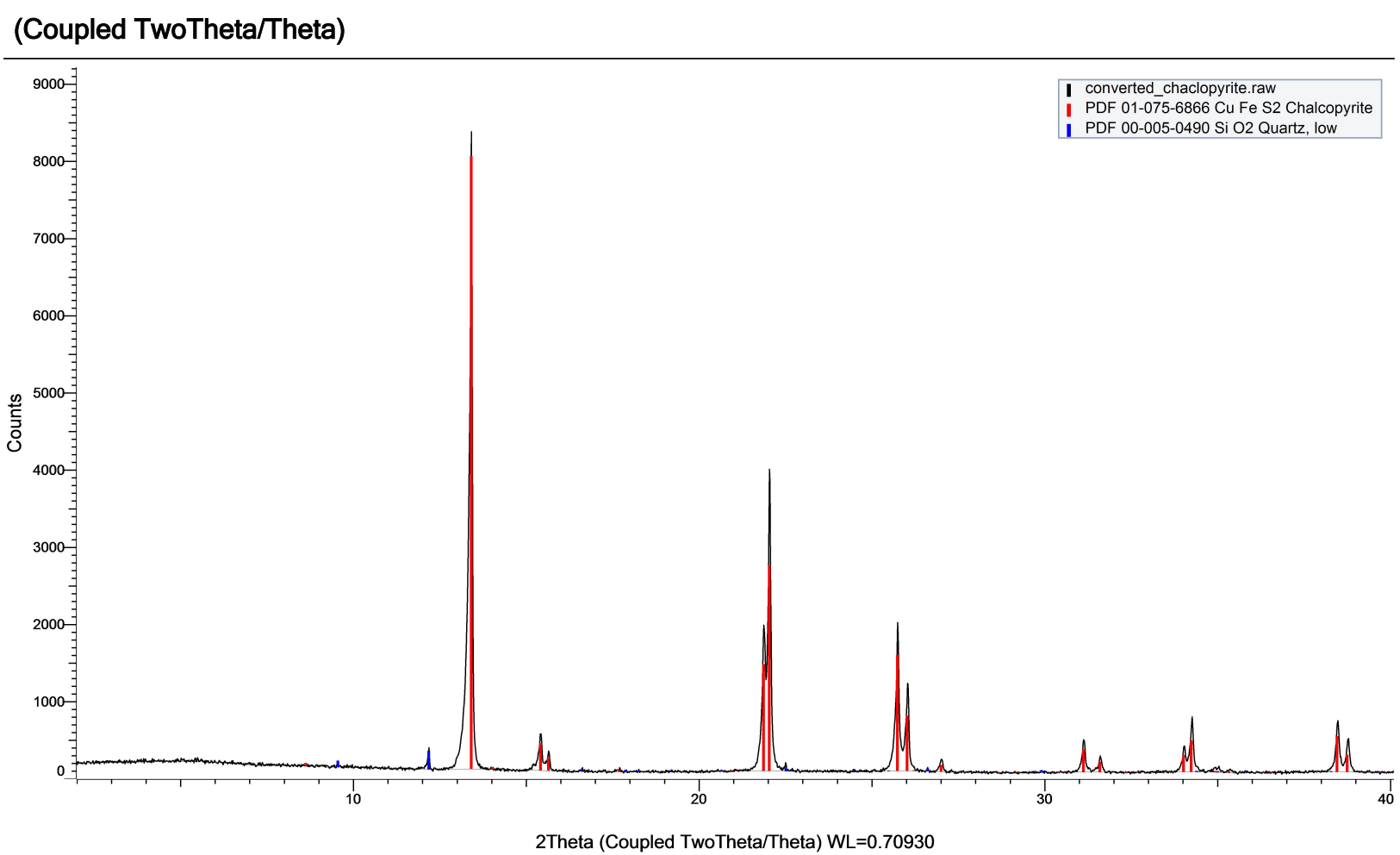

Figure 2.4 pXRD pattern for the laboratory grade chalcopyrite used in growth experiments. PXRD produces peaks which are characteristic of specific minerals. Red lines indicate peaks corresponding to chalcopyrite, blue lines indicate peaks corresponding to quartz

Total mineral dissolution in acid followed by ICP-OES corroborated the pXRD analysis. The overall composition of the mineral was revealed to be 33.8% Cu, 31.1% Fe, 32.5% S, (± standard deviations of 6.0, 5.4 and 5.19 respectively, Fig. 3.5). This result is in line with reported values for chalcopyrite (Lundström *et al.*, 2005).

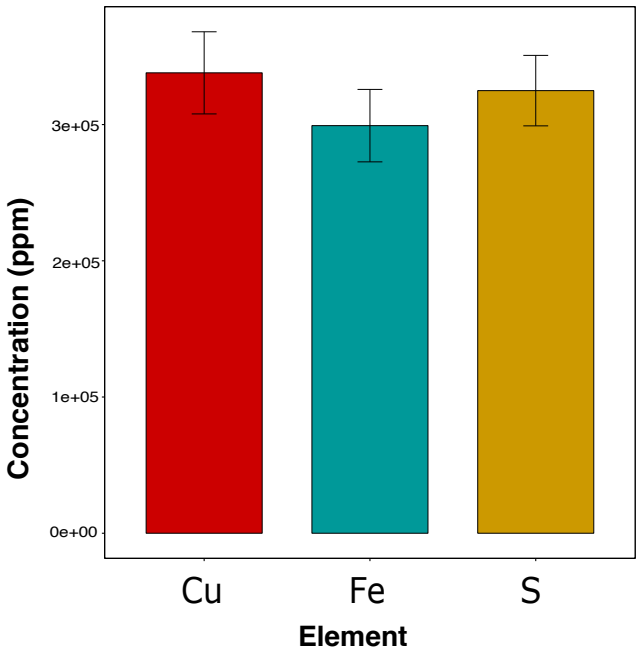

Figure 2.5 - Mean element concentrations (ppm) of the chalcopyrite examined in this chapter, dissolved in nitric acid, as measured by ICP-OES (n=3), error bars show standard error

The strong agreement of the pXRD and ICP-OES results confirmed that the mineral used in this chapter was high grade chalcopyrite. Additionally, this information established the baseline (pre-leaching) quantities of Cu, Fe and S in the mineral.

2.3.2 Scanning Electron Microscopy

Inspection under an optical microscope at 4 week intervals had confirmed that microbes were present in biotic samples and absent in abiotic samples. To explore whether there was microbial attachment to the mineral surface, biotic

samples were then examined using scanning electron microscopy (SEM) at 12 weeks' growth.

SEM images of the chalcopyrite are shown in Fig. 2.6A-C. These images confirm the chalcopyrite was colonised by microbes, and show multiple morphologies suggesting more than one species is present. Fig 2.6A shows a substance comparable to biofilms seen in sulfide mineral bioleaching and attachment studies (Q. Li *et al.*, 2018; Nascimento *et al.*, 2019).

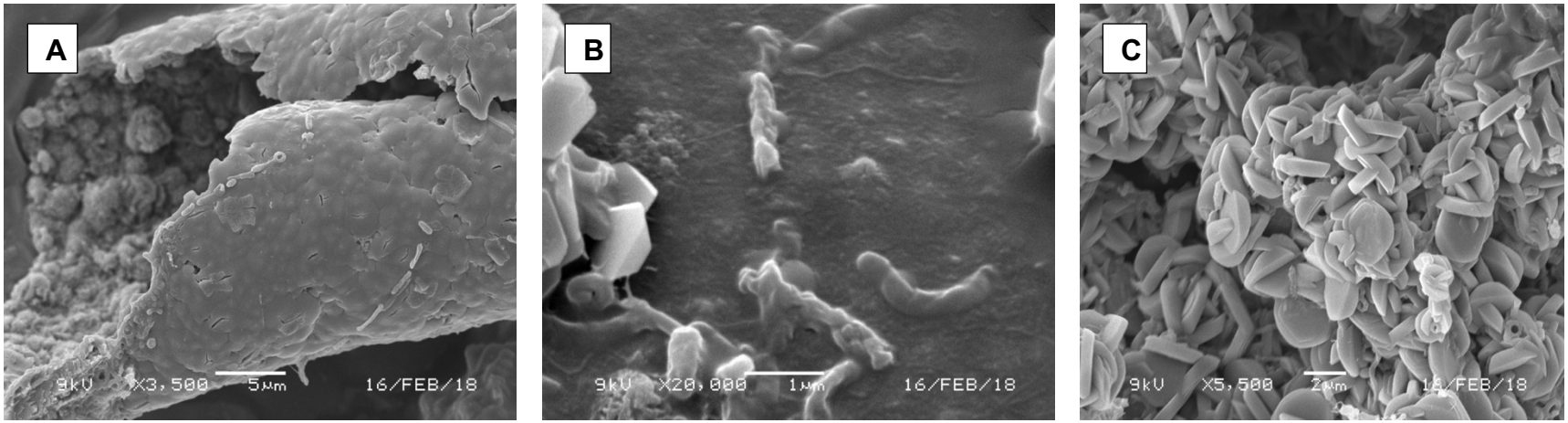

Figure 2.6 SEM images of SC3 consortium at 12 weeks' growth on chalcopyrite

2.3.3 Dissolution of Chalcopyrite in Biotic and Abiotic Conditions

To establish whether chalcopyrite breakdown is greater in the presence of a microbial consortium, the overall extent of mineral breakdown was established using ICP-OES. Quantities of Cu, Fe and S were measured at 0 time, 4, 8 and 12 weeks. Significant differences in quantities of Cu, Fe, and S present in supernatant were observed between biotic and abiotic conditions after 4, 8 and 12 weeks' growth (Fig 2.7 and Appendix III; linear mixed effects model, $p<0.01$).

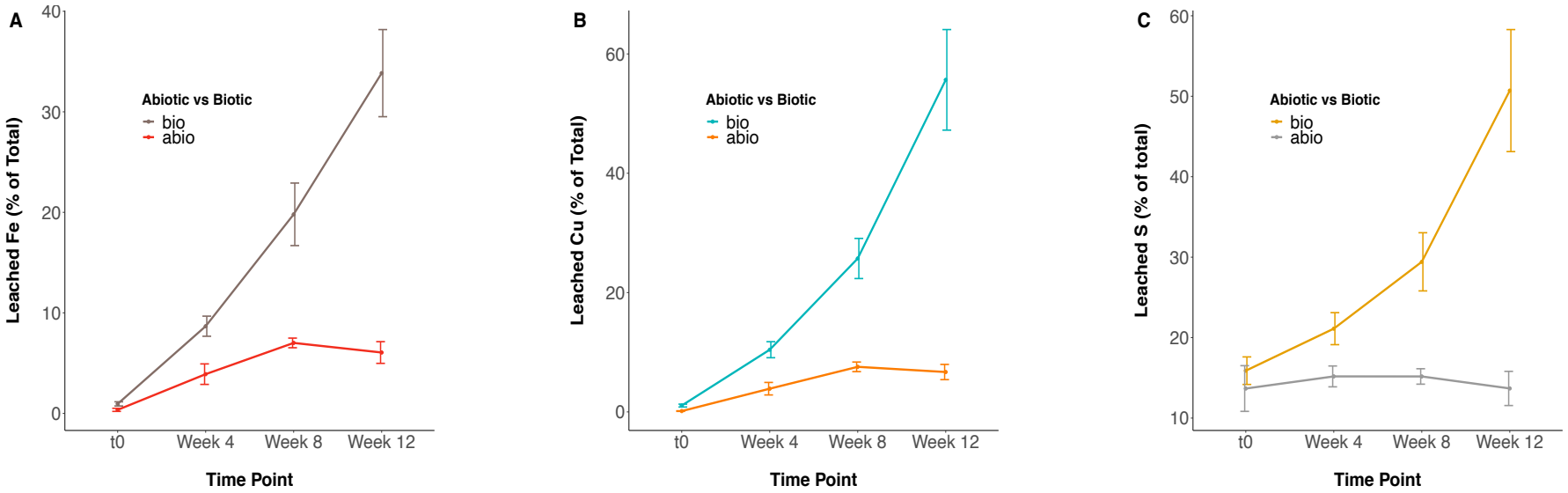

Figure 2.7 - mean supernatant ICP-OES results showing percentage of total A) iron, B) copper, and C) sulfur leached from chalcopyrite under biotic and abiotic conditions over 12 weeks (n=3). Error bars show the standard error of the mean.

At week 12, the mean leached percentages of Fe, S and Cu for the biotic samples are 33.8% (± st. dev. 7.5), 50.7% (±13.1) and 55.7% (±14.6) of the total, respectively. In comparison, in the abiotic samples at the same time point, a mean 6.1%(±1.9) Fe, 13.7%(± 3.7) and 6.7%(±2.21) of the total element was leached from the mineral.

As protons can be both produced and consumed during mineral dissolution, the pH of samples over time was measured as an additional indicator of sulfide mineral breakdown. Both abiotic and biotic samples showed increases in pH over time (Fig. 2.8), suggesting protons were being consumed in all samples. However, over time biotic samples showed a greater pH increase than the abiotic samples, with a mean 0.44 and 0.37 unit difference between the two conditions at week 8 and 12, respectively. This increase in pH could be indicative of increased iron oxidation in biotic samples, as this process consumes protons (Smith, Luthy and Middleton, 1988).

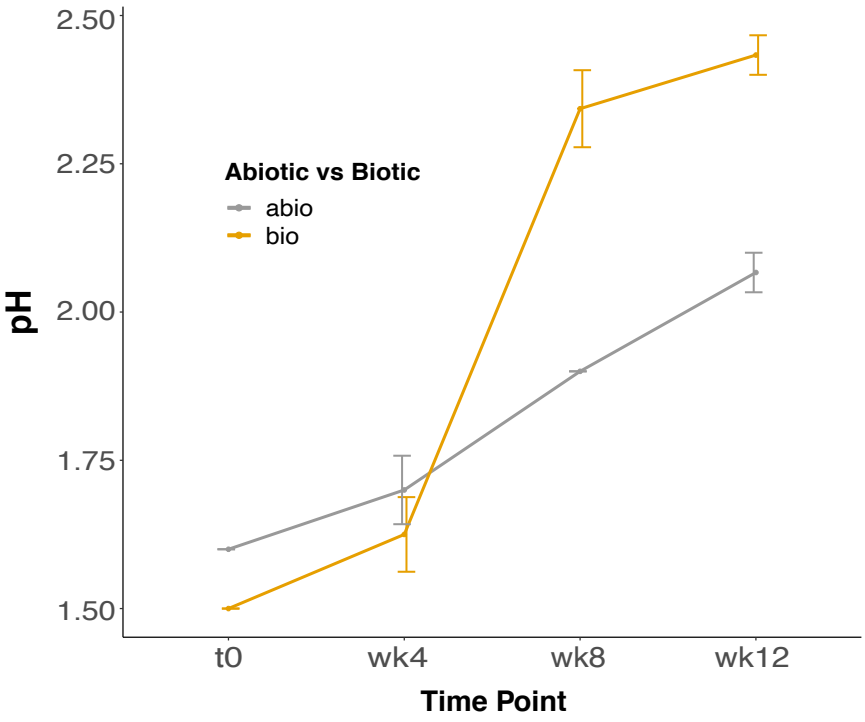

Figure 2.8 - mean pH values over time for biotic and abiotic $CuFeS_2$ samples. Error bars show standard error.

2.3.4 Establishing the Species of the SC3 Consortium Present during Chalcopyrite Bioleaching

In order to establish what roles are played by different consortium members during bioleaching, it was necessary to first verify the identity of the microbes present in the biotic samples. As detailed in Section 2.2.2, previous analyses had resolved 11 genomes from the SC3 consortium. To ensure the same strains were present and active during this chapter's experimental work, a combination of 16s rDNA sequencing and total RNA-seq transcript alignment was employed.

The results of 16s rDNA sequencing showed that all the families present in the SC3 consortium after 8 weeks' growth on chalcopyrite were in line with the species previously established via genome-resolved metagenomics (Fig 2.9).

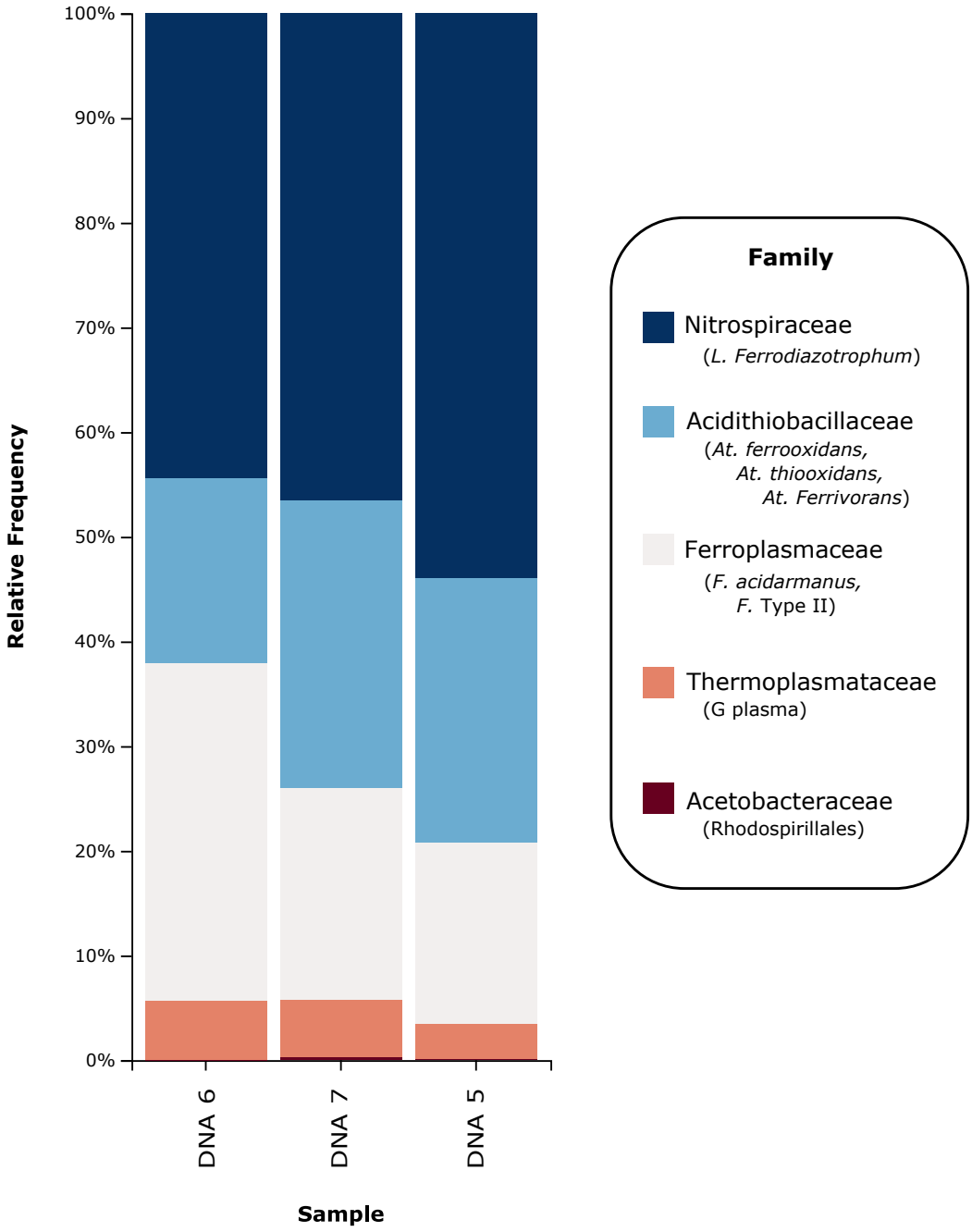

Figure 2.9 - Relative frequencies of microbial families in the SC3 consortium at 8 weeks' growth on chalcopyrite determined by 16s rRNA gene sequencing. Brackets show SC3 species that are within that family.

Total gene expression data was in broad agreement with these findings, with transcriptional data aligning to all expected species (Fig 2.10). This finding not only corroborates the presence of all expected species in the consortium, but also demonstrates that these taxa were actively transcribing genes when grown on chalcopyrite (*i.e.* all species were shown to be alive).

Total alignment of RNA-seq data can also function as a proxy for relative species abundance (Davids *et al.*, 2016; Marcelino *et al.*, 2019). It is notable, therefore, that Rhodospirillales is abundant in the RNA-seq data, whereas it was only found in one sample of the 16s rDNA data.

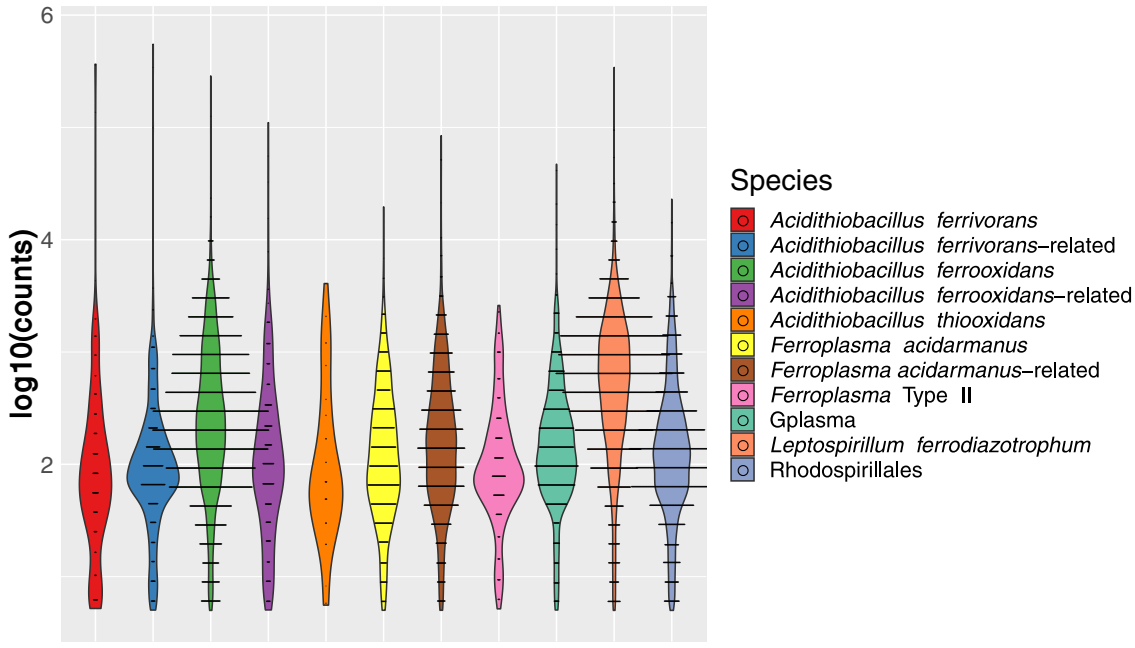

Figure 2.10 – violin plot of metatranscriptome RNA-seq counts per species. Wider lines indicate a greater number of genes expressed at that level, consequently wider lines at higher expression levels show a high level of reads aligned to this species' genome.

2.3.5 Genome Comparison of Unclassified SC3 Members to Known Genomes of Related Strains

To gain an understanding of the iron and sulfur oxidising metabolisms present within the SC3 consortium, it was important to first ascertain the identity of the

microbes. Although the previously described metagenomic work resolved the genome sequences of all the SC3 consortium members, two of the eleven strains within the SC3 consortium had not been assigned to known species. Instead, one of these strains had been solely labelled as potentially being a member of the Rhodospirillales order, and the other strain was dubbed as “G plasma” – an archaeal group known from culture-independent studies of the acidic environment at Iron Mountain and acidic cave sites (Bond, Druschel and Banfield, 2000; Jones, Schaperdoth and Macalady, 2014). In an attempt to identify their species, the genomes of these strains – G plasma and the Rhodospirillales strain - were compared to genomes available on the NCBI database.

Using Blast comparison of their protein sequences, it was established that the SC3 G plasma strain was highly similar to the two strains of *Cuniculiplasma divulgatum* available on the NCBI database, across the entire length of the genome. An extremely high percentage of sequence identity was observed for the 16s rRNA genes (>99.9%, Table 2.3). It is therefore probable that the SC3 G plasma constitutes a strain of *C. divulgatum.*

Table 2.3 – Blast results of G plasma genome against available genomes of *Cuniculiplasma divulgatum*

Strain	**Estimated genome size (bp)**	**Median percentage sequence identity (whole genome)**	**Percentage sequence identity (16s rRNA gene)**
SC3 G plasma	1,770,000		
Cuniculiplasma divulgatum strain S5	1,938,699	98.77%	99.93%
Cuniculiplasma divulgatum strain PM4	1,878,916	98.75%	99.93%

As the only Rhodospirillales family to appear in the results of the 16s rDNA analyses was the *Acetobacteraeceae*, it was concluded that the Rhodospirillales

strain in the SC3 consortium was likely a member of this family. This was in agreement with earlier conclusions by the Banfield group that this consortium member was potentially an *Acidisphaera* relative (Banfield, unpublished data). However, no significant similarities were found between the SC3 Rhodospirillales genome and any of the known *Acidisphaera* genomes available on NCBI. Therefore, it is possible that this genome represents a novel strain.

2.3.6 Identification of Genes of Interest within the SC3 Consortium Genomes

In Section 2.3.3, it was established that the presence of the SC3 consortium enhanced the breakdown of chalcopyrite. To understand more about *how* the SC3 consortium facilitates bioleaching, and consequently meet the research objectives of this work, genes of interest needed to be identified. Genes of interest were categorised as those associated with iron and sulfur oxidation, or those relevant to community functioning.

2.3.6.1 Genes Associated with Iron and Sulfur Metabolism

Iron and sulfur metabolism genes present within the SC3 consortium's genomes were identified using the Protein Blast bioinformatics tool. Figure 2.11, below, shows which putative sulfur metabolism genes were found to be present in the SC3 consortium and highlights the presence of novel genes. Further information, including Blast scores and references can be found in Appendix IV.

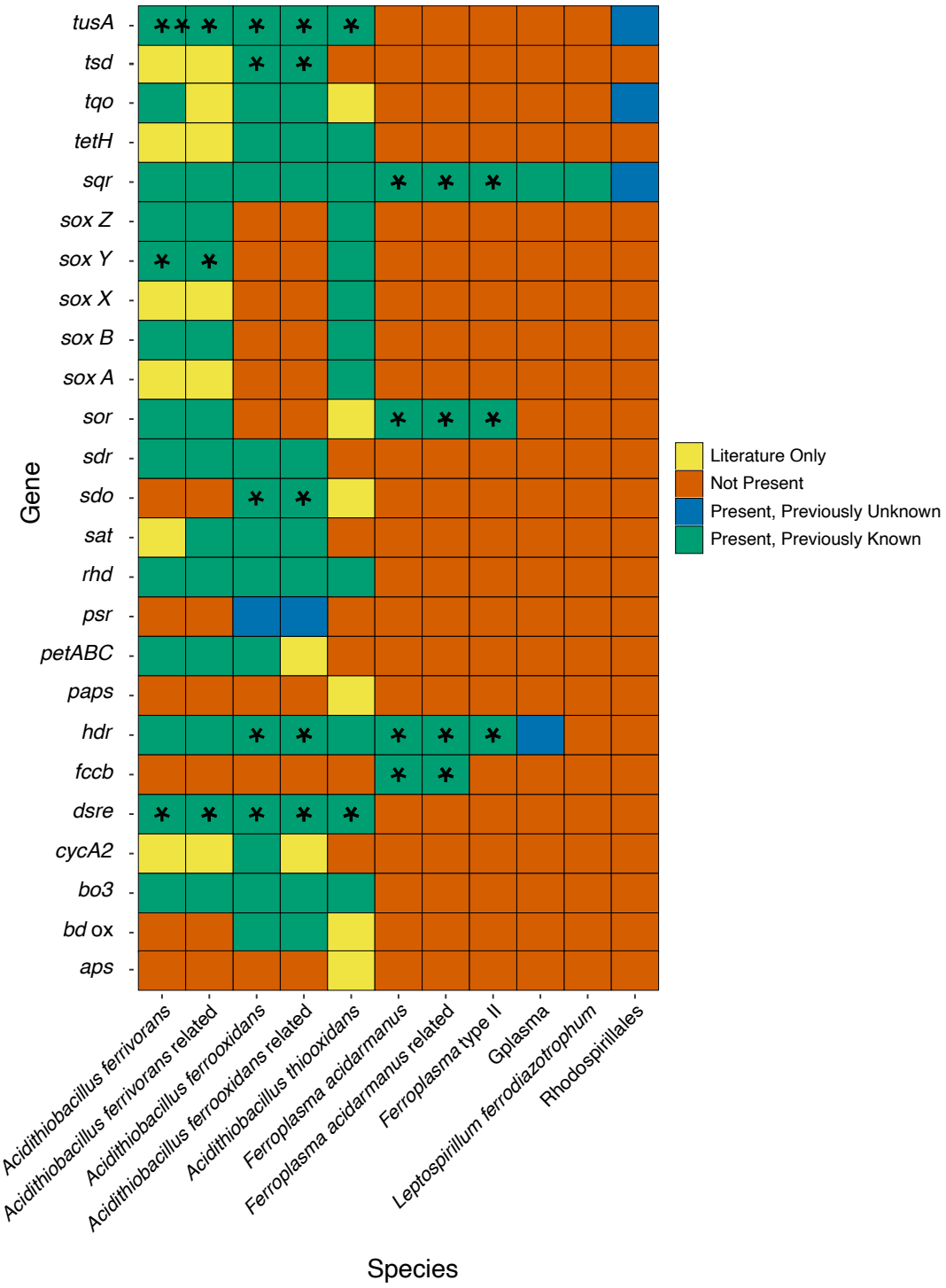

Figure 2.11 – Tile graph of proteins implicated in sulfur metabolism and associated electron transport chains, with colours indicating whether genes were found in species in the SC3 consortium, and whether they were previously known in this species. Asterisks indicate genes only confirmed by Protein Blast. aps: adenylylsulfate kinase paps: phosphoadenosine phosphosulfate reductase, psr: polysulfide reductase, sqr: sulfide-quinone reductase, fccb: flavocytochrome c sulfide dehydrogenase, sor: sulfur oxygenase reductase, sdo: sulfur

dioxygenase, hdr: heterodisulfide reductase, sat: sulfate adenylyltransferase, teth: tetrathionate hydrolase, tqo: thiosulfate-quinone oxidoreductase, tsd: thiosulfate dehydrogenase, sox: sulfur oxidation pathway

Of the sulfur oxidation genes known from the literature, only two genes were not present at all in the consortium - PAPS and APS. Notably, genes for the reduction of polysulfide, which is a key step in the dissolution of chalcopyrite were also found. These *psr* genes, were identified here for the first time in *At. ferrooxidans.* G plasma was found to possess an elemental sulfur oxidising *hdr* homologue, which was previously unknown in the literature. Comparably, the SC3 Rhodospirillales was found to possess homologues of *sqr, tqo* and the sulfur transferase *tusA,* all of which are unknown in *Acidisphaera spp. At. thiooxidans* had the most complete *sox* cluster in the consortium possessing *soxABXYZ,* while *At. ferrivorans* and its related strain had only *soxBYZ*. Some species were found to possess multiple copies of some genes. The *At. ferrooxidans* and related strain genomes included two *sqr,* and both *tsd*1 and t*sd*2 and five or six copies of the rhodanese transferase, respectively. *At. thiooxidans* contained four copies of *sqr* as previously reported for this species (Travisany *et al.*, 2014).

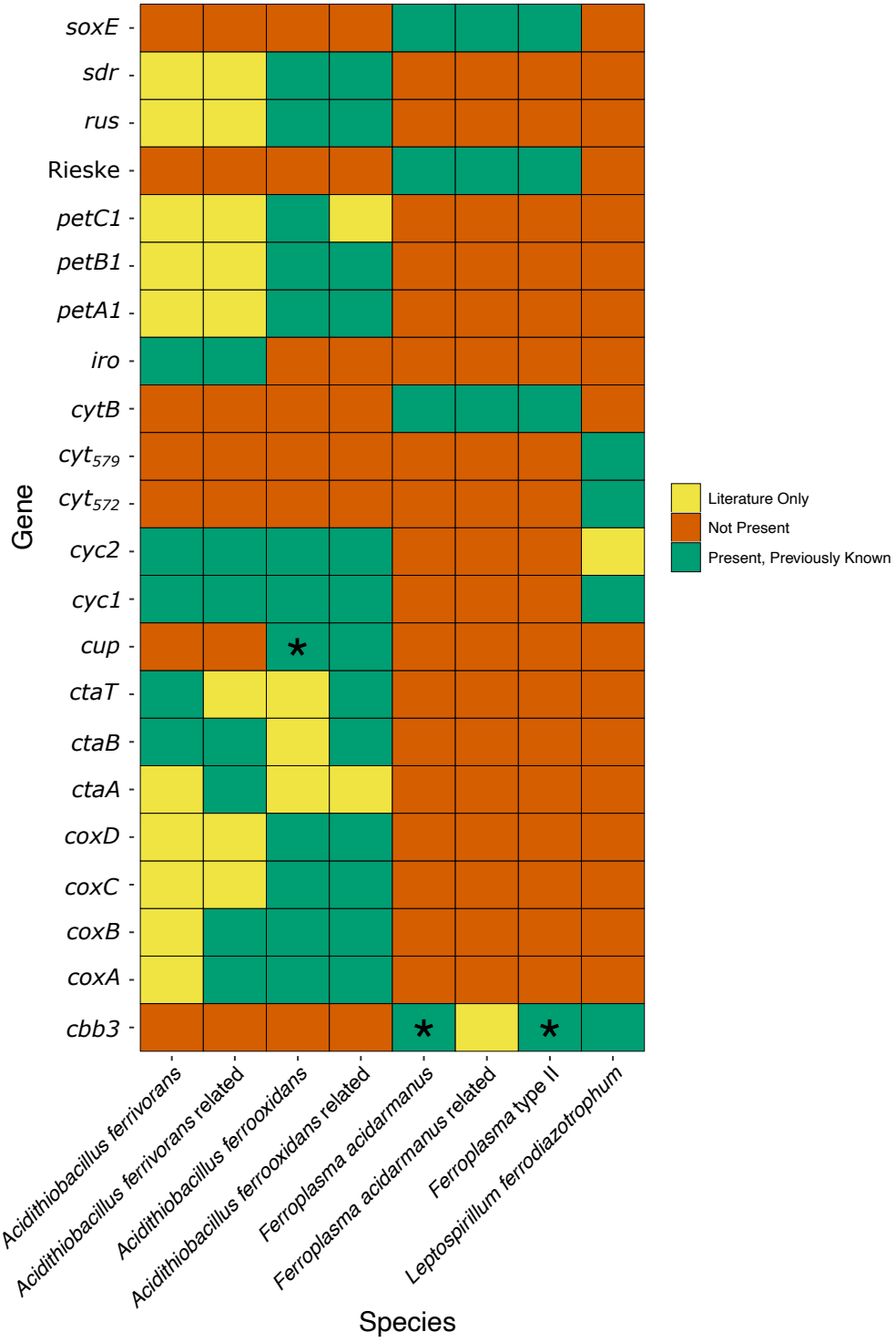

Figure 2.12 – Tile graph of proteins implicated in iron metabolism and associated electron transport chains, with colours indicating whether genes were found in species in the SC3 consortium. Asterisks indicate genes only confirmed by Blast. rus: rusticyanin, soxE: sulfocyanin, iro: high potential iron-sulfur protein, cyt_{572}: cytochrome 572.

Of the eleven species within the SC3 consortium, eight were found to possess genes for iron oxidation activity (Fig 2.12). This is in line with the species known to have confirmed iron metabolisms (Kelly and Wood, 2000; Dopson *et al.*, 2004). Genomes of G plasma, Rhodospirillales, and *At. thiooxidans* contained no iron oxidation genes, in line with what has previously been established for these species (Jones, Schaperdoth and Macalady, 2014; Golyshina *et al.*, 2016b). Notably, the *L. ferrodiazotrophum* genome was shown to include Cytochrome$_{579}$, thought to be involved in the electron transport chain during iron oxidation, the presence of which in the species had previously been the subject of debate (Levicán *et al.*, 2012).

2.3.6.2 Genes Associated with Nitrogen Fixation

Genes providing auxiliary information that could indicate how the consortium is functioning as a community were identified in the SC3 consortium's genomes. These included nitrogen fixation genes.

The nitrogen fixation related *nif* gene cluster (*nifHDKENX)* has previously been established in *L. ferrodiazotrophum*, *At. ferrooxidans*, and *At. ferrivorans* (Pretorius, Rawlings and Woods, 1986; Tyson *et al.*, 2005; Valdés *et al.*, 2008; Hallberg, González-Toril and Johnson, 2010). Genes from the cluster were found to be present in the genomes of these strains in the SC3 consortium (BLAST comparison scores can be found in Appendix IV). The complete cluster was found to be present in *L. ferrodiazotrophum, At. ferrooxidans* and the *At. ferrooxidans* related strain. In the *At. ferrivorans* and the *At. ferrivorans* related strain, the complete *nif* cluster was present, with the exception of the ferredoxins (*fer1,2*), of which, both are missing in the former, and *fer2* is absent in the latter genome.

2.3.7 RNA-seq Investigation of Gene Expression during SC3 Growth on Chalcopyrite

A metatranscriptomic study was conducted to examine the functional roles of SC3 consortium members during chalcopyrite bioleaching. RNA-seq was used to

capture which SC3 consortium genes were expressed after 8 weeks' growth. Genes were considered expressed if the number of transcript counts aligned to them was greater than 5.

2.3.7.1 RISC Metabolism Associated Gene Expression

The RNA transcript counts for RISC oxidation associated genes are presented below for bacteria and archaea in SC3 consortium (Fig 2.13). All species except *At. thiooxidans* were found to be expressing at least one gene associated with RISC oxidation, and at least one species was expressing every RISC gene identified in Section 2.3.7.1.

The sulfide oxidising *sqr* genes - present in all consortium members - were found to be expressed in 7 out of the 11 species, including both bacteria and archaea. Similarly, the sulfur oxidation gene, *hdr,* present in 9 species, was expressed by 6 consortium members. This gene was expressed by all archaea species, excluding G plasma, where expression below the threshold was found in one sample only.

The genes coding for an alternative elemental sulfur oxidation pathway of SOR were expressed by both *F. acidarmanus* strains. *At. ferrooxidans* was found to be expressing all sulfur metabolism genes and associated electron transport chains found in its genome, including all subunits of *bd* and bo_3 oxidases, two copies of *tsd*, *sqr* and four copies of *rhd*. With the exception of the *PetII* operon, and *bd* oxidase subunit II, the *At. ferrooxidans* related strain possesses all the RISC genes found in the confirmed strain of this species. However, notably fewer sulfur oxidation genes were expressed in the related strain, with only bd oxidase subunit I showing expression above the threshold. Sox genes were solely expressed in the *At. ferrivorans* related strain, where only *soxBYZ* is present.

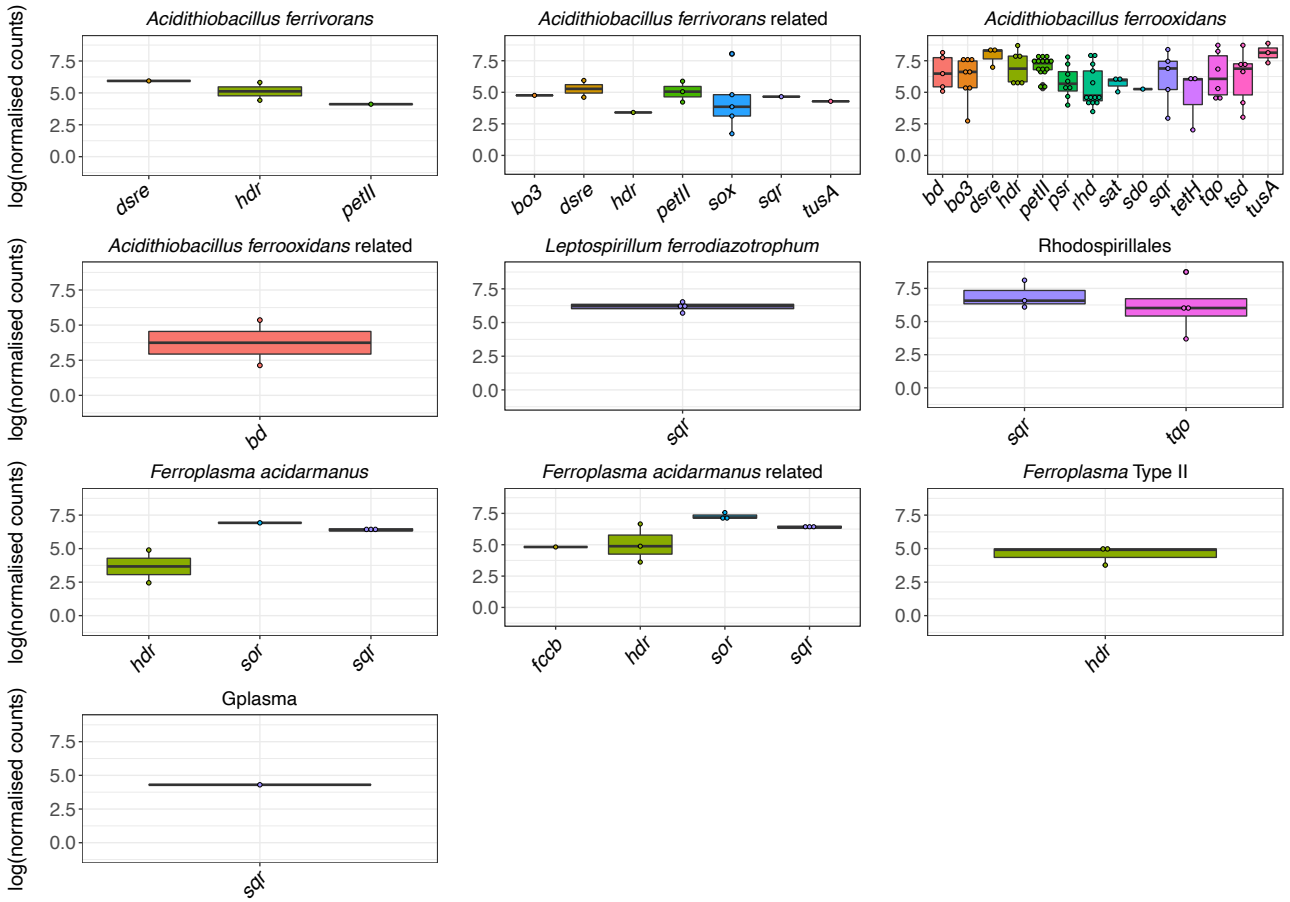

Figure 2.13 – Expression of known sulfur metabolism and associated electron transport chain genes in bacteria and archaea within the SC3 consortium, grown on chalcopyrite for 8 weeks. Normalisation was performed with Deseq2. PSR: polysulfide reductase, SQR: sulfide-quinone reductase, FCCB: Flavocytochrome c sulfide dehydrogenase, SOR: sulfur oxygenase reductase, SDO: sulfur dioxygenase, HDR: heterodisulfide reductase, SAT: sulfate adenylyltransferase, TetH: tetrathionate hydrolase, TQO: thiosulfate-quinone oxidoreductase, TSD: thiosulfate dehydrogenase, SOX: sulfur oxidation pathway.

2.3.7.2 Iron Metabolism Associated Gene Expression

The transcript counts for iron oxidation associated genes are presented in Fig 2.14. Similar to findings for RISC oxidation genes, *At. ferrooxidans* was found to express all identified genes associated with its iron oxidation pathway. In contrast, the *At. ferrooxidans* related strain did not express the rusticyanin responsible for the direct oxidation of iron, nor any of the associated genes for this pathway. Sulfocyanins were expressed in all *Ferroplasma spp.,* while the HIPIP encoded by *iro* - thought to be involved in an alternative iron oxidation pathway in this species - was expressed in *At. ferrivorans* related but not the confirmed strain.

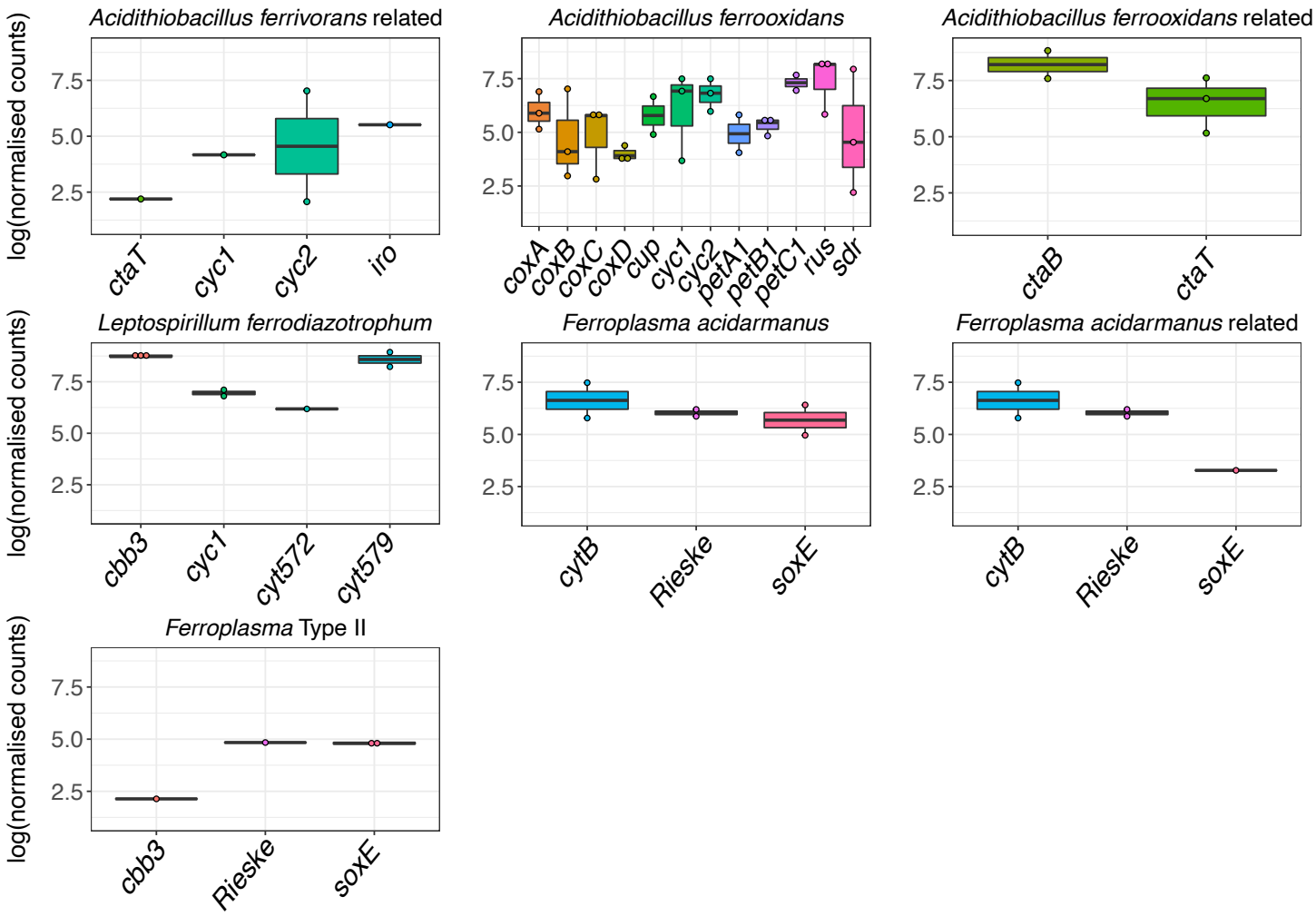

Figure 2.14 – Expression of putative iron oxidation genes and associated electron transport chain in the SC3 consortium, grown on chalcopyrite for 8 weeks. Normalisation was conducted with Deseq2.

RUS: rusticyanin, SoxE: Sulfocyanin, IRO: high potential iron-sulfur protein, Cyt_{572}: Cytochrome 572.

2.3.7.3 Expression of Genes Associated with Additional Metabolism Processes

2.3.7.3.1 Nitrogen Fixation Associated Gene Expression

In order to provide further insight into the functioning of the SC3 consortium during chalcopyrite dissolution, the expression of additional metabolism genes were also explored. The full gene cluster bar *nifX* was expressed in SC3's *L. ferrodiazotrophum.* In *At. ferrooxidans,* part of the *nif* gene cluster present in its genome (*nifDEKN)* was found to be expressed (Fig 2.15). However, no expression was found for any of the gene cluster in the *At. ferrooxidans* related species. Similarly, no expression was found for any of the *nif* cluster present in the *At. ferrivorans'* genome, nor in that of its related strain.

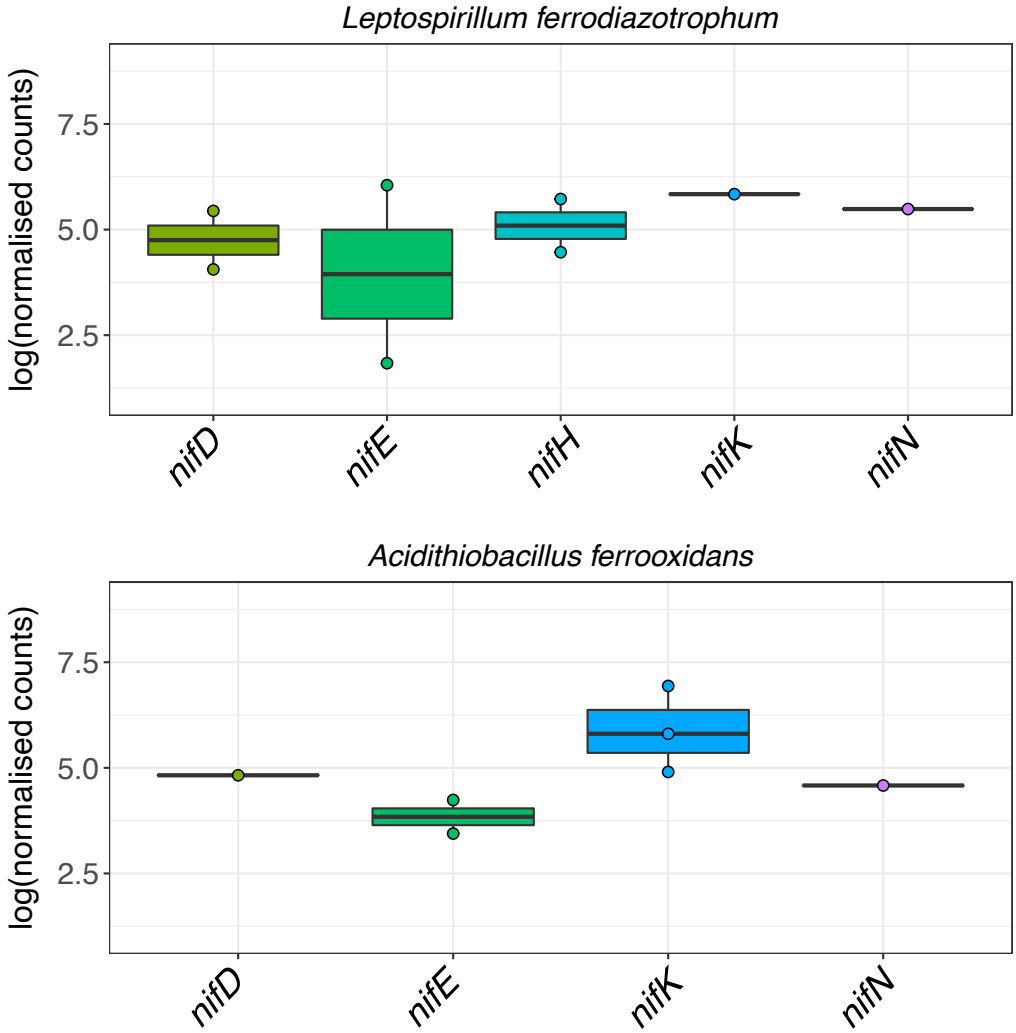

Figure 2.15 - Expression of genes in the nitrogen-fixation associated nif gene clusters of At. ferrooxidans and L. ferrodiazotrophum at 8 weeks growth on chalcopyrite. Normalisation was conducted with Deseq2.

2.3.7.3.2 Carbon Metabolism Associated Gene Expression

In earlier work conducted by Dr. T. Osborne, genes for carbon fixation were identified (unpublished data), and expression of these genes was explored in the present work. Genes for the Calvin Cycle CO_2 fixing enzyme, ribulose-1,5-bisphosphate carboxylase/oxygenase (EC 4.1.1.39, Rubisco) were found in all *Acidithiobacilli* as well as Rhodospirillales, but expression of these genes was only found for *At. ferrooxidans, At. ferrivorans* and their related strains (Fig. 2.16). Genes associated with the chimaeric CO_2 fixation pathway (Cárdenas *et al.*, 2009), which partially consists of proteins from Ljungdahl–

Wood pathway and some steps associated with the serine cycle, were expressed by all *Ferroplasma spp.* in the consortium.

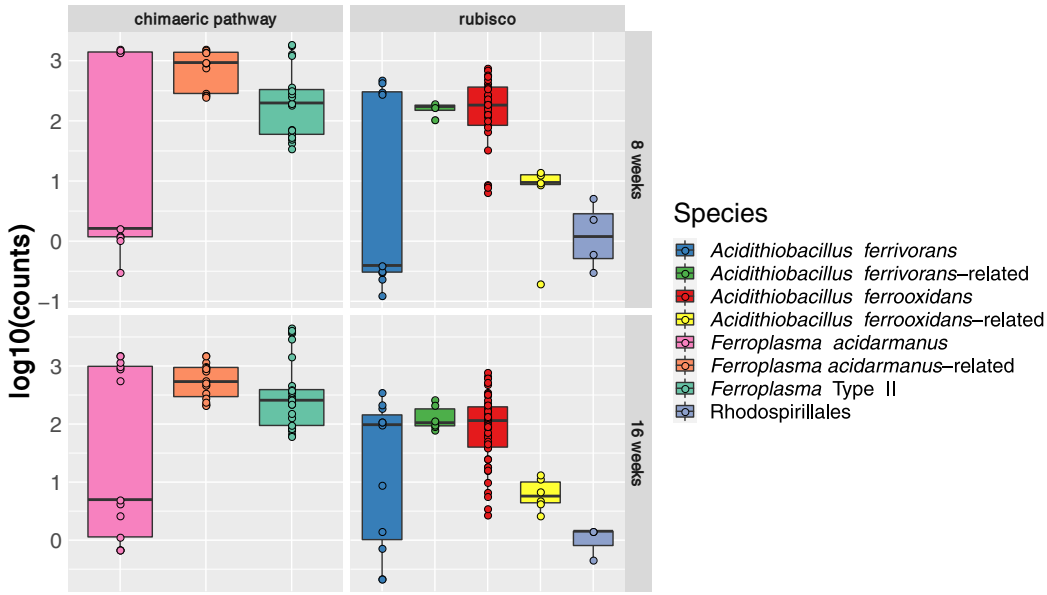

Figure 2.16 - Expression of genes associated with carbon fixation in SC3 consortium at 8 weeks' growth on chalcopyrite

2.3.8 Model of Chalcopyrite Dissolution by SC3 Consortium

The results given in Sections 2.3.1-2.3.7 established that chalcopyrite breakdown was greater in the presence of the typical bioleaching consortium dubbed "SC3". The strains present in the SC3 bioleaching consortium were identified, and the expression of genes associated with iron and sulfur metabolism within the consortium was analysed. These results were linked together to create an integrated model of chalcopyrite dissolution by the SC3 consortium (Figure 2.17).

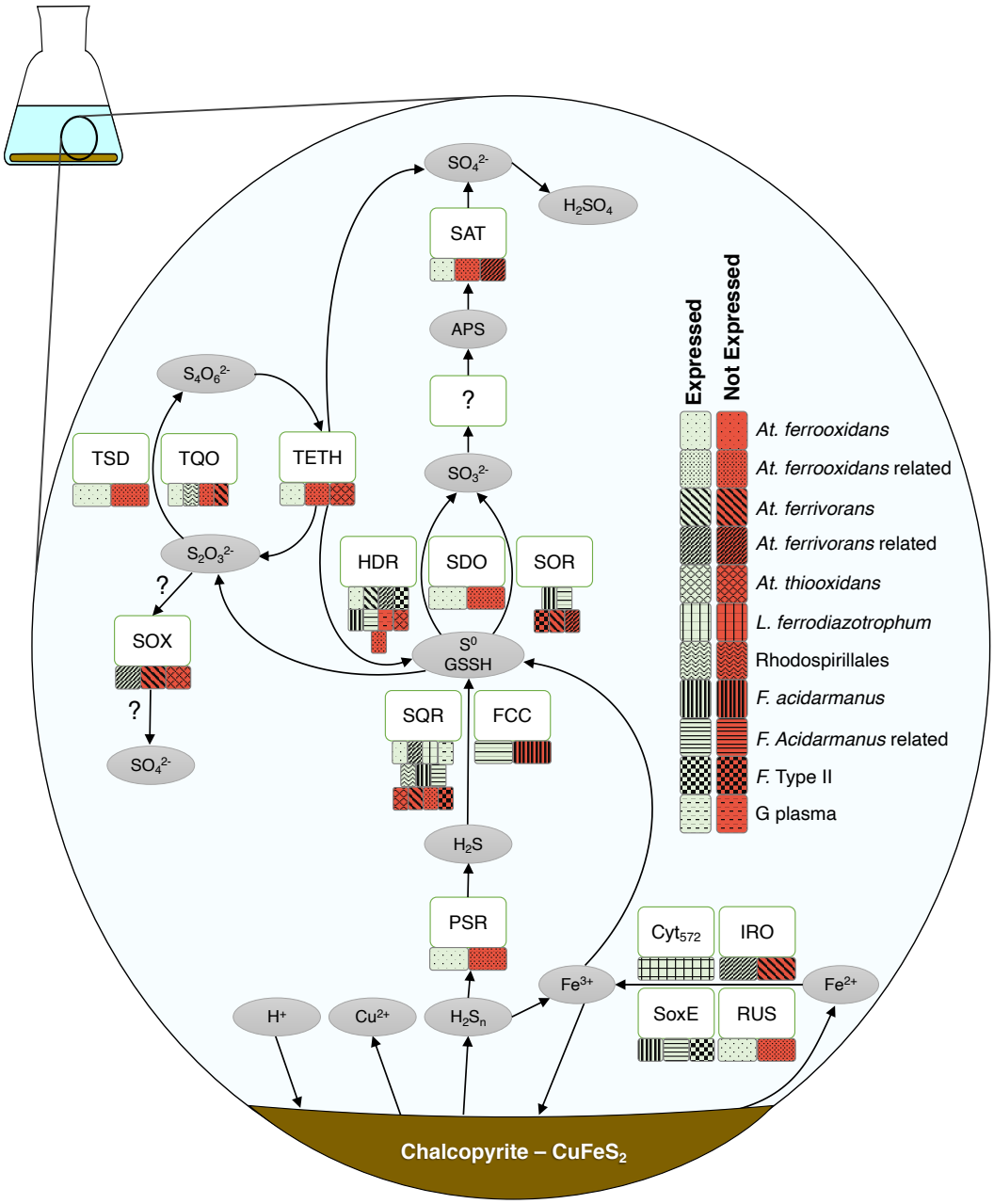

Figure 2.17 – Model of the proposed mechanism of chalcopyrite dissolution by the SC3 consortium. Patterns indicate whether the gene was found in the SC3 consortium, pale green indicates expression at 8 weeks' growth, orange indicates no expression found. PSR: polysulfide reductase, SQR: sulfide-quinone reductase, FCC: Flavocytochrome c sulfide dehydrogenase, SOR: sulfur oxygenase reductase, SDO: sulfur dioxygenase, HDR: heterodisulfide reductase, SAT: sulfate adenylyltransferase, TetH: tetrathionate hydrolase, TQO: thiosulfate-quinone oxidoreductase, TSD: thiosulfate dehydrogenase, SOX: sulfur oxidation pathway, RUS: rusticyanin, SoxE: Sulfocyanin, IRO: high potential iron-sulfur protein, Cyt_{572}: Cytochrome 572.

As chalcopyrite dissolution follows the polysulfide pathway, breakdown in acid conditions is initiated by proton attack, facilitating the release of sulfur and ferrous iron by cleaving metals away from the sulfur moiety. Copper, which exists as Cu^{+} within chalcopyrite is readily oxidised to Cu^{2+} when exposed to ferric iron in acidic aqueous conditions (Kimball, Rimstidt and Brantley, 2010). Iron is then oxidised to ferric iron by *At. ferrooxidans, the At. ferrivorans related strain, Ferroplasma spp.* and *L. ferrodiazotrophum.* As ferric iron is present, the released sulfur is in the form of a sulfide ion, which spontaneously dimerises to hydrogen disulfide (H_2S_2). Ferric iron can oxidise this hydrogen disulfide via intermediate polysulfides to elemental sulfur, or this conversion may occur enzymatically. Where this step is microbially mediated, it occurs in a stepwise manner. The *At. ferrooxidans* PSR catalyses the first step to hydrogen sulfide, which is then oxidised to elemental sulfur via the SQR expressed by seven members of the consortium (and possessed by all SC3 members), or the FCC expressed by the *F. acidarmanus* related strain. From this stage, elemental sulfur may continue along the pathway of sequential oxidation and be converted to glutathionate persulfide (GSSH) then oxidised to sulfite by HDR, as expressed by six SC3 members, *At. ferrooxidans'* SDO and the SOR expressed by *F. acidarmanus* and its related species. Alternatively, elemental sulfur may be converted to thiosulfate abiotically or by SOR (Ghosh and Dam, 2009). Thiosulfate is oxidised to tetrathionate via TQO (*At. ferrooxidans* and Rhodospirillales) and TSD (*At. ferrooxidans*). TETH can disproportionate tetrathionate to thiosulfate, elemental sulfur and sulfate. Thiosulfate may also chemically decompose to tetrathionate, sulfur or sulfite (Mizoguchi, Takei and Okabe, 1976). It is unclear whether SOX is playing a role in the SC3 consortium, as the only SOX genes expressed were *soxBYZ* in the *At. ferrivorans* related strain. It has previously been concluded that due to the incomplete *sox* cluster, TQO is the most likely pathway for oxidation in *At. ferrivorans* (Christel, Fridlund, Watkin, *et al.*, 2016). The mechanism of sulfite oxidation remains elusive, however the subsequent stage of APS oxidation to sulfate may be facilitated by *At. ferrooxidans'* SAT. Finally, as sulfate forms sulfuric acid when dissolved in water, protons are regenerated to serve as an oxidant by which

chalcopyrite is further broken down, aided by the ferric iron regenerated by the iron oxidising members of the consortium.

2.3.9 Results Summary

This chapter's experimental work improved the understanding of chalcopyrite breakdown by the naturally occurring SC3 consortium:

- Geochemical information confirmed that the overall breakdown of chalcopyrite was significantly greater in the biotic versus abiotic samples, indicating that the SC3 consortium has the capacity for use in copper bioleaching.
- The presence of genes that facilitate bioleaching (sulfur and iron oxidation) was shown in every consortium member, highlighting the potential of all consortium members for direct contribution to the bioleaching process.
- A model was created using metatranscriptomics data to show the overall metabolic pathways of sulfur and iron oxidation, demonstrating the bioleaching capacity of the consortium.

2.4 Discussion

2.4.1 The Bioleaching Potential of the SC3 Consortium

This study is the first to evaluate the bioleaching potential of the SC3 consortium. Geochemical analyses quantified the SC3 consortium's effect on chalcopyrite breakdown, compared to abiotic controls. Significant differences between biotic and abiotic samples were seen in the ICP-OES data, suggesting the SC3 consortium enhanced chalcopyrite breakdown. This is consistent with innumerate previous studies of acidophiles, especially mixed cultures, and their effect on chalcopyrite breakdown through the provision of oxidants (Qiu *et al.*, 2005b; Qiu, Xiong and Zhang, 2006; Akcil, Ciftci and Deveci, 2007; Zhang *et al.*, 2008; Ma *et al.*, 2017).

Contrary to some previous studies (Ma *et al.*, 2019), pH increased in both the biotic and abiotic samples over time. Although sulfide mineral dissolution is facilitated by the protons supplied by sulfur oxidation, this process does not continue uninhibited in bioleaching systems. In reality, the sulfide mineral dissolution process is a balance between acid-producing and acid-consuming reactions (Plumb, Muddle and Franzmann, 2008). In the case of chalcopyrite, an acid-soluble mineral, protons are consumed during its initial breakdown (Vilcáez and Inoue, 2009). Further, additional protons are consumed during iron oxidation (Eq. 2.7, Smith, Luthy and Middleton, 1988; Ojumu *et al.*, 2006), a process that is accelerated in the presence of iron oxidising microbes.

$$4\ Fe^{2+} + 4\ H^{+} + O_2 \rightarrow 4\ Fe^{3+} + 2\ H_2O \qquad \text{(Eq. 2.7)}$$

Greater pH increases were seen in biotic compared to abiotic samples, where the ICP-OES results indicated greater dissolution was also occurring. Therefore, the pH increase seen is indicative of processes associated with mineral breakdown, as opposed to barriers to breakdown. This finding is consistent with previous studies (*e.g.* He *et al.*, 2012). Indeed, at all times, the pH remained <3, the point at which proton concentration is sufficiently high to maintain effective bioleaching (Plumb, Muddle and Franzmann, 2008).

Overall, it can be concluded from the geochemical findings that the SC3 consortium enhances chalcopyrite breakdown. To understand exactly *how* the consortium is facilitating this, the genomes of the consortium must be discussed.

2.4.2 The Bioleaching Mechanisms of the SC3 Consortium

Microbial chalcopyrite breakdown requires microbes to possess sulfur and iron oxidation capabilities. Accordingly, sulfur oxidation associated genes were found in every genome of the SC3 consortium, and 9 of the species

expressed at least one of these genes. Additionally, iron oxidation genes were present in 8 of the SC3 species, and their expression was seen in more than half of the consortium members. Genes coding for all four of the iron-oxidation enzymes found in the SC3 metagenome were expressed during bioleaching: Cytochrome$_{572,}$ the *iro* high potential iron-sulfur protein, sulfocyanin and rusticyanin. These findings are consistent with the geochemical data, providing a potential mechanism underpinning the observed increase in chalcopyrite breakdown.

The metagenomic and metatranscriptomic data was integrated into a complete model of bioleaching, which confirmed that the overall chalcopyrite dissolution mechanism by the SC3 consortium fits the polysulfide pathway, as described previously (Schippers and Sand, 1999). This pathway is driven by a complex series of RISC oxidising enzymes. The final stage of this multi-step sulfur oxidation pathway has remained enigmatic for many bioleaching organisms. Previous studies have proposed enzymes that facilitate this step in some organisms. For example, PAPS and APS were hypothesised to form an alternate sulfite oxidation pathway in *At. thiooxidans* (Yin *et al.*, 2014; Camacho *et al.*, 2020). However, in the SC3 consortium, *At. thiooxidans* did not possess genes for the (P)APS pathway. Similarly, the multi-enzyme SOX system has been shown in bioleaching organisms to oxidise a range of RISCs, including sulfite (Yin *et al.*, 2014). However, in the SC3 consortium only *At. thiooxidans* was found to feature the full *soxABXYZ,* with no expression seen. Similarly, *At. ferrivorans* and its related strain were found to possess only *soxBYZ,* and these genes were only found to be expressed by the *At. ferrivorans* related strain. Indeed, oxidation of thiosulfate via TQO has previously been suggested to be the most likely pathway of RISC oxidation in this species (Christel, Fridlund, Buetti-Dinh, *et al.*, 2016). Overall, as no enzyme is apparent in any of the SC3 consortium genomes accounting for the oxidation of sulfite to APS, it is possible that thiosulfate cycling and tetrathionate disproportionation via TQO-TETH is the predominant pathway of RISC oxidation during bioleaching.

As well as clarifying the overall pathways of chalcopyrite dissolution, the integrated model demonstrated for the first time how different organisms within a typical bioleaching consortium fit together to facilitate the breakdown pathway. Notably, all the SC3 organisms were shown to be able to play a role in chalcopyrite bioleaching, including species for which bioleaching capabilities were previously unconfirmed. For example, the previous evidence for sulfur oxidation in G plasma was extremely limited. Jones *et al.* (2014), reported the presence of a gene for the sulfide oxidising enzyme *sqr,* however, these authors did not examine expression. This thesis demonstrated that the G plasma *sqr* gene is being expressed when the consortium is grown on chalcopyrite, concomitantly presenting the first evidence of sulfur oxidation gene expression in this archaeon. Potentially, this could suggest that this organoheterotrophic species (Golyshina *et al.*, 2016b) possesses some mixotrophic abilities.

Similarly, this study demonstrated sulfur oxidation potential in the SC3 Rhodospirillales species. The 16s rDNA gene sequencing indicated that the Rhodospirillales was likely an *Acetobacteraceae*. The *Acetobacteraceae* family have not previously been notably associated with sulfur cycling (Whaley-Martin *et al.*, 2019). However, in the SC3 Rhodospirillales genome, homologues of RISC oxidation associated genes were found to be present and expressed (*sqr* and *tqo*). This finding could indicate that the SC3 Rhodospiralles represents a novel *Acetobacteraceae* species, notably possessing the capacity to oxidise thiosulfate and sulfide.

Beyond highlighting the potential roles of species not previously linked to bioleaching, the research in this chapter also found novel sulfur oxidation genes in key bioleaching species, filling some long-standing gaps in the understanding of chalcopyrite breakdown. The first microbially driven step in the chalcopyrite breakdown pathway is the conversion of polysulfide to sulfide. Although this is an integral step to the entire breakdown process, the genes facilitating this step were previously unknown in the large majority of acidophiles, including the highly-studied *At. ferrooxidans.* This study resolved

this gap, by demonstrating the presence and expression of all sub-units of a polysulfide reductase homologue (*psrABC*) in this species. The *psr* genes have been demonstrated to facilitate the reduction of polysulfide coupled to the oxidation of hydrogen in *Wolinella succinogenes,* and quinone in sulfur-vent extremophiles (Jankielewicz *et al.*, 1994). By demonstrating the presence and expression of *psr* in *At. ferrooxidans*, this study has provided the first molecular evidence that this organism has the capability to facilitate sulfur oxidation from polysulfide all the way through to sulfite.

This chapter's experimental work also provided clarity to a debate regarding the iron oxidation mechanism of *L. ferrodiazotrophum.* Previous evidence for the periplasmic cyt_{579} thought to be involved in electron transport during iron oxidation in this species was relatively weak. It was initially detected in an environmental metagenome from sequence reads associated with *L. ferrodiazotrophum,* but not brought into the genome (Aliaga Goltsman *et al.*, 2009), while Levicán *et al.* (2012) found no copies of Cyt_{579} in the *L. ferrodiazotrophum* genome. Conversely, the SC3 consortium possessed and was expressing $cyt_{579,}$ providing a more complete picture of the iron oxidation mechanism in this species. Comparably, the consortium's *Ferroplasma spp.* were all found to possess and be expressing genes for the iron oxidising sulfocyanin, corroborating the sparse previous findings for *F. acidarmanus,* and providing new information about the poorly documented *F.* type II (Dopson *et al.*, 2004; Castelle *et al.*, 2015).

2.4.3 Metatranscriptomic Insights in SC3 Community Functioning

Species within microbial communities are highly dependent on one another for resources that allow them to survive and, in turn, facilitate processes such as bioleaching. This is especially true on the inherently nutrient poor surface of bioleaching ore; the low availability of organic matter and fixed nitrogen in this environment suggests that bioleaching consortia necessarily include autotrophs and diazotrophs capable of fixing carbon and nitrogen (Cárdenas, Quatrini and Holmes, 2016). Indeed, the molecular data collected in this

chapter revealed several SC3 species capable of fixing these essential macronutrients.

The *nif* operon genes are expressed in certain microbes in response to low fixed nitrogen concentrations. Two SC3 species were shown to possess and express genes from the *nif* operon: *At ferrooxidans* and *L. ferrodiazotrophum,* in line with previous findings for these species (Mackintosh, 1978; Norris, Colin Murrell and Hinson, 1995; Aliaga Goltsman *et al.*, 2009). *L. ferrodiazotrophum* has been dubbed a "keystone species" in acid mine and cave environments due to its ability to fix nitrogen at very low pH (Tyson *et al.*, 2004, 2005; Ram *et al.*, 2005). In fact, *L. ferrodiazotrophum* is the strain within the SC3 consortium found to be expressing the most complete *nif* operon, suggesting this organism could be playing a prominent role in SC3 community functioning through the provision of fixed nitrogen. This is a noteworthy prospect, as this species is not typically present in commercial bioleaching consortia, yet has been demonstrated in this study to be capable of contributing directly (S + Fe oxidation) and indirectly (N fixation).

The limited number of species within the consortium capable of nitrogen fixation highlights the reliance of consortium members to function as a whole. Another regard in which the consortium members may be interdependent is the provision of another macronutrient – carbon. Many species within the consortium were shown in the metatranscriptomic data to possess carbon fixation pathways, however, no carbon fixation pathways are found in G plasma and it is unclear exactly how this heterotroph is obtaining sufficient carbon to be present in observable quantities. It has previously been suggested that heterotrophs can metabolise organic substrates that could inhibit autotrophs during bioleaching (Bacelar-Nicolau and Johnson, 1999; Méndez-García *et al.*, 2015). It is possible, therefore, that a symbiotic relationship exists whereby G plasma receives fixed carbon via organic substrates produced by autotrophs, simultaneously aiding the autotrophs of the SC3 consortium by preventing the accumulation of inhibitors.

Overall, all members of the SC3 consortium were capable of contributing to chalcopyrite bioleaching, but only certain species can bring essential fixed carbon and nitrogen into the bioleaching environment. Without these organisms contributing essential nitrogen and carbon, microbial growth might be limited and bioleaching processes could be slowed (Levicán *et al.*, 2008).

2.4.4 Limitations

In this study, 16s rDNA sequencing was used to confirm the identities of the species present in the SC3 consortium. This technique remains widely used for microbial community profiling, as it is relatively simple, accessible and cost effective. Despite this, a number of limitations of 16s sequencing have been noted, including primer selection and PCR biases (Acinas *et al.*, 2005; Brooks *et al.*, 2015). For example, through its simplicity, 16s rDNA sequencing necessarily lacks much of the information that can be garnered from other metagenomic techniques. Additionally, the interpretation of 16s results can vary based on the bioinformatic pipeline used, although there is a greater degree of agreement between pipelines at higher taxonomic levels (Straub *et al.*, 2019). Indeed, in this chapter, the 16s rDNA results were resolved to a relatively high taxonomic level (Family), which was sufficient, when combined with RNA-seq data, for confirming the presence of expected species. However, there were some notable contrasts between the 16s rDNA sequencing findings, and the RNA-seq data. For example, the 16s rDNA sequencing data suggested that the Rhodospirillales family, *Acetobacteraceae,* was only found in one sample at a very low frequency. However, the converse picture can be seen from the RNA-seq data, where a large number of reads aligned to the genome. This discrepancy is likely attributable to 16s rDNA PCR bias (Poretsky *et al.*, 2014; Brooks *et al.*, 2015).

Overall, the 16s rDNA sequencing in this chapter helped to confirm that the RNA-seq data can be used to confirm species identities. This finding, combined with the lower accuracy of 16s rDNA sequencing for some of the

species, meant that 16s rDNA sequencing was not carried out for further studies in this thesis.

2.4.5 Conclusion

The results of this study established the copper bioleaching potential of the SC3 consortium through both geochemical and molecular data. Geochemical data showed that chalcopyrite breakdown was significantly greater in the presence of the SC3 bioleaching consortium (H_1). Similarly, metagenomic and metatranscriptomic work found novel genes associated with bioleaching within the SC3 consortium genomes (H_2), and that genes associated with sulfur and iron oxidation were expressed when the consortium was grown on chalcopyrite (H_3).

The experimental findings of this chapter represent the first metatranscriptomic study of sulfur and iron metabolism genes in a naturally occurring acidophilic bioleaching consortium. Focussing on a naturally occurring consortium offered the opportunity to examine the dissolution mechanisms occurring in acidic environments, while simultaneously filling gaps in our understanding of the sulfur and iron oxidation mechanisms of some very commonly used bioleaching organisms.

The meta-omic approach taken provided integrated information about the organisms in the consortium, without which it could not have been established that all species were capable of playing a role in bioleaching. Additionally, utilising a meta-omics approach can help us discover the potential of species not commonly used in bioleaching, as was demonstrated for *L. ferrodiazotrophum* in this chapter. Equally, by capturing information about auxiliary processes carried out at the same time as bioleaching, *e.g.* nitrogen and carbon fixation, the meta-omics approach allows us to consider how species can contribute indirectly to the consortium's overall ability to bioleach. Practitioners looking to optimise bioleaching consortia should take into consideration this holistic view of microbial capabilities when selecting

species in order to avoid unnecessary limitations on microbial growth and, in turn, enhance bioleaching efficacy.

The overall implication of this chapter's research is that the SC3 consortium enhances chalcopyrite breakdown, via mechanisms that are now better understood. This finding was an important baseline, establishing the mechanism by which copper can be removed from a pure mineral. However, real-world bioleaching scenarios often involve low-grade ore of mixed mineral assemblages. Whether the community functioning and mechanism of breakdown would be the same under these conditions is not yet known. Therefore, it is vital that the functioning of the consortium when grown on a low-grade ore is tested, to provide a clear view of how it would function in a practical application.

Chapter 3 - Metatranscriptomic Analysis of Low-grade Copper Ore Bioleaching

3.1 Introduction

3.1.1 General Introduction

In the previous chapter, bioleaching of very pure, laboratory grade chalcopyrite was studied. Indeed, a large proportion of copper bioleaching studies use chalcopyrite as the mineral substrate (*e.g.* Ahmadi *et al.*, 2010; Behrad Vakylabad, 2011; Ma *et al.*, 2019; Peng *et al.*, 2021). These high-grade chalcopyrite studies are important in providing a clear characterisation of the breakdown of an economically important mineral. It is equally imperative, however, that these studies are built upon with studies that more closely reflect "real-world" sulfide dissolution scenarios. In practice, the ore exploited for copper extraction is rarely pure chalcopyrite, and bioleaching is commonly employed to improve the economic viability of low-grade ores that would otherwise be discarded as waste products (Jia *et al.*, 2019). Exploitation of this type of ore is likely to increase in the following decades as demand for copper increases worldwide (Elshkaki *et al.*, 2016). Studying the breakdown of low-grade ore can therefore provide information that could optimise leaching of similar ores, and additionally, inform remediation plans to reduce the dissolution and subsequent pollution caused by waste sulfide mineral breakdown in spoil heaps (Johnson and Hallberg, 2005; Wu *et al.*, 2009, 2016). As demonstrated in Chapter 2, metatranscriptomic data can help elucidate which sulfur and iron oxidation genes are active during sulfide mineral bioleaching. In turn this can help us determine the mechanism of mineral dissolution by a bioleaching consortium. However, to date, there are no studies using metatranscriptomics to explore the breakdown of a low-grade ore by a native microbial community. In this chapter, gene expression data is used to develop a model of Phoukassa low-grade

copper ore dissolution by the native SC3 microbial consortium. This work represents the first metatranscriptomic study of copper ore dissolution by microbes naturally present in the ore's environment.

3.1.2 Low-Grade Copper Ore Mineralogy

Low-grade (*i.e.* low metal percentage, mixed mineral) copper ores are often the material targeted by bioleaching operations (Watling *et al.*, 2014). Low-grade ores can have various mineralogical compositions, and as each type of sulfide mineral breaks down in a different manner, the mineralogical composition of low grade ore has a bearing on its bioleaching mechanism (Olubambi *et al.*, 2007; Plumb, McSweeney and Franzmann, 2008).

Low-grade copper ores are predominantly comprised of sulfide minerals such as: pyrite, chalcopyrite, covellite, magnetite, muscovite, sphalerite, siderite, chlorite, galena; gangue materials are commonly quartz and feldspar (Singh, Sukla and Mishra, 2011; Watling *et al.*, 2014). Less commonly, they may also include copper oxides and carbonates (Bogdanovic *et al.*, 2016).

Previous analyses have shown the Phoukassa ore used in this chapter to be comprised predominantly of pyrite (Hudson-Edwards *et al.* unpublished data), with minor inclusions of chalcopyrite and other copper sulfides, and trace amounts of lattice-bound Cu within the pyrite itself. The mineralogy of this ore is typical of the low-grade material commonly discarded as waste at mining sites, where their breakdown presents an environmental hazard. Understanding the breakdown process of the Phoukassa ore could help improve the recovery of copper from similar low-grade ores, facilitating the removal of an environmental hazard by creating an economic opportunity. To date, however, there have been no studies examining the microbial breakdown of the Phoukassa ore.

3.1.3 Pyrite Dissolution

As the primary component of the Phoukassa ore is pyrite, the mechanism of pyrite dissolution is a key component of understanding Phoukassa ore breakdown. Pyrite is one of the most well studied sulfide minerals in terms of its dissolution, as a result of its environmental abundance and key role in the generation of acid mine drainage (Johnson and Hallberg, 2005).

Pyrite oxidation occurs when the mineral is exposed to oxygen and water, often as a result of human interventions, such as mining. The overall reactions for pyrite dissolution via dissolved oxygen and ferric iron are shown by Eq. 3.1 and Eq. 3.2, respectively (Moses *et al.*, 1987). The Fe^{2+} from dissolved oxygen oxidation can then be further oxidised to ferric iron via the equation 3.3 (Moses and Herman, 1991).

$$FeS_2 + 7/2O_2 + H_2O \rightarrow Fe^{2+} + 2SO_4^{2-} + 2H^+ \qquad \text{Eq. 3.1}$$

$$FeS_2 + 14Fe^{3+} + 8H_2O \rightarrow 15Fe^{2+} + 2SO_4^{2-} + 16H^+ \qquad \text{Eq. 3.2}$$

$$Fe^{2+} + 1/4O_2 + H^+ \rightarrow Fe^{3+} + 1/2H_2O \qquad \text{Eq. 3.3}$$

Although abiotic dissolution is possible via the mechanism above, dissolution is significantly enhanced in the presence of microorganisms (Yahya and Johnson, 2002). As pyrite is not acid soluble, biological dissolution of pyrite proceeds via the thiosulfate pathway, as described in Section 1.5.1 of this thesis. Overall, it is well established that sulfur and iron oxidising microbes facilitate pyrite dissolution by providing oxidants, and by preventing the build-up of ferrous iron and elemental sulfur that might otherwise accumulate on the surface of the pyrite and form a barrier to breakdown (Schippers, Rohwerder and Sand, 1999; Rodríguez *et al.*, 2003b). However, the underlying mechanisms of pyrite breakdown by

microbes are not yet fully elucidated, and its breakdown as part of the Phoukassa ore is yet to be studied.

3.1.4 Formation of Hypotheses

It was demonstrated in Chapter 2 that sulfide mineral breakdown increased in the presence of the SC3 consortium, in line with previous research on bioleaching with sulfur and iron oxidising acidophiles (Section 1.5). Additionally, the SC3 consortium were shown to possess metabolic genes relevant to the breakdown of sulfide minerals. These genes were shown to be expressed, and therefore active, during the breakdown of chalcopyrite. Gene expression levels in microbes fluctuate over time in response to environmental stimuli (Moreno-Paz *et al.*, 2010; Bunse *et al.*, 2016; Mahto, Kumari and Das, 2021). The increasing presence of iron and sulfur during the course of sulfide mineral bioleaching could lead to increased expression of genes associated with iron and sulfur oxidation. Indeed, previous studies have shown that some bioleaching organisms upregulate genes associated with iron and sulfur oxidation in the presence of these elements (Holmes and Bonnefoy, 2007; Liljeqvist, Rzhepishevska and Dopson, 2013; Ai *et al.*, 2019; Feng *et al.*, 2020). Based on this background, several hypotheses were formed regarding the microbial breakdown of Phoukassa ore:

H_1 - Phoukassa ore breakdown will be greater in the presence of the SC3 consortium than in the abiotic samples
H_2 - Genes predicted to be involved in sulfur and iron metabolism will be expressed when the consortium is grown on Phoukassa ore
H_3 - Genes predicted to be involved in sulfur and iron metabolism would be upregulated at 16 weeks compared to 8 weeks when the consortium was grown on Phoukassa ore

Testing these hypotheses will expand our understanding of the iron and sulfur oxidation pathways in acidophiles, while creating the first datasets

regarding the microbial dissolution of the Phoukassa ore. Further, testing H3 can help identify any changes in the roles played by different consortium members at different stages of bioleaching.

3.1.5 Aims and Objectives

The aims of the work outlined in this chapter were to improve the understanding of the roles played by different members of the SC3 bioleaching consortium during biotic dissolution of an environmentally relevant low-grade copper ore, and concomitantly, to produce the first study of Phoukassa ore breakdown mechanisms. To fulfil the aims, the following objectives were set out:

1. To collect geochemical information about Phoukassa ore breakdown by a naturally occurring bioleaching consortium and compare this to an abiotic control.
2. To use bioinformatic tools to explore which iron and sulfur oxidising genes are being expressed, and by which consortium members, during bioleaching.
3. To use bioinformatic tools to explore which genes associated with additional metabolism processes that may be relevant to community functioning, such as carbon and nitrogen fixation, and are being expressed during bioleaching.
4. To use bioinformatic tools to examine whether there is differential expression of genes relevant to bioleaching over time.
5. To create a model of Phoukassa ore breakdown using metatranscriptomic data over time

3.2 Materials and Methods

3.2.1 Experimental Design

Chapter 2 used a combination of genomic and transcriptomic data to identify genes associated with bioleaching by the SC3 consortium at a single time point. This chapter explores whether the same gene pathways are involved in the bioleaching of a low-grade ore, typical of those exploited in real-world bioleaching scenarios. Additionally, this chapter will build on the work carried out in Chapter 2, by testing whether the expression of genes associated with bioleaching changes over time.

An experimental plan was designed that would test the hypotheses and meet the outlined aims and objectives of this chapter. The experimental plan broadly followed that of Chapter 2 (Fig 2.2, Section 2.2.1), with some exceptions. Briefly, the composition of the Phoukassa ore was established via pXRD and ICP-OES analysis. Next, a bioleaching study was set up with the SC3 consortium grown on Phoukassa ore, alongside abiotic controls. The dissolution of the mineral was tracked over time using ICP-OES, and SEM observations of microbial samples were used to explore whether microbes were attached to the mineral surface.

In Chapter 2, a number of limitations were highlighted with regards to 16s rDNA sequencing. For example, it was found that 16s did not accurately capture some of the species in the consortium. Additionally, it was demonstrated that RNA-seq can be used to confirm species' presence. Consequently, 16s rDNA sequencing was not employed in this chapter as it was unnecessary to address the hypotheses in this chapter, and the resources instead were put towards the creation and sequencing of a greater number of RNA-seq samples.

Whole community RNA was extracted from 6 samples at 8, 12 and 16 weeks. In Chapter 2, there were some difficulties with extracting sufficient

RNA for sequencing. This was attributed to the well-known challenges associated with RNA extraction from low pH environments (Zammit *et al.*, 2011). Therefore, in order to extract sufficient levels of RNA the number of samples at each time-point was increased, and the timeframe of the experiment was increased to 16 weeks, thus providing an inceased growth time, for a greater chance of RNA recovery. It was also anticipated that sufficient RNA would be retrieved from at least two time points to examine whether there are changes in gene expression over time. By sequencing at multiple time points we can explore whether the individual roles of each species in the consortium change over time during bioleaching. Following quality control of the RNA-seq data, some samples were excluded due to low sequence quality, and 4 samples from week 8, and 5 samples from week 16 were taken forward to use in downstream analyses. In this process, all replicates from week 12 were excluded (see Section 3.2.7.2 for detailed explanation). RNA-seq data was processed using the novel pipeline developed in Chapter 2.

Finally, a model of Phoukassa ore dissolution was proposed, incorporating the previously collected metagenomic and this chapter's metatranscriptomic data to provide a novel and comprehensive picture of Phoukassa ore bioleaching over time by a naturally occurring bioleaching consortium.

The following sections provide further detail on the methods used to achieve this experimental plan.

3.2.2 Phoukassa Ore

Ore was obtained from the Phoukassa deposit, Skouriotissa Mine, Cyprus (provided by Hellenic Copper Mines Ltd). The Phoukassa deposit is one of multiple exploited within the The Skouritissa mine site. Previous analyses of this ore had established its non-silicate portion to comprise predominantly of pyrite, with frequent chalcopyrite inclusions, and some

replacement chalcocite, covellite and bornite. Gangue minerals were shown to be predominantly quartz. EPMA analysis of the pyrite, conducted away from obvious microscopic inclusions of the chalcopyrite, covellite, chalcocite and bornite, found an average Cu concentration of <0.01% (Hudson-Edwards *et al.,* unpublished data).

3.2.3 Phoukassa Ore Compositional Analysis

The phase identity of the Phoukassa ore was assessed using PXRD which was conducted as outlined in Chapter 2 of this thesis. To assess total amounts of Cu, Fe and S in both the Phoukassa ore, 3 samples (10mg) of mineral were dissolved in nitric acid and the concentration of elements was analysed using ICP-OES at the Wolfson Laboratory for Environmental Geochemistry, UCL.

3.2.4 Microbial Growth

In this section, the growth conditions for samples used in geochemical testing and RNA-seq are described.

Prior to setting up the bioleaching experiment, microbes were adapted to growth on the Phoukassa ore by serial sub-culturing. Sub-culturing involved a 5% inoculum of the consortium being transferred into minimal acid medium (MAM, Table 2.1, Section 2.2.2) containing the Phoukassa mineral 3 times (every 8 weeks). These adapted cultures were then used as the inoculum for the Phoukassa ore bioleaching experiment.

Growth medium and conditions of the bioleaching experiment were similar to those described in chapter 2. Briefly, samples were created by adding 50ml MAM and 1g Phoukassa ore to 100ml conical flasks (Fig 3.1). A 5% inoculum of the SC3 consortium was transferred to all biotic samples which were then incubated alongside abiotic controls at 28°C without shaking for up to 16 weeks. Sterile conditions were maintained throughout

experimental set-up to ensure contamination with non-target species did not occur, and to ensure the control samples remained abiotic. Further, samples (20 µl) were examined at 400x magnification under a Leica DM 2500 LED optical microscope (Leica Microsystems GmbH, Wetzlar, Germany) at 4 week intervals to confirm the presence or absence of microbes in biotic and abiotic samples, respectively.

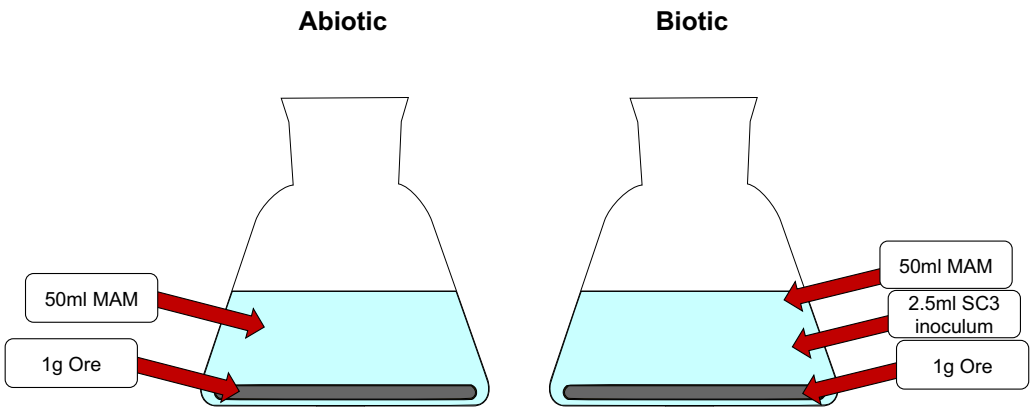

Figure 3.1 - Schematic of Phoukassa ore dissolution experiment flasks. Images of growth in flasks are in Appendix V

3.2.5 Scanning Electron Microscopy

At 16 weeks' growth, mineral samples from biotic Phoukassa samples were adhered to stubs, freeze-dried and imaged using SEM, as outlined in Section 2.3.2 of this thesis.

3.2.6 Geochemical Analyses of Supernatant

To establish the breakdown of Phoukassa ore over time in biotic and abiotic samples, ICP-OES and pH testing analyses were employed. Supernatant (10ml per sample) was collected from biotic and abiotic samples at 0 time, 8 weeks, and 16 weeks (as grown in Section 3.2.4). Samples were filtered to 0.22µm before being frozen at -20ºC until

analysis. Samples were acidified prior to analysis with 1% HNO_3. ICP-OES analysis was carried out using a Varian 720 ICP-OES (Varian Inc., CA, USA). Standards and blanks were matrix matched to the samples. Percentage of total Cu, Fe and S leached were calculated by dividing concentrations of Cu, Fe and S in the supernatant by total values for Cu, Fe and S in the mineral, as established in Section 3.2.3 and multiplying by 100. The pH values of sample supernatant were assessed using MilliporeSigma MColorpHast pH indicator strips (pH 0-2.5, Merck KGaA, Darmstadt, Germany).

3.2.7 RNA-seq

To meet the objective of analysing whether, and which, genes relevant to bioleaching are expressed during Phoukassa ore bioleaching, RNA sequencing of the SC3 consortium grown on Phoukassa ore was carried out. This process consisted of extracting and sequencing whole-community RNA, and bioinformatic processing of the sequence data, as detailed below.

3.2.7.1 RNA Isolation and Sequencing

RNA was isolated from six biotic samples at 8, 12 and 16 weeks' growth using the adapted protocol for the Mo Bio PowerMicrobiome RNA isolation kit (Mo Bio Laboratories, CA, USA), and RNA quantities assessed as outlined in Section 2.2.11 of this thesis. Samples were stored at -80ºC prior to sequencing.

Library preparation and RNA sequencing was conducted by LGC Genomics GmbH (Berlin, Germany). Samples were treated with bacterial RiboZero to enrich for mRNA, and library construction was achieved using an Ovation Complete Prokaryotic RNA-seq kit (NuGen). Sequencing was

150bp, paired-end (average 25 million read pairs per sample, minimum 12 million paired-end reads per sample, maximum 45 million paired-end reads per sample), non-stranded via an Illumina NextSeq 500 V2 platform.

3.2.7.2 RNA-seq Data Analysis

Bioinformatic processing of metatranscriptomic data was carried out as described in Section 2.2.11.2. Quality checks (FastQC and alignment metrics) indicated degraded RNA for all week 12 replicates; 2 week 8 replicates; and 1 week 16 replicate. These samples were therefore removed from downstream analyses. All remaining samples had a minimum of 50% aligned to the reference metatranscriptome, indicating high sequence quality.

Additionally, Wald tests in Deseq2 (Love, Huber and Anders, 2014) were used to establish intra-species differential expression between the two timepoints. The p values generated were adjusted for multiple testing using the Benjamini and Hochberg method for controlling the false discovery rate (Benjamini and Hochberg, 1995).

To further assess the quality of the RNA, a principal component analysis (PCA) was performed. To carry this out, genes that were present across genomes needed to be identified, so that data could be compared across species. This was achieved using InterProScan version 5.34-73.0 (Jones *et al.*, 2014) to annotate genes in the genomes. Following this, genes present in two or more species were used in the PCA. Where genes were not present in a species, their expression value was set to zero.

3.2.8 Graphics and Statistical Analysis

Diagrams illustrating experiment schematics, metabolic pathways and biogeochemical cycles were produced using Inkscape (Inkscape, 2019).

Statistical analyses were carried out and figures showing data were produced in R version 3.4.3 (R Core Team, 2017), using R studio version 1.1.423 (RStudio Team, 2016), with packages: “ggplot2” (Wickham, 2016), “ggpubr” (Kassambara, 2018), “forcats” (Wickham, 2019), “dplyr” (Wickham *et al.*, 2019) “tximport” (Soneson, Love and Robinson, 2016), “readr” (Wickham, Hester and Francois, 2018), “devtools” (Wickham, Hester and Chang, 2019), “ggbiplot” (Vincent Q Vu, 2011), “gridExtra” (Auguie and Antonov, 2017).

Linear mixed effects models for differences in elements between biotic and abiotic accounting for the effect of time point, Kruskal-Wallis analysis of variance testing, and Mann-Whitney U testing were used to establish differences between treatments.

3.3 Results

3.3.1 Growth Substrate Mineral Composition Analyses

To meet the aim of this chapter to improve the understanding of Phoukassa ore and its breakdown, it was essential to establish the composition of the ore. This was achieved via PXRD and ICP-OES analyses.

The PXRD analysis carried out determined the major phase within the sample of Phoukassa ore analysed to be pyrite, with secondary chalcopyrite and quartz (Fig. 3.2).

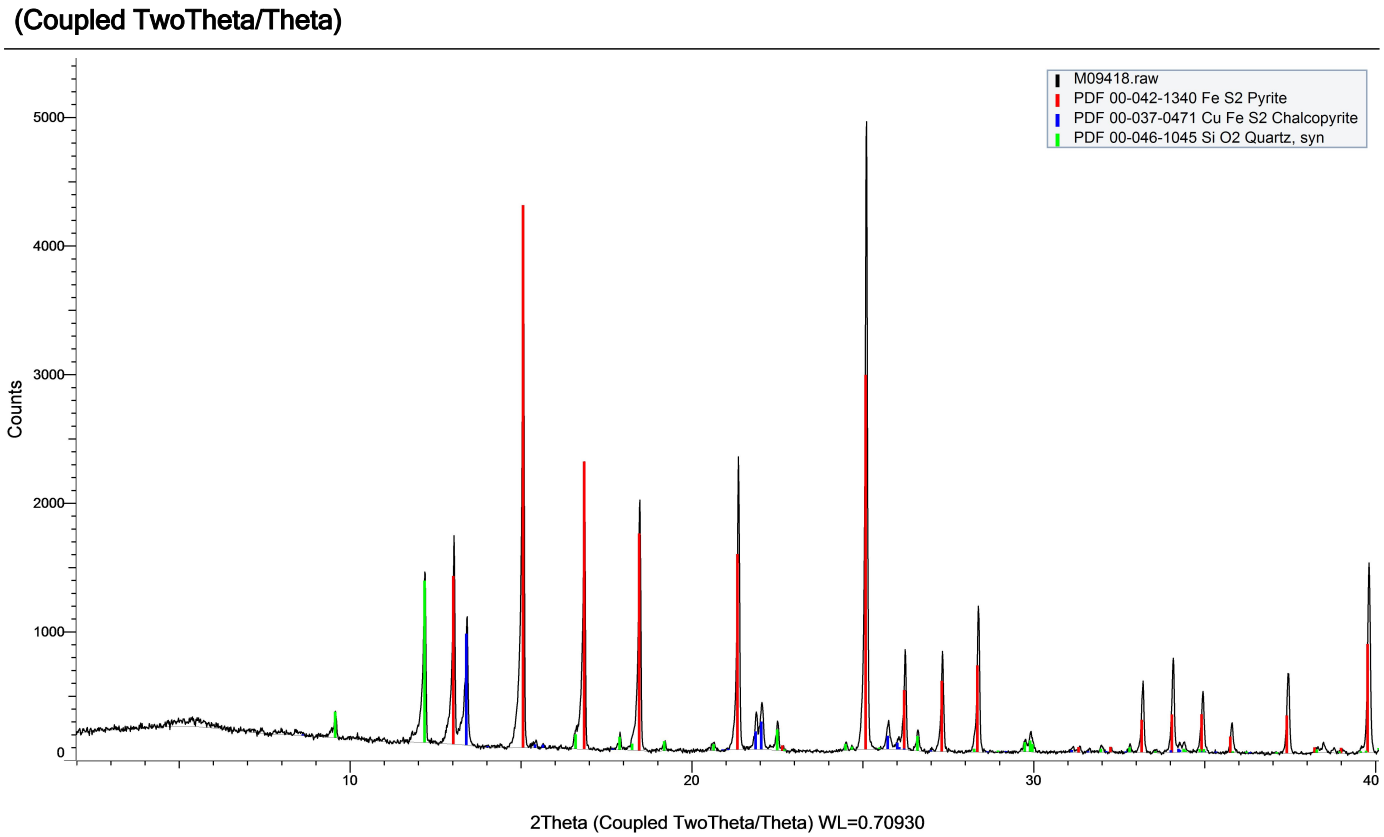

Figure 3.2 - PXRD pattern for the Phoukassa ore used in growth experiments. PXRD produces peaks which are characteristic of specific minerals. Red lines indicate peaks matching pyrite, blue lines highlight peaks corresponding to chalcopyrite and green lines highlight peaks analogous to quartz.

Subsequently the baseline (pre-leaching) quantities of Cu, Fe and S in the Phoukassa ore were ascertained via ICP-OES analysis of dissolved samples (Fig. 3.3). This analysis revealed the mean composition of the Phoukassa ore to be predominantly pyrite with a low level of copper, in line with the pXRD analysis for this mineral (2.2% ± 0.4 Cu, 39.1% ± 4.1 Fe, 43.5% ± 5.2 S).

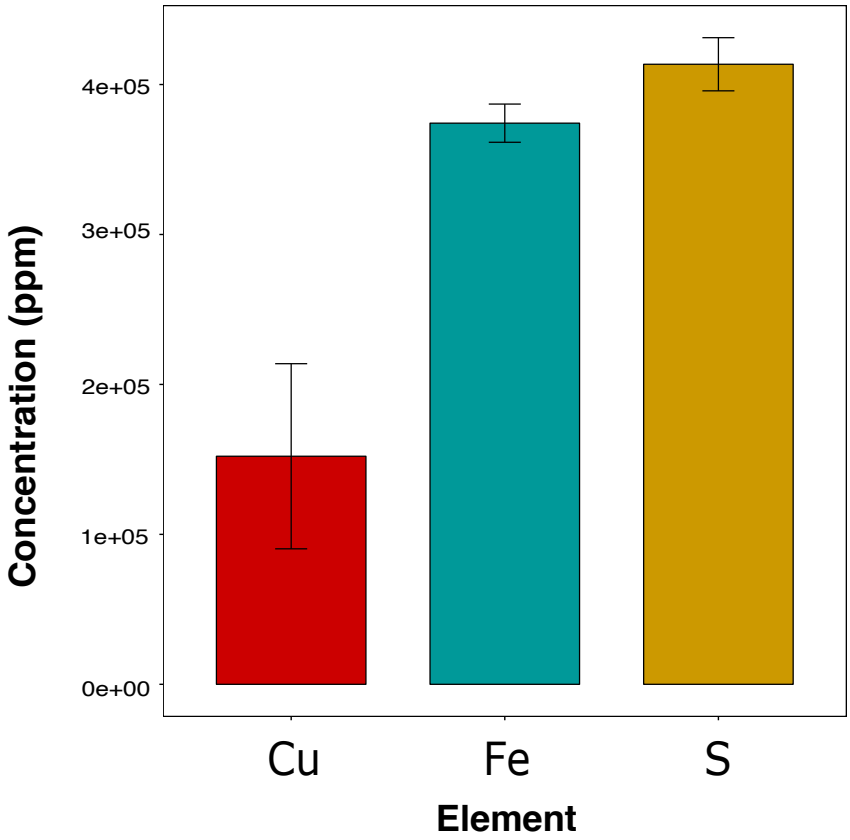

Figure 3.3 - Mean element concentrations (ppm) of the Phoukassa ore dissolved in nitric acid, as measured by ICP-OES (n=3), error bars show standard error

3.3.2 Scanning Electron Microscopy

Inspection under an optical microscope at 4 week intervals had confirmed that microbes were present in biotic samples and absent in abiotic samples. To explore whether there was microbial attachment to the mineral surface, biotic samples

were then examined using scanning electron microscopy (SEM) at 16 weeks' growth (Fig 3.4A-C). The SEM images confirm the Phoukassa ore was colonised by microbes, and show multiple morphologies suggesting more than one species is present.

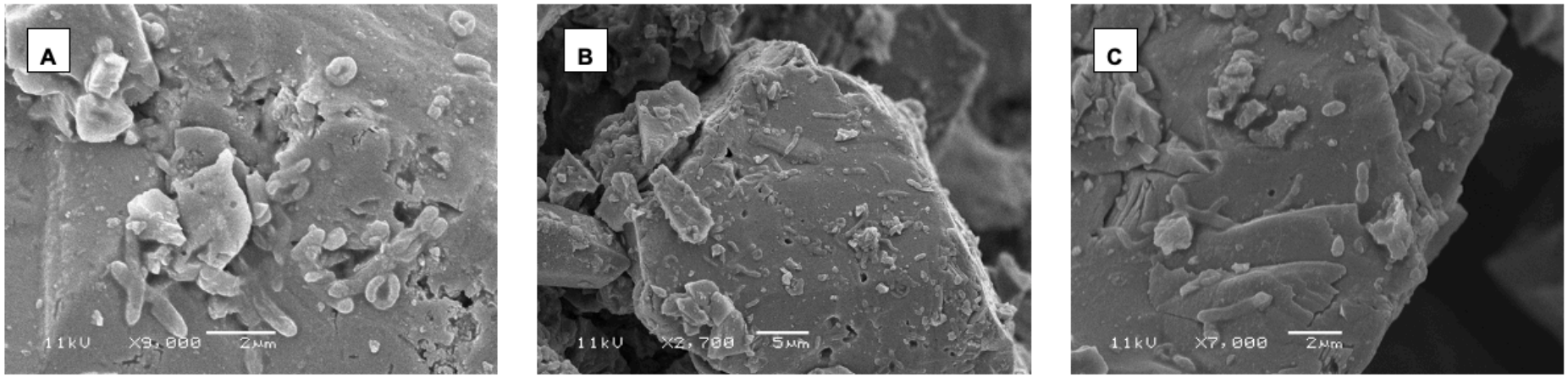

Figure 3.4 – SEM images of SC3 on Phoukassa ore at 16 weeks' growth

3.3.3 Dissolution of Phoukassa Ore in Biotic and Abiotic Conditions

To establish whether Phoukassa ore breakdown is greater in the presence of the SC3 consortium, quantities of Cu, Fe and S were measured at 0 time, 8 and 16 weeks using ICP-OES. Concentrations of Fe, Cu and S in the supernatant increased over time in all samples (Figure 3.5 and 3.6), and over time the Fe and S concentrations for the biotic samples significantly exceeded those of the abiotic samples (linear mixed effects model $p<0.001$). A contrasting trend was found for copper, with abiotic samples showing significantly increased concentrations over time compared to the biotic samples (linear mixed effects model $p=0.02$). However, overall copper concentrations were notably lower than Fe and S (Fig 3.6).

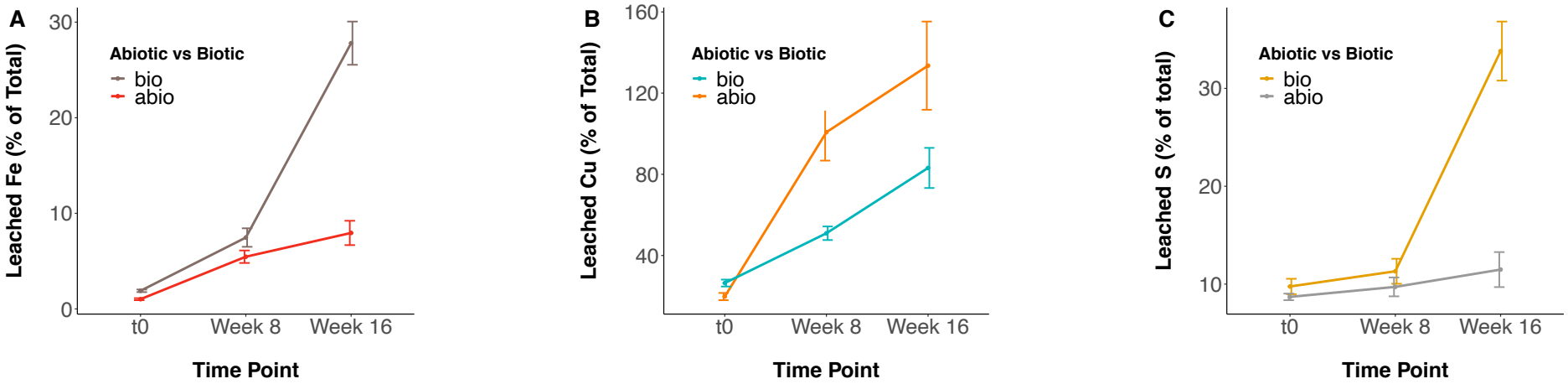

Figure 3.5 - mean supernatant ICP-OES results showing percentage of A) iron, B) copper, and C) sulfur leached from Phoukassa ore under biotic and abiotic conditions over 16 weeks (time0: n=3, Week 8,16: n=4). Error bars show the standard error of the mean.

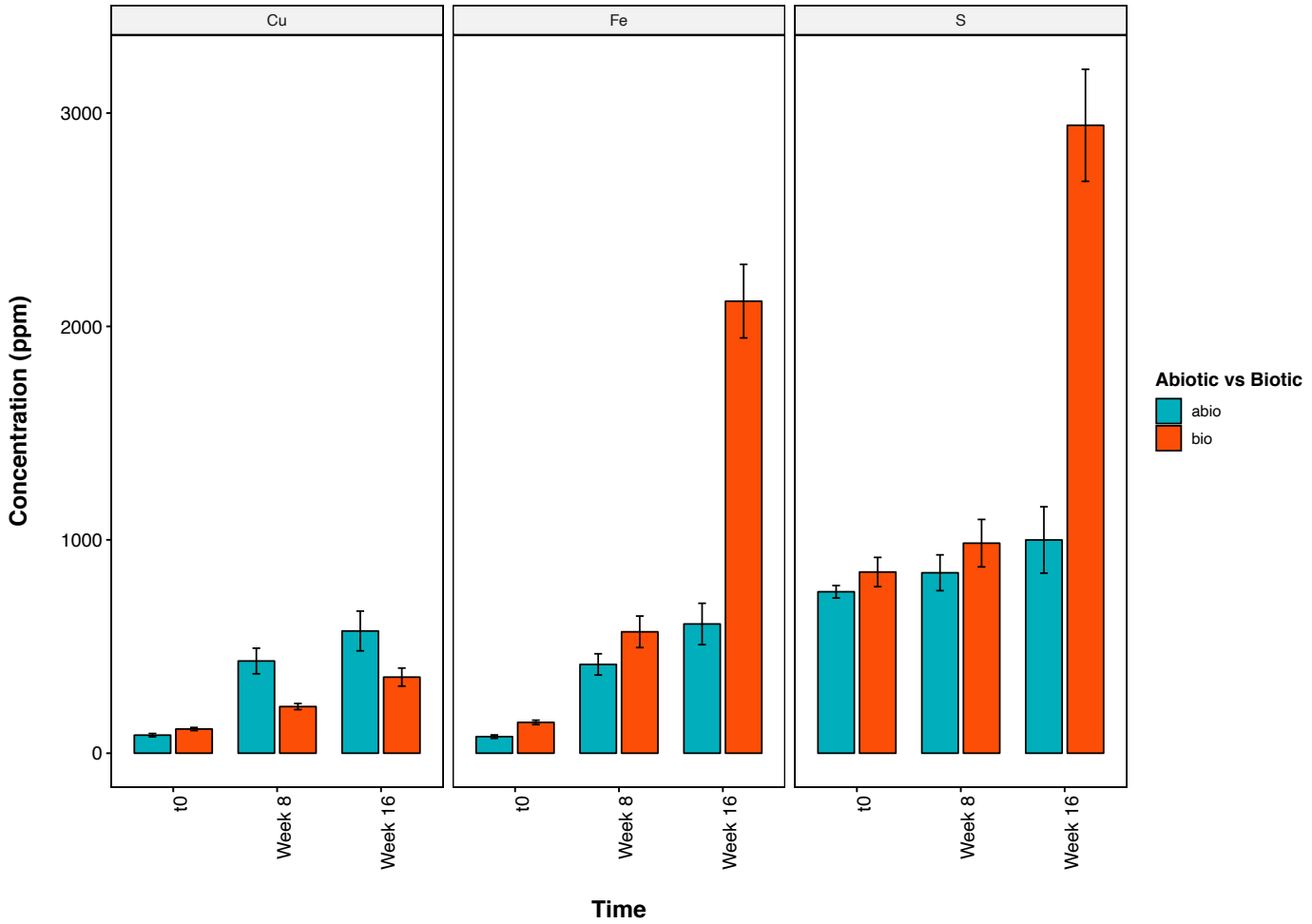

Figure 3.6 – mean supernatant ICP-OES results (ppm) for copper, iron and sulfur from Phoukassa ore under biotic and abiotic conditions. Error bars show the standard error of the mean.

To assess the regeneration of protons via sulfur oxidation, pH was measured throughout the Phoukassa bioleaching experiment. The pH values for the abiotic samples increased steadily over the 16 weeks, whereas the biotic samples showed a converse trend, becoming more acidic over time (Figure 3.7). By week 16, there was an average 0.64 difference in pH between the two conditions.

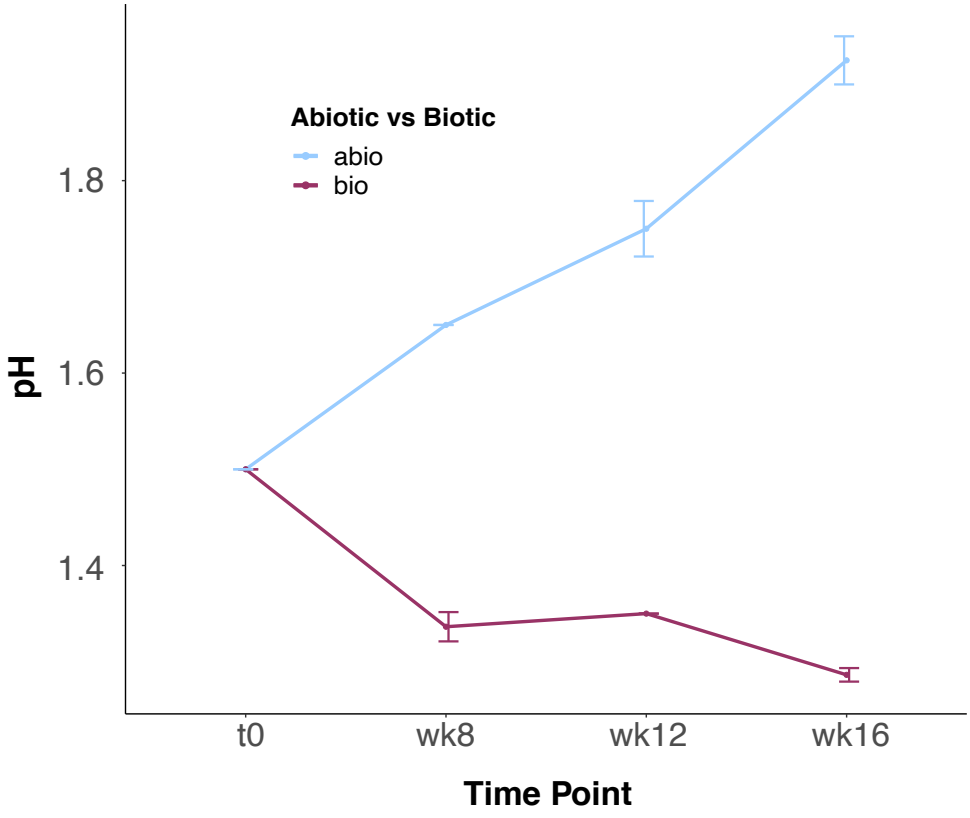

Figure 3.7 - mean pH values over time for biotic and abiotic Phoukassa samples. Error bars show standard error.

3.3.4 Metatranscriptomic Insights into Gene Expression during Growth of SC3 on Phoukassa Ore

A metatranscriptomic study using RNA-seq data was used to explore differential expression of metabolism associated genes between week 8 and 16 growth on the Phoukassa ore. Principal components analysis (PCA) was employed to visualise variation in the transcriptomic data. The results showed that species grouped together, helping to confirm that reads were correctly aligned and that the RNA sequenced produced a clear biological signal. There was also some phylogenetic clustering; for example, all of the archaea clustered together (Fig 3.8, below). Further, these results confirm that all SC3 species were still present when the consortium was grown on the Phoukassa ore.

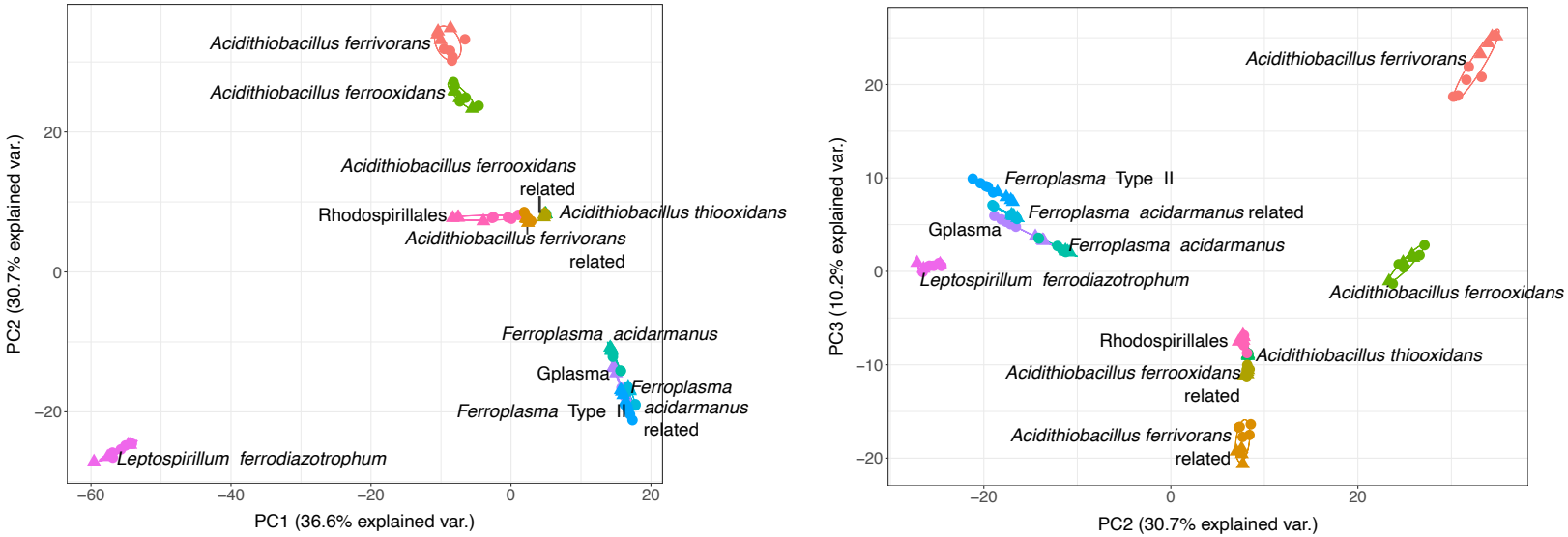

Figure 3.8 – Principal components analyses (PCA) using metatranscriptomic data at the two time points. Based on the top 3 principal components (which explain 77% of the variance, Appendix VI), samples cluster by species rather than timepoint.

Differential expression of metabolism genes was explored using Deseq2. Archaea demonstrated the greatest changes in overall gene expression between week 8 and 16, which could be indicative of changes in function, and/or changes in abundance (Fig 3.9).

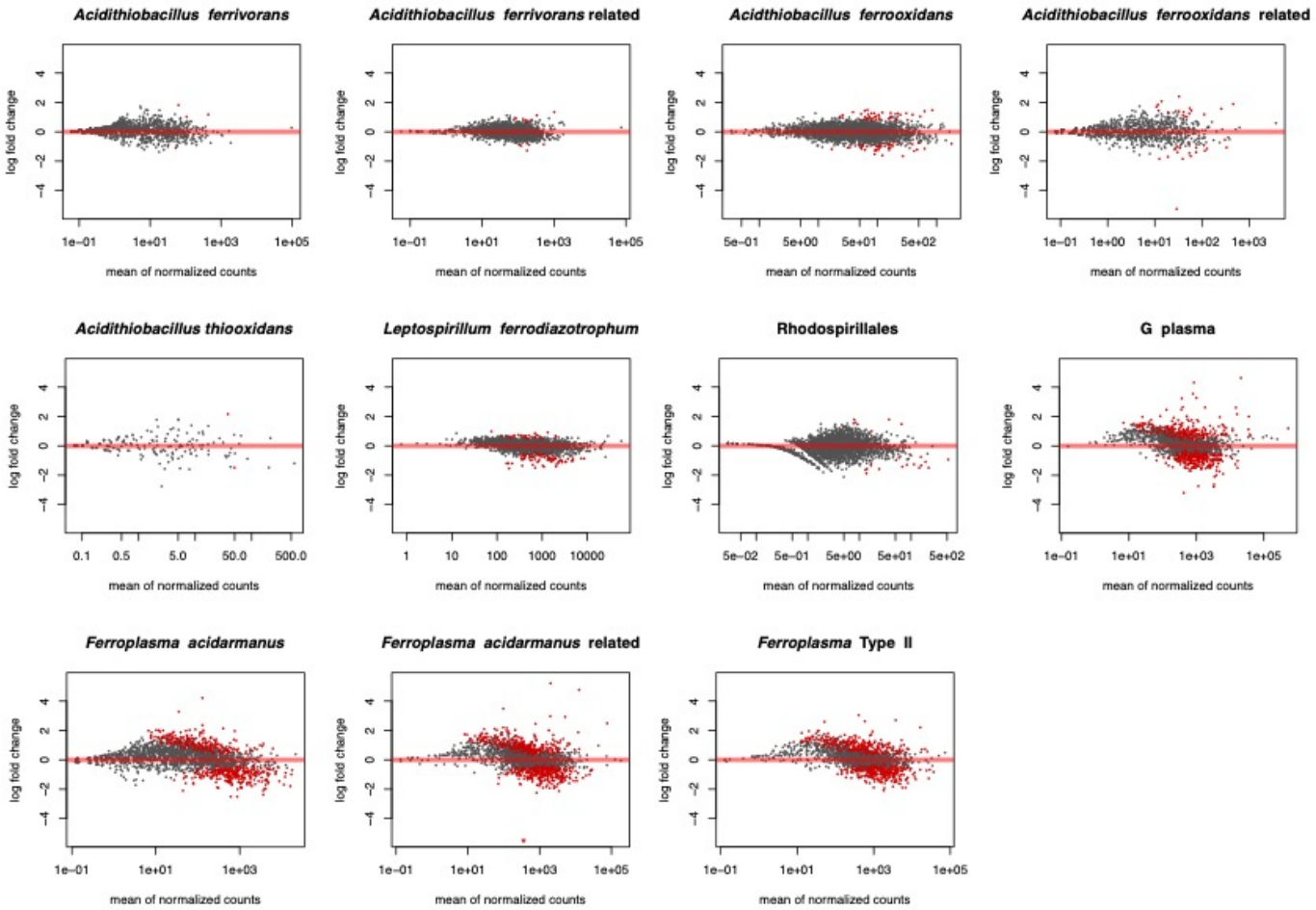

Figure 3.9 – Expression differences of all genes by species. Y axis shows the log^2 change of the ratio of expression between week 16 and 8. Positive values indicate higher expression at week 16, negative values indicate higher expression at week 8. Red dots show genes that are significantly differently higher expressed (Deseq2's Wald Test, p value <0.05). X axis shows the average level of expression per gene

To test whether iron and sulfur metabolism changed over time during bioleaching, the expression level of genes associated with these processes were compared across time points, alongside nitrogen and carbon fixation. Generalised functional categories were manually assigned based on the sulfur oxidation, iron oxidation, nitrogen and carbon fixation genes established in Chapter 2 (Appendix IV). These categories were used to explore whether functional change occurred over time across the whole consortium (Fig. 3.10). Linear regression of gene expression found that there were no significant differences between time points for iron, or sulfur metabolism ($p>0.05$). This finding suggests that at a functional community level, iron and sulfur oxidation are being carried out at a consistent level at week 8 and 16. Additionally, no significant differences between time points were seen between time points for carbon fixation ($p>0.05$). Nitrogen fixation was the only generalised function to be significantly different between the two time points ($p=0.02$).

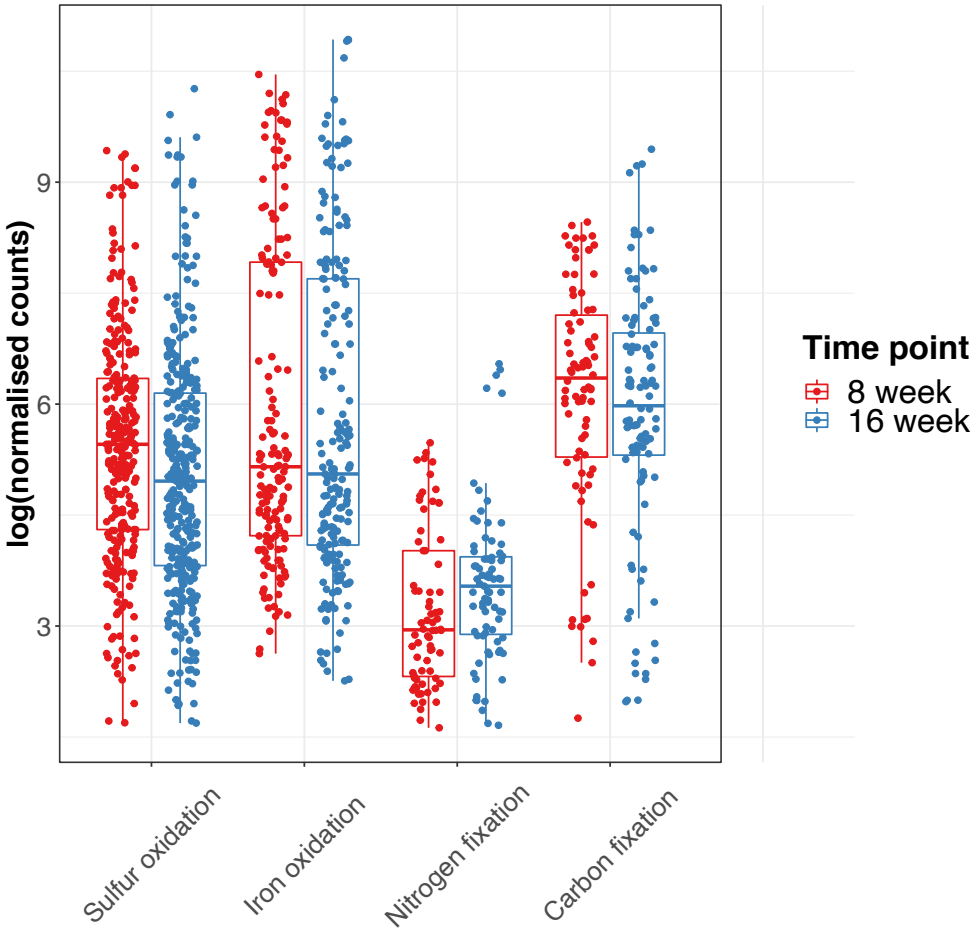

Figure 3.10 - Expression of known iron oxidation, sulfur oxidation, nitrogen fixation, and carbon fixation genes in the SC3 metatranscriptome at 8 and 16 weeks growth on Phoukassa ore.

3.3.4.1 Sulfur and Iron Metabolism Gene Expression during Growth of SC3 on Phoukassa Ore

Genes associated with sulfur oxidation were found to be expressed at both time points by all species except *At. thiooxidans* (Figs 3.11. – 3.12), however, in *At. ferrivorans,* overall expression of sulfur genes was very limited. Of the two direct RISC oxidising genes showing expression, *sqr* was not expressed above the threshold at week 8 and *hdr* was downregulated at week 16 (log^2 fold change -1.1, $p < 0.01$).

For many of the species, expression of sulfur oxidation genes was consistent over time. For example, *At. ferrooxidans* was expressing all sulfur oxidation genes present in its genome, maintaining expression levels between the two time points. Likewise, *L. ferrodiazotrophum* was expressing its only sulfur oxidation gene, *sqr*, consistently across both time points.

For individual genes within some of the species, differences in sulfur and iron oxidation gene expression were observed between the two time points. For example, G plasma was found to be expressing *sqr* and *hdr* significantly more at week 16 (log^2 fold change 2.6 and 2.4, respectively, $p < 0.01$). Similarly, *sor* was slightly upregulated at 16 weeks in *F. acidarmanus* (log^2 fold change 0.8, $p < 0.05$). In *F.* Type II, *sor* was determined to be upregulated at week 16 (log^2 fold change 2, $p < 0.01$), although the overall number of reads aligned to this gene was low (mean 13.4 across all samples).

In contrast, both of the expressed Rhodospirillales RISC oxidation genes, *sqr* and *tqo* were downregulated at week 16 (log^2 fold change -3.6, -2.6, respectively, $p < 0.01$). The *At. ferrivorans* related strain showed significant down regulation of almost all its sulfur oxidation associated genes at week 16 compared to week 8 (*soxBYZ, dsre, tusA, rhd, sqr, bo3, petII operon,* median log^2 fold change -1.3, $p \leq 0.03$).

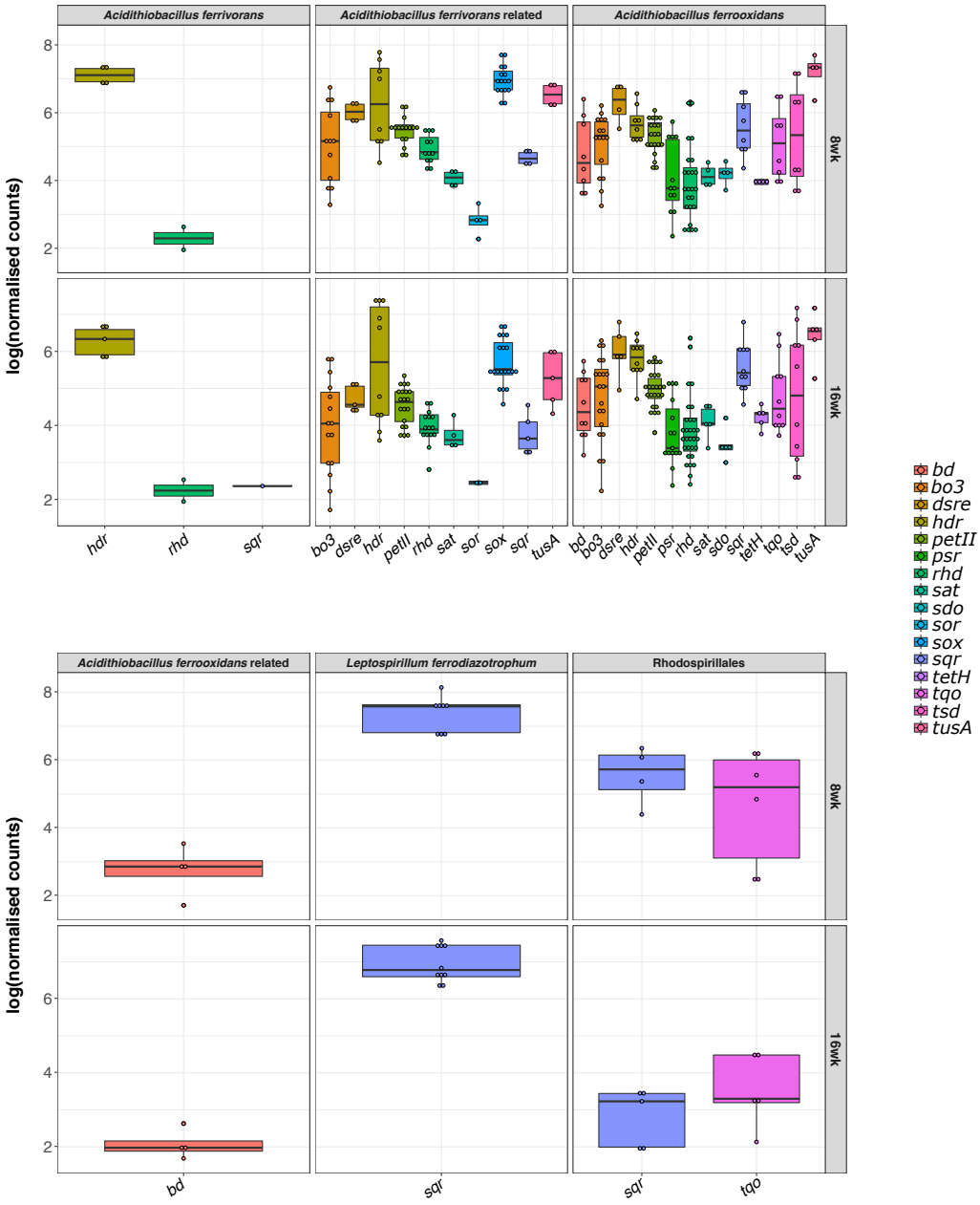

Figure 3.11 - Expression of known sulfur metabolism and associated electron transport chain genes in the bacteria of the SC3 consortium grown on Phoukassa ore for 8 and 16 weeks. Normalisation was performed with Deseq2. PSR: polysulfide reductase, SQR: sulfide-quinone reductase, FCCB: Flavocytochrome c sulfide dehydrogenase, SOR: sulfur oxygenase reductase, SDO: sulfur dioxygenase, HDR: heterodisulfide reductase, SAT: sulfate adenylyltransferase, TetH: tetrathionate hydrolase, TQO: thiosulfate-quinone oxidoreductase, TSD: thiosulfate dehydrogenase, SOX: sulfur oxidation pathway.

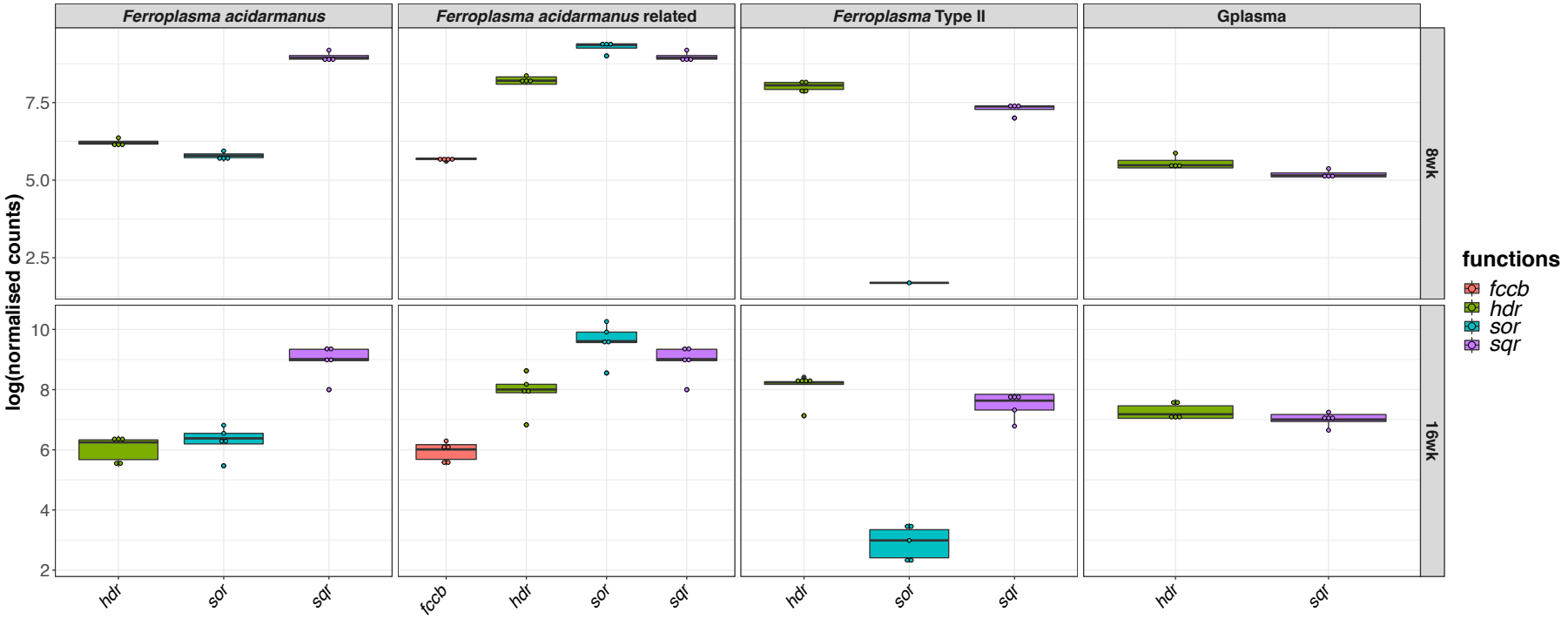

Figure 3.12 – Expression of known sulfur metabolism and associated electron transport chain genes in the archaea of the SC3 consortium grown on Phoukassa ore for 8 and 16 weeks. Normalisation was performed with Deseq2. SQR: sulfide-quinone reductase, FCCB: Flavocytochrome c sulfide dehydrogenase, SOR: sulfur oxygenase reductase, HDR: heterodisulfide reductase

Expression of iron oxidation associated genes was shown in all 8 of the consortium species that were demonstrated to possess them (Chapter 2). It was found that there was differential expression of some of the iron genes in *L. ferrodiazotrophum,* with *cycA1,* and one copy of the gene responsible for direct iron oxidation, cyt_{572}, downregulated at 16 weeks (-1.5, -0.8 log^2 fold change, respectively, $p < 0.05$). The *At. ferrivorans iro* gene was also downregulated at 16 weeks (-1.5 log^2 fold change, $p < 0.01$), as well as all of the additional iron oxidation associated genes in this organism, of which significant differential expression was found for *ctaT, coxA, Cyc1, Cyc2* (median log^2 fold change -1.1, $p<0.05$). Conversely, the *Ferroplasma acidarmanus* related strain and *Ferroplasma* Type II were found to be upregulating their sulfocyanin, *soxE* at 16 weeks (log^2 fold change 2.8 and 1.8, respectively, $p<0.01$) (Fig. 3.14). It was found that *soxE* was not expressed at all in *Ferroplasma acidarmanus,* despite this species showing expression of the other iron metabolism associated genes at both time points. No significant difference in expression was seen for *At. ferrooxidans*' rusticyanin encoding *rus,* which was moderately expressed at both time points (Fig. 3.13).

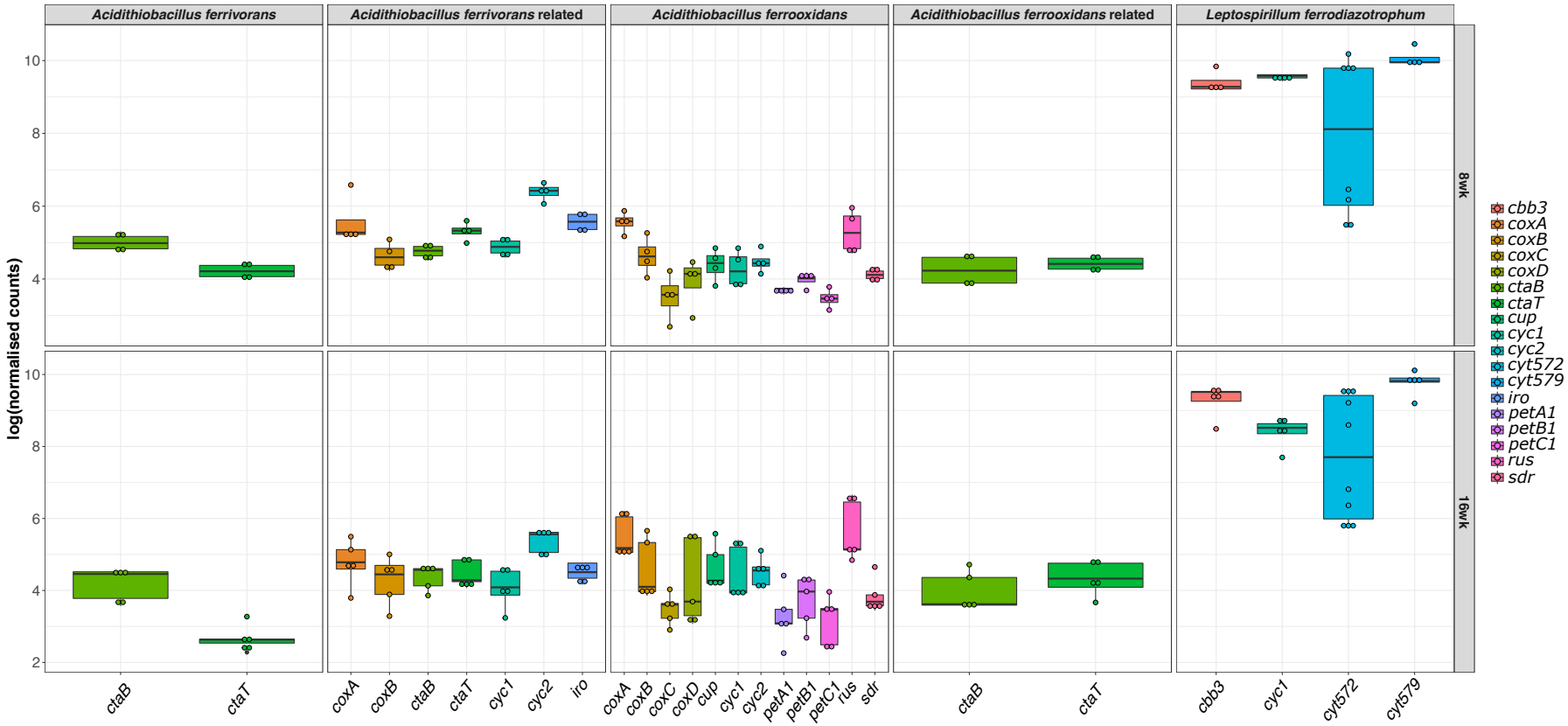

Figure 3.13 - Expression of iron oxidation and associated electron transport protein genes in the bacteria of the SC3 consortium grown on Phoukassa ore for 8 and 16 weeks. Normalisation was conducted with Deseq2.

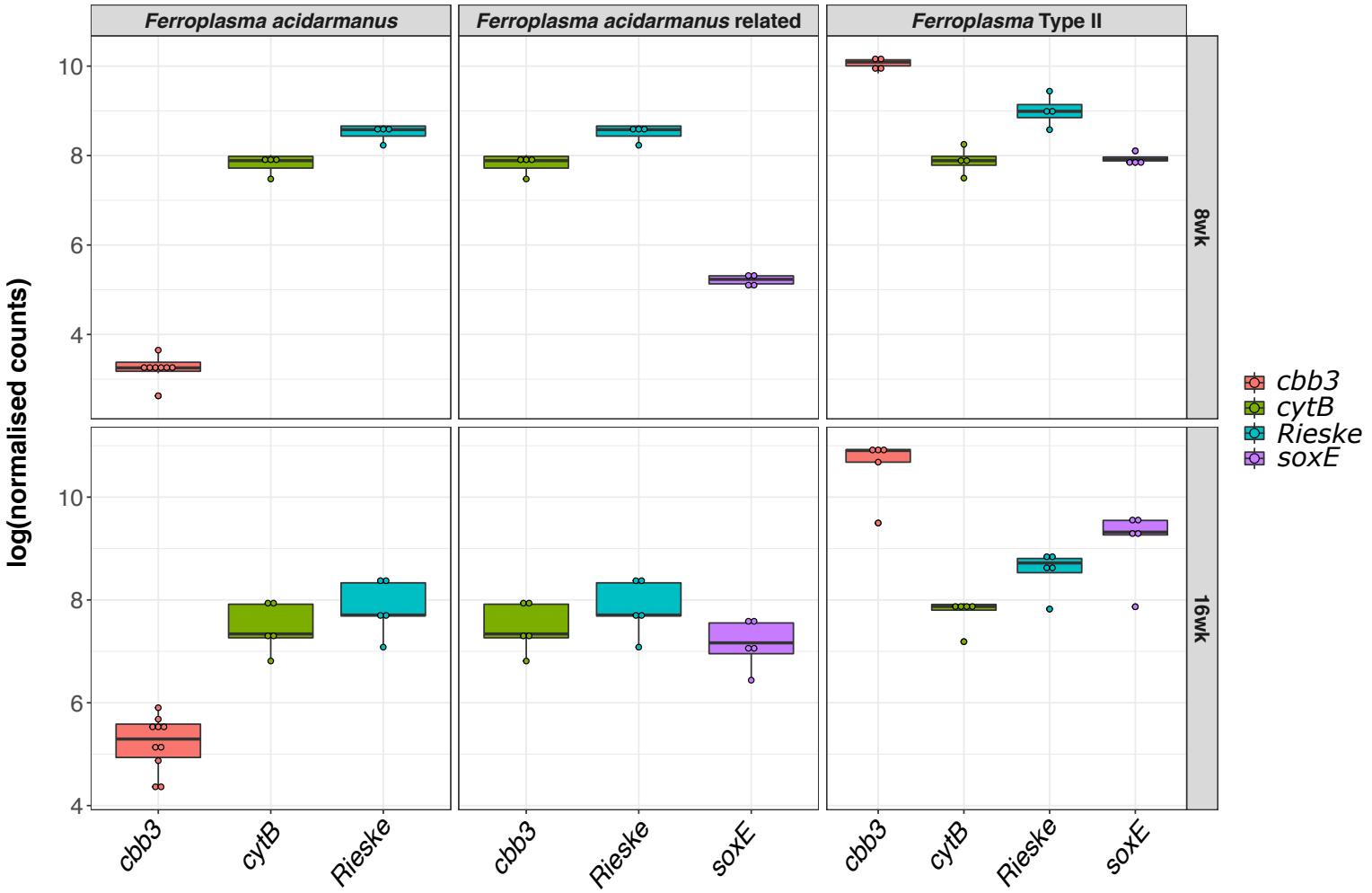

Figure 3.14 - Expression of iron oxidation genes in the archaea of the SC3 consortium grown on Phoukassa ore for 8 and 16 weeks. Normalisation was conducted with Deseq2. RUS: rusticyanin, SoxE: Sulfocyanin, IRO: high potential iron-sulfur protein, Cyt_{572}: Cytochrome 572. q

3.3.4.2 Nitrogen Fixation

As a generalized function (*i.e.* genes from all species taken together) nitrogen fixation genes were significantly different between time points (linear regression, p=0.02), suggesting an increase in nitrogen fixation activity over time. Nitrogen fixation genes were expressed in four of the five species that possessed them: *At. ferrivorans* and its related species, *At ferrooxidans* and *L. ferrodiazotrophum* (Fig. 3.15). At both week 8 and 16, the complete *nif* operon was expressed in both *L. ferrodiazotrophum* and *At. ferrooxidans.* Additionally, all of the *nif* operon genes present in *At. ferrivorans* related species were expressed, with the exception of *nifX. At. ferrivorans* was only found to express two of the *nif* genes, *nifEN.* At a species level, no individual genes were differentially expressed between the two time points for any consortium member. Overall, the number of reads aligned to the *L. ferrodiazotrophum nif* operon (mean across all samples: 102) was notably higher than any of the other species (mean across all samples: 5, 45, 12, for *At. ferrivorans, At. ferrivorans* related, and *At. ferrooxidans*, respectively).

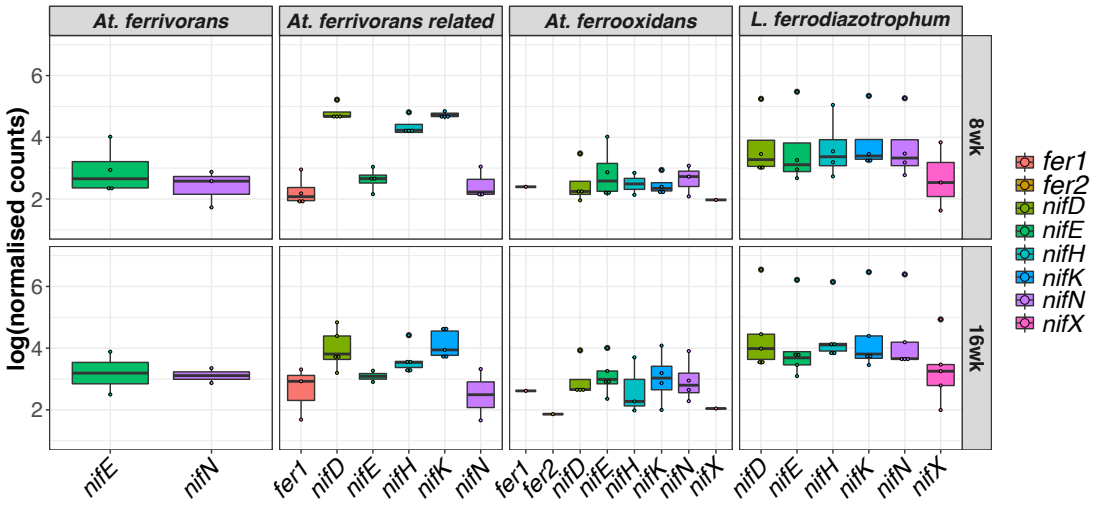

Figure 3.15 – Expression of nitrogen fixing nif genes in the SC3 consortium at week 8 and 16 of growth on Phoukassa ore. Normalisation was conducted with Deseq2.

3.3.4.3 Carbon Fixation

Genes for the Calvin Cycle CO_2 fixing enzyme, ribulose-1,5-bisphosphate carboxylase/oxygenase (EC 4.1.1.39, Rubisco) were expressed in *At. ferrooxidans, At. ferrivorans* and their related strains (Fig. 3.16), as well as Rhodospirillales. Genes associated with the chimaeric CO_2 fixation pathway (Cárdenas *et al.*, 2009), were expressed by all *Ferroplasma spp.* in the consortium. As a generalised function and within individual species and genes over time, no significant differences were seen in carbon fixation genes between the two time points (Linear regression, p>0.05).

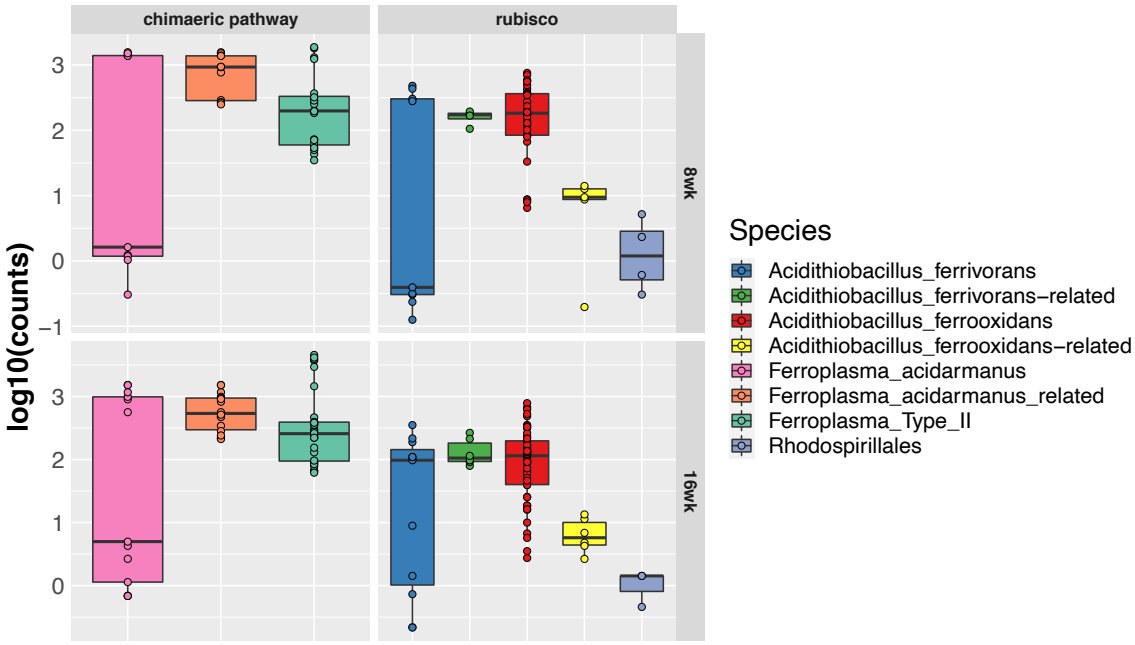

Figure 3.16 - Expression of genes associated with carbon fixation in SC3 consortium at 8 and 16 weeks' growth on Phoukassa Ore.

3.3.4.4 Model of Phoukassa Ore Bioleaching by the SC3 Consortium

The expression data given in the previous sections were linked together to create a model of Phoukassa ore dissolution by the SC3 consortium (Figure 3.17).

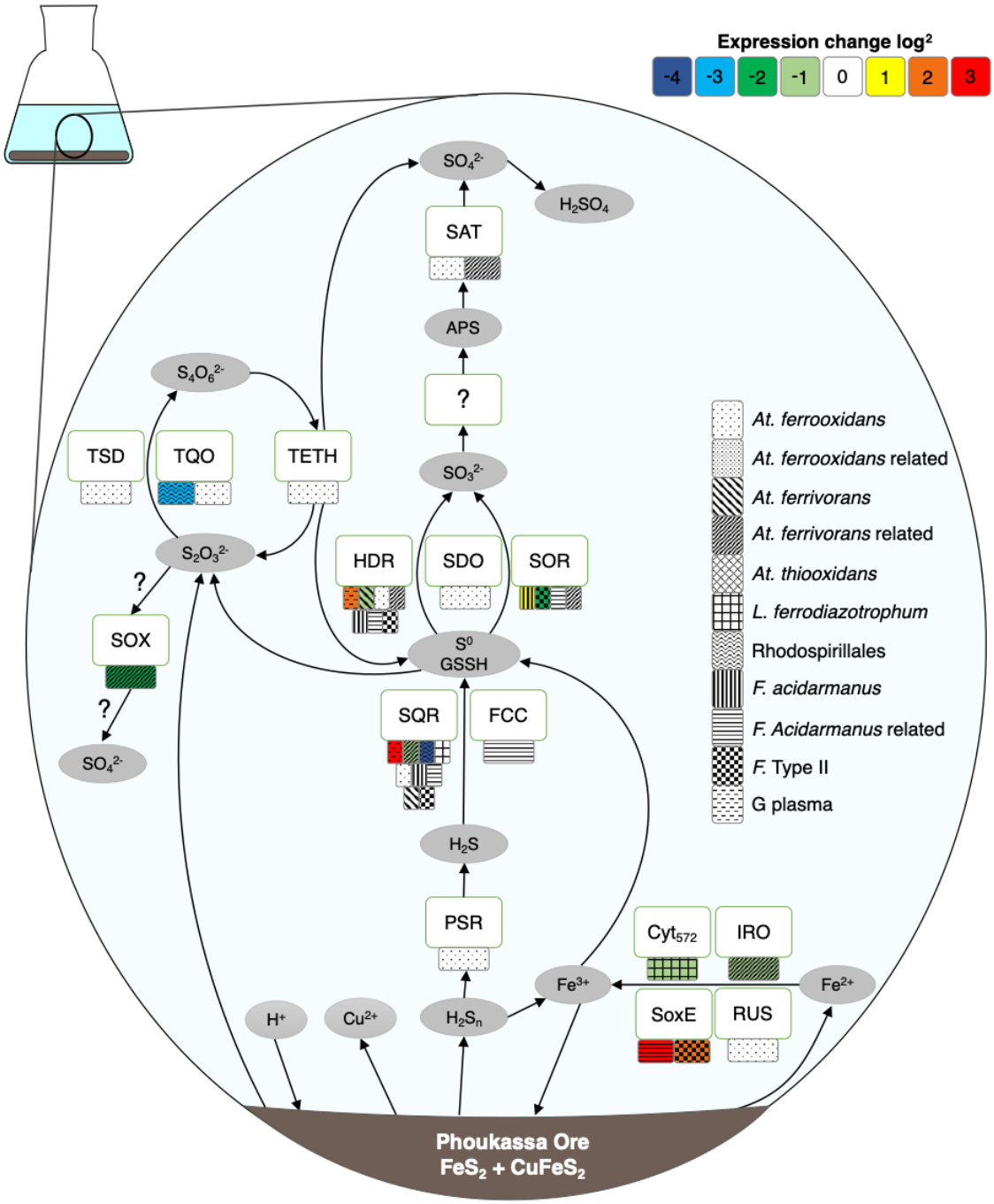

Figure 3.17 - Model of Phoukassa ore dissolution showing significant differences in gene expression between week 8 and week 16 ($p < 0.05$). Positive numbers indicate genes expressed more highly at 16 weeks, negative numbers suggest genes expressed more highly at 8 weeks. Species with white backgrounds show genes that were expressed but no significant difference was found in expression between time points. Genes that are present in species but not expressed are not shown. PSR: polysulfide reductase, SQR: sulfide-quinone reductase, FCC: Flavocytochrome c sulfide dehydrogenase, SOR: sulfur oxygenase reductase, SDO: sulfur dioxygenase, HDR: heterodisulfide reductase, SAT: sulfate adenylyltransferase, TetH: tetrathionate hydrolase, TQO: thiosulfate-quinone oxidoreductase, TSD: thiosulfate dehydrogenase, SOX: sulfur oxidation

pathway, RUS: rusticyanin, SoxE: Sulfocyanin, IRO: high potential iron-sulfur protein, Cyt_{572}: Cytochrome 572.

The bioleaching of the Phoukassa ore is more complex than pure chalcopyrite as it includes chalcopyrite alongside a primary phase of pyrite. As pyrite is acid insoluble, protons do not initiate the attack on this mineral. Instead, pyrite dissolution proceeds via the thiosulfate pathway during which thiosulfate is generated via ferric iron hexahydrate oxidation of the mineral (Schippers and Sand, 1999). This thiosulfate may then be oxidised by TQO (*At. ferrooxidans* and Rhodospirillales) or TSD (*At. ferrooxidans*) to tetrathionate, which can subsequently be disproportionated by *At. ferrooxidans'* TETH to sulfur, thiosulfate, and sulfate. Tetrathionate may also be abiotically hydrolysed to disulfane-monosulfonic acid, which can then be oxidised to trithionate by molecular oxygen or ferric iron, which in turn is hydrolysed to thiosulfate and sulfate (Schippers, Rohwerder and Sand, 1999). Pentathionate and elemental sulfur can also form as intermediary sulfur compounds due to side reactions of disulfane-monosulfonic acid with ferric iron, although the quantity of these products is limited compared to sulfate (Sand *et al.*, 2001; Tu *et al.*, 2017). Pentathionate may additionally be hydrolysed by TETH (De Jong *et al.*, 1997). Elemental sulfur formed via side reactions and tetrathionate disproportionation can be oxidised by the multispecies HDR, SDO (*At. ferrooxidans*) or SOR (*Ferroplasma spp.* and *At. ferrivorans* related). Although the mechanism of sulfite oxidation to APS remains unknown, both *At. ferrooxidans* and the *At. ferrivorans* related strain expressed APS oxidising SAT consistently at 8 and 16 weeks' growth, suggesting that this pathway of oxidation to sulfate was being mediated by microbes. Protons generated by pyrite breakdown can initiate the attack on chalcopyrite breakdown, which can then proceed as outlined in Chapter 2.

3.4 Discussion

3.4.1 The Potential of the SC3 Consortium to Bioleach Low-Grade Ore

This study examined the capability of the SC3 consortium to breakdown a low-grade copper ore derived from its native environment. Geochemical testing found that copper, sulfur and iron availability increased over time both with and without the consortium. This is in line with numerous previous studies that show sulfide ores break down in abiotic conditions, however, breakdown is enhanced in the presence of iron and sulfur oxidising microbes (Garcia, Bigham and Tuovinen, 1995; Bosecker, 1997; Sand *et al.*, 2001; Ma *et al.*, 2019). Overall, this trend was seen in this chapter, with significantly greater iron and sulfur retrieval in the presence of SC3.

Phoukassa ore is comprised of the elements iron, sulfur and copper. Given the increased breakdown of Phoukassa ore indicated by greater iron and sulfur availability in biotic samples, it would be expected that copper would follow the same trend. However, contrary to expectations, copper availability was greater in the abiotic samples than the biotic samples. These findings are in line with a previous study of low grade ore, where increased iron and sulfur release during bioleaching from a low grade ore did not result in a corresponding increase in copper release. The authors suggest this finding is due to copper release being a purely chemical process at low copper percentages (Bostelmann and Southam, 2020).

It is unlikely that this trend in Phoukassa ore is due to greater breakdown of the copper bearing phases in the abiotic samples. Firstly, the copper bearing phases within the mineral are predominantly chalcopyrite, and SC3 was demonstrated to enhance chalcopyrite breakdown in Chapter 2. Secondly, pH was decreasing in biotic samples only, and the regeneration of protons aids chalcopyrite dissolution (Sand *et al.*, 2001; Vera, Schippers

and Sand, 2013). Finally, it is well established that chalcopyrite dissolution is enhanced in the presence of pyrite due to galvanic interactions, and that this effect is greater in the presence of microbes (Berry, Murr and Hiskey, 1978). In line with this, copper retrieval reached above 80% in the biotic samples, indicating notable copper mineral breakdown in the presence of the microbes. Therefore, it is likely that the greater copper availability in the abiotic samples is due to an alternative factor, such as uneven distribution of copper minerals within the Phoukassa ore, owing to its mixed mineral assemblage. Uneven distribution of target minerals within mixed ores is an established feature of low-grade ores (Svetlov *et al.*, 2020; Mohanraj *et al.*, 2022). Indeed, supernatant copper as a percentage of the total available copper in the abiotic samples increased beyond 100%, reaching 101% at week 8 and 133% at week 16. This implies the proportion of copper available differed from that of the ore tested by total dissolution, *i.e.* the small sample quantity used in mineral dissolution tests (3 replicates of 10mg of mineral) likely had a different proportion of copper to the portion of mineral used for the bioleaching tests. Further, the overall proportion of copper in the ore is notably lower than that of iron and sulfur: only 2% of the mineral is copper, compared to 39% and 44% for iron and sulfur, respectively. It is possible, therefore, copper availability in leachate may not be the strongest indicator of overall breakdown for this ore. In support of this concept, iron and sulfur retrieval were significantly higher in the presence of the SC3 consortium. Therefore, overall Phoukassa ore breakdown was higher in the presence of the SC3 consortium. The pH data is in line with this conclusion, as mean pH decreased over time in the biotic samples. This indicates the SC3 microbes facilitated the greater release and oxidation of sulfur to sulfuric acid (Ma *et al.*, 2019).

The pH trend contrasts with the results of the previous chapter, where pH increased in the presence of the SC3 consortium. This finding does, however, fit with the expected mechanism of mineral breakdown: Phoukassa ore is comprised predominantly of pyrite, which is acid insoluble, whereas chalcopyrite is acid soluble and consumes protons

during its initial dissolution (Schippers and Sand, 1999; Vilcáez, Yamada and Inoue, 2009). The difference in acid solubility between the two minerals can also explain the contrast in the total mineral breakdown observed. A greater overall percentage of mineral breakdown was seen in the chalcopyrite of Chapter 2 compared to the Phoukassa ore. As an acid insoluble mineral, the pyrite of the Phoukassa ore requires ferric iron to initiate bioleaching (as detailed in Section 1.5.1), which is not initially present in the medium. Initial breakdown of this mineral therefore progresses slowly until iron is leached out of the mineral and oxidised (Kocaman, Cemek and Edwards, 2016). Conversely, as chalcopyrite is acid soluble, and thus vulnerable to proton attack, mineral breakdown could commence faster than that of pyrite. This is in line with previous findings for microbial chalcopyrite and pyrite dissolution (Kocaman, Cemek and Edwards, 2016). Therefore, where pyrite makes up a large proportion of an ore's mineralogy, bioleaching practitioners may consider adding ferric iron to the bioleaching system to enhance mineral breakdown.

3.4.2 Mechanisms of Phoukassa Ore Bioleaching by the SC3 Consortium

In Chapter 2, the bioleaching mechanism of the SC3 consortium was shown to be driven by the expression of iron and sulfur oxidation associated genes. To examine whether the same genes are involved in the breakdown of a low-grade copper ore, a metatranscriptomics study was conducted.

The metatranscriptomics results showed that as generalised functions, there were no significant differences in the expression of genes associated with iron and sulfur oxidation between the two time points. This suggests that, at a community level, sulfur and iron metabolism is maintained over time during bioleaching. Genes representing every step in the complex sulfur oxidation pathway are expressed at both time points. Therefore, as a whole, the oxidation pathways are similarly active over time. Previous research based on single species found that iron and sulfur oxidation

genes are upregulated in the presence of iron and sulfur (Ramírez *et al.*, 2004; Liljeqvist, Rzhepishevska and Dopson, 2013). However, the results of this chapter show that this upregulation is not seen at a community level over time; overall relative expression of these genes remains constant despite the increasing concentrations of sulfur and iron in the supernatant.

Individual genes within some species were differentially expressed between time points. For example, several of the putative sulfur and iron metabolism genes were significantly more highly expressed in the *Ferroplasma spp.* and G plasma in the second time point. This increase could be as a function of increased relative abundance of these species – the archaea had an overall greater number of reads aligned to them at 16 weeks compared to 8 weeks. Therefore, it is unclear whether this change in expression level is due to changes in relative abundance of these species, or due to upregulation of the genes. However, in either scenario, it would appear that the archaea are playing a larger role in RISC and iron oxidation at the latter stage of Phoukassa ore bioleaching, compared to week 8. As overall sulfur and iron metabolism gene expression at the community level did not increase over time, these findings could be indicative of some degree of shift from bacteria to archaea for these functions. In line with this, the bacterial species of Rhodospirillales and the *At. ferrivorans* related strain downregulated their sulfur oxidation genes at week 16. This is a notable finding, as the archaeal species in the consortium are not generally associated with playing major roles in direct bioleaching. They would not be traditionally added to “created” bioleaching consortia and, in naturally occurring communities, are broadly regarded as predominantly playing an indirect role in community functioning (Baker and Banfield, 2003; Shiers, Collinson and Watling, 2016)

As well as indicating the potential changing roles of individual species during bioleaching, the gene expression results also highlighted the expression of some novel genes. Notably, the elemental sulfur oxidising *hdr* gene identified in G plasma was shown to be expressed at both of the

studied time points. This gene was unidentified in this species prior to this thesis. The presence and expression of *sqr* and *hdr* homologues in this species provides a putative pathway of oxidation from sulfide through to sulfite. In combination with the results of Chapter 2, this offers the first evidence of expression of this sulfur oxidation pathway in this species, and provides evidence that this organism is capable of facilitating more of the sulfur oxidation pathway than ever previously theorised. As it has been previously noted that the *sqr* found in G plasma is genetically distant from *sqr* sequences in other organisms (Jones, Schaperdoth and Macalady, 2014), there is a degree of possibility that G plasma could facilitate even more of the RISC oxidation pathway, utilising additional enzymes that are as yet unidentifiable as being associated with sulfur metabolism. Further work is needed to identify additional sulfur oxidation associated genes in this species, and to establish whether a complete RISC oxidation pathway is present.

To provide a complete picture of Phoukassa ore breakdown mechanisms, sulfur and iron metabolism gene expression data was fitted into a community bioleaching model (Figure 3.17). This model suggested that the mechanism of ore breakdown was likely a hybrid pathway combining the previously described polysulfide and thiosulfate pathways (Schippers and Sand, 1999), leading to the breakdown of the two major mineral components of the ore: pyrite and chalcopyrite. This work represents, for the first time, an evidenced view of the Phoukassa ore breakdown mechanisms.

The metatranscriptomic study also facilitated examination of nitrogen fixation processes that can help to sustain the community. Relative expression of genes associated with nitrogen fixation were upregulated over time at the community level. As a small quantity of fixed nitrogen was provided in the initial growth medium, this finding fits a pattern of gene upregulation over time in response to depletion of initial nitrogen (Marín *et al.*, 2021).

3.4.3 Conclusion

This study fulfilled the outlined aims of the chapter by using geochemical and molecular data to establish the role and mechanism of the SC3 consortium in the dissolution of a low-grade ore found in the consortium's native environment. This study used the first metatranscriptomic dataset of low-grade ore bioleaching to create the first ever model of Phoukassa ore breakdown. Geochemical data showed that ore breakdown was overall significantly greater in the presence of the SC3 bioleaching consortium (H_1). However, an upscaled study is required to confirm enhanced retrieval of copper, due to the uneven distribution and comparatively low quantities of this element within the ore. Genes associated with sulfur and iron oxidation were expressed at both time points when grown on the Phoukassa ore (H_2). Notably, they were not differentially expressed between time points at a community level, however, within species, some up- and down-regulation of these genes was seen (H_3). This shows that while the relative contribution of each species may change, overall bioleaching processes are consistently maintained by the consortium as a whole.

In compliment to the findings of Chapter 2, this study confirms that more species may be playing a direct role in bioleaching than previously thought, and that species may play unexpected roles. In turn, this could have implications for the selection of optimised bioleaching consortia. The metatranscriptomic approach taken was essential to this finding, as it provided a picture of how the community functions as a whole to maintain consistent bioleaching over time. This has never previously been demonstrated, as this chapter's study represents the first whole-community study of iron and sulfur gene expression over time during bioleaching.

Chapter 4 – Characterisation of Trace Elements and Exploration of Bioleaching Potential in Stibnite

4.1 Introduction

4.1.1 General Introduction

The previous results chapters improved the understanding of the mechanisms behind the breakdown of copper sulfide minerals. For copper sulfide minerals, bioleaching is already employed industrially worldwide. However, not all sulfide minerals have been equally studied. For some sulfide minerals, not only is bioleaching not yet commercially exploited, but even the feasibility of bioleaching has not been adequately explored. Stibnite is one such sulfide mineral (Dembele, Akcil and Panda, 2022).

Stibnite is the primary ore of the metalloid antimony. Antimony (Sb) is increasingly in demand for a range of industrial uses, and consequently has high global extraction rates - worldwide antimony production was estimated to be 160,000 tons in 2019 (USGS, 2020). Despite the high extraction rates and economic importance of stibnite, very little is known about the geochemistry of this mineral. Consequently, it is currently unclear whether bioleaching could enhance antimony recovery from stibnite. Additionally, improving the understanding of stibnite dissolution is important because where this process takes place in the environment (*e.g.* in mining spoil heaps), it results in the release of antimony into the environment (Ashley *et al.*, 2003). Antimony exposure has been associated with negative human health impacts such as impaired liver function, pneumoconiosis and gastrointestinal symptoms (Sundar and Chakravarty, 2010; You *et al.*, 2020). It is important therefore to establish the factors affecting the release of antimony from sulfide minerals.

In this chapter, very preliminary trials attempting to establish microbial growth on stibnite were unsuccessful. Therefore, to improve future attempts to explore stibnite bioleaching, a better background characterisation of the mineral is required. Stibnite is poorly studied not just with regards to its breakdown, but also with regards to its geochemical characteristics. Significantly less research has been conducted with regards to stibnite than copper bearing sulfide minerals. Consequently, much of the background information that is available for historically more valuable sulfide minerals (*e.g.* chalcopyrite) is absent in the literature for stibnite. This is a significant gap as geochemical characteristics of minerals are important to their mechanisms of breakdown. For example, the presence of trace elements in minerals has been shown to affect how sulfide minerals break down (Fallon *et al.*, 2019). However, the types and typical concentrations of trace elements in stibnite are one of the key areas where no formal study has previously been conducted. Therefore, this chapter attempts to fill the gaps regarding stibnite characteristics to help provide a background understanding of stibnite on which further dissolution studies can be based.

4.1.2 Stibnite

Stibnite (Sb_2S_3, Fig. 4.1) is an opaque sulfide mineral found in hydrothermal deposits worldwide. Typically made up of 72% antimony, stibnite is commonly mined for this element's retrieval (Schwarz-Schampera, 2014).

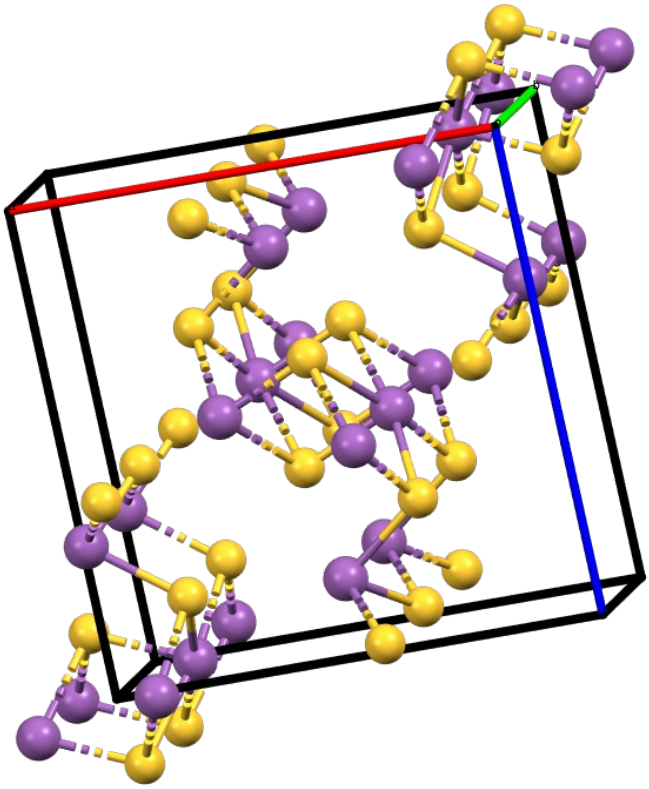

Figure 4.1 – Structure of stibnite created in Mercury (Macrae et al., 2020) based on structural data from (Bayliss and Nowacki, 1972). Purple atoms represent Sb; yellow atoms, S. Bayliss & Nowacki (1972) determined the cell parameters to be: a = 11.31Å, b = 3.84Å, c = 11.23Å, with the structure of stibnite made up of infinite Sb_4S_6 chains parallel to the b axis which form crumpled sheets (two in each unit cell, with interatomic distances between sheets of 3.373 and 3.642 Å). The bonds joining Sb-S were found to be largely covalent.

Antimony is increasingly in demand due to its wide range of applications, which include as a fire retardant, an alloy in lead-acid batteries, and for plastic production (Sundar and Chakravarty, 2010; Belzile, Chen and Filella, 2011). Very pure antimony is also employed for niche electronics uses, such as in semiconductor devices (Cooper and Harrison, 2009). As well as being mined as a target mineral for antimony extraction, stibnite may also be retrieved then discarded as a by-product of precious metal mining (*e.g.* Au, Ag) (Ashley *et al.*, 2003; Schwarz-Schampera, 2014). Due to the increasing mining and disposal of stibnite ores, there is growing

concern regarding the breakdown of this mineral and the concomitant environmental consequences (Filella, Belzile and Chen, 2002). However, due to the very limited previous study of this mineral, there are many notable gaps in relation to our understanding of stibnite. What is currently understood regarding the characteristics of stibnite and its breakdown are discussed in the following Sections (4.1.3 - 4.1.5).

4.1.3 Stibnite Dissolution

Antimony is released from stibnite into the environment when the mineral is exposed to oxidising conditions, *i.e.* when it is mined and lower quality ores are discarded (Wilson *et al.*, 2010; Hiller *et al.*, 2012; M. He *et al.*, 2012). The formal dissolution of stibnite under abiotic conditions, generating acid, is represented by Eq. 4.1, (Biver and Shotyk, 2012b):

$$Sb_2S_3 + 6O_2 + 6H_2O \rightarrow 2Sb(OH)_3 + 32H_2SO_4 \quad \text{(Eq. 4.1)}$$

Although sulfide mineral dissolution at mining sites is typically thought of as an acidic process, in the natural environment, pH may be buffered by the surrounding geology (*e.g.* pH may be elevated if carbonates are present)(Ashley *et al.* 2003). As a result, neutral or alkaline conditions may sometimes prevail, and there is evidence to suggest stibnite breakdown can occur in these conditions. For example, elevated antimony loads have been observed in mine drainage waters with neutral and alkaline pH (Ashley *et al.*, 2003; Klimko *et al.*, 2011). To date, only one study has explored the effect of pH on stibnite dissolution rates, with highest dissolution rates found to be under acid and alkaline conditions, compared to neutral (Biver and Shotyk, 2012b).

4.1.4 Bioleaching Potential of Stibnite

The first paper to demonstrate the potential for stibnite bioleaching used the acidophile *Acidithiobacillus* (then *Thiobacillus*) *ferrooxidans* (Torma

and Gabra, 1977), while an earlier report provided an overall equation of stibnite breakdown by *At. ferrooxidans* within acid mine drainage environments (Eq.4.2, Rossi (1971)):

$Sb_2S_3 + 6O_2 \rightarrow Sb_2(SO_4)_3$ (Eq. 4.2)

In more than four decades since the publication of these studies, very little work has been conducted to further the understanding of stibnite bioleaching. *Acidithiobacillus ferrooxidans* remains the only acidophile confirmed to be capable of mediating stibnite dissolution (Ubaldini *et al.*, 2000). There are only two reports of stibnite bioleaching under non-acidic conditions, where the neutrophiles *Paraccocus versutus* XT0.6 and *Bosea* sp. AS-1 were demonstrated to mediate the dissolution of stibnite under circumneutral conditions (Loni *et al.*, 2020; Xiang *et al.*, 2022). To date, no alkaliphiles have been demonstrated to grow on, or enhance the dissolution of, stibnite. Overall, much remains unknown about the mechanisms of stibnite breakdown with microbes. For example, it is not currently known whether stibnite is acid soluble or insoluble, a notable gap in our understanding of this mineral's geochemistry.

While only a small number of organisms have been confirmed to facilitate stibnite breakdown, a wide range of microbes have been shown to oxidise the element antimony once released from the mineral. These include both acidophiles and neutrophiles (Casiot *et al.*, 2007; Sun *et al.*, 2016; J. Li *et al.*, 2018; Xiang *et al.*, 2022). Current evidence suggests that the greatest effect of the presence of microbes on antimony oxidation is at circumneutral conditions, where antimony oxidation occurs significantly faster compared to abiotic conditions (Leuz and Johnson, 2005; Biver and Shotyk, 2012b; Hamamura, Fukushima and Itai, 2013; Nguyen and Lee, 2015). Whether microbial antimony oxidation has an effect on stibnite breakdown remains unknown, as to date no antimony-oxidation based stibnite breakdown has been identified at any pH.

4.1.5 The Presence of Trace Elements as Impurities in Stibnite

Establishing the quantity and nature of impurities in sulfide minerals is important in determining the environmental impact of their breakdown, as some elements commonly found within sulfide minerals are toxic. Additionally, impurities within minerals, including sulfide minerals, can have an effect on the rate and mechanism of their dissolution (Eisenlohr *et al.*, 1999; Xuehong *et al.*, 2006; Dos Santos *et al.*, 2017; Gartman, Whisman and Hein, 2020). For example, Dutrizac & MacDonald (1973) found that chalcopyrite dissolution could increase or decrease, depending on the type of impurity present. Improving the knowledge base with regards to the impurities in sulfide minerals can therefore be an important first step in understanding factors affecting dissolution.

The current understanding of the types of impurities typically present in stibnite is very limited. There are small number of technical and scientific reports describing the types of elements that are present in specific antimony ore deposits. These elements include: Au, Se, Pb, Fe, Zn, Cu, U, As and Ba (Davidson, 1960; Seal, Bliss and Campbell, 1986; Ashley *et al.*, 2003). Nonetheless, no formal study has yet been conducted examining the types of element present as impurities from stibnites collected from different deposits worldwide, and to date, there has been no study examining the speciation of trace elements in naturally-occurring stibnite. It is known that certain factors can influence the types and quantities of elements found within sulfide minerals, for example, the temperature of mineral formation and the surrounding geology (Pfaff *et al.*, 2011; Tanner *et al.*, 2016; Grant *et al.*, 2018). Therefore, these categorisations should be considered when examining trace elements in stibnite.

4.1.6 Hypotheses Formation

Based on the information in this introduction, the following hypotheses were formed and tested in this chapter:

H_1 - Acidophilic and neutrophilic bacteria will facilitate stibnite breakdown by oxidising sulfur or antimony
H_2 - All stibnites will contain a range of elements as impurities
H_3 - Greater quantities of trace elements will be present in stibnites formed at higher temperatures compared to lower temperatures
H_4 - The trace element profile of the stibnites will vary depending on host rock
H_5 - Selenium substitutes for sulfur within the structure of stibnite

To summarise how these hypotheses were reached:

H_1 – Neutrophiles and acidophiles have both been previously demonstrated to facilitate stibnite breakdown (Section 4.1.4).
The acidophilic SC3 consortium has been demonstrated in this thesis to mediate sulfide mineral dissolution and to possess sulfur oxidising genes. Consequently, it is hypothesised that this consortium will mediate stibnite breakdown through sulfur oxidation, as theorised previously for *At. ferrooxidans* (Torma and Gabra, 1977).
One of the neutrophilic bacteria used in this chapter, NT-26, has been previously shown to oxidise arsenic for energy generation (Santini *et al.*, 2000; Andres *et al.*, 2013). Arsenic and antimony share similar chemical properties (Liu *et al.*, 2010), arsenic oxidisers and arsenite oxidase have been shown to oxidise antimony (Wang *et al.*, 2015). It is possible therefore that this arsenic oxidising microbe could oxidise antimony, and consequently facilitate stibnite breakdown.

H_2 - Sulfide minerals typically contain impurities in the form of minor or trace elements, as inclusions or within the mineral lattice (Fontboté *et al.*, 2017).

H_3 -The temperature at which sulfide minerals form has been shown to affect quantities of trace elements within minerals (Wang *et al.*, 2017), with sulfide mineral deposits that form at higher temperatures typically contain higher concentrations of elements (Metz and Trefry, 2000; Fontboté *et al.*, 2017).

H_4 - The geology surrounding the mineral, *i.e.* the "host rocks" have been shown to affect trace element characteristics in sulfide minerals .

H_5 – Results of the initial geochemical analyses indicated that selenium was consistently present as a trace element in stibnite. Selenium substitution for sulfur has been demonstrated in synthetic stibnite (Kyono, Hayakawa and Horiki, 2015). It is possible therefore that selenium can fit within the mineral lattice of naturally occurring stibnite by replacing antimony.

4.1.7 Aims and Objectives

The aims of this chapter were to improve the understanding of stibnite geochemistry and potential for microbial breakdown. An initial objective of this chapter was to establish whether neutrophilic and/or acidophilic microbes could mediate stibnite dissolution and then to determine the mechanism of microbial stibnite dissolution. Initial trials indicated that the trialled organisms did not grow on stibnite under the tested range of conditions. Consequently, it was determined that a better background characterisation of the mineral is required to understand the geochemical factors that could affect mineral breakdown, which could improve future attempts to explore stibnite bioleaching. Therefore the following objectives

were set out to improve the overall geochemical characterisation of stibnite:

1. To use a range of analytical techniques to determine which elements, at what quantities, are present as impurities in stibnite.
2. To use WDS mapping and μXRF to assess whether there is zonation of trace elements in stibnite.
3. To analyse whether there are differences in the type or quantity of trace elements based on the type of deposit the stibnites originated from, or the type of rock the stibnites were hosted in.
4. Utilise μXANES to investigate the speciation state of Se in stibnite.

4.2 Materials and Methods

4.2.1 Experimental Overview

Previous study of stibnite has been extremely limited, with many gaps remaining regarding both this mineral's geochemical characterisation and its viability as a substrate for bioleaching. An experimental plan was designed that would improve the overall understanding of stibnite, test the outlined hypotheses and meet the aims and objectives of this chapter. Preliminary trials were set up to examine if microbial growth could be established and whether neutrophiles and/or acidophiles could facilitate mineral breakdown. As these trials did not indicate microbial growth on stibnite, focus was placed on improving the background understanding of stibnite geochemistry, which could help inform future dissolution studies. A series of geochemical analyses were conducted to characterise a range of stibnites derived from diverse deposits across the globe and the types and quantities of trace elements present within them. Further detail on the analyses conducted is provided in the following sections.

4.2.2 Preliminary Microbial Growth Trials on Stibnite

In an attempt to establish whether sulfur oxidising microbes could grow on stibnite, and the effect this would have on the dissolution of the mineral, two preliminary growth trials were set up, one with the acidophilic SC3 consortium, and one with neutrophile strains. As optimum growth conditions have not been previously established for this mineral, a number of different parameters were tested to explore if growth and stibnite dissolution could be established. As no alkaliphiles have yet been demonstrated to oxidise antimony or to mediate the dissolution of stibnite, acidophilic and neutrophilic microbes were trialled in this chapter.

4.2.2.1 Acidophilic Growth Trials on Stibnite

The acidophilic microbes selected for growth trials were the SC3 consortium described in Section 1.8.1, and used in bioleaching experiments in Chapters 2 and 3. These organisms were selected due to their known sulfur oxidation abilities and well documented ability to break sulfide minerals down in acidic conditions. An *Acidithiobacillus ferrooxidans* isolate was also trialled, as this species had been previously suggested to contribute to the dissolution of stibnite (Torma and Gabra, 1977; Ubaldini *et al.*, 2000).

Several environmentally relevant stibnites obtained from currently active mine sites were trialled for suitability as a growth substrate for the acidophiles. The stibnites were samples Stb 6, Stb 7 and Stb 8 (mineralogical data listed in Section 4.2.3). These stibnites were selected in line with the previous studies of acidophile growth on stibnite which have both been conducted on stibnites derived from mine sites (Torma and Gabra, 1977; Ubaldini *et al.*, 2000).

An *At. ferrooxidans* isolate grown on an iron medium and the acidophilic SC3 consortium were used as the inocula for stibnite growth trials. These

inocula (5% v/v) were transferred to McCartney bottles containing 10ml minimal acid medium (MAM, as listed in Section 2.2.2) and 0.25g of stibnite samples 6, 7 or 8. This is in line with numerous recent bioleaching studies where the mineral is typically added at between 1-3% wt/vol (He *et al.*, 2010, 2014; Yu *et al.*, 2011; Buetti-Dinh *et al.*, 2020). This set up was repeated three times. All biotic samples were then incubated alongside abiotic controls at 28°C without shaking for up to 8 weeks.

In each attempt, after 4 and 8 weeks growth, a 20µl sub-sample of each sample was viewed at 400x magnification under a Leica DM 2500 LED optical microscope (Leica Microsystems GmbH, Wetzlar, Germany). In every attempt, at 4 and 8 weeks incubation no, or <5 cells per view were seen in any sample, compared to hundreds of cells per view in the inocula. Additionally, pH was measured at 4 and 8 weeks using MilliporeSigma MColorpHast pH indicator strips (Merck KGaA, Darmstadt, Germany) and pH did not change from the initial ~pH 1.5 in any sample over this period. Therefore, it was determined that growth on stibnite could not be established with these organisms. Consequently, the original experimental plan could not be followed. Had these growth attempts been successful, a full scale experiment would have been set up in line with those of Chapter 3 to explore the effect of the SC3 on stibnite dissolution and the expression of sulfur related genes in the consortium during growth on a mineral that lacks iron.

4.2.2.2 Neutrophilic growth trials on stibnite

The neutrophilic microbes selected for growth trials were the strains “NT-24” and “NT-26” (now *Pseudorhizobium banfieldiae* (Lassalle *et al.*, 2021), which had been isolated from a mine environment (Granites Goldmine, North West Territory, Australia) (Santini *et al.*, 2000). NT-26 is a known sulfur and arsenite oxidiser (Andres *et al.*, 2013). NT-24 is an unpublished *Comamonas* species which oxidises sulfur (J. Santini, Pers. Comm., 2017, confirmed 2022). This strain was therefore included to examine whether

sulfur oxidation could facilitate mineral breakdown at neutral pH. Both strains can grow autotrophically (Ibid).

It has been suggested that antimony and arsenic oxidation could share biogeochemical oxidation pathways in microbes (Terry *et al.*, 2015; Li *et al.*, 2017). Therefore, these organisms were trialled to examine whether they were capable of facilitating stibnite breakdown via antimony or sulfur oxidation.

In this trial, laboratory grade stibnite was used to ensure that neutrophiles were growing on stibnite only. This conservative approach was taken as at the time of designing this experiment, no neutrophiles had been demonstrated to grow on stibnite. In the time since the research in this thesis was carried out, two neutrophilic studies of microbial growth on stibnite have been conducted, which also utilise laboratory grade stibnite for dissolution experiments, in line with the methodology of this chapter (Loni *et al.*, 2020; Xiang *et al.*, 2022).

Microbes were cultivated in line with previous work on these strains (Andres *et al.*, 2013). Microbes grown in 0.04% yeast extract and minimal salts medium (MSM, Table 4.1, below) aseptically transferred daily (1% inoculum). Transfers were carried out by pipetting 1% of the previous culture into a new sterile bottle of media. Once steady growth was established, bacteria were transferred to 0.004% yeast extract (1% inoculum) + MSM to acclimatise them to lower amounts of organic substrate. After several transfers at this concentration of yeast extract, bacteria were transferred to an inorganic MSM (5% inoculum), with 10mM thiosulfate as the electron donor. A minimum of 6 inorganic transfers occurred before transferring to the mineral without any additional electron donors. The bacteria (1% inoculum) were then transferred to McCartney bottles containing 0.2g autoclaved laboratory grade stibnite, ground and sieved to leave the 200-500um fraction, and 10ml MSM (aseptically created and transferred to the sterilised bottle containing the mineral).

Samples were incubated alongside abiotic controls at 28ºC without shaking.

Table 4.1 – Minimal Salts Medium (Santini *et al.*, 2000)

Reagent	**Concentration**
$Na_2SO_4 \cdot 10H_2O$	0.7 g L^{-1}
KH_2PO_4	0.17 g L^{-1}
$MgCl_2 \cdot 6H_2O$	0.04 g L^{-1}
KCL	0.05 g L^{-1}
$CaCl_2 \cdot 2H_2O$	0.05 g L^{-1}
KNO_3	0.15 g L^{-1}
$(NH_4)_2SO_4$	0.1 g L^{-1}
$NaHCO_3$	0.05 g L^{-1}
Trace elements SL8 containing W & Se (Macy *et al.*, 1996)	1ml L^{-1}

At all stages, bacterial samples were checked periodically for purity by transferring a small amount (20µl) onto an LB plate and incubating for 24-48 hours. Samples were viewed under an optical microscope as described in Section 4.2.2.1. Small numbers of cells (<20 per view) were visible at weeks 2 and 4. Samples were analysed for pH once per fortnight, assessed using MilliporeSigma MColorpHast pH indicator strips (Merck KGaA, Darmstadt, Germany). Quantities of antimony and sulfur in supernatant samples over time were analysed using ICP-OES as described in Section 2.2.7, to establish whether stibnite had been broken down in biotic and abiotic samples.

4.2.3 Stibnite Characterisation Study

Stibnite samples collected from around the world were examined using a range of analyses to establish the presence, quantity, zonation and speciation of trace elements. Phase identity was confirmed for a

subsection of the stibnites using PXRD; the micro-analytical techniques of EPMA (WDS) and LA-ICP-MS were used to identify trace elements and confirm whether any zonation of trace elements was present; speciation of Se in the samples was established using XANES. These methods are explained in detail in Sections 4.2.3.1-4.2.3.6, below.

4.2.3.1 Stibnite Collection and Sample Preparation

Table 4.2, below shows a list of all the stibnite samples (total number: 34), including the geographic location they were collected and their source. Further information on the samples is included in Appendix VII.

Table 4.2 – Stibnite Samples and Origins

Sample ID	**Location of origin**	**Source**
Stb 1	Medas, Portugal	Private seller
Stb 2	Knipes Mine, Scotland	Private seller
Stb 3	Su-Suergiu-Martalai, Sardinia	Private seller
Stb 4	Bau Mine, Malaysia	Private seller
Stb 5	Les Biards Mine, France	Private seller
Stb 6	Reefton, NZ	Private mine contact
Stb 7	Xiknangshan XKS Mine, Hunan Province	Private mine contact
Stb 8	Xiknangshan XKS Mine, Hunan Province	Private mine contact
Stb 9	Hillgrove, NSW, Australia	Smithsonian, DC, USA
Stb 10	Black Warrior Mine, AZ, USA	Private collector
Stb 11	Hampton Mine, UT, USA	Private collector
Stb 12	Bajuz Mine, Romania	Private collector
Stb 13	Red Devil Mine, AK, USA	Smithsonian, DC, USA

Stb 14	Antimony Peak, San Benito County, CA, USA	Smithsonian, DC, USA
Stb 15	Isle of Pines, Cuba	Smithsonian, DC, USA
Stb 16	Caspari-Zeche, Arnsberg, Germany	Smithsonian, DC, USA
Stb 17	Boccheggiano, Tuscany, Italy	Smithsonian, DC, USA
Stb 18	Echinokawa Mine, Near Saijo, Ehime, Japan	Smithsonian, DC, USA
Stb 19	Estado de San Luis Potosi, Mexico	Smithsonian, DC, USA
Stb 20	Manhattan, Nye County, NV, USA	Smithsonian, DC, USA
Stb 21	Kremnica, Stredne Slovensko, Slovakia	Smithsonian, DC, USA
Stb 22	Asturias, Spain	NHM*, London, UK
Stb 23	“Busoh, India”**	NHM, London, UK
Stb 24	Rawdon, Hants Co., Nova Scotia, Canada	NHM, London, UK
Stb 25	Clontibret mine, Co. Monaghan, Ireland	NHM, London, UK
Stb 26	San Antonio de Esquilache mine, Puno, Peru	NHM, London, UK
Stb 27	Stolica mine, Podrinje, Krupanj, Serbia	NHM, London, UK
Stb 28	Lucette mines, Le Genest, Mayenne, France	NHM, London, UK
Stb 29	Sherwood siding, Gwelo, Zimbabwe	NHM, London, UK
Stb 30	Alcacoya mine, San Vincente Prov., Bolivia	NHM, London, UK

Stb 31	[Berndorf, Lower Austria] ***	NHM, London, UK
Stb 32	San Martin mine, Zacatecas, Mexico	NHM, London, UK
Stb 33	Montauto, Grosseto, Toscana, Italy	NHM, London, UK
Stb 34	Niarbyl trial, Traie Vrish, Isle of Man	NHM, London, UK

* Natural History Museum.

** NHM historic labelling, Busoh does not exist in India. There is a Busoh in Indonesia. No records can be found of an antimony mine in this region, but gold-mining from sulfide deposits is known.

*** Probable location.

Upon receipt, each stibnite was photographed to retain visual mineralogical information (see Appendix VIII). For samples where a larger quantity of material was available (Stb 1-8, *i.e.* those not obtained from museums or private collections), subsamples were removed with a hammer. As far as possible, gangue material (non-stibnite mineral *e.g.* quartz) was manually excluded. Part of these subsamples were ground and sieved to <200μm for XRD analysis. As Stb 9-34 had been sampled from museum and private collections, only a very small amount of material was available, hence the whole sample was mounted for LA-ICP-MS and EPMA analysis. Each sample was mounted in resin and a thin section was polished and mounted on a glass slide by Vancouver Petrographics Ltd (Langley, BC, Canada). Samples were categorised by both deposit type: epithermal (14) or mesothermal (7); and host rock: granites (6), greywackes-phyllites (5), carbonates-limestones (11). For some samples, no information could be obtained about their deposit of origin.

The types, quantities and distribution of the elements present is a function of the prevalent physical and geochemical conditions during formation (Fu *et al.*, 2020). Stibnite samples were therefore categorised by deposit type (*i.e.* formation conditions) and host rock surrounding deposits. The most common host rocks for stibnite deposits are sedimentary and meta-sedimentary rocks such as limestone, calcareous shales, sandstone; or

granitic terranes (Seal, Bliss and Campbell, 1986; Bliss and Orris, 1989). Additional surrounding geology can include phyllites (Ibid). Mesothermal stibnite veins predominantly form under moderate pressure in the temperature range of 250 to 350ºC (Pirajno, 1992). Epithermal deposits have been generally agreed to form under medium pressure, at temperatures in the range of 160 to 270ºC (Hedenquist, Arribas and Gonzalez-Urien, 2000).

4.2.3.2 Powder X-ray Diffraction (PXRD)

Stibnite samples 1-8 were analysed with PXRD to confirm their identities. In order to conduct this analysis, a sample of the mineral was ground and sieved to < 200 μm. PXRD was carried out using a Stoe Stadi-P Mo diffractometer (Stoe & Cie GmbH, Darmstadt, Germany), with operating conditions of 2θ=2°-40°, 0.5 step, 5 s count time per step. The resulting diffraction patterns were analysed using DIFFRAC.SUITE EVA v3.1 (Bruker, Germany), and phase identification was achieved using the International Centre for Diffraction Data PDF database (Gates-Rector and Blanton, 2019).

4.2.3.3 Electron Probe Micro Analysis (EPMA)

All stibnite samples were analysed using EPMA. EPMA has been used in numerous previous mineral composition studies, including to examine trace and minor elements in sulfide minerals (Huston *et al.*, 1995; Desborough *et al.*, 2010; Marques de Sá, Noronha and Ferreira da Silva, 2014).

For each sample in this chapter's study, one site was selected at random and analysed by energy dispersive spectroscopy (EDS), using the Oxford Instrument Inca system (Oxford Instruments Plc., Abingdon, UK). This

allowed qualitative identification of minor elements present within the stibnite. Ten sites were then selected at random per sample and analysed by wavelength dispersive spectroscopy (WDS), using a JEOL 8100 Superprobe (JEOL Ltd., Tokyo, Japan; accelerating voltage 15 kV, 2.5 mA current, beam diameter 1 μm, counting time 20s on peaks and 10s on high and low backgrounds), to allow quantification of the trace elements identified by WDS. The elements analysed by WDS were: O, Al, Sb, S, Si, As, Fe, Se, Cu, Zn, Au, Ag, Pd, Pb, Mo, W. Additionally, ~400 μm^2 WDS maps were used to identify any possible chemical zonation within a subset of the stibnite samples, no obvious zonation was seen (Appendix XI). All data were normalised to 100%. The data for stibnite 14 had four points with very low values for Sb and S, indicating that these samples had not been taken from stibnite grains. These points were therefore removed from the dataset.

4.2.3.4 Laser Inductively Coupled Plasma Mass Spectrometry (LA-ICP-MS)

Laser ablation inductively coupled mass spectrometry (LA-ICP-MS) is a rapid and accurate method of element analysis, that has been used to establish trace element concentrations in a wide variety of minerals, including sulfide minerals (Belousova *et al.*, 2002; Cook *et al.*, 2009, 2011; George *et al.*, 2015; Wang *et al.*, 2017). LA-ICP-MS instruments can determine quantities of trace elements at lower concentrations in minerals than is possible using EPMA (lower limits approaching parts per billion (ppb) concentrations, compared to parts per million (ppm) for EPMA-WDS (Cook *et al.*, 2011; Batanova, Sobolev and Magnin, 2018)). Therefore, after establishing a baseline and any elements present at larger quantities using EPMA, many studies follow up with LA-ICP-MS analysis, to provide finer detail (*e.g.* Belissont *et al.*, 2014; Cook *et al.*, 2015).

In work undertaken (by me) at the School of Earth and Ocean Sciences, Cardiff University, 15 of the stibnite samples were analysed using a New

Wave Research P213 laser ablation system (Elemental Scientific, Portland, OR, USA) attached to a Thermo X Series ICP-MS (Thermo Fisher Scientific, Inc., Waltham, MA, USA). Three points were analysed per sample. Samples were analysed in time-resolved mode using a spot diameter of 55 μm and 80 μm (depending on grain size) with a frequency of 10 Hz. Acquisition lasted 45s and a gas blank was measured for 20s prior to the start of analysis. ^{33}S was used as an internal standard for all analyses and subtraction of gas blanks and internal standard corrections were performed using Thermo Plasmalab software (Prichard et al., 2013). The isotopes analysed were: ^{57}Fe, ^{59}Co, ^{61}Ni, ^{65}Cu, ^{66}Zn, ^{75}As, ^{77}Se, ^{95}Mo, ^{99}Ru, ^{101}Ru, ^{103} Rh, ^{105}Pd, ^{106}Pd, ^{108}Pd, ^{109}Ag, ^{111}Cd, ^{121}Sb, ^{125}Te, ^{185}Re, ^{189}Os, ^{195}Pt, ^{197}Au, ^{206}Pb, ^{209}Bi.

LA-ICP-MS data contained some data points below the detection limit (the detection limit (D.L.) was variable from element to element). In light of this, in order the ensure that data trends were accurate, all statistical testing was carried out with data points below D.L. set to zero and then repeated with these data points set to the D.L. No differences in results of statistical tests were observed between the two treatments of the data. The data presented in this thesis is with the points in question treated as zero.

4.2.3.5 μXRF and X-ray Absorption Near Edge Structure (XANES)

Microfocus X-ray fluorescence (μXRF) is a method that allows analysing very small sample areas for trace quantities of elements. Due to small spatial resolution, micro XRF can pick up much smaller features on a sample than conventional XRF. The technique can be used to create detailed trace element maps of sulfide mineral surfaces (Courtin-Nomade *et al.*, 2009; Cook *et al.*, 2015)

X-ray absorption near-edge structure (μXANES) is a type of inner shell spectroscopy that involves using photon energy interacting with a deep-core electron to determine XANES. This technique is well established as

a method of determining the speciation of impurities within minerals, including sulfide minerals (Simon *et al.*, 1999; Savage *et al.*, 2000; Cook *et al.*, 2012). Determining the speciation state of trace elements within a mineral can help to establish which elements they may be substituting for within the crystal structure, and consequently improve our understanding of factors that could facilitate mineral breakdown.

To determine the zonation of trace elements and speciation of Se in a subset of stibnite samples, μXRF mapping (Stb 1, 7, 12, 14, 16, 18) and μXANES mapping (Stb 1, 7, 14, 16) was carried out on I18 beamline at Diamond Light Source Synchotron Facility (Didcot, UK). For two of the samples, Stb 12 and 18, μXRF maps were carried out, however as no notable areas of Se could be established, μXANES maps were not pursued.

The data were collected with the beamline in fluorescence mode, with a spot size of 2μm x 3.5μm, and exposure time of 0.05 sec per point for μXRF. The standards used were: sodium selenite pentahydrate (+4), sodium selenate anhydrous (+6), selenium sulfide (+4), elemental Se shot (0). Further information on the standards, as well as a full summary of beam energies and scans carried out is available in Appendix IX. Data analysis and map visualisations were carried out with DAWN ('Data Analysis Workbench') (Basham *et al.*, 2015) for μXRF. Data from XANES analyses were extracted and normalised in Mantis ('Multivariate data analysis for spectromicroscopy') (Lerotic *et al.*, 2014).

4.2.3.6 Statistical Analysis

Statistical analysis of data and production of graphs was conducted using R version 3.4.3 (R Core Team, 2017) in R studio version 1.1.423 (RStudio Team, 2016), using packages: "ggplot2" (Wickham, 2016), "ggpubr" (Kassambara, 2018), "forcats" (Wickham, 2019), "dplyr" (Wickham *et al.*,

2019), “effectsize” (Ben-Shachar, Makowski and Lüdecke, 2020), “reshape2” (Wickham, 2007) and “picante” (Kembel *et al.*, 2010).

Data distributions were tested for normality using Shapiro-Wilk tests, and were found not to be normally distributed ($P<0.01$). Consequently, non-parametric statistical tests were employed to ascertain the significance of results. Kruskal-Wallis analysis of variance testing and Mann-Whitney U testing were used to establish differences between host rock and deposit types, respectively. Pairwise correlations between elements were explored first visually with the creation of pairwise plot matrices, then tested for significance using Spearman correlation testing.

4.3 Results

4.3.1 Bacterial Growth Trials

4.3.1.1 Acidophile Trials

Experiments with acidophiles could not be set up as growth of *At. ferrooxidans* isolates or the SC3 consortium could not be established in any of the stibnites. Therefore, it was determined that the original experimental plan could not be followed and no data was obtained.

4.3.1.2 Neutrophile Trials

Following two weeks’ growth, pH values for the samples were consistent across biotic and abiotic samples. After a further 2 weeks growth, pH had decreased slightly in the abiotic sample and for NT-26 (Table 4.3).

Table 4.3 - pH values during growth on stibnite

Time	0 weeks	2 weeks	4 weeks
Abiotic Sb_2S_3	8	8	7.5
NT-26 Sb_2S_3	8	8	7.5
NT-24 Sb_2S_3	8	8	8

Table 4.4 – ICP-OES data concentrations of S and Sb in biotic and abiotic samples after 4 weeks growth on stibnite, at 0 time values were below detection limit (<D.L.)

Sample	Sb (mM) 4 weeks	S (mM) 4 weeks
Abiotic Sb_2S_3	0.55	1.32
NT-26 Sb_2S_3	0.46	4.21
NT-24 Sb_2S_3	0.52	<D.L.

It has been noted that sulfur may not be a reliable indicator of quantity of stibnite dissolution, as sulfur precipitates may form on the mineral surface and some S may be lost as gaseous H_2S, instead Sb should be used as the core measure of stibnite dissolution (Biver and Shotyk, 2012b, 2012a), and indeed is used as the sole measure of stibnite breakdown in the only studies of neutrophilic stibnite bioleaching (Loni *et al.*, 2020; Xiang *et al.*, 2022). There was a similar, or slightly lower, concentration of antimony in biotic compared to abiotic samples, indicating that microbes did not enhance mineral breakdown (Table 4.4). As the geochemical data indicated that the bacteria were not contributing to stibnite dissolution, neutrophilic trials were ended.

4.3.2 Confirmation of Mineral Identity

To confirm that the mineral samples studied were stibnite, pXRD, a technique that identifies unique minerals (or “phases”), was employed.

Diffraction patterns for samples Stb 1-8 can be found in Appendix X. As shown in Table 4.5, below, the major phases for all the samples analysed were stibnite and quartz.

Table 4.5 – major phases in each of the stibnite samples, with PDF database identifiers

Stb	**Phase 1**	**Phase 2**
1	00-046-1045 Si O_2 Quartz, syn	00-042-1393 Sb_2S_3 Stibnite
2	00-042-1393 Sb_2S_3 Stibnite	00-046-1045 Si O_2 Quartz, syn
3	00-042-1393 Sb_2S_3 Stibnite	00-046-1045 Si O_2 Quartz, syn
4	00-042-1393 Sb_2S_3 Stibnite	00-046-1045 Si O_2 Quartz, syn
5	00-046-1045 Si O_2 Quartz low, syn	00-042-1393 Sb_2S_3 Stibnite
6	01-079-1910 Si O_2 Quartz, syn	00-042-1393 Sb_2S_3 Stibnite
7	00-042-1393 Sb_2S_3 Stibnite	00-046-1045 Si O_2 Quartz, syn
8	00-042-1393 Sb_2S_3 Stibnite	00-46-1045 Si O_2 Quartz, syn

4.3.3 Quantification of Trace Elements via Electron Probe Micro Analysis - Wavelength Dispersive Spectroscopy (EPMA-WDS)

Across all 34 samples, the mean percentages of the two major elements, Sb and S, were highly consistent (Fig 4.2, below). The notable exception is Stb 5, where mean sulfur is recorded as is 13.45% ($\pm$ 5.08). This notably lower mean has been attributed to 4 analysis points for Stb 5 having values of 0.01 - 0.02%; the remaining analysis points for sample 5 had values between 26.41 and 27.29%, in line with the other stibnite samples analysed (*i.e.*, these samples were likely sampled in gangue material as opposed to the stibnite phase). The S values for the remaining samples ranged between 23.79 - 35.96%, with a median value of 27.53%, in line with theoretical/reported values for stibnite. The range for Sb across all samples was 62.4 - 75.88%, with a median value of 70.75%, in line with reported/theoretical values for stibnite (Kadıoğlu *et al.*, 2009).

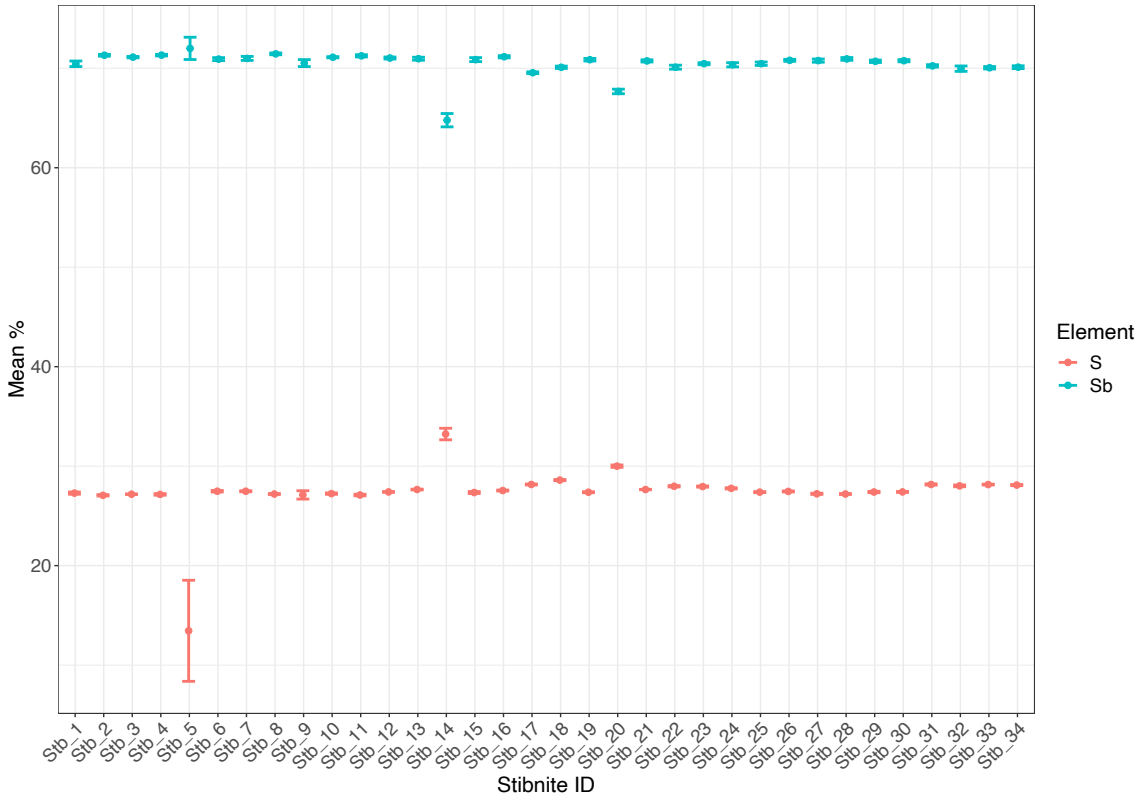

Figure 4.2 – WDS Mean and Standard Error of Sb and S percentages in stibnite samples

As well as Sb and S, a further 16 elements were analysed using WDS, of which 7 were found to be present at trace element quantities: Ag, Au, Mo, Pb, Pd, Se and Zn (Fig 4.3). Across all stibnite samples, trace elements were present at average percentages of Au (0.46%), Mo (0.42%), Se (0.35%), Pb (0.08%), Zn (0.02%), Pd (0.008%), Ag (0.005%).

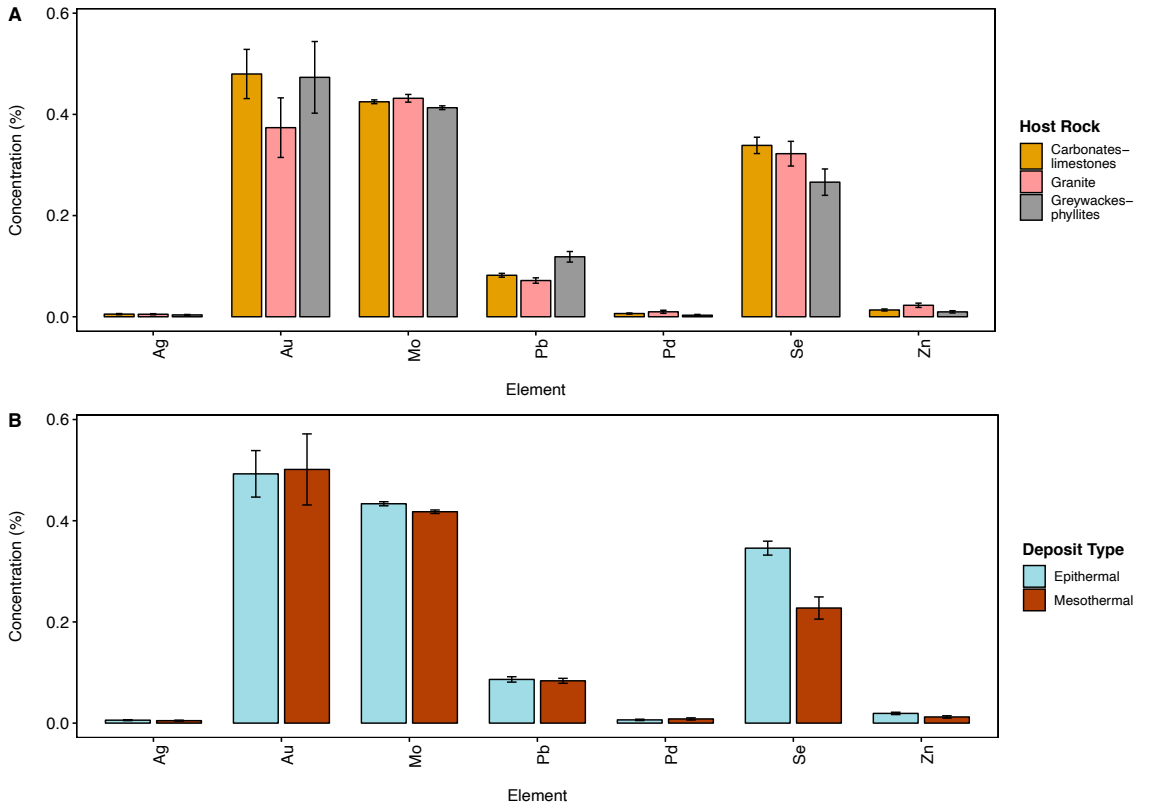

Figure 4.3 - Mean concentration (%) of trace elements in stibnites split by host rock (a), and deposit type (b) as analysed by WDS. Error bars show standard error of mean.

Significant differences between different deposit types were found for Mo ($p=0.02$) and Se ($p<0.01$). Significant differences were found between all host rock types for Pd ($p=0.04$). Pairwise follow-up tests found significant differences between greywacke-phyllites and carbonates-limestones for this element. Pairwise follow-up testing also identified significant differences for Pb and Se values between greywacke-phyllites and carbonates-limestones ($p<0.01$); and for Pb values between greywacke-phyllites and granite ($p<0.01$). Correlation testing via Spearman testing of WDS data from all stibnite samples found that the strongest correlation of elements was a negative association between Au and Sb (-0.56, $p<0.01$). The WDS data suggested that there was a strong negative correlation between gold and antimony in the mesothermal deposits (-0.77, $p<0.01$).

4.3.4 Quantification of Trace Elements via Laser Inductively Coupled Plasma Mass Spectrometry (LA-ICP-MS)

Of the twenty-four isotopes measured by LA-ICP-MS analysis, eight were found to be present at trace element quantities (*i.e.* below 0.1%): ^{109}Ag, ^{197}Au, ^{209}Bi, ^{125}Te, ^{75}As, ^{206}Pb, ^{77}Se, ^{66}Zn. Mean concentrations of these trace elements are shown in Fig. 4.4, below. Antimony was found to have a mean concentration of 71.2% (±1.66 st. dev), in line with the stoichiometric values for stibnite (Kadıoğlu *et al.*, 2009). Measurements for each of the remaining 15 isotopes (^{57}Fe, ^{59}Co, ^{61}Ni, ^{65}Cu, ^{95}Mo, ^{99}Ru, ^{101}Ru, ^{103} Rh, ^{105}Pd, ^{106}Pd, ^{108}Pd, ^{111}Cd, ^{185}Re, ^{189}Os, ^{195}Pt) were all, or predominantly, below the detection limit.

Significant differences were found within concentrations of Ag, Pb and Bi (Kruskal-Wallis $p=0.02,<0.01,<0.01$, respectively) that were dependent on the rock types within which the minerals were hosted. Ag was notably higher in samples with host rocks of granites and greywackes-phyllites compared to carbonates-limestones. Post-hoc pairwise Mann-Whitney U tests were performed to establish which pairs were significantly different to one another. This established that there were significant differences in Ag concentrations between stibnites hosted in granite versus carbonates-limestones ($p=0.01$), and in Pb concentrations for greywackes-phyllites versus carbonates-limestones ($p<0.01$). Bi was determined to be present in significantly higher concentrations in samples hosted in greywackes-phyllites to both carbonates-limestones ($p=0.02$) and granite ($p=0.03$).

Differences in element concentrations between deposit types were established using Mann-Whitney-U testing. Ag was determined to be present in significantly higher quantities in epithermal compared to mesothermal deposits ($p<0.01$). Se, As and Te were also present in higher quantities in epithermal deposits, however this difference could not be established as significant using the employed non-parametric tests.

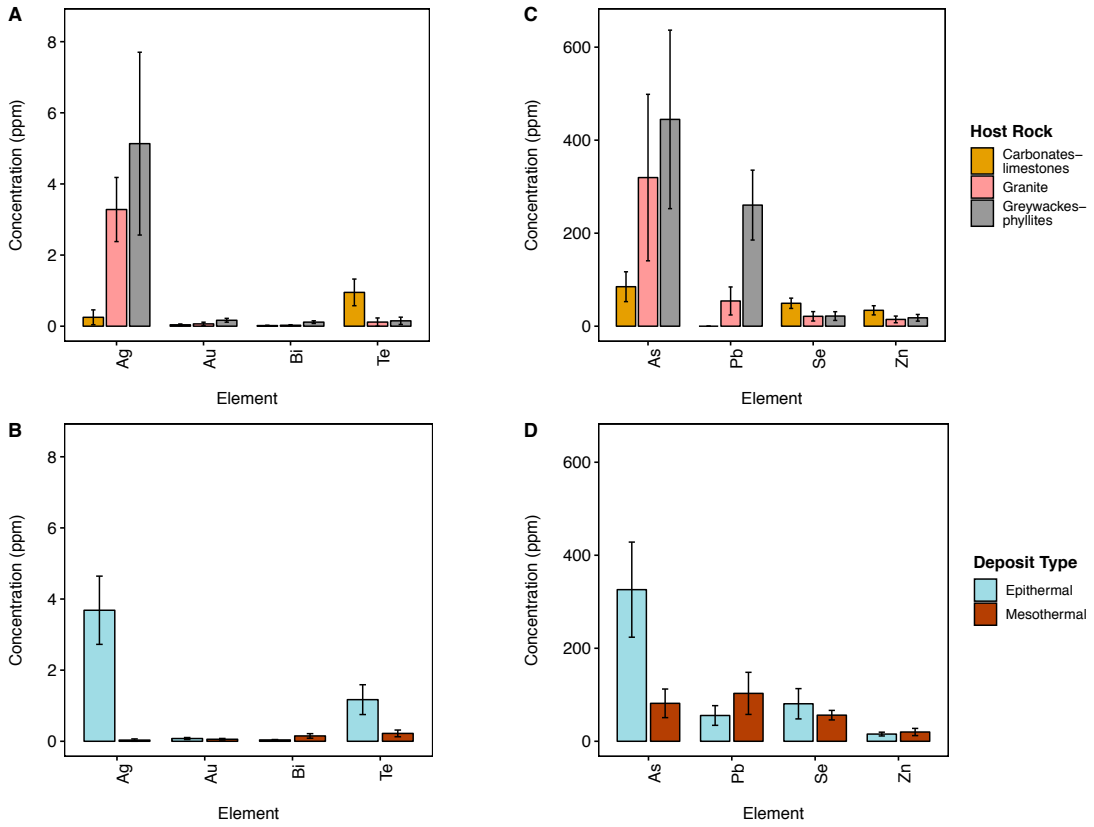

Figure 4.4 – Mean concentration (ppm) of trace elements in stibnites split by host rock (a & c), and deposit type (b & d) as analysed by LA-ICP-MS. Elements have been split into those with mean concentrations below 10ppm (a & b) and those above 10ppm (c & d). Error bars show standard error of mean.

Fig 4.5, below demonstrates the variability that was present within the conditions. For As, there is a high degree of intra-condition variability in the data within all categorisations, with pooled standard deviations (PSD) of 483.61 and 421.24 for host rock (HoRo) and deposit type (Dep), respectively. There is also notable intra-condition variability in the Pb (PSD_{HoRo} = 132.45, PSD_{Dep} = 147.94) Se (PSD_{HoRo} = 34.59, PSD_{Dep} = 134.36) and Zn (PSD_{HoRo} = 27.88, PSD_{Dep} = 26.44) data. This high degree of intra-condition variability may suggest that there is heterogeneity of trace elements across the samples. Within individual samples, variability was lower (Per stibnite PSDs for: As = 292.04, Pb = 59.70, Se = 22.03, Zn = 21.03), suggesting that variation was not a function of outliers, but rather the presence of different concentrations of these elements in different samples. Conversely, intra-condition values for Ag (PSD_{HoRo} = 4.43, PSD_{Dep} = 3.88), Au (PSD_{HoRo} = 0.14,

PSD_{Dep} = 0.13), Bi (PSD_{HoRo} = 0.07, PSD_{Dep} = 0.18) and Te (PSD_{HoRo} = 0.84, PSD_{Dep} = 1.71) were highly homogeneous.

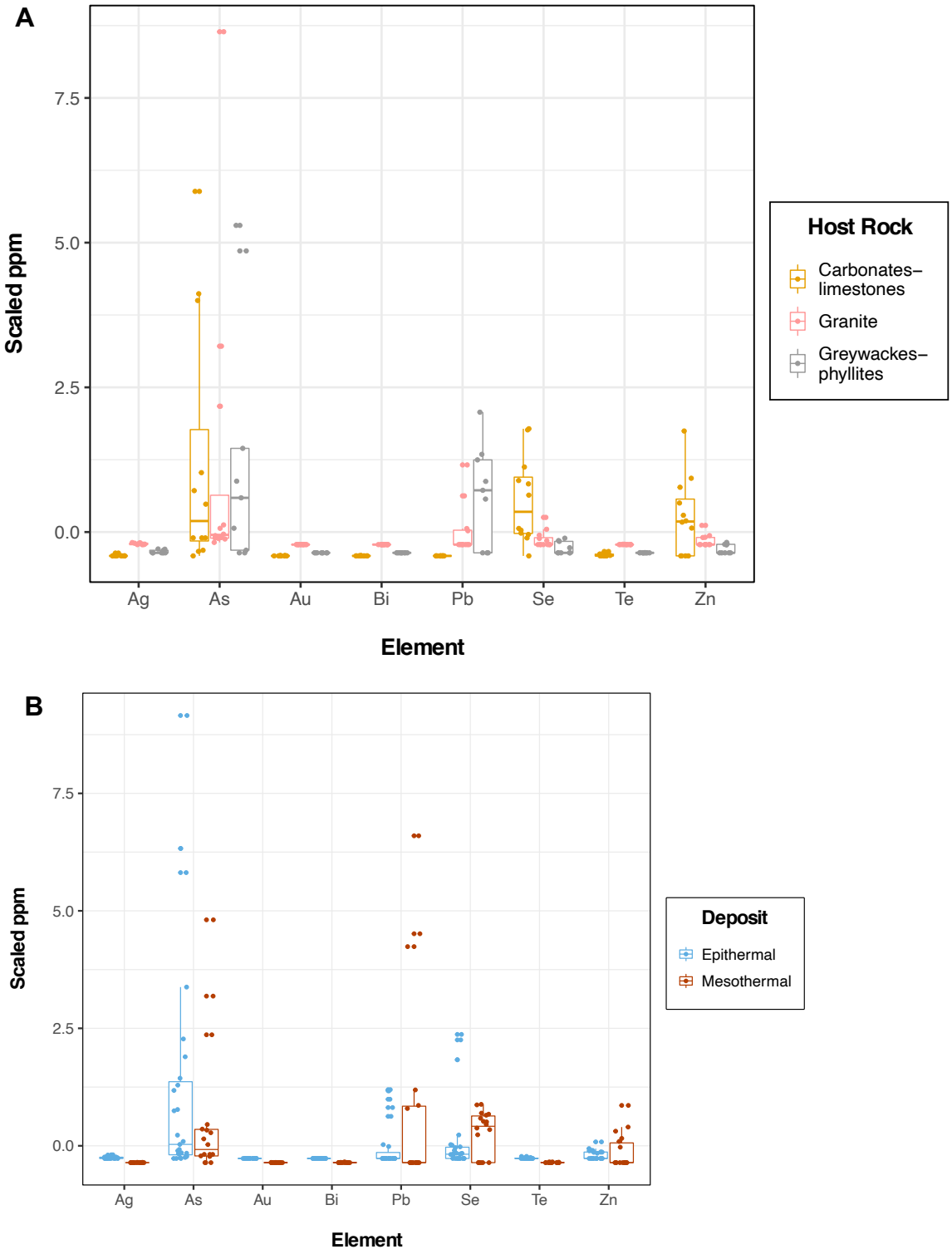

Figure 4.5 – Boxplot of scaled LA-ICP-MS data for all stibnite samples measured, showing variability in the data.

Correlation testing of elements did not reveal any strong patterns across conditions. However, a positive correlation was found between Au and Pb across all samples (0.54, $p<0.01$), with this correlation stronger in stibnites from mesothermal deposits (0.86, <0.01) than epithermal deposits (0.43, $p=0.03$). A similar trend was seen for Pb-Bi, which showed a positive correlation overall, and had a stronger correlation in mesothermal than epithermal deposits (all= 0.63, meso = 0.53, epi = 0.51, $p<0.02$). No strong negative correlations were found across the data as a whole, although a very strong negative correlation was seen between Se and As in the stibnites derived from Greywacke-phyllite host rock (-0.91, $p<0.01$), a trend also seen in the stibnites derived from the mesophilic deposits (-0.7, $p<0.01$).

4.3.5 Qualitative Assessment of Trace Element Presence and Zonation Spectroscopy

To help establish whether there was zonation of elements and identify areas with high Se to conduct XANES mapping, μXRF was employed. μXRF scans of areas selected for μXANES are shown in Fig 4.6, below. Qualitative analysis of samples 1, 7, 14 and 16 by μXRF mapping indicated that Au, Ag, As, Se and Pb were present in all samples. These elements were not homogeneously distributed within the areas studied, indicating some degree of zonation within the minerals. In Stb 7, Fe and Zn were present in small patches. In Stb 12 small patches of Pb and As were visible, whereas no notable areas of trace elements could be found in Stb 18. Bismuth was not established in any sample. The presence of other elements detected using WDS and LA-ICP-MS (Mo, Te, and Pd) could not be evaluated due to their $K\alpha$ X-ray emission energies being above the energy used in this study (maximum 13200 eV).

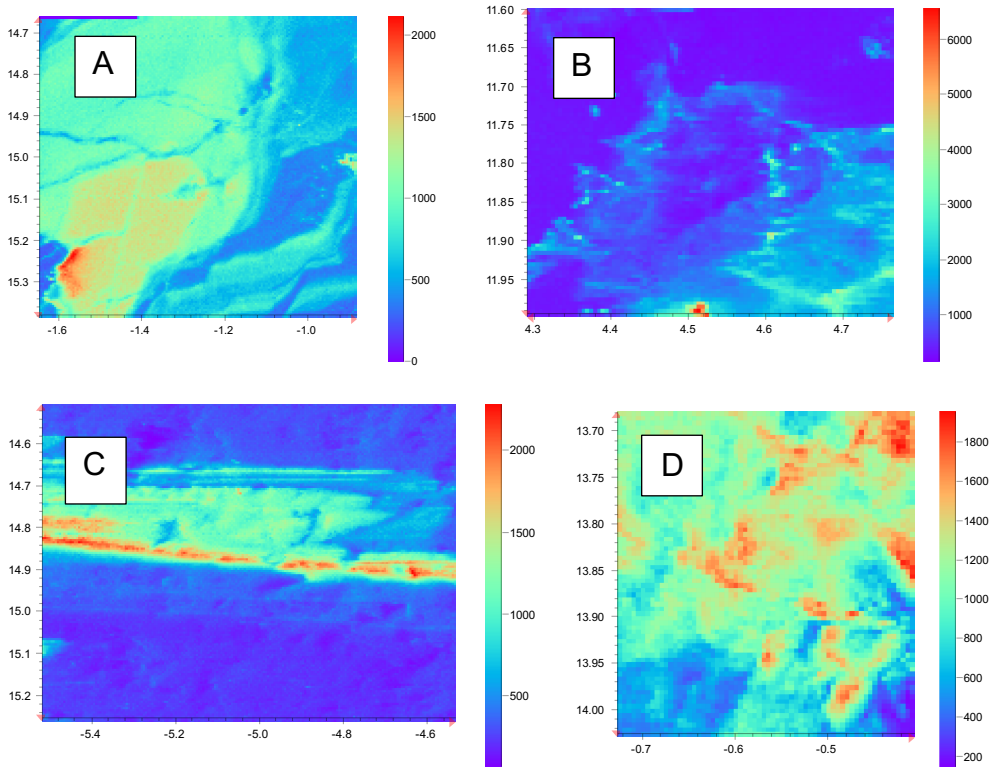

Figure 4.6 - Intensity of Se in Stb 1(A), 7(B), 14(C), 16(D) analysed with μXRF. Arbitrary units.

4.3.6 Speciation of Se in Stibnites

The oxidation state of Se was explored to determine how this trace element was fitting within the stibnite structure. This element was selected as it was present in both EPMA-WDS and LA-ICP-MS assessments. Selenium K-edge XANES spectra for samples 1, 7, 14 and 16 are shown in Figure 4.7, below. The standards used for comparison (selenite pentahydrate (+4), sodium selenate anhydrous (+6), selenium sulfide (+4), elemental Se shot (0)) are also plotted.

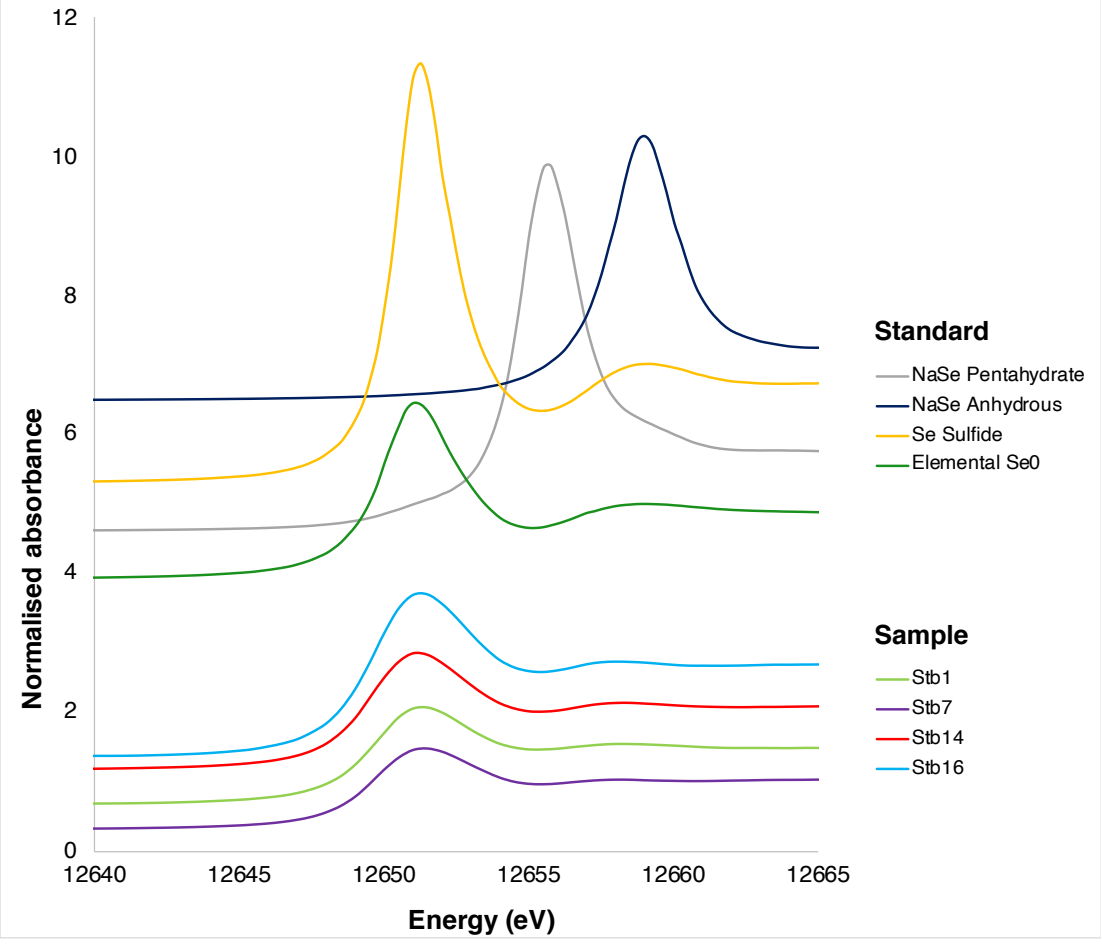

Figure 4.7 – Selenium K-edge averaged, normalised XANES spectra for stibnite samples and standards

By comparing XANES spectra to the standards analysed (position of white line peaks and second peaks), it appears that stibnite samples measured could correspond to either Se(4+) sulfide or elemental selenium (0). The white line peaks for the stibnites were 12651.5 eV, 12651.25 eV for Se sulfide, and 12651.5 eV for elemental selenium.

4.4 Discussion

4.4.1 Trace Element Trends in Stibnite

This study represents the first comprehensive study of trace elements in stibnites from a wide variety of origins. In line with findings for other sulfide minerals (Fontboté *et al.*, 2017), the experimental data collected by WDS, LA-ICP-MS and μXRF confirmed the presence of a range of trace elements in the analysed stibnite samples. There was consensus between the analytical techniques that Se, Au, Ag, Pb and Zn were present in stibnite. Additionally, the presence of As was confirmed by LA-ICP-MS and μXRF. These results are in agreement with the small number of previous studies which examined single stibnite samples (Murao *et al.*, 1999; Ashley *et al.*, 2003; Fu *et al.*, 2020). Overall, these findings demonstrate that stibnite breakdown could contribute potentially toxic elements to the environment.

The replacement of major elements in a sulfide mineral with trace elements can lead to the creation of defects in the mineral structure, which has been shown to lead to more breakdown compared to sulfide minerals free of impurities (Lehner *et al.*, 2007; Liu *et al.*, 2008). This is as a result of element substitutions changing the structural and electronic properties of the mineral (Chen, Chen and Guo, 2010). The nature of the trace elements found in this study can inform what properties of the mineral may be changed by their inclusion. The majority of the elements present as trace elements in the stibnites were chalcophile elements, which preferentially form bonds with sulfur (As, Se, Te, Pb, Zn, Ag, Mo and Bi (Dare *et al.*, 2011)). Additional elements identified in this study included Au and Pd, which can act as chalcophiles in some magmatic ore deposits (Barnes and Ripley, 2015). These findings could imply that trace elements found within the mineral lattice of stibnite are more likely to be replacing antimony than sulfur. As most of the elements found to be present in stibnite in this study (As, Se, Te, Pb, Zn, Ag, Mo, Au and Pd) have atomic radii smaller than antimony, if these elements are replacing antimony, changes to the size of the mineral lattice could occur. This could create defects and/or affect the bonds within the mineral, with potential implications for the rate of mineral breakdown (Chen, Chen and Guo, 2010). A

detailed electrochemical study is required to establish the complex effects of mineral substitutions in stibnite.

A key challenge to interpreting the results collected in this chapter was the conflicting data collected by the different analytical techniques. The percentage of Sb determined by both EPMA-WDS and LA-ICP-MS was highly similar, suggesting the two methods are accurate at higher concentrations. At trace element concentrations, however, there were many contrasts between the techniques in terms of quantities detected. For example, the EPMA-WDS data indicated that Mo was present in notable quantities, while this element was not detected by LA-ICP-MS. It is unlikely that high levels of Mo would be present in the stibnite samples studied, as Mo is poorly soluble in sulfide hydrothermal vent fluids below 350ºC (Metz and Trefry, 2000). Epithermal and mesothermal deposits (*i.e.* the conditions of formation of the stibnites studied in this chapter) predominantly form below this temperature (Pirajno, 1992; Hedenquist, Arribas and Gonzalez-Urien, 2000). Indeed, Mo potentially had an overlapping L alpha X-ray line with sulfur, potentially indicating that this element was recorded erroneously in place of sulfur (see plot of EPMA-WDS X-ray values in Appendix XII). Previous authors have concluded that LA-ICP-MS is more accurate than WDS at trace element concentrations. For example, Fu *et al.* (2020) could not use EPMA-WDS to detect trace elements in stibnite due to many values being recorded below the detection limit. Therefore, where data conflicts occur, focus should be placed on LA-ICP-MS results at trace element concentration levels.

Mapping carried out via WDS suggested homogeneity of trace elements within the samples. Conversely, zonation and heterogenous distribution of trace elements in the stibnites was implied by the μXRF and LA-ICP-MS (due to intra-sample variability). As the μXRF findings corroborate the accuracy of LA-ICP-MS, the LA-ICP-MS results will be focussed on in the following section.

4.4.2 The Effect of Host Rock and Deposit Type on Trace Elements in Stibnite

A number of factors can affect the quantity and types of trace elements in sulfide minerals, including the type of deposit they form in and the surrounding geology (*i.e.* the host rock). This is the first study to examine whether these factors affect the characteristics of trace elements in stibnite.

General trends for sulfide minerals are that solubility and therefore quantities of trace elements decrease as temperatures decrease (Metz and Trefry, 2000; Fontboté *et al.*, 2017). Consequently, the lower temperature epithermal deposits might be expected to contain fewer trace elements. However, no elements were present at significantly lower quantities in the epithermal stibnite group. In fact, LA-ICP-MS analysis established that the concentration of Ag was significantly higher in epithermal deposits. This specific result is in line with findings that Ag may be enriched in some sulfide minerals formed at lower <200ºC temperatures (Trefry *et al.*, 1994; Metz and Trefry, 2000). Similarly, there were no differences between the conditions in quantities of Au, despite the well-documented Au-Sb association in mesothermal ore, making enrichment in this condition likely (Madu, Nesbitt and Muehlenbachs, 1990; Ortega, Vindel and Beny, 1991; Bortnikov *et al.*, 2010; Yang *et al.*, 2017). The reasons for the contrasting findings of this study compared to findings for some other sulfide minerals could be due to a range of factors. For example, the two deposit types in which stibnite is found (epithermal and mesothermal) are closer in temperature formation range than the temperature ranges for other minerals; the precipitation of sulfide minerals from hydrothermal fluids ranges from 100-500ºC (compared to 160-350 for meso- and epithermal deposits) (Fontboté *et al.*, 2017). Indeed, there is some overlap in formation temperatures between the two (250-270ºC). Additionally, compounding effects of other factors could explain why intra-condition variability was greater than inter-condition. For example, fluid salinity, pH and sulfide concentration in hydrothermal fluids during mineral formation can all affect the deposition of trace elements in sulfide minerals (Fontboté *et al.*, 2017). Due to this range of influencing factors, it has been noted that making creation of a simplified model of trace element distribution extremely challenging (Metz and Trefry, 2000).

Host rock also did not appear to be a strong indicator of trace element trends, with very limited differences between the three conditions. This is consistent with some previous authors who have attributed differences in trace elements in sulfide minerals to variations in fluid composition and redox conditions during formation, as opposed to, or in combination with, host lithology (Bonnet *et al.*, 2016; Maslennikov *et al.*, 2019).

As a whole, the results of this chapter found very limited significant differences between the different conditions studied in terms of trace element composition or quantities. Instead, much variability between samples, within conditions was seen in LA-ICP-MS data, suggesting that neither host rock nor deposit type is a reliable predictor of the variability between samples.

4.4.3 Selenium Speciation in Stibnite

The speciation of trace elements found within stibnite can help us to establish whether an element is substituting for sulfur or antimony in the crystal structure, or whether it is present outside the mineral structure as an inclusion. In turn, this can help us understand factors that could affect stibnite breakdown. This chapter provides the first study of the speciation state of any element in naturally occurring stibnite.

No obvious inclusions were visible in the stibnites via EDS, although micron-scale inclusions may possible based on μXRF data. Consequently, μXANES was employed to determine the oxidation state of Se, as this element had been shown to be present in both LA-ICP-MS and EPMA-WDS analyses. There was a high degree of similarity in the XANES spectra across the four samples analysed. However, it could not be established whether Se was present as elemental selenium (possibly as an inclusion) or as selenium sulfide (within the mineral structure). These results are comparable to the findings of Matamoros-Veloza, Peacock and Benning (2014) for Se oxidation in pyrite from shales. These authors noted that the white line peaks and inflection points of the Se μXANES spectra for

the pyrite grains examined were very similar to their selenium sulfide and elemental selenium standards.

If Se is present as selenium sulfide, then it would potentially be substituting for Sb in the mineral structure. However, as no negative correlation was found between Sb and Se in either EPMA-WDS or LA-ICP-MS data, it was determined this was unlikely to be the case. Additionally, Kyono *et al.* (2015) suggest that in synthetic stibnite, Se substitutes for S, forming antimonselite, and it has been proposed that stibnite and antimonselite occur in solid solution, with Se substituting for S. In order for Se to substitute for S within the stibnite structure, Se would need to be present in the -2 oxidation state, as opposed to the +4 oxidation state of selenium sulfide. Therefore, it was determined that Se within the stibnite samples is unlikely to be occurring as a substitution. Instead, it could be considered more likely that the Se is occurring as elemental selenium. Furthermore, it has been suggested that identification of Se based solely on the position of peaks may be inaccurate due to the close positions of K-edge energies for the different oxidation states of Se. Instead, overall spectra shape should be employed (Shah *et al.*, 2007). Visual inspection of the spectra suggested that the selenium in the stibnite samples more closely matched elemental selenium. Therefore, it is likely that Se in stibnites is occurring as a microscale inclusion, rather than substituting for S or Sb within the mineral structure. This finding demonstrates that Se is unlikely to affect the mineral structure and therefore breakdown of stibnite. This is particularly notable, as Se was one of the trace elements measured with the highest concentrations in stibnite, and was present in all samples.

4.4.4 Stibnite as a Substrate for Microbial Growth

Despite its economic and environmental importance, the potential for microbial breakdown of stibnite has received limited study, and consequently, is poorly understood. Here, attempts to shed light on stibnite bioleaching by establishing microbial growth on stibnite were unsuccessful. Nonetheless, this outcome can provide some insights into stibnite, which could inform future bioleaching studies.

Although *At. ferrooxidans* and other members of the SC3 consortium have been comprehensively established to grow using a wide range of sulfide minerals as substrates, in this study, sustained growth of acidophiles in the SC3 consortium could not be achieved on stibnite. This observation could help inform our understanding of stibnite geochemistry and its susceptibility to breakdown in different conditions. For example, it is widely recognised that for certain sulfide minerals in acidic conditions, breakdown cannot be instigated by protons, but instead ferric iron is required. These minerals are considered acid-insoluble (Schippers and Sand, 1999). However, as limited information is available regarding stibnite dissolution, it has not previously been established whether or not it is acid-soluble. Indeed, both previous studies of stibnite breakdown with acidophiles have used stibnites that contained iron in the form of pyrite and as inclusions (Torma and Gabra, 1977; Ubaldini *et al.*, 2000). Conversely, in this chapter, iron was not detected even at trace element level by either WDS nor LA-ICP-MS in the stibnites used as growth substrates for the acidophiles. It is therefore possible that where acidophilic dissolution of stibnite has been suggested in previous studies, the actual mechanism of stibnite dissolution was via pyrite dissolution followed by iron oxidation by *At. ferrooxidans,* with ferric iron then acting as an oxidant for stibnite dissolution. This could indicate that stibnite might be acid insoluble. Further bioleaching studies with and without iron are required to corroborate this finding.

At the initiation of this chapter's work, no studies existed demonstrating the existence of neutrophilic stibnite oxidisers. Arsenic and antimony could share biogeochemical oxidation pathways in microbes (Liu *et al.*, 2010), and microbially produced arsenite oxidase has been shown to oxidise antimony (Wang *et al.*, 2015). It is possible, therefore, the arsenic oxidising microbes could oxidise antimony, and consequently facilitate stibnite breakdown. This study therefore explored whether an arsenic oxidising neutrophile derived from a mining site could mediate stibnite breakdown. Enhanced mineral breakdown could not be established in the presence of the studied neutrophiles. Consequently, it is unlikely that the neutrophiles were oxidising antimony or sulfur from the mineral, but rather using thiosulfate left over from the initial inoculum for growth. This is in line with findings of previous work that showed that the neutrophile *Bosea Sp.* WAO

resulted in no sustained stibnite oxidation and at the end of the experiment, no difference was found in soluble sulfate between the biotic samples and abiotic controls (Walczak, 2016). Since this chapter's work was conducted, two neutrophiles have been ostensibly demonstrated to facilitate stibnite breakdown (Loni *et al.*, 2020; Xiang *et al.*, 2022). In both instances, however, iron was present in the medium. Additionally, the mechanism of stibnite dissolution by microbes is accompanied by changes to pH and greatest oxidation was found under heterotrophic conditions. As it has been previously demonstrated that organic ligands can facilitate stibnite breakdown (Biver and Shotyk, 2012a), the basis for the enhanced stibnite dissolution with these organisms remains unclear.

Overall, it can be concluded that under the conditions tested, NT-24 and NT-26 are not capable of facilitating autotrophic stibnite breakdown. Additionally, despite similarities in chemistry between the elements, arsenite oxidising ability does not necessarily indicate the ability to oxidise antimony and facilitate stibnite breakdown.

4.4.5 Conclusion

In this chapter, the first comprehensive study of trace elements in stibnites from different sources around the world was presented. All techniques indicated that Se, Au, Ag, As, Pb and Zn were present as trace elements in the stibnites studied (H_2). These results indicate that the potential environmental consequences of stibnite breakdown include the release of toxic elements. Additionally, these findings could be used as a basis for understanding the types of trace elements present in stibnite for metal extraction.

Limited significant differences were seen between conditions in terms of quantities of the trace elements present, and it was consequently concluded that neither deposit type nor host rock provided a strong explanation for the variation seen between samples. A μXANES study allowed for the first insight into the speciation of Se as a trace element in naturally occurring stibnites, with conclusions drawn that Se is likely present in the elemental zero oxidation state, possibly as micro-

inclusions. These results indicate that the hypotheses 3-5 (H_3 -H_5) cannot be accepted.

Similarly, H_1 cannot be accepted as bacteria did not grow using stibnite under the tested conditions, nor did they facilitate stibnite breakdown. The lack of growth in the acidophilic strains could be indicative of the mineral being acid insoluble, therefore requiring iron to break down. This idea was supported by the collected geochemical data which indicated the lack of iron in the studied stibnite samples. Future stibnite bioleaching trials should be conducted in the presence and absence of iron to confirm this concept.

Some authors have suggested that abiotic stibnite breakdown is greatest at very alkaline pH (Hu, He and Kong, 2015; Hu *et al.*, 2016, 2017). Therefore, it is possible that the same may be true for biological dissolution of stibnite, *i.e.* in the absence of iron, alkaline conditions may be required to initiate microbial mineral breakdown. However, at present, there are very few studies of alkaliphilic bioleaching on any mineral, and to date, no alkaliphiles have been found to oxidise either stibnite or antimony.

Chapter 5 - General Discussion

5.1 Thesis Overview

Sulfide minerals are an ubiquitous and important group of minerals, both economically and environmentally. The impact of their breakdown can be desirable (for the retrieval of precious metals) or damaging (the creation of toxic acid mine waters). Despite the global impact of sulfide minerals and their dissolution (both intentional and unintentional), key aspects of their breakdown were poorly understood. This thesis aimed to add to the knowledge base regarding sulfide minerals and factors affecting their breakdown. To meet this aim, a series of objectives were outlined in Chapter 1 of this thesis, and these objectives were fulfilled as follows:

1. In Chapters 2 and 3, the collected ICP-OES and pH data indicated that, compared to abiotic conditions, chalcopyrite and Phoukassa ore breakdown was enhanced by the presence of the naturally occurring SC3 bioleaching consortium. In Chapter 4, geochemical data could not be collected, as growth of the SC3 consortium was not established, suggesting that stibnite is an unsuitable growth substrate for these microbes.
2. In Chapter 2, genes associated with the metabolic processes of the SC3 consortium were identified and RNA-seq analysis found expression of genes associated with iron and sulfur metabolism across the whole consortium during bioleaching. This work led to the detection of sulfur oxidation genes previously unknown in their respective species.
3. RNA-seq demonstrated that all identified iron and sulfur genes were expressed during dissolution of Phoukassa copper sulfide ore in Chapter 3, and several of these genes were differentially expressed over time.
4. The expression and geochemical data collected in Chapters 2 and 3 were used to create models of mineral breakdown for chalcopyrite and Phoukassa ore, respectively.

5. In Chapter 4, data collected from a range of analytical methods offered an improved understanding of the the types of impurities in stibnites from around the world, providing an enhanced geochemical background of this poorly studied mineral.

By meeting these objectives, this thesis has improved the understanding of the make-up of sulfide minerals and their breakdown. In turn, this information could be used to enhance the efficacy of bioleaching, and inform remediation strategies to reduce the environmental impact of sulfide minerals. Additionally, the research detailed in this thesis has provided a number of notable contributions to the field, including:

- The creation of a reproducible, novel bioinformatic pipeline for metatranscriptomic analyses
- The first community transcriptomic data sets of the SC3 bioleaching consortium
- The first metatranscriptomic study of sulfur and iron genes in a naturally occurring bioleaching consortium
- The first evidence of sulfur oxidation gene expression in the Archaeon G plasma
- A novel polysulfide reductase (*psr*) gene was shown to be expressed in *At. ferrooxidans*, providing the first evidence for a polysulfide reduction step in this organism
- The first geochemical dataset for the breakdown of Phoukassa ore
- The first model of Phoukassa ore dissolution by microbes
- The first comprehensive data set of stibnite impurities, providing key information regarding this poorly studied mineral
- The first ever data regarding speciation of any trace element in stibnite

These contributions to knowledge and their implications, with regards to sulfide minerals and the metabolisms of the SC3 bioleaching consortium, are discussed in the following sections. Additionally, potential practical applications of this work

are discussed. Finally, the limitations of this work and possible future directions are highlighted.

5.2 Metabolisms of the SC3 Consortium

Previous literature detailing metatranscriptomic studies of acidophiles is very limited, potentially due to the practical challenges associated with extracting sufficient high-quality RNA at low pH (Zammit *et al.*, 2011). To date, only two studies have used whole-community RNA-seq to examine gene expression during bioleaching processes (Marín *et al.*, 2017; Ma *et al.*, 2019). The metatranscriptomics studies carried out in Chapters 2 and 3 of this thesis represent the first whole community RNA-seq datasets exploring iron and sulfur oxidation genes in a bioleaching consortium. In the absence of metatranscriptomic studies, previous analyses of iron and sulfur oxidation gene expression have only been carried out for individual species (*e.g.* Carlos *et al.*, 2008; Quatrini *et al.*, 2009; Liljeqvist, Rzhepishevska and Dopson, 2013). Such studies cannot capture the interactions between species in a community during the active process of bioleaching. Therefore, the datasets in this thesis build the first comprehensive picture of inter-species sulfide mineral dissolution pathways.

The findings demonstrated that genes facilitating every step of the complex sulfide mineral dissolution process were consistently expressed by the consortium when faced with varying conditions (different mineral substrates of Chapter 2 and 3), and over time (Chapter 3). Indeed, as generalised functions of the whole consortium, expression of sulfur and iron oxidation genes were not significantly different over time in Chapter 3. Changes were, however, seen over time at the species level in Chapter 3, where the data indicated a potential shift over time in the types of species dominating sulfur and iron oxidation. Similarly, certain organisms were expressing some RISC oxidising genes when grown on the Phoukassa ore, but not when grown on chalcopyrite. Nonetheless, all sulfur oxidation steps were shown to be mediated by at least one species in both conditions. Therefore, while the roles played by individual species may vary over time, and in response to changing mineral substrates, the overall processes of sulfur and iron oxidation are

consistently facilitated by the community as a whole. This finding is significant as it indicates that bioleaching as a community-level function is robust in this consortium, and could suggest SC3 is capable of facilitating bioleaching under a range of conditions.

As well as exploring inter-species and community-level gene expression, the use of metatranscriptomics to explore a naturally occurring consortium also allows the study of the transcriptomes of species that are not yet isolated. For G plasma, this enabled the first ever gene expression analyses to be carried out in the species. Additionally, for the *Ferroplasma spp.* in the consortium, this study represented the first report of sulfur oxidation gene expression. That these archaeal species were found to be expressing iron and sulfur oxidation genes in the experimental work of both Chapters 2 and 3 broadens the evidence for bioleaching capabilities in these previously poorly studied species. Indeed, all SC3 members were shown in Chapters 2 and 3 to be expressing genes that could directly contribute to bioleaching. This finding could have implications for how we view the roles of heterotrophs in AMD and bioleaching communities, as G plasma has been posited to be organoheterotrophic (Golyshina *et al.*, 2016b). It has traditionally been concluded that heterotrophs predominantly play a supporting role in bioleaching communities, providing nutrients or removing organic acids that could inhibit the growth of the chemolithotrophs (Rawlings, 2005; Fang and Zhou, 2006; Vardanyan and Vyrides, 2019). Nonetheless, there have been some previous suggestions that heterotrophs can directly oxidise iron and sulfur to facilitate bioleaching (Valdés *et al.*, 2010). This thesis corroborates this proposition, by demonstrating that G plasma not only possesses sulfur oxidising enzymes, but also that these genes are expressed during bioleaching, consequently indicating an active role for this species in sulfide mineral oxidation pathways. Alternatively, it is possible that these findings indicate that G plasma, previously categorised as heterotrophic, possesses the ability to gain energy mixotrophically. Indeed, if this were the case it would represent a first step in understanding how presumed “heterotrophs” are surviving and obtaining energy in the barren environment of a mineral surface. Extrapolating further, these findings could make us reconsider how many species in acid mine drainage environments are true heterotrophs, or whether the

inhospitable environment necessitates diversification of mechanisms for obtaining energy. High resolution metagenomic and metatranscriptomic studies will be essential to resolving this in future work.

5.3 Sulfide Mineral Dissolution

The results chapters of this thesis clearly demonstrated differences in the geochemical properties of the sulfide minerals studied. A key example of this is the differences in susceptibility to bioleaching observed. Growth of the SC3 consortium was not observed on stibnite, and no evidence of mineral breakdown was seen in the presence of microbes. In contrast, mineral breakdown was observed during SC3 growth on chalcopyrite and the Phoukassa ore. This indicates that the presence of acidic conditions and sulfur and iron oxidising microbes (*i.e.* the fundamental components of bioleaching), is not sufficient to initiate bioleaching across sulfide minerals. Indeed, differences in metal-sulfur bonds across different sulfide minerals affect the susceptibility of minerals to acid attack (Schippers and Sand, 1999). When chalcopyrite was bioleached by SC3, pH increased over time, suggesting proton consumption. This observation is in line with previous studies that demonstrate that chalcopyrite breakdown is initiated by proton attack, and its breakdown is a proton-consuming reaction (Vilcáez and Inoue, 2009). Conversely, pH fell over time in the Phoukassa ore, in line with previous findings for pyritic ores, which are not vulnerable to acid attack (Rohwerder *et al.*, 2003a).

The vulnerability to initial proton attack can also provide information regarding the impact of ferric iron presence on mineral breakdown. No iron was present in the minimal growth medium of the SC3 consortium studies. As chalcopyrite is vulnerable to proton attack, lack of added ferric iron would not inhibit breakdown, and iron and sulfur would be released into solution for oxidation by the SC3 consortium, leading to a feedback loop of mineral breakdown. Comparatively, pyrite, the major mineral phase of the Phoukassa ore is not vulnerable to initial attack by protons. Consequently, microbial mineral breakdown may have been

delayed until the abiotic oxidation of pyrite via dissolved oxidation (Moses *et al.*, 1987) released iron into solution.

Unlike the sulfide substrates studied in Chapters 2 and 3, stibnite (Sb_2S_3) does not contain iron as a constituent element, and indeed, geochemical analyses suggested iron was not present even in trace element quantities in the stibnites used in microbial trials. No known study has been conducted regarding the susceptibility of stibnite to initial proton attack. However, all previous studies demonstrating microbial growth on stibnite have been conducted in the presence of iron (within the medium or as pyrite in a mixed assemblage). It is possible, therefore, that stibnite is not vulnerable to initial proton attack, and requires iron to be added to initiate and sustain mineral breakdown. Studies conducted to corroborate this suggestion would provide interesting insights into the interplay between iron and sulfur metabolisms in bioleaching organisms.

5.4 Contributions to the Field of Metatranscriptomics

Data analysis techniques for acidophile whole-community RNA sequencing are not consistent in the small number of studies published to date, and no standard protocol exists for metatranscriptomic analyses more generally. Further, the small number of bioinformatic tools that have been specifically developed for metatranscriptomics are aimed at creating de novo assemblies from samples containing unknown microbial assemblages (Kuske *et al.*, 2015; Shakya, Lo and Chain, 2019). De novo assembly for metatranscriptomics has a number of drawbacks, notably including errors in assembly and limited gene identification in non-model organisms (Ungaro *et al.*, 2017; Shakya, Lo and Chain, 2019). In the work detailed in this thesis, the genomes of the SC3 consortium were known through genome resolved metagenomics. Consequently, a higher level of detail could be achieved by using the resolved genomes as a reference transcriptome. To leverage these data in this way, it was necessary to develop a reproducible, dedicated bioinformatics pipeline, which incorporated a number of bioinformatic tools (as detailed in Section 2.2.10.2). With decreasing sequencing prices,

assembled metagenomes of entire communities are likely to become increasingly common. As a result the opportunity to perform analyses such as conducted in this thesis will gain relevance. Therefore this pipeline is likely to become useful for a wide variety of users.

5.5 Practical Applications of Experimental Findings

The significance of improving the knowledge surrounding sulfide minerals and their breakdown lies in their potential to provide valuable metals, or create environmental damage. The research conducted in this thesis adds to our general background understanding of both these minerals and bioleaching consortia. In addition, some of the findings could be considered for practical applications to improve bioleaching. For example, in Chapter 4, microbial growth could not be established on stibnite which was demonstrated to not contain iron as an impurity. Similarly, in Chapter 3, it was posited that due to the acid-insoluble nature of pyrite and lack of iron present in the medium (Rohwerder *et al.*, 2003b), onset of breakdown may have been delayed. Bioleaching practitioners should therefore take into consideration the specific mineral assemblages of ores being used in bioleaching, and consider whether the addition of ferric iron is necessary to initiate the bioleaching process. This may be particularly relevant for low-grade ores where the target mineral may only represent a minor proportion of the overall ore. In such instances, it would be worthwhile to consider whether the major mineral components are likely constrain the overall rate of bioleaching.

At present, a limited range of sulfur and iron-oxidising microbes are typically used in commercial bioleaching operations (*e.g. Acidthiobacillus spp., Leptospirillum spp.*). While some archaea are used in bioleaching (*e.g.* the obligate autotroph *Ferroplasma ferriphilum*), some of the SC3 archaeal species are not yet reported to be used in bioleaching in any published study (G plasma and *Ferroplasma* Type II), and indeed, none of the SC3 archaeal species are commonly added to constructed bioleaching consortia. The results of the metatranscriptomic analyses highlighted the potential for notable contributions to bioleaching from the archaeal

species in the SC3 consortium. Bioleaching practitioners should therefore take a holistic approach to selecting organisms for bioleaching consortia, including considering the opportunities provided by “non-traditional” microbes, such as the archaeal SC3 species.

5.6 Limitations of Laboratory Studies on Bioleaching Consortia

The work detailed in this thesis provided new information on the mechanisms of breakdown of Phoukassa ore and chalcopyrite in the presence of an acidophilic consortium. For practical and budgetary reasons, this work was conducted using flasks in a laboratory environment. This offered some advantages over field-based studies of bioleaching consortia. For example, the differences in conditions and differences in abiotic and biotic mineral dissolution would be impossible to monitor in the environment due to the universal presence of microbes. Additionally, control of variables such as temperature and initial pH allows for differences in condition to be accurately assessed. However, due to the variable geochemical factors influencing microbial activity in the environment, care should be exercised in extrapolating the results of this study to the functioning of large-scale heap bioleaching or environmental samples (Edwards *et al.*, 2000).

Crushed sulfide minerals on a larger scale, as in industrial heap or dump bioleaching system, may face varying aeration gradients, with anaerobic or microaerophilic sub-environments (Pradhan *et al.*, 2008). This thesis focussed on aerobic oxidation of sulfur and iron, however many chemolithoautotrophs, for example *At. ferrooxidans,* are also capable of anaerobic sulfur oxidation (Osorio *et al.*, 2013). Additionally, in anaerobic conditions, some of the species in the SC3 consortium are capable of iron reduction (Dopson *et al.*, 2004; Hallberg, González-Toril and Johnson, 2010). The effects of anaerobic growth during bioleaching should be investigated further to further increase the understanding of mineral breakdown mechanisms, and also to inform environmental protection measures, as creating anaerobic environments surrounding sulfide minerals is sometimes used as a method of AMD remediation (Vera, Schippers and Sand, 2013).

5.7 Future Directions for Research

As highlighted in the previous section, there are some constraints on what can be extrapolated from laboratory scale studies. Future research could address this cap by scaling-up studies of bioleaching with the SC3 consortium. For example, extraction and sequencing of RNA from the consortium grown in a bioleaching column (*e.g.* as in Marín *et al.*, 2017). This project would be a significant undertaking, as RNA extraction protocols would need to be adapted to account for the difference in scale, and the practicalities would likely dictate that the experiment would need to be conducted in the field. Such a project would, nonetheless, further illuminate the expression of metabolism genes in bioleaching consortia and clarify the effect of scale.

Additionally, a scaled-up study of bioleaching could include trials with thermophilic species. In some bioleaching set-ups (*e.g.* heap leaching), mesophiles (*i.e.* microbes that operate at an optimum temperature range of 20-40ºC) are the primary colonisers of sulfide minerals, then, as sulfide mineral dissolution is an exothermic process, thermophiles (optimum temperature range of 40-80ºC) begin to take over later in the breakdown (Natarajan, 2018a). The species present in the SC3 consortium are widely reported as being mesophiles (Table 1.2, Section 1.8.1.2), however trials to establish the specific optimum temperature for the consortium could further enhance the efficacy of bioleaching.

As well as trials incorporating new species, such as thermophiles, future work could look to isolate and re-combine the consortium in a number of different groupings to explore whether this effects the roles played by different consortium members. This work could be a crucial step in tailoring optimal bioleaching consortia.

A key challenge presented by the work described in this thesis was the difficulty in extracting sufficient RNA from the bioleaching consortium for sequencing. Time and funding constraints prevented further exploration of this, however, future work could include investigation of RNA protocols to develop an optimised method of extracting RNA from low pH consortia, and including steps to account for biofilm

formation. Biofilm formation using extracellular polymeric substances (EPS) has been shown to commonly occur during copper bioleaching by acidophiles (Bobadilla-Fazzini and Poblete-Castro, 2021). As it is well established that the EPS matrix binding microbes is a key inhibiting factor to RNA extraction from biofilms, modification of the RNA extraction method to include steps to remove the EPS could help improve the quantity of RNA recovered from acidophiles (Vera *et al.*, 2009). Trials to remove EPS could include enzymes, mechanical or chemical techniques (Callahan, 2010). However, inclusion of additional steps must be demonstrated to not affect the quality of the extracted RNA, as both quantity and quality of RNA affect the success of the sequencing and analysis (França, Melo and Cerca, 2011). Indeed, due to the very acidic conditions involved, it was necessary to carry out the RNA extractions described in this thesis very quickly to avoid RNA degradation. The addition of steps such as EPS removal must therefore establish a balance between the potential for enhanced quantity against possible reduced quality of the extracted RNA.

Due to funding constraints, only a limited number of samples could be sequenced via RNA-seq. Consequently the entirety of the sample was treated as one environment and RNA extracted together, as opposed to extracting RNA from the supernatant and mineral surface separately. The SEM images obtained in Chapters 2 and 3 suggest that some consortium cells are attached to the mineral surface. As it has previously been suggested that microbial communities attached to mineral surfaces are different to those in solution (Watling *et al.*, 2014), future work could explore the potential differences between sessile and planktonic members of the bioleaching consortium in terms of community dynamics and gene expression. For example, using a similar approach to previous studies exploring the different activities of biofilm and planktonic *Clostridium thermocellum* (Dumitrache *et al.*, 2017) and the functioning of river microbial communities (Nakamura *et al.*, 2016). This work could help further elucidate the exact function of consortiums during bioleaching breakdown.

This thesis utilised a metatranscriptome concatenated from the known genomes of the species in the SC3 consortium as a reference for alignment of RNA-seq reads,

however, due to the nature of most metatranscriptomic studies, where species present are unknown, de novo assembly is often employed. In de novo metatranscriptome assembly, the transcripts are assembled without alignment to a reference genome. There are limitations of this approach, as errors affecting results are more frequent in de novo assembly, for example, erroneous contig assembly (Hsieh, Oyang and Chen, 2018). Therefore, although alignment to a genome, as conducted in this thesis, is considerably more robust in terms of transcriptomic analysis, a complimentary de novo alignment could potentially highlight additional genes not present in the current metagenome, as the genomes used in this thesis were not complete. However, the majority of genes known from literature associated with S and Fe metabolism were already present in the reference SC3 metatranscriptome. Instead, de novo alignment may be useful for researchers interested in exploring other aspects of the genome, for example, acid resistance associated genes, other metabolisms and the types of features present on the plasmids.

Contrary to some previous studies, microbial growth on stibnite could not be established with the tested microbes under the trial conditions in Chapter 4. Future work could therefore explore the factors that affect the success of microbial growth on stibnite, for example, the presence of iron, as discussed in Section 4.4.4. To determine whether iron is essential to microbial growth on stibnite, a future study could trial microbes previously posited to grow on stibnite (*e.g. At. ferrooxidans*) in the presence and absence of iron. This would also help establish the mechanism of stibnite bioleaching, as the sulfide minerals that break down following the thiosulfate bioleaching mechanism require iron (Schippers and Sand, 1999).

As it has been demonstrated that trace elements effect the rate of sulfide mineral dissolution (Fallon *et al.*, 2019), additional studies that could build on the stibnite research conducted in this thesis could include examining in detail the effect of different trace elements on stibnite breakdown, these studies could include a combination of laboratory and computational studies (*e.g.* as conducted by Xuehong *et al.*, 2006; Chen and Chen, 2010; Dos Santos *et al.*, 2017). The trace

elements that were established in Chapter 4 as being commonly present in stibnite can provide the foundation for these studies.

5.8 Conclusion

Multidisciplinary research techniques were used to address the aims and objectives of this thesis, enhancing the knowledge surrounding sulfide minerals and their dissolution. In particular, the presence of sulfur and iron oxidising genes were identified in a naturally occurring bioleaching consortium, and it was demonstrated that these genes were expressed during sulfide mineral breakdown. This work has not only helped to fill core gaps in the understanding of bioleaching mechanisms for some of the most important acidophiles, but also highlighted the potential role of less commonly applied bioleaching microbes during sulfide mineral breakdown.

The common thread of experimental work in this thesis has been the interactions between bioleaching microbes and their geological substrate. Microbes have been demonstrated to affect their host sulfide mineral through facilitating breakdown (Chapter 2 and 3). In turn, minerals have been shown to affect the bioleaching organisms studied by providing iron and sulfur, which are electron donors for microbial growth. Where one of these factors was not provided *(i.e.* no iron by stibnite) microbial growth was not achieved. Nonetheless, much remains to be examined regarding sulfide mineral-microbe interactions. The work in this thesis sets the foundation for new avenues of research in this field, including the potential for using metatranscriptomics to engineer optimal bioleaching consortia.

References

Acinas, S. G. *et al.* (2005) 'PCR-induced sequence artifacts and bias: Insights from comparison of two 16s rRNA clone libraries constructed from the same sample', *Applied and Environmental Microbiology*. American Society for Microbiology, 71(12), pp. 8966–8969. doi: 10.1128/AEM.71.12.8966-8969.2005.

Adamides, N. G. (2010) 'Mafic-dominated volcanogenic sulphide deposits in the troodos ophiolite, Cyprus Part 2 - A review of genetic models and guides for exploration', *Transactions of the Institutions of Mining and Metallurgy, Section B: Applied Earth Science*, pp. 193–204. doi: 10.1179/1743275811Y.0000000011.

Ahmadi, A. *et al.* (2010) 'Electrochemical bioleaching of high grade chalcopyrite flotation concentrates in a stirred bioreactor', *Hydrometallurgy*. Elsevier, 104(1), pp. 99–105. doi: 10.1016/j.hydromet.2010.05.001.

Ai, C. *et al.* (2019) 'Increased chalcopyrite bioleaching capabilities of extremely thermoacidophilic Metallosphaera sedula inocula by mixotrophic propagation', *Journal of Industrial Microbiology and Biotechnology*. Oxford Academic, 46(8), pp. 1113–1127. doi: 10.1007/S10295-019-02193-3.

Akcil, A., Ciftci, H. and Deveci, H. (2007) 'Role and contribution of pure and mixed cultures of mesophiles in bioleaching of a pyritic chalcopyrite concentrate', *Minerals Engineering*. Pergamon, 20(3), pp. 310–318. doi: 10.1016/j.mineng.2006.10.016.

Akcil, A. and Koldas, S. (2006) 'Acid Mine Drainage (AMD): causes, treatment and case studies', *Journal of Cleaner Production*. Elsevier, pp. 1139–1145. doi: 10.1016/j.jclepro.2004.09.006.

Aliaga Goltsman, D. S. *et al.* (2009) 'Community genomic and proteomic analyses of chemoautotrophic iron-oxidizing "Leptospirillum rubarum" (Group II) and

"Leptospirillum ferrodiazotrophum" (Group III) bacteria in acid mine drainage biofilms', *Applied and Environmental Microbiology*. American Society for Microbiology, 75(13), pp. 4599–4615. doi: 10.1128/AEM.02943-08.

Aliaga Goltsman, D. S. *et al.* (2013) 'New group in the leptospirillum clade: Cultivation-independent community genomics, proteomics, and transcriptomics of the new species "leptospirillum group IV UBA BS"', *Applied and Environmental Microbiology*, 79(17), pp. 5384–5393. doi: 10.1128/AEM.00202-13.

Almeida, A. *et al.* (2018) 'Benchmarking taxonomic assignments based on 16S rRNA gene profiling of the microbiota from commonly sampled environments', *GigaScience*. Oxford Academic, 7(5), pp. 1–10. doi: 10.1093/gigascience/giy054.

Altschul, S. F. *et al.* (1990) 'Basic local alignment search tool', *Journal of Molecular Biology*. J Mol Biol, 215(3), pp. 403–410. doi: 10.1016/S0022-2836(05)80360-2.

Andres, J. *et al.* (2013) 'Life in an arsenic-containing gold mine: genome and physiology of the autotrophic arsenite-oxidizing bacterium rhizobium sp. NT-26.', *Genome biology and evolution*, 5(5), pp. 934–53. doi: 10.1093/gbe/evt061.

Andrews, S. (2010) *FastQC - A quality control tool for high throughput sequence data. http://www.bioinformatics.babraham.ac.uk/projects/fastqc/*, *Babraham Bioinformatics*. doi: citeulike-article-id:11583827.

Ashley, P. M. *et al.* (2003) 'Environmental mobility of antimony around mesothermal stibnite deposits, New South Wales, Australia and southern New Zealand', *Journal of Geochemical Exploration*, 77(1), pp. 1–14. doi: 10.1016/S0375-6742(02)00251-0.

Auguie, B. and Antonov, A. (2017) *gridExtra: Miscellaneous Functions for 'Grid'' Graphics'*. Available at: https://rdrr.io/cran/gridExtra/ (Accessed: 29 October 2020).

Ayala-Muñoz, D. *et al.* (2020) 'Metagenomic and Metatranscriptomic Study of

Microbial Metal Resistance in an Acidic Pit Lake', *Microorganisms 2020, Vol. 8, Page 1350*. Multidisciplinary Digital Publishing Institute, 8(9), p. 1350. doi: 10.3390/MICROORGANISMS8091350.

Ayling, M., Clark, M. D. and Leggett, R. M. (2019) 'New approaches for metagenome assembly with short reads', *Briefings in Bioinformatics*, 21(2), pp. 584–594. doi: 10.1093/bib/bbz020.

Baba, A. A. *et al.* (2011) 'Bioleaching of Zn(II) and Pb(II) from Nigerian sphalerite and galena ores by mixed culture of acidophilic bacteria', *Transactions of Nonferrous Metals Society of China*. Elsevier, 21(11), pp. 2535–2541. doi: 10.1016/S1003-6326(11)61047-9.

Bacelar-Nicolau, P. and Johnson, D. B. (1999) 'Leaching of pyrite by acidophilic heterotrophic iron-oxidizing bacteria in pure and mixed cultures', *Applied and Environmental Microbiology*. American Society for Microbiology, 65(2), pp. 585–590. doi: 10.1128/aem.65.2.585-590.1999.

Baker, B. J. and Banfield, J. F. (2003) 'Microbial communities in acid mine drainage.', *FEMS microbiology ecology*. The Oxford University Press, 44(2), pp. 139–52. doi: 10.1016/S0168-6496(03)00028-X.

Barco, R. A. *et al.* (2015) 'New insight into microbial iron oxidation as revealed by the proteomic profile of an obligate iron-oxidizing chemolithoautotroph', *Applied and Environmental Microbiology*. American Society for Microbiology, 81(17), pp. 5927–5937. doi: 10.1128/AEM.01374-15/SUPPL_FILE/ZAM999116520SO1.PDF.

Barnes, S. J. and Ripley, E. M. (2015) 'Highly siderophile and strongly chalcophile elements in magmatic ore deposits', *Reviews in Mineralogy and Geochemistry*. Mineralogical Society of America, pp. 725–774. doi: 10.2138/rmg.2016.81.12.

Basham, M. *et al.* (2015) 'Data Analysis WorkbeNch (DAWN)', *Journal of Synchrotron Radiation*, 22, pp. 853–858. doi: 10.1107/S1600577515002283.

Batanova, V. G., Sobolev, A. V. and Magnin, V. (2018) 'Trace element analysis by EPMA in geosciences: Detection limit, precision and accuracy', in *IOP Conference Series: Materials Science and Engineering*. Institute of Physics Publishing. doi: 10.1088/1757-899X/304/1/012001.

Bayliss, P. and Nowacki, W. (1972) 'Refinement of the crystal structure of stibnite, Sb2S3', 135, pp. 308–315. Available at: https://rruff-2.geo.arizona.edu/uploads/ZK135_308.pdf (Accessed: 15 May 2017).

Behrad Vakylabad, A. (2011) 'A comparison of bioleaching ability of mesophilic and moderately thermophilic culture on copper bioleaching from flotation concentrate and smelter dust', *International Journal of Mineral Processing*. Elsevier, 101(1–4), pp. 94–99. doi: 10.1016/J.MINPRO.2011.09.003.

Belissont, R. *et al.* (2014) 'LA-ICP-MS analyses of minor and trace elements and bulk Ge isotopes in zoned Ge-rich sphalerites from the Noailhac – Saint-Salvy deposit (France): Insights into incorporation mechanisms and ore deposition processes', *Geochimica et Cosmochimica Acta*. Pergamon, 126, pp. 518–540. doi: 10.1016/J.GCA.2013.10.052.

Belousova, E. A. *et al.* (2002) 'Apatite as an indicator mineral for mineral exploration: Trace-element compositions and their relationship to host rock type', *Journal of Geochemical Exploration*. Elsevier, 76(1), pp. 45–69. doi: 10.1016/S0375-6742(02)00204-2.

Belzile, N., Chen, Y.-W. and Filella, M. (2011) 'Human Exposure to Antimony: I. Sources and Intake', *Critical Reviews in Environmental Science and Technology*. Taylor & Francis Group, 41(14), pp. 1309–1373. doi: 10.1080/10643381003608227.

Ben-Shachar, M., Makowski, D. and Lüdecke, D. (2020) 'Compute and interpret indices of effect size', *CRAN*. Available at: https://github.com/easystats/effectsize.

Benjamini, Y. and Hochberg, Y. (1995) 'Controlling the False Discovery Rate: A Practical and Powerful Approach to Multiple Testing', *Journal of the Royal Statistical Society: Series B (Methodological)*. Wiley, 57(1), pp. 289–300. doi: 10.1111/j.2517-6161.1995.tb02031.x.

Berry, V. K., Murr, L. E. and Hiskey, J. B. (1978) 'Galvanic interaction between chalcopyrite and pyrite during bacterial leaching of low-grade waste', *Hydrometallurgy*. Elsevier, 3(4), pp. 309–326. doi: 10.1016/0304-386X(78)90036-1.

Bini, E. (2010) 'Archaeal transformation of metals in the environment', *FEMS Microbiology Ecology*. Oxford Academic, 73(1), pp. 1–16. doi: 10.1111/J.1574-6941.2010.00876.X.

Bird, L. J., Bonnefoy, V. and Newman, D. K. (2011) 'Bioenergetic challenges of microbial iron metabolisms.', *Trends in microbiology*. Elsevier, 19(7), pp. 330–40. doi: 10.1016/j.tim.2011.05.001.

Biver, M. and Shotyk, W. (2012a) 'Experimental study of the kinetics of ligand-promoted dissolution of stibnite (Sb2S3)', *Chemical Geology*, 294, pp. 165–172. doi: 10.1016/j.chemgeo.2011.11.009.

Biver, M. and Shotyk, W. (2012b) 'Stibnite (Sb2S3) oxidative dissolution kinetics from pH 1 to 11', *Geochimica et Cosmochimica Acta*, 79, pp. 127–139. doi: 10.1016/j.gca.2011.11.033.

Blake, R. C. (2012) 'In situ spectroscopy on intact Leptospirillum ferrooxidans reveals that reduced cytochrome 579 is an obligatory intermediate in the aerobic iron respiratory chain', *Frontiers in Microbiology*. Frontiers Research Foundation, 3(APR), p. 136. doi: 10.3389/fmicb.2012.00136.

Bliss, J. D. and Orris, G. J. (1989) 'Descriptive model of simple Sb deposits', *Journal of Chemical Information and Modeling*, 53, p. 160.

Bobadilla-Fazzini, R. A. *et al.* (2017) 'Primary copper sulfides bioleaching vs. chloride leaching: Advantages and drawbacks', *Hydrometallurgy*. Elsevier, 168, pp. 26–31. doi: 10.1016/J.HYDROMET.2016.08.008.

Bobadilla-Fazzini, R. A. and Poblete-Castro, I. (2021) 'Biofilm Formation Is Crucial for Efficient Copper Bioleaching From Bornite Under Mesophilic Conditions: Unveiling the Lifestyle and Catalytic Role of Sulfur-Oxidizing Bacteria', *Frontiers in Microbiology*. Frontiers Media S.A., 12, p. 3133. doi: 10.3389/FMICB.2021.761997/BIBTEX.

Bogdanovic, G. *et al.* (2016) 'Leaching of low-grade copper ores: A case study for "Kraku Bugaresku-Cementacija" deposits (Eastern Serbia)', *Journal of Mining and Metallurgy A: Mining*. Centre for Evaluation in Education and Science (CEON/CEES), 52(1), pp. 45–56. doi: 10.5937/jmma1601045b.

Bokulich, N. A. *et al.* (2018) 'Optimizing taxonomic classification of marker-gene amplicon sequences with QIIME 2's q2-feature-classifier plugin', *Microbiome*, 6(1), p. 90. doi: 10.1186/s40168-018-0470-z.

Bolyen, E. *et al.* (2018) 'QIIME 2: Reproducible, interactive, scalable, and extensible microbiome data science', *PeerJ Preprints*, 6, p. e27295v1. doi: 10.7287/peerj.preprints.27295v1.

Bolyen, E. *et al.* (2019) 'Reproducible, interactive, scalable and extensible microbiome data science using QIIME 2', *Nature Biotechnology*. Nature Publishing Group, pp. 852–857. doi: 10.1038/s41587-019-0209-9.

Bond, P. L., Druschel, G. K. and Banfield, J. F. (2000) 'Comparison of acid mine drainage microbial communities in physically and geochemically distinct ecosystems', *Applied and Environmental Microbiology*. American Society for Microbiology, 66(11), pp. 4962–4971. doi: 10.1128/AEM.66.11.4962-4971.2000.

Bonnefoy, V. and Holmes, D. S. (2011) 'Genomic insights into microbial iron oxidation and iron uptake strategies in extremely acidic environments', *Environmental Microbiology*, pp. 1597–1611. doi: 10.1111/j.1462-2920.2011.02626.x.

Bonnet, J. *et al.* (2016) 'Trace Element Distribution (Cu, Ga, Ge, Cd, and Fe) IN Sphalerite From the Tennessee MVT Deposits, USA, By Combined EMPA, LA-ICP-MS, Raman Spectroscopy, and Crystallography', *The Canadian Mineralogist*. Mineralogical Association of Canada, 54(5), pp. 1261–1284. doi: 10.3749/canmin.1500104.

Borja, D. *et al.* (2019) 'Continuous bioleaching of arsenopyrite from mine tailings using an adapted mesophilic microbial culture', *Hydrometallurgy*. Elsevier, 187, pp. 187–194. doi: 10.1016/J.HYDROMET.2019.05.022.

Bortnikov, N. S. *et al.* (2010) 'The Sarylakh and Sentachan Gold–Antimony Deposits, Sakha-Yakutia: A Case of Combined Mesothermal Gold–Quartz and Epithermal Stibnite Ore', *Geology of Ore Deposits*, 52(5), pp. 339–372.

Bosecker, K. (1997) 'Bioleaching: metal solubilization by microorganisms', *FEMS Microbiology Reviews*. Oxford University Press, 20(3–4), pp. 591–604. doi: 10.1111/j.1574-6976.1997.tb00340.x.

Bostelmann, H. and Southam, G. (2020) 'A Column Leaching Model of Low-Grade Chalcopyrite Ore: Mineral Preferences and Chemical Reactivity', *Minerals 2020, Vol. 10, Page 1132*. Multidisciplinary Digital Publishing Institute, 10(12), p. 1132. doi: 10.3390/MIN10121132.

Brar, K. K. *et al.* (2021) 'Integrated bioleaching-electrometallurgy for copper recovery - A critical review', *Journal of Cleaner Production*. Elsevier, 291, p. 125257. doi: 10.1016/J.JCLEPRO.2020.125257.

Bray, N. L. *et al.* (2016) 'Near-optimal probabilistic RNA-seq quantification', *Nature*

Biotechnology. Nature Publishing Group, 34(5), pp. 525–527. doi: 10.1038/nbt.3519.

Brierley, C. L. and Brierley, J. A. (2013) 'Progress in bioleaching: Part B: Applications of microbial processes by the minerals industries', *Applied Microbiology and Biotechnology*, pp. 7543–7552. doi: 10.1007/s00253-013-5095-3.

Brierley, J. A. and Kuhn, M. C. (2009) 'From laboratory to application heap bioleach or not', in *Advanced Materials Research*, pp. 311–317. doi: 10.4028/www.scientific.net/AMR.71-73.311.

Brierley, J. A. and Kuhn, M. C. (2010) 'Fluoride toxicity in a chalcocite bioleach heap process', in *Hydrometallurgy*. Elsevier, pp. 410–413. doi: 10.1016/j.hydromet.2010.01.013.

Brooks, J. P. *et al.* (2015) 'The truth about metagenomics: Quantifying and counteracting bias in 16S rRNA studies Ecological and evolutionary microbiology', *BMC Microbiology*. BioMed Central Ltd., 15(1), p. 66. doi: 10.1186/s12866-015-0351-6.

Brune, D. C. (1989) 'Sulfur oxidation by phototrophic bacteria', *Biochimica et Biophysica Acta (BBA) - Bioenergetics*. Elsevier, 975(2), pp. 189–221. doi: 10.1016/S0005-2728(89)80251-8.

Buetti-Dinh, A. *et al.* (2020) 'Reverse engineering directed gene regulatory networks from transcriptomics and proteomics data of biomining bacterial communities with approximate Bayesian computation and steady-state signalling simulations', *BMC Bioinformatics*. BioMed Central Ltd., 21(1), pp. 1–15. doi: 10.1186/S12859-019-3337-9/TABLES/1.

Bunse, C. *et al.* (2016) 'Response of marine bacterioplankton pH homeostasis gene expression to elevated CO2', *Nature Climate Change 2016 6:5*. Nature

Publishing Group, 6(5), pp. 483–487. doi: 10.1038/nclimate2914.

Callahan, H. (2010) ‘Improved DNA and RNA isolation from biofilms’, *BioTechniques*. Future Science Ltd London, UK , 48(5), p. 413. doi: 10.2144/000113424/ASSET/IMAGES/LARGE/TABLE1.JPEG.

Camacho, D. *et al.* (2020) ‘New Insights Into Acidithiobacillus thiooxidans Sulfur Metabolism Through Coupled Gene Expression, Solution Chemistry, Microscopy, and Spectroscopy Analyses’, *Frontiers in Microbiology*. Frontiers Media S.A., 11, p. 411. doi: 10.3389/fmicb.2020.00411.

Caporaso, J. G. *et al.* (2010) ‘QIIME allows analysis of high-throughput community sequencing data’, *Nature Methods*. Nat Methods, pp. 335–336. doi: 10.1038/nmeth.f.303.

Cárdenas, J. P. *et al.* (2009) ‘Predicted CO/CO2 fixation in Ferroplasma spp. via a novel chimaeric pathway’, in *Advanced Materials Research*, pp. 219–222. doi: 10.4028/www.scientific.net/AMR.71-73.219.

Cárdenas, J. P. *et al.* (2010) ‘Lessons from the genomes of extremely acidophilic bacteria and archaea with special emphasis on bioleaching microorganisms’, *Applied Microbiology and Biotechnology*. Springer, pp. 605–620. doi: 10.1007/s00253-010-2795-9.

Cárdenas, J. P., Quatrini, R. and Holmes, D. S. (2016) ‘Genomic and metagenomic challenges and opportunities for bioleaching: a mini-review’, *Research in Microbiology*. Elsevier Masson, 167(7), pp. 529–538. doi: 10.1016/J.RESMIC.2016.06.007.

Carlos, C. *et al.* (2008) ‘The rus operon genes are differentially regulated when Acidithiobacillus ferrooxidans LR is kept in contact with metal sulfides’, *Current Microbiology*, 57(4), pp. 375–380. doi: 10.1007/s00284-008-9208-7.

Casiot, C. *et al.* (2007) 'Antimony and arsenic mobility in a creek draining an antimony mine abandoned 85 years ago (upper Orb basin, France)', *Applied Geochemistry*. Pergamon, 22(4), pp. 788–798. doi: 10.1016/J.APGEOCHEM.2006.11.007.

Cassman, N. A. *et al.* (2018) 'Genome-resolved metagenomics of sugarcane vinasse bacteria', *Biotechnology for Biofuels*. BioMed Central Ltd., 11(1), pp. 1–16. doi: 10.1186/s13068-018-1036-9.

Castelle, C. *et al.* (2008) 'A New Iron-oxidizing O2-reducing Supercomplex Spanning Both Inner and Outer Membranes, Isolated from the Extreme Acidophile Acidithiobacillus ferrooxidans', *Journal of Biological Chemistry*, 283(38), pp. 25803–25811. doi: 10.1074/jbc.M802496200.

Castelle, C. J. *et al.* (2015) 'The aerobic respiratory chain of the acidophilic archaeon Ferroplasma acidiphilum: A membrane-bound complex oxidizing ferrous iron', *Biochimica et Biophysica Acta - Bioenergetics*. Elsevier, 1847(8), pp. 717–728. doi: 10.1016/j.bbabio.2015.04.006.

Chaerun, S. K., Putri, E. A. and Mubarok, M. Z. (2020) 'Bioleaching of Indonesian Galena Concentrate With an Iron- and Sulfur-Oxidizing Mixotrophic Bacterium at Room Temperature', *Frontiers in Microbiology*. Frontiers, 0, p. 2427. doi: 10.3389/FMICB.2020.557548.

Chen, J. and Chen, Y. (2010) 'A first-principle study of the effect of vacancy defects and impurities on the adsorption of O2 on sphalerite surfaces', *Colloids and Surfaces A: Physicochemical and Engineering Aspects*. Elsevier, 363(1–3), pp. 56–63. doi: 10.1016/J.COLSURFA.2010.04.013.

Chen, L. *et al.* (2015) 'Comparative metagenomic and metatranscriptomic analyses of microbial communities in acid mine drainage', *The ISME Journal*. Nature Publishing Group, 9(7), pp. 1579–1592. doi: 10.1038/ismej.2014.245.

Chen, L. X. *et al.* (2015) 'Comparative metagenomic and metatranscriptomic

analyses of microbial communities in acid mine drainage', *ISME Journal*. Nature Publishing Group, 9(7), pp. 1579–1592. doi: 10.1038/ismej.2014.245.

Chen, P. *et al.* (2011) 'Bioleaching of realgar by Acidithiobacillus ferrooxidans using ferrous iron and elemental sulfur as the sole and mixed energy sources', *Bioresource Technology*. Elsevier, 102(3), pp. 3260–3267. doi: 10.1016/J.BIORTECH.2010.11.059.

Chen, Y., Chen, J. and Guo, J. (2010) 'A DFT study on the effect of lattice impurities on the electronic structures and floatability of sphalerite', *Minerals Engineering*. Pergamon, 23(14), pp. 1120–1130. doi: 10.1016/J.MINENG.2010.07.005.

Chen, Z. W. *et al.* (2007) 'Novel bacterial sulfur oxygenase reductases from bioreactors treating gold-bearing concentrates', *Applied Microbiology and Biotechnology*. Springer, 74(3), pp. 688–698. doi: 10.1007/s00253-006-0691-0.

Christel, S., Fridlund, J., Watkin, E. L., *et al.* (2016) 'Acidithiobacillus ferrivorans SS3 presents little RNA transcript response related to cold stress during growth at 8 °C suggesting it is a eurypsychrophile', *Extremophiles*. Springer Japan, 20(6), pp. 903–913. doi: 10.1007/s00792-016-0882-2.

Christel, S., Fridlund, J., Buetti-Dinh, A., *et al.* (2016) 'RNA transcript sequencing reveals inorganic sulfur compound oxidation pathways in the acidophile *Acidithiobacillus ferrivorans*', *FEMS Microbiology Letters*. Edited by R. Boden. Narnia, 363(7), p. fnw057. doi: 10.1093/femsle/fnw057.

Christel, S. *et al.* (2018) 'Weak Iron Oxidation by Sulfobacillus thermosulfidooxidans Maintains a Favorable Redox Potential for Chalcopyrite Bioleaching', *Frontiers in Microbiology*. Frontiers Media S.A., 9(DEC), p. 3059. doi: 10.3389/fmicb.2018.03059.

Constantinou, G. (1975) 'Idaite from the Skouriotissa Massive Sulfide Orebody, Cyprus', *American Mineralogist*, 60, pp. 3–8.

Constantinou, G. and Govett, G. J. S. (1973) 'Geology, geochemistry, and genesis of Cyprus sulfide deposits', *Economic Geology*, 68(6), pp. 843–858. doi: 10.2113/gsecongeo.68.6.843.

Cook, N. J. *et al.* (2009) 'Trace and minor elements in sphalerite: A LA-ICPMS study', *Geochimica et Cosmochimica Acta*. Pergamon, 73(16), pp. 4761–4791. doi: 10.1016/J.GCA.2009.05.045.

Cook, N. J. *et al.* (2011) 'Minor and trace elements in bornite and associated Cu–(Fe)-sulfides: A LA-ICP-MS studyBornite mineral chemistry', *Geochimica et Cosmochimica Acta*. Pergamon, 75(21), pp. 6473–6496. doi: 10.1016/J.GCA.2011.08.021.

Cook, N. J. *et al.* (2012) 'Determination of the oxidation state of Cu in substituted Cu-In-Fe-bearing sphalerite via -XANES spectroscopy', *American Mineralogist*. GeoScienceWorld, 97(2–3), pp. 476–479. doi: 10.2138/am.2012.4042.

Cook, N. J. *et al.* (2015) 'Distribution and Substitution Mechanism of Ge in a Ge-(Fe)-Bearing Sphalerite', *Minerals 2015, Vol. 5, Pages 117-132*. Multidisciplinary Digital Publishing Institute, 5(2), pp. 117–132. doi: 10.3390/MIN5020117.

Cooper, E. D. *et al.* (2014) 'Metatranscriptome profiling of a harmful algal bloom', *Harmful Algae*. Elsevier, 37, pp. 75–83. doi: 10.1016/j.hal.2014.04.016.

Cooper, R. G. and Harrison, A. P. (2009) 'The exposure to and health effects of antimony.', *Indian journal of occupational and environmental medicine*, 13(1), pp. 3–10. doi: 10.4103/0019-5278.50716.

Corkhill, C. L. *et al.* (2008) 'The oxidative dissolution of arsenopyrite (FeAsS) and enargite (Cu3AsS4) by Leptospirillum ferrooxidans', *Geochimica et Cosmochimica Acta*, 72(23), pp. 5616–5633. doi: 10.1016/j.gca.2008.09.008.

Courtin-Nomade, A. *et al.* (2009) 'The weathering of a sulfide orebody: Speciation and fate of some potential contaminants', *Canadian Mineralogist*, 47(3), pp. 493–508. doi: 10.3749/CANMIN.47.3.493.

Cravotta, C. A. and Kirby, C. S. (2004) 'ACIDITY AND ALKALINITY IN MINE DRAINAGE : THEORETICAL', *2004 National Meeting of the American Society of Mining and Reclamation and the 25th West Virginia Surface Mine Drainage Task Force, A*, pp. 334–365. doi: 10.21000/JASMR04010334.

Crowson, P. (2012) 'Some observations on copper yields and ore grades', *Resources Policy*. Pergamon, 37(1), pp. 59–72. doi: 10.1016/J.RESOURPOL.2011.12.004.

Crundwell, F. K. (2015) 'The semiconductor mechanism of dissolution and the pseudo-passivation of chalcopyrite', *Canadian Metallurgical Quarterly*. Maney Publishing, 54(3), pp. 279–288. doi: 10.1179/1879139515Y.0000000007.

Cyprus Geological Survey (2017) *Copper and Copper Mines In Cyprus*. Available at: www.moa.gov.cy/gsd (Accessed: 3 September 2020).

D'Amore, R. *et al.* (2016) 'A comprehensive benchmarking study of protocols and sequencing platforms for 16S rRNA community profiling', *BMC Genomics*, 17(1), p. 55. doi: 10.1186/s12864-015-2194-9.

D'Hugues, P. *et al.* (2002) 'Continuous bioleaching of chalcopyrite using a novel extremely thermophilic mixed culture', *International Journal of Mineral Processing*. Elsevier, 66(1–4), pp. 107–119. doi: 10.1016/S0301-7516(02)00004-2.

Dare, S. A. S. *et al.* (2011) 'Chalcophile and platinum-group element (PGE) concentrations in the sulfide minerals from the McCreedy East deposit, Sudbury, Canada, and the origin of PGE in pyrite', *Mineralium Deposita*, 46(4), pp. 381–407. doi: 10.1007/s00126-011-0336-9.

Das, A. P. and Ghosh, S. (2018) 'Bioleaching of Manganese from mining waste materials', *Materials Today: Proceedings*. Elsevier, 5(1), pp. 2381–2390. doi: 10.1016/J.MATPR.2017.11.459.

Davids, M. *et al.* (2016) 'Functional Profiling of Unfamiliar Microbial Communities Using a Validated De Novo Assembly Metatranscriptome Pipeline', *PLOS ONE*. Edited by I. K. Jordan. Public Library of Science, 11(1), p. e0146423. doi: 10.1371/journal.pone.0146423.

Davidson, D. F. (1960) *Selenium in Some Epithermal Deposits of Antimony, Mercury and Silver and Gold*, *Geological Survey Bulletin*.

Delforno, T. P. *et al.* (2019) 'Comparative metatranscriptomic analysis of anaerobic digesters treating anionic surfactant contaminated wastewater', *Science of The Total Environment*. Elsevier, 649, pp. 482–494. doi: 10.1016/J.SCITOTENV.2018.08.328.

Dembele, S., Akcil, A. and Panda, S. (2022) 'Technological trends, emerging applications and metallurgical strategies in antimony recovery from stibnite', *Minerals Engineering*. Pergamon, 175, p. 107304. doi: 10.1016/J.MINENG.2021.107304.

Deng, S. *et al.* (2017) 'Bioleaching of arsenopyrite by mixed cultures of iron-oxidizing and sulfur-oxidizing microorganisms', *Chemosphere*. Chemosphere, 185, pp. 403–411. doi: 10.1016/j.chemosphere.2017.07.037.

Desborough, G. A. *et al.* (2010) 'Mineralogical and chemical characteristics of some natural jarosites', *Geochimica et Cosmochimica Acta*, 74(3), pp. 1041–1056. doi: 10.1016/j.gca.2009.11.006.

Dhir, B. (2018) 'Biotechnological Tools for Remediation of Acid Mine Drainage (Removal of Metals From Wastewater and Leachate)', in *Bio-Geotechnologies for Mine Site Rehabilitation*. Elsevier, pp. 67–82. doi: 10.1016/B978-0-12-812986-

9.00004-X.

Dimitrijević, M. *et al.* (2009) 'Influence of pyrometallurgical copper production on the environment', *Journal of Hazardous Materials*. Elsevier, 164(2–3), pp. 892–899. doi: 10.1016/j.jhazmat.2008.08.099.

Donati, E. *et al.* (1996) 'Bioleaching of covellite using pure and mixed cultures of Thiobacillus ferrooxidans and Thiobacillus thiooxidans', *Process Biochemistry*. Elsevier BV, 31(2), pp. 129–134. doi: 10.1016/0032-9592(95)00037-2.

Dopson, M. *et al.* (2004) 'Characterization of Ferroplasma Isolates and Ferroplasma acidarmanus sp. nov., Extreme Acidophiles from Acid Mine Drainage and Industrial Bioleaching Environments', *Applied and Environmental Microbiology*. American Society for Microbiology, 70(4), pp. 2079–2088. doi: 10.1128/AEM.70.4.2079-2088.2004.

Dopson, M., Baker-Austin, C. and Bond, P. (2007) 'Towards determining details of anaerobic growth coupled to ferric iron reduction by the acidophilic archaeon "Ferroplasma acidarmanus" Fer1', *Extremophiles*, 11(1), pp. 159–168. doi: 10.1007/s00792-006-0029-y.

Dopson, M., Baker-Austin, C. and Bond, P. L. (2005) 'Analysis of differential protein expression during growth states of Ferroplasma strains and insights into electron transport for iron oxidation', *Microbiology*. Microbiology Society, 151(12), pp. 4127–4137. doi: 10.1099/mic.0.28362-0.

Dopson, M. and Johnson, D. B. (2012) 'Biodiversity, metabolism and applications of acidophilic sulfur-metabolizing microorganisms', *Environmental Microbiology*. John Wiley & Sons, Ltd, 14(10), pp. 2620–2631. doi: 10.1111/j.1462-2920.2012.02749.x.

Dopson, M. and Lindström, E. B. (2004) 'Analysis of community composition during moderately thermophilic bioleaching of pyrite, arsenical pyrite, and chalcopyrite',

Microbial Ecology. Springer-Verlag, 48(1), pp. 19–28. doi: 10.1007/s00248-003-2028-1.

Dugat-Bony, E. *et al.* (2015) 'Overview of a Surface-Ripened Cheese Community Functioning by Meta-Omics Analyses'. doi: 10.1371/journal.pone.0124360.

Dumitrache, A. *et al.* (2017) 'Specialized activities and expression differences for Clostridium thermocellum biofilm and planktonic cells', *Scientific Reports*. Nature Publishing Group, 7(1), pp. 1–14. doi: 10.1038/srep43583.

Dutrizac, J. E. and MacDonald, R. J. C. (1973) 'The effect of some impurities on the rate of chalcopyrite dissolution', *Canadian Metallurgical Quarterly*. Taylor & Francis, 12(4), pp. 409–420. doi: 10.1179/cmq.1973.12.4.409.

Edgar, R. C. (2013) 'UPARSE: Highly accurate OTU sequences from microbial amplicon reads', *Nature Methods*, 10(10), pp. 996–998. doi: 10.1038/nmeth.2604.
Edlund, A. *et al.* (2018) 'Uncovering complex microbiome activities via metatranscriptomics during 24 hours of oral biofilm assembly and maturation', *Microbiome*. BioMed Central Ltd., 6(1), pp. 1–22. doi: 10.1186/s40168-018-0591-4.

Edwards, Katrina J. *et al.* (2000) 'An Archaeal iron-oxidizing extreme acidophile important in acid mine drainage', *Science*, 287(5459), pp. 1796–1799. doi: 10.1126/science.287.5459.1796.

Edwards, Katrina J *et al.* (2000) 'Geochemical and biological aspects of sulfide mineral dissolution: lessons from Iron Mountain, California', *Chemical Geology*, 169(3), pp. 383–397. doi: 10.1016/S0009-2541(00)00216-3.

Eisenlohr, L. *et al.* (1999) 'The inhibiting action of intrinsic impurities in natural calcium carbonate minerals to their dissolution kinetics in aqueous H2O–CO2 solutions', *Geochimica et Cosmochimica Acta*, 63(7), pp. 989–1001. doi: 10.1016/S0016-7037(98)00301-9.

Elshkaki, A. *et al.* (2016) ‘Copper demand, supply, and associated energy use to 2050’, *Global Environmental Change*. Elsevier Ltd, 39, pp. 305–315. doi: 10.1016/j.gloenvcha.2016.06.006.

European Environment Agency (2019) *EMEP/EEA air pollutant emission inventory guidebook 2019. Technical guidance to prepare national emission inventories. EEA Report No 13/2019.* Available at: https://www.eea.europa.eu/publications/emep-eea-guidebook-2019/part-b-sectoral-guidance-chapters/2-industrial-processes/2-c-metal-production/2-c-7-a-copper/view (Accessed: 11 January 2022).

European Planetary Science Congress (2013) ‘The Skouriotissa mine: a new terrestrial analogue for hydrated mineral formation on Early Mars’, 8. Available at: www.isar.cnrs- (Accessed: 3 September 2020).

Evans, J. S., López-Legentil, S. and Erwin, P. M. (2018) ‘Comparing Two Common DNA Extraction Kits for the Characterization of Symbiotic Microbial Communities from Ascidian Tissue’, *Microbes and Environments*. Nakanishi Printing, 33(4), p. 435. doi: 10.1264/JSME2.ME18031.

Fallon, E. K. *et al.* (2019) ‘Geological, Mineralogical and Textural Impacts on the Distribution of Environmentally Toxic Trace Elements in Seafloor Massive Sulfide Occurrences’, *Minerals 2019, Vol. 9, Page 162*. Multidisciplinary Digital Publishing Institute, 9(3), p. 162. doi: 10.3390/MIN9030162.

Fang, D. and Zhou, L. X. (2006) ‘Effect of Sludge Dissolved Organic Matter on Oxidation of Ferrous Iron and Sulfur by Acidithiobacillus Ferrooxidans and Acidithiobacillus Thiooxidans’, *Water, Air, & Soil Pollution 2005 171:1*. Springer, 171(1), pp. 81–94. doi: 10.1007/S11270-005-9014-9.

Fantauzzi, M. *et al.* (2011) ‘Arsenopyrite and pyrite bioleaching: Evidence from XPS, XRD and ICP techniques’, *Analytical and Bioanalytical Chemistry*. Springer,

401(7), pp. 2237–2248. doi: 10.1007/S00216-011-5300-0/TABLES/7.

Fenchel, T., King, G. M. and Blackburn, T. H. (2012) '7. Aquatic Sediments', in *Bacterial Biogeochemistry: The Ecophysiology of Mineral Cycling*. 3rd edn. London: Academic Press, pp. 138–142. Available at: https://books.google.co.uk/books?hl=en&lr=&id=PUilCEGS1osC&oi=fnd&pg=PP2&dq=COLOURLESS+SULFUR+BACTERIA&ots=RCFqxu7nPb&sig=SSHQCT9jyTTlU_FT1EzBXtHYWoc#v=onepage&q=COLOURLESS SULFUR BACTERIA&f=false (Accessed: 13 August 2020).

Feng, S. *et al.* (2013) 'A novel and highly efficient system for chalcopyrite bioleaching by mixed strains of Acidithiobacillus', *Bioresource Technology*. Elsevier Ltd, 129, pp. 456–462. doi: 10.1016/j.biortech.2012.11.110.

Feng, S. *et al.* (2020) 'Metabolic transcriptional analysis on copper tolerance in moderate thermophilic bioleaching microorganism Acidithiobacillus caldus', *Journal of Industrial Microbiology and Biotechnology*. Oxford Academic, 47(1), pp. 21–33. doi: 10.1007/s10295-019-02247-6.

Filella, M., Belzile, N. and Chen, Y.-W. (2002) 'Antimony in the environment: a review focused on natural waters I', *Earth-Science Reviews*, 57(1–2), pp. 125–176. doi: 10.1016/S0012-8252(01)00070-8.

De Filippis, F. *et al.* (2016) 'Metatranscriptomics reveals temperature-driven functional changes in microbiome impacting cheese maturation rate', *Scientific Reports 2016 6:1*. Nature Publishing Group, 6(1), pp. 1–11. doi: 10.1038/srep21871.

Fontboté, L. *et al.* (2017) 'Sulfide minerals in hydrothermal deposits', *Elements*. GeoScienceWorld, 13(2), pp. 97–103. doi: 10.2113/gselements.13.2.97.

França, A., Melo, L. D. and Cerca, N. (2011) 'Comparison of RNA extraction methods from biofilm samples of Staphylococcus epidermidis', *BMC Research*

Notes. BioMed Central, 4, p. 572. doi: 10.1186/1756-0500-4-572.

Friedrich, C. G. *et al.* (2000) 'Novel genes coding for lithotrophic sulfur oxidation of Paracoccus pantotrophus GB17', *Journal of Bacteriology*. American Society for Microbiology Journals, 182(17), pp. 4677–4687. doi: 10.1128/JB.182.17.4677-4687.2000.

Friedrich, C. G. *et al.* (2001) 'Oxidation of reduced inorganic sulfur compounds by bacteria: emergence of a common mechanism?', *Applied and environmental microbiology*, 67(7), pp. 2873–82. doi: 10.1128/AEM.67.7.2873-2882.2001.

Friedrich, C. G. *et al.* (2005) 'Prokaryotic sulfur oxidation', *Current Opinion in Microbiology*. Elsevier Current Trends, 8(3), pp. 253–259. doi: 10.1016/J.MIB.2005.04.005.

Frigaard, N. U. and Dahl, C. (2008) 'Sulfur Metabolism in Phototrophic Sulfur Bacteria', *Advances in Microbial Physiology*. Academic Press, pp. 103–200. doi: 10.1016/S0065-2911(08)00002-7.

Fu, S. *et al.* (2020) 'Trace element composition of stibnite: Substitution mechanism and implications for the genesis of Sb deposits in southern China', *Applied Geochemistry*. Pergamon, p. 104637. doi: 10.1016/j.apgeochem.2020.104637.

Fullerton, H. *et al.* (2017) 'Hidden diversity revealed by genome-resolved metagenomics of iron-oxidizing microbial mats from Lo'ihi Seamount, Hawai'i', *ISME Journal*. Nature Publishing Group, 11(8), pp. 1900–1914. doi: 10.1038/ismej.2017.40.

Galleguillos, P. *et al.* (2008) 'Identification of differentially expressed genes in an industrial bioleaching heap processing low-grade copper sulphide ore elucidated by RNA arbitrarily primed polymerase chain reaction', *Hydrometallurgy*, 94(1), pp. 148–154. doi: 10.1016/j.hydromet.2008.05.031.

Garcia, O., Bigham, J. M. and Tuovinen, O. H. (1995) 'Oxidation of galena by Thiobacillus ferrooxidans and Thiobacillus thiooxidans', *Canadian Journal of Microbiology*. Canadian Science Publishing, 41(6), pp. 508–514. doi: 10.1139/M95-067.

Gartman, A., Whisman, S. P. and Hein, J. R. (2020) 'Sphalerite Oxidation in Seawater with Covellite: Implications for Seafloor Massive Sulfide Deposits and Mine Waste', *ACS Earth and Space Chemistry*. American Chemical Society, 4(12), pp. 2261–2269. doi: 10.1021/ACSEARTHSPACECHEM.0C00177/ASSET/IMAGES/LARGE/SP0C00177_0008.JPEG.

Gates-Rector, S. and Blanton, T. (2019) 'The Powder Diffraction File: a quality materials characterization database', *Powder Diffraction*. Cambridge University Press, 34(4), pp. 352–360. doi: 10.1017/S0885715619000812.

George, L. *et al.* (2015) 'Trace and minor elements in galena: A reconnaissance LA-ICP-MS study', *American Mineralogist*. Walter de Gruyter GmbH, 100(2–3), pp. 548–569. doi: 10.2138/am-2015-4862.

Ghosh, A., Mehta, A. and Khan, A. M. (2018) 'Metagenomic analysis and its applications', in *Encyclopedia of Bioinformatics and Computational Biology: ABC of Bioinformatics*. Elsevier, pp. 184–193. doi: 10.1016/B978-0-12-809633-8.20178-7.

Ghosh, W. and Dam, B. (2009) 'Biochemistry and molecular biology of lithotrophic sulfur oxidation by taxonomically and ecologically diverse bacteria and archaea', *FEMS Microbiology Reviews*. Oxford University Press, pp. 999–1043. doi: 10.1111/j.1574-6976.2009.00187.x.

Gilbertson, B. P. (2000) 'Creating value through innovation: biotechnology in mining', *Mineral Processing and Extractive Metallurgy*. Taylor & Francis, 109(2), pp. 61–67. doi: 10.1179/mpm.2000.109.2.61.

Gleisner, M., Herbert, R. B. and Frogner Kockum, P. C. (2006) 'Pyrite oxidation by Acidithiobacillus ferrooxidans at various concentrations of dissolved oxygen', *Chemical Geology*, 225(1), pp. 16–29. doi: 10.1016/j.chemgeo.2005.07.020.

Golyshina, O. V *et al.* (2016) 'The novel extremely acidophilic, cell-wall-deficient archaeon Cuniculiplasma divulgatum gen. Nov., sp. nov. represents a new family, Cuniculiplasmataceae fam. nov., of the order Thermoplasmatales', *International Journal of Systematic and Evolutionary Microbiology*. Microbiology Society, 66(1), pp. 332–340. doi: 10.1099/ijsem.0.000725.

Grant, H. L. J. *et al.* (2018) 'Constraints on the behavior of trace elements in the actively-forming TAG deposit, Mid-Atlantic Ridge, based on LA-ICP-MS analyses of pyrite', *Chemical Geology*. Elsevier, 498, pp. 45–71. doi: 10.1016/J.CHEMGEO.2018.08.019.

Gribble, C. D. and Hall, A. J. (1985) 'Sulphides', in *A Practical Guide to Optical Mineralogy*. George Allen & Unwin.

Grout, J. A. and Levings, C. D. (2001) 'Effects of acid mine drainage from an abandoned copper mine, Britannia Mines, Howe Sound, British Columbia, Canada, on transplanted blue mussels (Mytilus edulis)', *Marine Environmental Research*. Elsevier, 51(3), pp. 265–288. doi: 10.1016/S0141-1136(00)00104-5.

Gu, G. *et al.* (2015) 'Formation of passivation film during pyrrhotite bioleached by pure L. ferriphilum and mixed culture of L. ferriphilum and A. caldus', *Journal of Central South University 2015 22:3*. Springer, 22(3), pp. 880–886. doi: 10.1007/S11771-015-2597-4.

Guerra-Bieberach, G. *et al.* (2017) 'Expression of candidate cold stress and metabolic related genes in Acidithiobacillus ferrivorans PQ33 strain using ferrous iron as electron donor', in *Solid State Phenomena*, pp. 368–371. doi: 10.4028/www.scientific.net/SSP.262.368.

Haghshenas, D. F. *et al.* (2009) 'Kinetics of sphalerite bioleaching by Acidithiobacillus ferrooxidans', *Hydrometallurgy*. Elsevier, 99(3–4), pp. 202–208. doi: 10.1016/J.HYDROMET.2009.08.007.

Halinen, A. K. *et al.* (2012) 'Microbial community dynamics during a demonstration-scale bioheap leaching operation', *Hydrometallurgy*, 125–126, pp. 34–41. doi: 10.1016/j.hydromet.2012.05.001.

Hallberg, K. B., González-Toril, E. and Johnson, D. B. (2010) 'Acidithiobacillus ferrivorans, sp. nov.; facultatively anaerobic, psychrotolerant iron-, and sulfur-oxidizing acidophiles isolated from metal mine-impacted environments', *Extremophiles*. Springer Japan, 14(1), pp. 9–19. doi: 10.1007/s00792-009-0282-y.

Hamamura, N., Fukushima, K. and Itai, T. (2013) 'Identification of Antimony- and Arsenic-Oxidizing Bacteria Associated with Antimony Mine Tailing', *Microbes and Environments*, 28(2), pp. 257–263. doi: 10.1264/jsme2.ME12217.

Han, X. Y. *et al.* (2002) 'Rapid and Accurate Identification of Mycobacteria by Sequencing Hypervariable Regions of the 16S Ribosomal RNA Gene', *American Journal of Clinical Pathology*. Oxford University Press, 118(5), pp. 796–801. doi: 10.1309/HN44-XQYM-JMAQ-2EDL.

Hawkes, R. B., Franzmann, P. D. and Plumb, J. J. (2006) 'Moderate thermophiles including "Ferroplasma cupricumulans" sp. nov. dominate an industrial-scale chalcocite heap bioleaching operation', *Hydrometallurgy*. Elsevier, 83(1–4), pp. 229–236. doi: 10.1016/J.HYDROMET.2006.03.027.

He, H. *et al.* (2012) 'Analysis of sulfur speciation on chalcopyrite surface bioleached with Acidithiobacillus ferrooxidans', *Minerals Engineering*. Pergamon, 27–28, pp. 60–64. doi: 10.1016/j.mineng.2011.12.012.

He, M. *et al.* (2012) 'Antimony pollution in China', *Science of the Total Environment*.

Elsevier, pp. 41–50. doi: 10.1016/j.scitotenv.2011.06.009.

He, Z. *et al.* (2010) 'Insights into the dynamics of bacterial communities during chalcopyrite bioleaching', *FEMS Microbiology Ecology*. Oxford Academic, 74(1), pp. 155–164. Available at: https://academic.oup.com/femsec/article-lookup/doi/10.1111/j.1574-6941.2010.00943.x (Accessed: 27 October 2020).

He, Z. G. *et al.* (2014) 'Effect of pyrite, elemental sulfur and ferrous ions on EPS production by metal sulfide bioleaching microbes', *Transactions of Nonferrous Metals Society of China (English Edition)*. Nonferrous Metals Society of China, 24(4), pp. 1171–1178. doi: 10.1016/S1003-6326(14)63176-9.

Hedenquist, J. W., Arribas, A. and Gonzalez-Urien, E. (2000) 'Exploration for Epithermal Gold Deposits', in Hagemann, S. G. and Brown, P. E. (eds) *Gold in 2000*, pp. 245–277. doi: 10.5382/rev.13.07.

Hedrich, S. *et al.* (2016) 'Quantitative Monitoring of Microbial Species during Bioleaching of a Copper Concentrate', *Frontiers in Microbiology*. Frontiers Media SA, 7(DEC). doi: 10.3389/FMICB.2016.02044.

Hedrich, S. *et al.* (2018) 'Enhanced chalcopyrite dissolution in stirred tank reactors by temperature increase during bioleaching', *Hydrometallurgy*. Elsevier, 179, pp. 125–131. doi: 10.1016/J.HYDROMET.2018.05.018.

Hedrich, S., Schlömann, M. and Barrie Johnson, D. (2011) 'The iron-oxidizing proteobacteria', *Microbiology*. Microbiology Society, pp. 1551–1564. doi: 10.1099/mic.0.045344-0.

Herath, I., Vithanage, M. and Bundschuh, J. (2017) 'Antimony as a global dilemma: Geochemistry, mobility, fate and transport', *Environmental Pollution*, 223, pp. 545–559. doi: 10.1016/j.envpol.2017.01.057.

Hiller, E. *et al.* (2012) 'Arsenic and antimony contamination of waters, stream

sediments and soils in the vicinity of abandoned antimony mines in the Western Carpathians, Slovakia', *Applied Geochemistry*. Pergamon, 27(3), pp. 598–614. doi: 10.1016/j.apgeochem.2011.12.005.

Hiraishi, A. (2015) 'Acidisphaera', in *Bergey's Manual of Systematics of Archaea and Bacteria*. Chichester, UK: John Wiley & Sons, Ltd, pp. 1–5. doi: 10.1002/9781118960608.gbm00878.

Holmes, D. S. and Bonnefoy, V. (2007) 'Genetic and bioinformatic insights into iron and sulfur oxidation mechanisms of bioleaching organisms', *Biomining*. Springer-Verlag Berlin Heidelberg, pp. 281–307. doi: 10.1007/978-3-540-34911-2_14.

Hsieh, P.-H., Oyang, Y.-J. and Chen, C.-Y. (2018) 'Effect of de novo transcriptome assembly on transcript quantification', *bioRxiv*, p. 380998. doi: 10.1101/380998.

Hu, X. *et al.* (2016) 'pH-dependent release characteristics of antimony and arsenic from typical antimony-bearing ores', *Journal of Environmental Sciences (China)*. Chinese Academy of Sciences, 44, pp. 171–179. doi: 10.1016/j.jes.2016.01.003.

Hu, X. *et al.* (2017) 'The leaching characteristics and changes in the leached layer of antimony-bearing ores from China', *Journal of Geochemical Exploration*. Elsevier B.V., 176, pp. 76–84. doi: 10.1016/j.gexplo.2016.01.009.

Hu, X., He, M. and Kong, L. (2015) 'Photopromoted oxidative dissolution of stibnite', *Applied Geochemistry*, 61, pp. 53–61. doi: 10.1016/j.apgeochem.2015.05.014.

Huang, C. *et al.* (2018) 'Chalcopyrite bioleaching of an in situ leaching system by introducing different functional oxidizers', *RSC Advances*. Royal Society of Chemistry, 8(65), pp. 37040–37049. doi: 10.1039/C8RA07085G.

Huerta, L. and Burke, M. (2020) *Number of replicates | Functional genomics II*. Available at: https://www.ebi.ac.uk/training/online/courses/functional-genomics-ii-

common-technologies-and-data-analysis-methods/rna-sequencing/performing-a-rna-seq-experiment/design-considerations/number-of-replicates/ (Accessed: 13 April 2022).

Huston, D. L. *et al.* (1995) 'Trace elements in sulfide minerals from eastern Australian volcanic-hosted massive sulfide deposits; Part I, Proton microprobe analyses of pyrite, chalcopyrite, and sphalerite, and Part II, Selenium levels in pyrite; comparison with delta 34 S values and implications for the source of sulfur in volcanogenic hydrothermal systems', *Economic Geology*. GeoScienceWorld, 90(5), pp. 1167–1196. doi: 10.2113/gsecongeo.90.5.1167.

Hyatt, D. *et al.* (2010) 'Prodigal: Prokaryotic gene recognition and translation initiation site identification', *BMC Bioinformatics*. BioMed Central, 11(1), pp. 1–11. doi: 10.1186/1471-2105-11-119.

Ilbert, M. and Bonnefoy, V. (2013) 'Insight into the evolution of the iron oxidation pathways', *Biochimica et Biophysica Acta - Bioenergetics*. Elsevier, pp. 161–175. doi: 10.1016/j.bbabio.2012.10.001.

Ingledew, W. J. (1982) 'Thiobacillus Ferrooxidans the bioenergetics of an acidophilic chemolithotroph', *Biochimica et Biophysica Acta (BBA) - Reviews on Bioenergetics*. Elsevier, 683(2), pp. 89–117. doi: 10.1016/0304-4173(82)90007-6.
Inkscape (2019) 'Inkscape: Open Source Scalable Vector Graphics Editor'. Available at: https://inkscape.org/.

Ishii, T. *et al.* (2015) 'From chemolithoautotrophs to electrolithoautotrophs: CO2 fixation by Fe(II)-oxidizing bacteria coupled with direct uptake of electrons from solid electron sources', *Frontiers in Microbiology*. Frontiers, 6, p. 994. doi: 10.3389/fmicb.2015.00994.

Jankielewicz, A. *et al.* (1994) 'Polysulfide reductase and formate dehydrogenase from Wolinella succinogenes contain molybdopterin guanine dinucleotide', *Archives of Microbiology*. Springer-Verlag, 162(4), pp. 238–242. doi:

10.1007/BF00301844.

Jeans, C. *et al.* (2008) ‘Cytochrome 572 is a conspicuous membrane protein with iron oxidation activity purified directly from a natural acidophilic microbial community’, *ISME Journal*. Nature Publishing Group, 2(5), pp. 542–550. doi: 10.1038/ismej.2008.17.

Jia, Y. *et al.* (2019) ‘Sulfide mineral dissolution microbes: Community structure and function in industrial bioleaching heaps’, *Green Energy and Environment*. KeAi Publishing Communications Ltd., pp. 29–37. doi: 10.1016/j.gee.2018.04.001.

Jin, J. *et al.* (2012) ‘Arsenopyrite bioleaching by Acidithiobacillus ferrooxidans in a rotating-drum reactor’, *Minerals Engineering*. Pergamon, 39, pp. 19–22. doi: 10.1016/J.MINENG.2012.07.018.

Johnson, B. D. and Hallberg, K. B. (2008) ‘Carbon, Iron and Sulfur Metabolism in Acidophilic Micro-Organisms’, *Advances in Microbial Physiology*. Academic Press, 54, pp. 201–255. doi: 10.1016/S0065-2911(08)00003-9.

Johnson, D. (2018) ‘The Evolution, Current Status, and Future Prospects of Using Biotechnologies in the Mineral Extraction and Metal Recovery Sectors’, *Minerals*, 8(8), p. 343. doi: 10.3390/min8080343.

Johnson, D. B. (2003) ‘Chemical and Microbiological Characteristics of Mineral Spoils and Drainage Waters at Abandoned Coal and Metal Mines’, *Water, Air and Soil Pollution: Focus*. Kluwer Academic Publishers, 3(1), pp. 47–66. doi: 10.1023/A:1022107520836.

Johnson, D. B. (2014) ‘Biomining-biotechnologies for extracting and recovering metals from ores and waste materials’, *Current Opinion in Biotechnology*. Elsevier Ltd, pp. 24–31. doi: 10.1016/j.copbio.2014.04.008.

Johnson, D. B. and Hallberg, K. B. (2005) ‘Acid mine drainage remediation options: a review’, *Science of The Total Environment*, 338(1–2), pp. 3–14. doi:

10.1016/j.scitotenv.2004.09.002.

Johnson, D. B., Kanao, T. and Hedrich, S. (2012) 'Redox transformations of iron at extremely low pH: Fundamental and applied aspects', *Frontiers in Microbiology*. Frontiers Media SA, 3(MAR), p. 96. doi: 10.3389/fmicb.2012.00096.

Johnson, D. B. and Quatrini, R. (2020) 'Acidophile Microbiology in Space and Time', *Current Issues in Molecular Biology 2020, Vol. 39, Pages 63-76*. Multidisciplinary Digital Publishing Institute, 39(1), pp. 63–76. doi: 10.21775/CIMB.039.063.

Johnson, D. B. and Roberto, F. F. (1997) 'Heterotrophic Acidophiles and Their Roles in the Bioleaching of Sulfide Minerals', in *Biomining*. Springer Berlin Heidelberg, pp. 259–279. doi: 10.1007/978-3-662-06111-4_13.

Johnston, A. *et al.* (2017) 'Exploration of Diffuse and Discrete Sources of Acid Mine Drainage to a Headwater Mountain Stream in Colorado, USA', *Mine Water and the Environment*, 36(4), pp. 463–478. doi: 10.1007/s10230-017-0452-6.

Jones, D. S., Schaperdoth, I. and Macalady, J. L. (2014) 'Metagenomic Evidence for Sulfide Oxidation in Extremely Acidic Cave Biofilms', *Geomicrobiology Journal*. Taylor & Francis Group , 31(3), pp. 194–204. doi: 10.1080/01490451.2013.834008.

Jones, P. *et al.* (2014) 'InterProScan 5: Genome-scale protein function classification', *Bioinformatics*, 30(9), pp. 1236–1240. doi: 10.1093/bioinformatics/btu031.

De Jong, G. A. H. *et al.* (1997) 'Polythionate degradation by tetrathionate hydrolase of Thiobacillus ferrooxidans', *Microbiology*. Microbiology Society, 143(2), pp. 499–504. doi: 10.1099/00221287-143-2-499.

Kadıoğlu, Y. K. *et al.* (2009) 'XRF and Raman Characterization of Antimonite'.

Taylor & Francis Group , 37(6), pp. 683–696. doi: 10.1080/10739140903252956.

Kanao, T. *et al.* (2013) 'Crystallization and preliminary X-ray diffraction analysis of tetrathionate hydrolase from Acidithiobacillus ferrooxidans', *Acta Crystallographica Section F: Structural Biology and Crystallization Communications*. International Union of Crystallography, 69(6), pp. 692–694. doi: 10.1107/S1744309113013419.

Kantor, R. S. *et al.* (2015) 'Bioreactor microbial ecosystems for thiocyanate and cyanide degradation unravelled with genome-resolved metagenomics', *Environmental Microbiology*. Blackwell Publishing Ltd, 17(12), pp. 4929–4941. doi: 10.1111/1462-2920.12936.

Kappler, A. *et al.* (2015) 'Geomicrobiology of iron', in *Ehrlich's Geomicrobiology*. 6th edn. CRC Press, pp. 343–400. doi: 10.1201/b19121.

Karavaiko, G. I., Dubinina, G. A. and Kondrat'eva, T. F. (2006) 'Lithotrophic microorganisms of the oxidative cycles of sulfur and iron', *Microbiology*. Maik Nauka-Interperiodica Publishing, pp. 512–545. doi: 10.1134/S002626170605002X.

Kassambara, A. (2018) 'ggpubr: "ggplot2" Based Publication Ready Plots'. Available at: https://rpkgs.datanovia.com/ggpubr/.

Kay, C. M., Haanela, A. and Johnson, D. B. (2014) 'Microorganisms in subterranean acidic waters within Europe's deepest metal mine', *Research in Microbiology*, 165(9), pp. 705–712. doi: 10.1016/j.resmic.2014.07.007.

Kelly, D. P. and Wood, A. P. (2000) 'Reclassification of some species of Thiobacillus to the newly designated genera Acidithiobacillus gen. nov., Halothiobacillus gen. nov. and Thermithiobacillus gen. nov.', *International Journal of Systematic and Evolutionary Microbiology*, 50(2), pp. 511–516. doi: 10.1099/00207713-50-2-511.

Kembel, S. W. *et al.* (2010) 'Picante: {R} tools for integrating phylogenies and

ecology', *Bioinformatics*, 26, pp. 1463–1464.

Kikumoto, M. *et al.* (2013) 'Tetrathionate-forming thiosulfate dehydrogenase from the acidophilic, chemolithoautotrophic bacterium Acidithiobacillus ferrooxidans', *Applied and Environmental Microbiology*. American Society for Microbiology, 79(1), pp. 113–120. doi: 10.1128/AEM.02251-12.

Kim, B.-J., Koh, Y.-K. and Kwon, J.-S. (2021) 'Bioleaching of Pyrrhotite with Bacterial Adaptation and Biological Oxidation for Iron Recovery', *Metals 2021, Vol. 11, Page 295*. Multidisciplinary Digital Publishing Institute, 11(2), p. 295. doi: 10.3390/MET11020295.

Kimball, B. E., Rimstidt, J. D. and Brantley, S. L. (2010) 'Chalcopyrite dissolution rate laws', *Applied Geochemistry*. Pergamon, 25(7), pp. 972–983. doi: 10.1016/j.apgeochem.2010.03.010.

Klimko, T. *et al.* (2011) 'Chemical composition of weathering products in neutral and acidic mine tailings from stibnite exploitation in Slovakia', *Journal of Geosciences*, 5, pp. 327–340. doi: 10.3190/jgeosci.104.

Knight, K. S., Marshall, W. G. and Zochowski, S. W. (2011) 'The low-temperature and high-pressure thermoelastic and structural properties of chalcopyrite, CuFeS2', *Canadian Mineralogist*, 49(4), pp. 1015–1034. doi: 10.3749/canmin.49.4.1015.

Kocaman, A. T., Cemek, M. and Edwards, K. J. (2016) 'Kinetics of pyrite, pyrrhotite, and chalcopyrite dissolution by Acidithiobacillus ferrooxidans', *Canadian Journal of Microbiology*, 62(8), pp. 629–642. doi: 10.1139/cjm-2016-0085.

Konhauser, K. (2007) 'Microbial Weathering', in *Introduction to Geomicrobiology*. Blackwell Publishing Ltd, pp. 192–234.

Konishi, Y., Asai, S. and Yoshida, N. (1995) 'Growth Kinetics of Thiobacillus

thiooxidans on the Surface of Elemental Sulfur.', *Applied and environmental microbiology*. American Society for Microbiology, 61(10), pp. 3617–22. Available at: http://www.ncbi.nlm.nih.gov/pubmed/16535145 (Accessed: 28 March 2020).

Konishi, Y., Nishimura, H. and Asai, S. (1998) 'Bioleaching of sphalerite by the acidophilic thermophile Acidianus brierleyi', *Hydrometallurgy*. Elsevier, 47(2–3), pp. 339–352. doi: 10.1016/S0304-386X(97)00057-1.

Krafft, T., Gross, R. and Kröger, A. (1995) 'The Function of Wolinella succinogenes psr Genes in Electron Transport with Polysulphide as the Terminal Electron Acceptor', *European Journal of Biochemistry*. Eur J Biochem, 230(2), pp. 601–606. doi: 10.1111/j.1432-1033.1995.0601h.x.

Król, A., Mizerna, K. and Bożym, M. (2020) 'An assessment of pH-dependent release and mobility of heavy metals from metallurgical slag', *Journal of Hazardous Materials*. Elsevier, 384, p. 121502. doi: 10.1016/J.JHAZMAT.2019.121502.

Kulczycka, J. *et al.* (2016) 'Environmental Impacts of Energy-Efficient Pyrometallurgical Copper Smelting Technologies: The Consequences of Technological Changes from 2010 to 2050', *Journal of Industrial Ecology*. John Wiley & Sons, Ltd, 20(2), pp. 304–316. doi: 10.1111/JIEC.12369.

Kuske, C. R. *et al.* (2015) 'Prospects and challenges for fungal metatranscriptomics of complex communities', *Fungal Ecology*. Elsevier Ltd, pp. 133–137. doi: 10.1016/j.funeco.2014.12.005.

Kyono, A., Hayakawa, A. and Horiki, M. (2015) 'Selenium substitution effect on crystal structure of stibnite (Sb2S3)', *Physics and Chemistry of Minerals*. Springer Berlin Heidelberg, 42(6), pp. 475–490. doi: 10.1007/s00269-015-0737-x.

Lassalle, F. *et al.* (2021) 'Phylogenomics reveals the basis of adaptation of Pseudorhizobium species to extreme environments and supports a taxonomic revision of the genus', *Systematic and Applied Microbiology*. Urban & Fischer,

44(1), p. 126165. doi: 10.1016/J.SYAPM.2020.126165.

Lee, J. *et al.* (2011) 'Comparative bioleaching and mineralogy of composited sulfide ores containing enargite, covellite and chalcocite by mesophilic and thermophilic microorganisms', *Hydrometallurgy*. Elsevier, 105(3–4), pp. 213–221. doi: 10.1016/j.hydromet.2010.10.001.

Lee, S. T. M. *et al.* (2017) 'Tracking microbial colonization in fecal microbiota transplantation experiments via genome-resolved metagenomics', *Microbiome*. BioMed Central Ltd., 5(1), pp. 1–10. doi: 10.1186/S40168-017-0270-X.

Lehner, S. *et al.* (2007) 'The effect of As, Co, and Ni impurities on pyrite oxidation kinetics: An electrochemical study of synthetic pyrite', *Geochimica et Cosmochimica Acta*. Pergamon, 71(10), pp. 2491–2509. doi: 10.1016/J.GCA.2007.03.005.

Lerotic, M. *et al.* (2014) '{\it MANTiS}: a program for the analysis of X-ray spectromicroscopy data', *Journal of Synchrotron Radiation*, 21(5), pp. 1206–1212. doi: 10.1107/S1600577514013964.

Leuz, A.-K. and Johnson, C. A. (2005) 'Oxidation of Sb(III) to Sb(V) by O2 and H2O2 in aqueous solutions', *Geochimica et Cosmochimica Acta*, 69(5), pp. 1165–1172. doi: 10.1016/j.gca.2004.08.019.

Levicán, G. *et al.* (2008) 'Comparative genomic analysis of carbon and nitrogen assimilation mechanisms in three indigenous bioleaching bacteria: Predictions and validations', *BMC Genomics*. BioMed Central, 9(1), pp. 1–19. doi: 10.1186/1471-2164-9-581/FIGURES/7.

Levicán, G. *et al.* (2012) 'Comparative genomic analysis reveals novel facts about leptospirillum spp. cytochromes', *Journal of Molecular Microbiology and Biotechnology*. J Mol Microbiol Biotechnol, 22(2), pp. 94–104. doi: 10.1159/000338105.

Li, A. and Huang, S. (2011) ‘Comparison of the electrochemical mechanism of chalcopyrite dissolution in the absence or presence of Sulfolobus metallicus at 70 °c’, *Minerals Engineering*. Pergamon, 24(13), pp. 1520–1522. doi: 10.1016/j.mineng.2011.08.009.

Li, J. *et al.* (2017) ‘Abiotic and biotic factors responsible for antimonite oxidation in Agrobacterium tumefaciens GW4’, *Scientific Reports*. Nature Publishing Group, 7. doi: 10.1038/SREP43225.

Li, J. *et al.* (2018) ‘Novel Hyper Antimony-Oxidizing Bacteria Isolated from Contaminated Mine Soils in China’, *Geomicrobiology Journal*. Taylor and Francis Inc., 35(8), pp. 713–720. doi: 10.1080/01490451.2018.1454556/SUPPL_FILE/UGMB_A_1454556_SM4058.DOCX.

Li, Q. *et al.* (2018) ‘Comparative analysis of attachment to chalcopyrite of three mesophilic iron and/or sulfur-oxidizing acidophiles’, *Minerals*. MDPI AG, 8(9). doi: 10.3390/min8090406.

Li, Y. *et al.* (2013) *A review of the structure, and fundamental mechanisms and kinetics of the leaching of chalcopyrite*, *Advances in Colloid and Interface Science*. Elsevier B.V. doi: 10.1016/j.cis.2013.03.004.

Liljeqvist, M. *et al.* (2011) ‘Draft Genome of the Psychrotolerant Acidophile Acidithiobacillus ferrivorans SS3’, *JOURNAL OF BACTERIOLOGY*, 193(16), pp. 4304–4305. doi: 10.1128/JB.05373-11.

Liljeqvist, M., Rzhepishevska, O. I. and Dopson, M. (2013) ‘Gene identification and substrate regulation provide insights into sulfur accumulation during bioleaching with the psychrotolerant acidophile Acidithiobacillus ferrivorans’, *Applied and Environmental Microbiology*, 79(3), pp. 951–957. doi: 10.1128/AEM.02989-12.

Liu, F. *et al.* (2010) 'Antimony speciation and contamination of waters in the Xikuangshan antimony mining and smelting area, China', *Environmental Geochemistry and Health*. Springer Netherlands, 32(5), pp. 401–413. doi: 10.1007/s10653-010-9284-z.

Liu, H. C. *et al.* (2015) 'Investigation of copper, iron and sulfur speciation during bioleaching of chalcopyrite by moderate thermophile Sulfobacillus thermosulfidooxidans', *International Journal of Mineral Processing*. Elsevier, 137, pp. 1–8. doi: 10.1016/J.MINPRO.2015.02.008.

Liu, H., Gu, G. and Xu, Y. (2011) 'Surface properties of pyrite in the course of bioleaching by pure culture of Acidithiobacillus ferrooxidans and a mixed culture of Acidithiobacillus ferrooxidans and Acidithiobacillus thiooxidans', *Hydrometallurgy*. Elsevier, 108(1–2), pp. 143–148. doi: 10.1016/J.HYDROMET.2011.03.010.

Liu, R. *et al.* (2008) 'Comparison of dissolution under oxic acid drainage conditions for eight sedimentary and hydrothermal pyrite samples', *Environmental Geology*. Springer, 56(1), pp. 171–182. doi: 10.1007/S00254-007-1149-0/TABLES/5.

Liu, S.-J. (2008) 'Archaeal and Bacterial Sulfur Oxygenase-Reductases: Genetic Diversity and Physiological Function', in *Microbial Sulfur Metabolism*. Berlin, Heidelberg: Springer Berlin Heidelberg, pp. 217–224. doi: 10.1007/978-3-540-72682-1_17.

Loni, P. C. *et al.* (2020) 'Mechanism of microbial dissolution and oxidation of antimony in stibnite under ambient conditions', *Journal of Hazardous Materials*. Elsevier B.V., 385, p. 121561. doi: 10.1016/j.jhazmat.2019.121561.

Love, M. I., Huber, W. and Anders, S. (2014) 'Moderated estimation of fold change and dispersion for RNA-seq data with DESeq2', *Genome Biology*. BioMed Central Ltd., 15(12), p. 550. doi: 10.1186/s13059-014-0550-8.

Lu, X. and Wang, H. (2012) 'Microbial Oxidation of Sulfide Tailings and the

Environmental Consequences', *Elements*, 8(2), pp. 119–124. doi: 10.2113/gselements.8.2.119.

Lundström, M. *et al.* (2005) 'Leaching of chalcopyrite in cupric chloride solution', *Hydrometallurgy*, 77(1–2), pp. 89–95. doi: 10.1016/j.hydromet.2004.10.013.
Luo, J. *et al.* (2019) 'SLR: a scaffolding algorithm based on long reads and contig classification', *BMC bioinformatics*. NLM (Medline), 20(1), p. 539. doi: 10.1186/s12859-019-3114-9.

Ma, L. *et al.* (2017) 'Co-culture microorganisms with different initial proportions reveal the mechanism of chalcopyrite bioleaching coupling with microbial community succession', *Bioresource Technology*. Elsevier Ltd, 223, pp. 121–130. doi: 10.1016/j.biortech.2016.10.056.

Ma, L. *et al.* (2018) 'Intensified bioleaching of chalcopyrite by communities with enriched ferrous or sulfur oxidizers', *Bioresource Technology*. Elsevier Ltd, 268, pp. 415–423. doi: 10.1016/j.biortech.2018.08.019.

Ma, L. *et al.* (2019) 'Metatranscriptomics reveals microbial adaptation and resistance to extreme environment coupling with bioleaching performance', *Bioresource Technology*. Elsevier Ltd, 280, pp. 9–17. doi: 10.1016/j.biortech.2019.01.117.

Mackintosh, M. E. (1978) 'Nitrogen fixation by Thiobacillus ferrooxidans', *Journal of General Microbiology*, 105(2), pp. 215–218. doi: 10.1099/00221287-105-2-215.
Macrae, C. F. *et al.* (2020) '*Mercury 4.0* : from visualization to analysis, design and prediction', *Journal of Applied Crystallography*. International Union of Crystallography, 53(1), pp. 226–235. doi: 10.1107/S1600576719014092.

Macy, J. M. *et al.* (1996) 'Chrysiogenes arsenatis gen. nov., sp. nov., a new arsenate-respiring bacterium isolated from gold mine wastewater', *International journal of systematic bacteriology*. Int J Syst Bacteriol, 46(4), pp. 1153–1157. doi: 10.1099/00207713-46-4-1153.

Madu, B. E., Nesbitt, B. E. and Muehlenbachs, K. (1990) 'A mesothermal gold-stibnite-quartz vein occurrence in the Canadian Cordillera', *Economic Geology*. Society of Economic Geologists, 85(6), pp. 1260–1268. doi: 10.2113/gsecongeo.85.6.1260.

Mahmoudi, N., Slater, G. F. and Fulthorpe, R. R. (2011) 'Comparison of commercial DNA extraction kits for isolation and purification of bacterial and eukaryotic DNA from PAH-contaminated soils', *https://doi.org/10.1139/w11-049*. NRC Research Press , 57(8), pp. 623–628. doi: 10.1139/W11-049.

Mahto, K. U., Kumari, S. and Das, S. (2021) 'Unraveling the complex regulatory networks in biofilm formation in bacteria and relevance of biofilms in environmental remediation', *https://doi.org/10.1080/10409238.2021.2015747*. Taylor & Francis, 57(3), pp. 305–332. doi: 10.1080/10409238.2021.2015747.

Malmstrom, R. R. and Eloe-Fadrosh, E. A. (2019) 'Advancing Genome-Resolved Metagenomics beyond the Shotgun', *mSystems*. American Society for Microbiology, 4(3). doi: 10.1128/msystems.00118-19.

Marcelino, V. R. *et al.* (2019) 'Metatranscriptomics as a tool to identify fungal species and subspecies in mixed communities – A proof of concept under laboratory conditions', *IMA Fungus*. BioMed Central Ltd., 10(1), pp. 1–10. doi: 10.1186/s43008-019-0012-8.

Marín, S. *et al.* (2017) 'Is the growth of microorganisms limited by carbon availability during chalcopyrite bioleaching?', *Hydrometallurgy*, 168, pp. 13–20. doi: 10.1016/j.hydromet.2016.10.003.

Marín, S. *et al.* (2021) 'From Laboratory towards Industrial Operation: Biomarkers for Acidophilic Metabolic Activity in Bioleaching Systems', *Genes 2021, Vol. 12, Page 474*. Multidisciplinary Digital Publishing Institute, 12(4), p. 474. doi: 10.3390/GENES12040474.

Marlenne, G.-R., Fernanda, M.-V. and Norma G, R.-A. (2020) 'Acidithiobacillus thiooxidans DSM 26636: An Alternative for the Bioleaching of Metallic Burrs', *Catalysts*. MDPI AG, 10(11), p. 1230. doi: 10.3390/catal10111230.

Marotz, L. *et al.* (2018) 'Earth Microbiome Project (EMP) high throughput (HTP) DNA extraction protocol', (2), pp. 4–9. Available at: https://www.protocols.io/view/earth-microbiome-project-emp-high-throughput-htp-d-8epv5qqjv1bz/v1 (Accessed: 14 July 2022).

Marques de Sá, C., Noronha, F. and Ferreira da Silva, E. (2014) 'Factor analysis characterization of minor element contents in sulfides from Pb–Zn–Cu–Ag hydrothermal vein deposits in Portugal', *Ore Geology Reviews*. Elsevier, 62, pp. 54–71. doi: 10.1016/J.OREGEOREV.2014.03.001.

Martin, M. (2011) 'Cutadapt removes adapter sequences from high-throughput sequencing reads', *EMBnet.journal*. EMBnet Stichting, 17(1), p. 10. doi: 10.14806/ej.17.1.200.

Martins, F. L., Patto, G. B. and Leão, V. A. (2019) 'Chalcopyrite bioleaching in the presence of high chloride concentrations', *Journal of Chemical Technology & Biotechnology*. John Wiley & Sons, Ltd, 94(7), pp. 2333–2344. doi: 10.1002/JCTB.6028.

Maslennikov, V. *et al.* (2019) 'High-Tech Elements in Minerals of Massive Sulfide Deposits: LA-ICP-MS Data', in. Springer, Cham, pp. 107–110. doi: 10.1007/978-3-030-22974-0_24.

Matamoros-Veloza, A., Peacock, C. L. and Benning, L. G. (2014) 'Selenium speciation in framboidal and euhedral pyrites in shales', *Environmental Science and Technology*. American Chemical Society, 48(16), pp. 8972–8979. doi: 10.1021/es405686q.

Memary, R. *et al.* (2012) ‘Life cycle assessment: a time-series analysis of copper’, *Journal of Cleaner Production*. Elsevier, 33, pp. 97–108. doi: 10.1016/J.JCLEPRO.2012.04.025.

Méndez-García, C. *et al.* (2015) ‘Microbial diversity and metabolic networks in acid mine drainage habitats’, *Frontiers in Microbiology*. Frontiers Media S.A. doi: 10.3389/fmicb.2015.00475.

Metz, S. and Trefry, J. H. (2000) ‘Chemical and mineralogical influences on concentrations of trace metals in hydrothermal fluids’, *Geochimica et Cosmochimica Acta*. Pergamon, 64(13), pp. 2267–2279. doi: 10.1016/S0016-7037(00)00354-9.

Milanese, A. *et al.* (2019) ‘Microbial abundance, activity and population genomic profiling with mOTUs2’, *Nature Communications*. Nature Publishing Group, 10(1), pp. 1–11. doi: 10.1038/s41467-019-08844-4.

Mizoguchi, T., Takei, Y. and Okabe, T. (1976) ‘The Chemical Behavior of Low Valence Sulfur Compounds. X. Disproportionation of Thiosulfate, Trithionate, Tetra-thionate and Sulfite under Acidic Conditions’, *Bulletin of the Chemical Society of Japan*. The Chemical Society of Japan, 49(1), pp. 70–75. doi: 10.1246/bcsj.49.70.

Mohanraj, G. T. *et al.* (2022) ‘Characterization study and recovery of copper from low grade copper ore through hydrometallurgical route’, *Advanced Powder Technology*. Elsevier, 33(1), p. 103382. doi: 10.1016/J.APT.2021.12.001.

Moreno-Paz, M. *et al.* (2010) ‘Environmental transcriptome analysis reveals physiological differences between biofilm and planktonic modes of life of the iron oxidizing bacteria Leptospirillum spp. in their natural microbial community’, *BMC Genomics*. BioMed Central, 11(1), pp. 1–14. doi: 10.1186/1471-2164-11-404/FIGURES/6.

Moses, C. O. *et al.* (1987) ‘Aqueous pyrite oxidation by dissolved oxygen and by

ferric iron', *Geochimica et Cosmochimica Acta*. Pergamon, 51(6), pp. 1561–1571. doi: 10.1016/0016-7037(87)90337-1.

Moses, C. O. and Herman, J. S. (1991) 'Pyrite oxidation at circumneutral pH', *Geochimica et Cosmochimica Acta*. Pergamon, 55(2), pp. 471–482. doi: 10.1016/0016-7037(91)90005-P.

Murao, S. *et al.* (1999) 'Contrasting distribution of trace elements between representative antimony deposits in southern China', *Nuclear Instruments and Methods in Physics Research, Section B: Beam Interactions with Materials and Atoms*. Elsevier Science Publishers B.V., 150(1–4), pp. 502–509. doi: 10.1016/S0168-583X(98)00947-1.

Naden, J. *et al.* (2006) 'New methodologies for volcanic-hosted copper sulphide mineralization on Cyprus: A GIS-prospectivity analysis-based approach Economic Minerals Programme', *British Geological Survey Internal Report*. Available at: http://nora.nerc.ac.uk/id/eprint/510717/1/CR06129N.pdf (Accessed: 3 September 2020).

Nakamura, Y. *et al.* (2016) 'Establishment of a multi-species biofilm model and metatranscriptomic analysis of biofilm and planktonic cell communities', *Applied Microbiology and Biotechnology*. Springer Verlag, 100(16), pp. 7263–7279. doi: 10.1007/s00253-016-7532-6.

Narasingarao, P. *et al.* (2012) 'De novo metagenomic assembly reveals abundant novel major lineage of Archaea in hypersaline microbial communities', *ISME Journal*. Nature Publishing Group, 6(1), pp. 81–93. doi: 10.1038/ismej.2011.78.

Nascimento, D. *et al.* (2019) 'Bioleaching for Copper Extraction of Marginal Ores from the Brazilian Amazon Region', *Metals*. MDPI AG, 9(1), p. 81. doi: 10.3390/met9010081.

Nguyen, V. K. *et al.* (2015) 'Bioleaching of arsenic and heavy metals from mine

tailings by pure and mixed cultures of Acidithiobacillus spp.', *Journal of Industrial and Engineering Chemistry*. Elsevier, 21, pp. 451–458. doi: 10.1016/J.JIEC.2014.03.004.

Nguyen, V. K. and Lee, J.-U. (2015) 'Antimony-Oxidizing Bacteria Isolated from Antimony-Contaminated Sediment – A Phylogenetic Study', *Geomicrobiology Journal*, 32(1), pp. 50–58. doi: 10.1080/01490451.2014.925009.

Ni, Z. *et al.* (2014) 'Bioleaching of pyrrhotite by Sulfobacillus thermosulfidooxidans', *Journal of Central South University 2014 21:7*. Springer, 21(7), pp. 2638–2644. doi: 10.1007/S11771-014-2224-9.

Nilakanta, H. *et al.* (2014) 'A review of software for analyzing molecular Sequences', *BMC Research Notes*. BioMed Central Ltd., pp. 1–9. doi: 10.1186/1756-0500-7-830.

Nordstrom, D. K. (2000) 'Advances in the Hydrogeochemistry and Microbiology of Acid Mine Waters', *International Geology Review*. Taylor & Francis Group , 42(6), pp. 499–515. doi: 10.1080/00206810009465095.

Nordstrom, D. Kirk and Alpers, C. N. (1999) 'Geochemistry of Acid Mine Waters', in Plumlee, G. S. and Logsdon, M. J. (eds) *Reviews in Economic Geology. V. 6A: The Environmental Geochemistry of Mineral Deposits, Part A: Processes, Techniques, and Health Issues*, pp. 133–156. doi: 10.5382/rev.06.06.

Nordstrom, D Kirk and Alpers, C. N. (1999) 'Negative pH, efflorescent mineralogy, and consequences for environmental restoration at the Iron Mountain Superfund site, California', *Proceedings of the National Academy of Sciences*, 96(7), pp. 3455–3462. doi: 10.1073/pnas.96.7.3455.

Norris, P. R., Colin Murrell, J. and Hinson, D. (1995) 'The potential for diazotrophy in iron-and sulfur-oxidizing acidophilic bacteria', *Archives of Microbiology*. Springer-Verlag, 164(4), pp. 294–300. doi: 10.1007/BF02529964.

Ogunade, I., Pech-Cervantes, A. and Schweickart, H. (2019) 'Metatranscriptomic Analysis of Sub-Acute Ruminal Acidosis in Beef Cattle', *Animals 2019, Vol. 9, Page 232*. Multidisciplinary Digital Publishing Institute, 9(5), p. 232. doi: 10.3390/ANI9050232.

Ojumu, T. V. *et al.* (2006) 'A review of rate equations proposed for microbial ferrous-iron oxidation with a view to application to heap bioleaching', *Hydrometallurgy*. Elsevier, 83(1–4), pp. 21–28. doi: 10.1016/j.hydromet.2006.03.033.

Okibe, N. and Johnson, D. B. (2004) 'Biooxidation of pyrite by defined mixed cultures of moderately thermophilic acidophiles in pH-controlled bioreactors: Significance of microbial interactions', *Biotechnology and Bioengineering*. John Wiley & Sons, Ltd, 87(5), pp. 574–583. doi: 10.1002/bit.20138.

Olm, M. R. *et al.* (2019) 'Genome-resolved metagenomics of eukaryotic populations during early colonization of premature infants and in hospital rooms', *Microbiome*. BioMed Central Ltd., 7(1), p. 26. doi: 10.1186/s40168-019-0638-1.

Olson, G. J. and Clark, T. R. (2008) 'Bioleaching of molybdenite', *Hydrometallurgy*. Elsevier, 93(1–2), pp. 10–15. doi: 10.1016/J.HYDROMET.2008.02.013.

Olubambi, P. A. *et al.* (2007) 'Effects of ore mineralogy on the microbial leaching of low grade complex sulphide ores', *Hydrometallurgy*. Elsevier, 86(1–2), pp. 96–104. doi: 10.1016/J.HYDROMET.2006.10.008.

Ortega, L., Vindel, E. and Beny, C. (1991) 'C-O-H-N fluid inclusions associated with gold-stibnite mineralization in low-grade metamorphic rocks, Mari Rosa mine, Caceres, Spain', *Mineralogical Magazine*, 55(379), pp. 235–247. doi: 10.1180/minmag.1991.055.379.12.

Osorio, H. *et al.* (2013) 'Anaerobic sulfur metabolism coupled to dissimilatory iron

reduction in the extremophile Acidithiobacillus ferrooxidans', *Applied and Environmental Microbiology*. American Society for Microbiology, 79(7), pp. 2172–2181. doi: 10.1128/AEM.03057-12.

Panda, S. *et al.* (2015) 'Current scenario of chalcopyrite bioleaching: A review on the recent advances to its heap-leach technology', *Bioresource Technology*, 196, pp. 694–706. doi: 10.1016/j.biortech.2015.08.064.

Pappas, R. S. (2012) 'Sample Preparation Problem Solving for Inductively Coupled Plasma-Mass Spectrometry with Liquid Introduction Systems I. Solubility, Chelation, and Memory Effects', *Spectroscopy (Springfield, Or.)*. NIH Public Access, 27(5), p. 20. Available at: /pmc/articles/PMC4550584/ (Accessed: 2 February 2022).

Park, C.-Y., Kim, S.-O. and Kim, B.-J. (2010) 'Bioleaching of Galena by Indigenous Bacteria at Room Temperature', *Journal of the Mineralogical Society of Korea*, 23(4), pp. 331–346. Available at: https://www.koreascience.or.kr/article/JAKO201015537950028.page (Accessed: 27 July 2021).

Pearson, W. R. (2013) 'An Introduction to Sequence Similarity ("Homology") Searching', *Current protocols in bioinformatics / editoral board, Andreas D. Baxevanis ... [et al.]*. NIH Public Access, 0 3(SUPPL.42). doi: 10.1002/0471250953.BI0301S42.

Pedregosa, F. *et al.* (2011) 'Scikit-learn: Machine learning in Python', *Journal of machine learning research*, 12(Oct), pp. 2825–2830.

Peng, T. *et al.* (2021) 'Bioleaching and Electrochemical Behavior of Chalcopyrite by a Mixed Culture at Low Temperature', *Frontiers in Microbiology*. Frontiers Media S.A., 12, p. 1103. doi: 10.3389/FMICB.2021.663757/BIBTEX.

Pfaff, K. *et al.* (2011) 'Trace and minor element variations and sulfur isotopes in

crystalline and colloform ZnS: Incorporation mechanisms and implications for their genesis', *Chemical Geology*. Elsevier, 286(3–4), pp. 118–134. doi: 10.1016/j.chemgeo.2011.04.018.

Pirajno, F. (1992) 'Crustal Hydrothermal Fluids and Mesothermal Mineral Deposits', in *Hydrothermal Mineral Deposits*. Springer Berlin Heidelberg, pp. 612–691. doi: 10.1007/978-3-642-75671-9_16.

Pistaccio, L. *et al.* (1994) 'Analysis of molybdenite bioleaching by Thiobacillus ferrooxidans in the absence of iron (II)', *Biotechnology Letters 1994 16:2*. Springer, 16(2), pp. 189–194. doi: 10.1007/BF01021669.

Plumb, J. J., McSweeney, N. J. and Franzmann, P. D. (2008) 'Growth and activity of pure and mixed bioleaching strains on low grade chalcopyrite ore', *Minerals Engineering*. Pergamon, 21(1), pp. 93–99. doi: 10.1016/J.MINENG.2007.09.007.

Plumb, J. J., Muddle, R. and Franzmann, P. D. (2008) 'Effect of pH on rates of iron and sulfur oxidation by bioleaching organisms', *Minerals Engineering*. Pergamon, 21(1), pp. 76–82. doi: 10.1016/J.MINENG.2007.08.018.

Poretsky, R. *et al.* (2014) 'Strengths and Limitations of 16S rRNA Gene Amplicon Sequencing in Revealing Temporal Microbial Community Dynamics', *PLoS ONE*. Edited by F. Rodriguez-Valera. Public Library of Science, 9(4), p. e93827. doi: 10.1371/journal.pone.0093827.

Pradhan, N. *et al.* (2008) 'Heap bioleaching of chalcopyrite: A review', *Minerals Engineering*, 21(5), pp. 355–365. doi: 10.1016/j.mineng.2007.10.018.

Pretorius, I. M., Rawlings, D. E. and Woods, D. R. (1986) 'Identification and cloning of Thiobacillus ferrooxidans structural nif genes in Escherichia coli', *Gene*. Elsevier, 45(1), pp. 59–65. doi: 10.1016/0378-1119(86)90132-0.

Qiu, M. Q. *et al.* (2005a) 'A comparison of bioleaching of chalcopyrite using pure

culture or a mixed culture', *Minerals Engineering*. Pergamon, 18(9), pp. 987–990. doi: 10.1016/J.MINENG.2005.01.004.

Qiu, M. Q. *et al.* (2005b) 'A comparison of bioleaching of chalcopyrite using pure culture or a mixed culture', *Minerals Engineering*. Pergamon, 18(9), pp. 987–990. doi: 10.1016/j.mineng.2005.01.004.

Qiu, M., Xiong, S. and Zhang, W. (2006) 'Efficacy of chalcopyrite bioleaching using a pure and a mixed bacterium', *Journal of University of Science and Technology Beijing: Mineral Metallurgy Materials (Eng Ed)*. University of Science and Technology Beijing, 13(1), pp. 7–10. doi: 10.1016/S1005-8850(06)60004-2.

Quast, C. (2013) 'SILVA ribosomal RNA gene database project: improved data processing and web-based tools', *Nucleic Acids Research*, 41(1), pp. D590–D596. Available at: https://academic.oup.com/nar/article/41/D1/D590/1069277 (Accessed: 13 July 2020).

Quatrini, R. *et al.* (2009) 'Extending the models for iron and sulfur oxidation in the extreme Acidophile Acidithiobacillus ferrooxidans', *BMC Genomics*. BioMed Central, 10(1), p. 394. doi: 10.1186/1471-2164-10-394.

Quatrini, R. and Johnson, D. B. (2018) 'Microbiomes in extremely acidic environments: functionalities and interactions that allow survival and growth of prokaryotes at low pH', *Current Opinion in Microbiology*. Elsevier Current Trends, 43, pp. 139–147. doi: 10.1016/J.MIB.2018.01.011.

R Core Team (2017) 'R: A language and environment for statistical computing.' Vienna, Austria: R Foundation for Statistical Computing.

Ram, R. J. *et al.* (2005) *Community Proteomics of a Natural Microbial Biofilm*, *Science*. Available at: https://www.jstor.org/stable/3841454 (Accessed: 20 January 2020).

Rameez, M. J. *et al.* (2020) ‘Two pathways for thiosulfate oxidation in the alphaproteobacterial chemolithotroph Paracoccus thiocyanatus SST’, *Microbiological Research*. Elsevier GmbH, 230, p. 126345. doi: 10.1016/j.micres.2019.126345.

Ramírez, P. *et al.* (2004) ‘Differential protein expression during growth of Acidithiobacillus ferooxidans on ferrous iron, sulfur compounds, or metal sulfides’, *Applied and Environmental Microbiology*. American Society for Microbiology, 70(8), pp. 4491–4498. doi: 10.1128/AEM.70.8.4491-4498.2004/ASSET/DA663D6B-7982-46E0-8FC4-675A12ADCC09/ASSETS/GRAPHIC/ZAM0080446790006.JPEG.

Rawlings, D. E. (2002) ‘Heavy Metal Mining Using Microbes’, *Annual Review of Microbiology*, 56(1), pp. 65–91. doi: 10.1146/annurev.micro.56.012302.161052.

Rawlings, D. E. (2005) ‘Characteristics and adaptability of iron- and sulfur-oxidizing microorganisms used for the recovery of metals from minerals and their concentrates’, *Microbial Cell Factories*. BioMed Central, pp. 1–15. doi: 10.1186/1475-2859-4-13.

Rawlings, D. E. (2011) ‘Some important developments in biomining during the past thirty years’. Central South University Press, Lushan South Road 932, 410083 Changsha, Hunan Province, PR China.

Rawlings, D. E. and Johnson, D. B. (2007) ‘The microbiology of biomining: development and optimization of mineral-oxidizing microbial consortia’, *Microbiology*. Microbiology Society, 153(2), pp. 315–324. doi: 10.1099/mic.0.2006/001206-0.

Reck, M. *et al.* (2015) ‘Stool metatranscriptomics: A technical guideline for mRNA stabilisation and isolation’, *BMC Genomics*. BioMed Central Ltd., 16(1), pp. 1–18. doi: 10.1186/S12864-015-1694-Y/FIGURES/7.

Rodríguez, Y. *et al.* (2003a) *New information on the chalcopyrite bioleaching mechanism at low and high temperature*, *Hydrometallurgy*. Elsevier. doi: 10.1016/S0304-386X(03)00173-7.

Rodríguez, Y. *et al.* (2003b) 'New information on the pyrite bioleaching mechanism at low and high temperature', in *Hydrometallurgy*. Elsevier, pp. 37–46. doi: 10.1016/S0304-386X(03)00172-5.

Roger, M. *et al.* (2012) 'Mineral respiration under extreme acidic conditions: From a supramolecular organization to a molecular adaptation in Acidithiobacillus ferrooxidans', in *Biochemical Society Transactions*, pp. 1324–1329. doi: 10.1042/BST20120141.

Rognes, T. *et al.* (2016) 'VSEARCH: a versatile open source tool for metagenomics', *PeerJ*. PeerJ Inc., 4, p. e2584. doi: 10.7717/peerj.2584.

Rohwerder, T. *et al.* (2003a) 'Bioleaching review part A: Progress in bioleaching: Fundamentals and mechanisms of bacterial metal sulfide oxidation', *Applied Microbiology and Biotechnology*. Springer-Verlag, pp. 239–248. doi: 10.1007/s00253-003-1448-7.

Rohwerder, T. *et al.* (2003b) 'Bioleaching review part A: Progress in bioleaching: Fundamentals and mechanisms of bacterial metal sulfide oxidation', *Applied Microbiology and Biotechnology*. Springer, pp. 239–248. doi: 10.1007/s00253-003-1448-7.

Rohwerder, T. and Sand, W. (2003) 'The sulfane sulfur of persulfides is the actual substrate of the sulfur-oxidizing enzymes from Acidithiobacillus and Acidiphilium spp', *Microbiology*, pp. 1699–1709. doi: 10.1099/mic.0.26212-0.

Rohwerder, T. and Sand, W. (2007) 'Oxidation of inorganic sulfur compounds in acidophilic prokaryotes', *Engineering in Life Sciences*, pp. 301–309. doi: 10.1002/elsc.200720204.

RStudio Team (2016) ‘RStudio: Integrated Development for R. RStudio, Inc.’ Boston, MA. Available at: http://www.rstudio.com/.

Sand, W. *et al.* (1995) ‘Sulfur chemistry, biofilm, and the (in)direct attack mechanism — a critical evaluation of bacterial leaching’, *Applied Microbiology and Biotechnology*, 43(6), pp. 961–966. doi: 10.1007/BF00166909.

Sand, W. *et al.* (2001) ‘(Bio)chemistry of bacterial leaching - direct vs. indirect bioleaching’, *Hydrometallurgy*. Elsevier Science Publishers B.V., 59(2–3), pp. 159–175. doi: 10.1016/S0304-386X(00)00180-8.

Santini, J. M. *et al.* (2000) ‘A New Chemolithoautotrophic Arsenite-Oxidizing Bacterium Isolated from a Gold Mine: Phylogenetic, Physiological, and Preliminary Biochemical Studies’, *Applied and Environmental Microbiology*, 66(1), pp. 92–97. doi: 10.1128/AEM.66.1.92-97.2000.

Dos Santos, E. C. *et al.* (2017) ‘Stability, Structure, and Electronic Properties of the Pyrite/ Arsenopyrite Solid−Solid Interface−A DFT Study’. doi: 10.1021/acs.jpcc.7b02642.

Savage, K. S. *et al.* (2000) ‘Arsenic speciation in pyrite and secondary weathering phases, Mother Lode Gold District, Tuolumne County, California’, *Applied Geochemistry*. Pergamon, 15(8), pp. 1219–1244. doi: 10.1016/S0883-2927(99)00115-8.

Schippers, A. *et al.* (2019) ‘Sphalerite bioleaching comparison in shake flasks and percolators’, *Minerals Engineering*. Pergamon, 132, pp. 251–257. doi: 10.1016/J.MINENG.2018.12.007.

Schippers, A., Rohwerder, T. and Sand, W. (1999) ‘Intermediary sulfur compounds in pyrite oxidation: Implications for bioleaching and biodepyritization of coal’, *Applied Microbiology and Biotechnology*. Springer, 52(1), pp. 104–110. doi:

10.1007/s002530051495.

Schippers, A. and Sand, W. (1999) ‘Bacterial leaching of metal sulfides proceeds by two indirect mechanisms via thiosulfate or via polysulfides and sulfur’, *Applied and Environmental Microbiology*, 65(1), pp. 319–321. doi: 10.1128/aem.65.1.319-321.1999.

Schloss, P. D. *et al.* (2009) ‘Introducing mothur: Open-source, platform-independent, community-supported software for describing and comparing microbial communities’, *Applied and Environmental Microbiology*. American Society for Microbiology, 75(23), pp. 7537–7541. doi: 10.1128/AEM.01541-09.

Schwarz-Schampera, U. (2014) ‘Antimony’, in Gunn, G. (ed.) *Critical Metals Handbook*. Oxford: John Wiley & Sons. doi: 10.1002/9781118755341.
Seal, R. R., Bliss, J. D. and Campbell, D. L. (1986) ‘Stibnite-Quartz Deposits’. Berger, (204), pp. 204–208.

Serbula, S. M. *et al.* (2017) ‘Extreme air pollution with contaminants originating from the mining–metallurgical processes’, *Science of The Total Environment*. Elsevier, 586, pp. 1066–1075. doi: 10.1016/J.SCITOTENV.2017.02.091.

Shaffer, J. P. *et al.* (2022) ‘A comparison of six DNA extraction protocols for 16S, ITS and shotgun metagenomic sequencing of microbial communities’, *BioTechniques*. doi: 10.2144/btn-2022-0032.

Shah, P. *et al.* (2007) ‘Speciation of arsenic and selenium in coal combustion products’, in *Energy and Fuels*. American Chemical Society , pp. 506–512. doi: 10.1021/ef0604083.

Shakya, M., Lo, C. C. and Chain, P. S. G. (2019) ‘Advances and challenges in metatranscriptomic analysis’, *Frontiers in Genetics*. Frontiers Media S.A., p. 904. doi: 10.3389/fgene.2019.00904.

Shiers, D. W., Collinson, D. M. and Watling, H. R. (2016) ‘Life in heaps: a review of microbial responses to variable acidity in sulfide mineral bioleaching heaps for metal extraction’, *Research in Microbiology*, 167(7), pp. 576–586. doi: 10.1016/j.resmic.2016.05.007.

Silverman, M. P. and Lundgren, D. G. (1959) ‘Studies on the chemoautotrophic iron bacterium Ferrobacillus ferrooxidans. I. An improved medium and a harvesting procedure for securing high cell yields’, *Journal of bacteriology*. J Bacteriol, 77(5), pp. 642–647. doi: 10.1128/JB.77.5.642-647.1959.

Simon, G. *et al.* (1999) ‘Oxidation state of gold and arsenic in gold-bearing arsenian pyrite’, *American Mineralogist*. GeoScienceWorld, 84(7–8), pp. 1071–1079. doi: 10.2138/am-1999-7-809.

Singer, P. C. and Stumm, W. (1970) ‘Acidic Mine Drainage: The Rate-Determining Step’, *Science*, 167(3921). Available at: http://science.sciencemag.org/content/167/3921/1121 (Accessed: 16 May 2017).

Singh, S., Sukla, L. B. and Mishra, B. K. (2011) ‘Extraction of Copper from Malanjkhand Low-Grade Ore by Bacillus stearothermophilus’, *Indian Journal of Microbiology*. Springer, 51(4), pp. 477–481. doi: 10.1007/s12088-011-0073-x.

Smith, J. R., Luthy, R. G. and Middleton, A. C. (1988) ‘Microbial ferrous iron oxidation in acidic solution’, *Journal of the Water Pollution Control Federation*, 60(4), pp. 518–530. Available at: https://www.jstor.org/stable/25043528?seq=1 (Accessed: 26 October 2020).

Soneson, C., Love, M. I. and Robinson, M. D. (2016) ‘Differential analyses for RNA-seq: Transcript-level estimates improve gene-level inferences [version 2; referees: 2 approved]’, *F1000Research*. Faculty of 1000 Ltd, 4, p. 1521. doi: 10.12688/F1000RESEARCH.7563.2.

Stewart, R. *et al.* (2018) ‘The genomic and proteomic landscape of the rumen

microbiome revealed by comprehensive genome-resolved metagenomics', *Nature Biotechnology*. Cold Spring Harbor Laboratory, p. 489443. doi: 10.1101/489443.

Stolze, Y. *et al.* (2018) 'Targeted *in situ* metatranscriptomics for selected taxa from mesophilic and thermophilic biogas plants', *Microbial Biotechnology*. John Wiley and Sons Ltd, 11(4), pp. 667–679. doi: 10.1111/1751-7915.12982.

Straub, D. *et al.* (2019) 'Interpretations of microbial community studies are biased by the selected 16S rRNA gene amplicon sequencing pipeline', *bioRxiv*. Cold Spring Harbor Laboratory, p. 2019.12.17.880468. doi: 10.1101/2019.12.17.880468.

Sun, W. *et al.* (2016) 'Profiling microbial community in a watershed heavily contaminated by an active antimony (Sb) mine in Southwest China.', *The Science of the total environment*, 550, pp. 297–308. doi: 10.1016/j.scitotenv.2016.01.090.

Sundar, S. and Chakravarty, J. (2010) 'Antimony toxicity.', *International journal of environmental research and public health*. Molecular Diversity Preservation International, 7(12), pp. 4267–77. doi: 10.3390/ijerph7124267.

Svetlov, A. *et al.* (2020) 'Processing of Cut-Off Grade Ores and Copper and Nickel Industry Process Waste: A Feasibility Study TRAKT-2018: Transferable Knowledge and Technologies for High-Resolution Environmental Impact Assessment and Management View project Sumilcere View project'. doi: 10.37614/978.5.91137.424.2.

Talla, E. *et al.* (2014) 'Insights into the pathways of iron- and sulfur-oxidation, and biofilm formation from the chemolithotrophic acidophile Acidithiobacillus ferrivorans CF27', *Research in Microbiology*. Elsevier Masson, 165(9), pp. 753–760. doi: 10.1016/J.RESMIC.2014.08.002.

Tanne, C. K. and Schippers, A. (2019) 'Electrochemical investigation of chalcopyrite (bio)leaching residues', *Hydrometallurgy*. Elsevier B.V., 187, pp. 8–17. doi: 10.1016/j.hydromet.2019.04.022.

Tanner, D. *et al.* (2016) ‘Sulfur isotope and trace element systematics of zoned pyrite crystals from the El Indio Au–Cu–Ag deposit, Chile’, *Contributions to Mineralogy and Petrology*. Springer Verlag, 171(4), pp. 1–17. doi: 10.1007/S00410-016-1248-6/FIGURES/11.

Tano, T. *et al.* (1996) ‘Purification and some properties of a tetrathionate decomposing enzyme from thiobacillus thiooxidans’, *Bioscience, Biotechnology and Biochemistry*. Taylor & Francis, 60(2), pp. 224–227. doi: 10.1271/bbb.60.224.
Tao, H. and Dongwei, L. (2014) ‘Presentation on mechanisms and applications of chalcopyrite and pyrite bioleaching in biohydrometallurgy - A presentation’, *Biotechnology Reports*. Elsevier B.V., pp. 107–119. doi: 10.1016/j.btre.2014.09.003.

Tao, J. *et al.* (2021) ‘An integrated insight into bioleaching performance of chalcopyrite mediated by microbial factors: Functional types and biodiversity’, *Bioresource Technology*. Elsevier, 319, p. 124219. doi: 10.1016/J.BIORTECH.2020.124219.

Taylor, C. D. *et al.* (1986) *Volcanic-associated massive sulfide deposits.* Available at: https://pubs.usgs.gov/of/1995/ofr-95-0831/CHAP16.pdf (Accessed: 31 January 2020).

Taylor, K. G. and Konhauser, K. O. (2011) ‘In earth surface systems: A major player in chemical and biological processes’, *Elements*. GeoScienceWorld, 7(2), pp. 83–88. doi: 10.2113/gselements.7.2.83.

Terry, L. R. *et al.* (2015) ‘Microbiological oxidation of antimony(III) with oxygen or nitrate by bacteria isolated from contaminated mine sediments.’, *Applied and environmental microbiology*. American Society for Microbiology, 81(24), pp. 8478–88. doi: 10.1128/AEM.01970-15.

Torma, A. E. and Gabra, G. G. (1977) ‘Oxidation of stibnite byThiobacillus

ferrooxidans', *Antonie van Leeuwenhoek*, 43(1), pp. 1–6. doi: 10.1007/BF02316204.

Tran, T. T. T. *et al.* (2017) 'Comparative genome analysis provides insights into both the lifestyle of Acidithiobacillus ferrivorans Strain CF27 and the chimeric nature of the iron-oxidizing acidithiobacilli genomes', *Frontiers in Microbiology*. Frontiers Media SA, 8(JUN). doi: 10.3389/fmicb.2017.01009.

Travisany, D. *et al.* (2014) 'A new genome of Acidithiobacillus thiooxidans provides insights into adaptation to a bioleaching environment', *Research in Microbiology*. Elsevier Masson SAS, 165(9), pp. 743–752. doi: 10.1016/j.resmic.2014.08.004.

Trefry, J. H. *et al.* (1994) 'Trace metals in hydrothermal solutions from Cleft segment on the southern Juan de Fuca Ridge', *Journal of Geophysical Research: Solid Earth*. John Wiley & Sons, Ltd, 99(B3), pp. 4925–4935. doi: 10.1029/93JB02108.

Tributsch, H. (2001) 'Direct versus indirect bioleaching', *Hydrometallurgy*. Elsevier Science Publishers B.V., 59(2–3), pp. 177–185. doi: 10.1016/S0304-386X(00)00181-X.

Truper, H. G. and Fischer, U. (1982) 'Anaerobic Oxidation of Sulphur Compounds as Electron Donors for Bacterial Photosynthesis', *Philosophical Transactions of the Royal Society B: Biological Sciences*. The Royal Society, 298(1093), pp. 529–542. doi: 10.1098/rstb.1982.0095.

Tu, Z. *et al.* (2017) 'Investigation of intermediate sulfur species during pyrite oxidation in the presence and absence of Acidithiobacillus ferrooxidans', *Hydrometallurgy*. Elsevier B.V., 167, pp. 58–65. doi: 10.1016/j.hydromet.2016.11.001.

Tyson, G. W. *et al.* (2004) 'Community structure and metabolism through reconstruction of microbial genomes from the environment', *Nature*, 428(6978), pp.

37–43. doi: 10.1038/nature02340.

Tyson, G. W. *et al.* (2005) ‘Genome-directed isolation of the key nitrogen fixer Leptospirillum ferrodiazotrophum sp. nov. from an acidophilic microbial community.’, *Applied and Environmental Microbiology*. American Society for Microbiology, 71(10), pp. 6319–24. doi: 10.1128/AEM.71.10.6319-6324.2005.

Ubaldini, S. *et al.* (2000) ‘Combined bio-hydrometallurgical process for gold recovery from refractory stibnite’, *Minerals Engineering*, 13(14–15), pp. 1641–1646. doi: 10.1016/S0892-6875(00)00148-5.

Ungaro, A. *et al.* (2017) ‘Challenges and advances for transcriptome assembly in non-model species’, *PLoS ONE*. Public Library of Science, 12(9). doi: 10.1371/JOURNAL.PONE.0185020.

Urich, T. *et al.* (2004) ‘The sulphur oxygenase reductase from Acidianus ambivalens is a multimeric protein containing a low-potential mononuclear non-haem iron centre’, *Biochemical Journal*. Portland Press Ltd, 381(1), pp. 137–146. doi: 10.1042/BJ20040003.

Uritskiy, G. and Di Ruggiero, J. (2019) ‘Applying genome-resolved metagenomics to deconvolute the halophilic microbiome’, *Genes*. MDPI AG. doi: 10.3390/genes10030220.

USGS (2020) *Antimony. United States Geological Survey, Mineral Commodity Summaries.* Available at: https://pubs.usgs.gov/periodicals/mcs2020/mcs2020-antimony.pdf (Accessed: 27 June 2020).

Valdes, J. *et al.* (2011) ‘Draft genome sequence of the extremely acidophilic biomining bacterium Acidithiobacillus thiooxidans ATCC 19377 provides insights into the evolution of the Acidithiobacillus genus’, *Journal of Bacteriology*, pp. 7003–7004. doi: 10.1128/JB.06281-11.

Valdés, J. *et al.* (2008) 'Acidithiobacillus ferrooxidans metabolism: from genome sequence to industrial applications', *BMC Genomics*. BioMed Central, 9(1), p. 597. doi: 10.1186/1471-2164-9-597.

Valdés, J. *et al.* (2010) 'Comparative genomics begins to unravel the ecophysiology of bioleaching', in *Hydrometallurgy*. Elsevier, pp. 471–476. doi: 10.1016/j.hydromet.2010.03.028.

Vardanyan, A. and Vyrides, I. (2019) 'Acidophilic bioleaching at high dissolved organic compounds: Inhibition and strategies to counteract this', *Minerals Engineering*. Pergamon, 143, p. 105943. doi: 10.1016/J.MINENG.2019.105943.

Vaughan, D. J. and Coker, V. S. (2016) 'Biogeochemical Redox Processes of Sulphide Minerals', in *Redox-active Minerals: Properties, Reactions and Applications in Natural Systems and Clean Technologies*. European Mineralogical Union and the Mineralogical Society of Great Britain and Ireland. doi: 10.1180/EMU-notes.17.5.

Vaughan, D. J. and Corkhill, C. L. (2017) 'Mineralogy of Sulfides', *Elements*, 13(2). Available at: http://elements.geoscienceworld.org/content/13/2/81 (Accessed: 7 August 2017).

Vegliò, F. *et al.* (2000) 'Bioleaching of a pyrrhotite ore by a sulfooxidans strain: kinetic analysis', *Chemical Engineering Science*. Pergamon, 55(4), pp. 783–795. doi: 10.1016/S0009-2509(99)00354-1.

Vera, M. *et al.* (2009) 'Characterization of biofilm formation by the bioleaching acidophilic bacterium Acidithiobacillus ferrooxidans by a microarray transcriptome analysis', in *Advanced Materials Research*, pp. 175–178. doi: 10.4028/www.scientific.net/AMR.71-73.175.

Vera, M., Schippers, A. and Sand, W. (2013) 'Progress in bioleaching: Fundamentals and mechanisms of bacterial metal sulfide oxidation-part A', *Applied*

Microbiology and Biotechnology, pp. 7529–7541. doi: 10.1007/s00253-013-4954-2.

Vilcáez, J. and Inoue, C. (2009) 'Mathematical modeling of thermophilic bioleaching of chalcopyrite', *Minerals Engineering*. Pergamon, 22(11), pp. 951–960. doi: 10.1016/j.mineng.2009.03.001.

Vilcáez, J., Suto, K. and Inoue, C. (2008) 'Bioleaching of chalcopyrite with thermophiles: Temperature-pH-ORP dependence', *International Journal of Mineral Processing*. Elsevier, 88(1–2), pp. 37–44. doi: 10.1016/j.minpro.2008.06.002.

Vilcáez, J., Yamada, R. and Inoue, C. (2009) 'Effect of pH reduction and ferric ion addition on the leaching of chalcopyrite at thermophilic temperatures', *Hydrometallurgy*. Elsevier, 96(1–2), pp. 62–71. doi: 10.1016/j.hydromet.2008.08.003.

Vincent Q Vu (2011) *ggbiplot package*. Available at: https://www.rdocumentation.org/packages/ggbiplot/versions/0.55 (Accessed: 29 October 2020).

Walczak, A. B. (2016) 'Characterization of Bosea sp. WAO and exploration of chemolithoautotrophic growth on lead and antimony'. doi: 10.7282/T3BG2R54.

Wang, J. *et al.* (2016) 'Dissolution and passivation mechanisms of chalcopyrite during bioleaching: DFT calculation, XPS and electrochemistry analysis', *Minerals Engineering*. Elsevier Ltd, 98, pp. 264–278. doi: 10.1016/j.mineng.2016.09.008.

Wang, J. *et al.* (2021) 'Metagenomic and metatranscriptomic profiling of Lactobacillus casei Zhang in the human gut', *npj Biofilms and Microbiomes 2021 7:1*. Nature Publishing Group, 7(1), pp. 1–10. doi: 10.1038/s41522-021-00227-2.

Wang, Q. *et al.* (2015) 'Arsenite oxidase also functions as an antimonite oxidase.', *Applied and environmental microbiology*, 81(6), pp. 1959–65. doi:

10.1128/AEM.02981-14.

Wang, R. *et al.* (2019) 'Sulfur oxidation in the acidophilic autotrophic Acidithiobacillus spp.', *Frontiers in Microbiology*. Frontiers Media S.A., p. 3290. doi: 10.3389/fmicb.2018.03290.

Wang, S. *et al.* (2008) 'Comparative study of external addition of Fe2+ and inoculum on bioleaching of marmatite flotation concentrate using mesophilic and moderate thermophilic bacteria', *Hydrometallurgy*. Elsevier, 93(1–2), pp. 51–56. doi: 10.1016/J.HYDROMET.2008.02.019.

Wang, X. *et al.* (2020) 'Effective bioleaching of low-grade copper ores: Insights from microbial cross experiments', *Bioresource Technology*. Elsevier, 308, p. 123273. doi: 10.1016/J.BIORTECH.2020.123273.

Wang, Y. *et al.* (2012) 'Bioleaching of chalcopyrite by defined mixed moderately thermophilic consortium including a marine acidophilic halotolerant bacterium', *Bioresource Technology*. Elsevier, 121, pp. 348–354. doi: 10.1016/j.biortech.2012.06.114.

Wang, Y. *et al.* (2017) 'Mineralogy and trace element geochemistry of sulfide minerals from the Wocan Hydrothermal Field on the slow-spreading Carlsberg Ridge, Indian Ocean', *Ore Geology Reviews*, 84, pp. 1–19. doi: 10.1016/j.oregeorev.2016.12.020.

Wang, Y. J. *et al.* (2013) 'Bioxidative dissolution of cinnabar by iron-oxidizing bacteria', *Biochemical Engineering Journal*. Elsevier, 74, pp. 102–106. doi: 10.1016/J.BEJ.2013.02.013.

Watling, H. R. (2006) 'The bioleaching of sulphide minerals with emphasis on copper sulphides - A review', *Hydrometallurgy*. Elsevier, 84(1–2), pp. 81–108. doi: 10.1016/j.hydromet.2006.05.001.

Watling, H. R. *et al.* (2014) 'Bioleaching of a low-grade copper ore, linking leach chemistry and microbiology', *Minerals Engineering*. Pergamon, 56, pp. 35–44. doi: 10.1016/j.mineng.2013.10.023.

Wenk, H.-R. and Bulakh, A. (2005) *Minerals: Their Constitution and Origin*. Cambridge University Press.

Whaley-Martin, K. *et al.* (2019) 'The potential role of Halothiobacillus spp. In sulfur oxidation and acid generation in circum-neutral mine tailings reservoirs', *Frontiers in Microbiology*. Frontiers Media S.A., 10(MAR), p. 297. doi: 10.3389/fmicb.2019.00297.

Wickham, H. (2007) 'Reshaping data with the reshape package', *Journal of Statistical Software*. University of California at Los Angeles, 21(12), pp. 1–20. doi: 10.18637/jss.v021.i12.

Wickham, H. (2016) 'ggplot2: Elegant Graphics for Data Analysis.' Springer-Verlag, New York.

Wickham, H. *et al.* (2019) 'dplyr: A Grammar of Data Manipulation'.

Wickham, H. (2019) 'forcats: Tools for Working with Categorical Variables (Factors)'. Available at: https://cran.r-project.org/package=forcats.

Wickham, H., Hester, J. and Chang, W. (2019) 'devtools: Tools to Make Developing R Packages Easier. R package version 2.0.2'. Available at: https://rdrr.io/cran/devtools/ (Accessed: 29 October 2020).

Wickham, H., Hester, J. and Francois, R. (2018) 'readr: Read Rectangular Text Data'. Available at: https://cran.r-project.org/package=readr.

Wilson, S. C. *et al.* (2010) 'The chemistry and behaviour of antimony in the soil environment with comparisons to arsenic: A critical review', *Environmental*

Pollution. Elsevier, pp. 1169–1181. doi: 10.1016/j.envpol.2009.10.045.

Winogradsky, S. (1887) 'Über schwefelbakterien. "About Sulfur Bacteria."', *Bot. Ztg*, 45(31--37), pp. 489--ff.

Woese, C. R. and Fox, G. E. (1977) 'Phylogenetic structure of the prokaryotic domain: the primary kingdoms', *Proceedings of the National Academy of Sciences*, (74(11)), pp. 5088–5090.

Wong, H. L. *et al.* (2018) 'Disentangling the drivers of functional complexity at the metagenomic level in Shark Bay microbial mat microbiomes', *ISME Journal*. Nature Publishing Group, 12(11), pp. 2619–2639. doi: 10.1038/s41396-018-0208-8.

Wu, A. *et al.* (2009) 'Technological assessment of a mining-waste dump at the Dexing copper mine, China, for possible conversion to an in situ bioleaching operation', *Bioresource Technology*. Elsevier, 100(6), pp. 1931–1936. doi: 10.1016/j.biortech.2008.10.021.

Wu, G. D. *et al.* (2011) 'Linking long-term dietary patterns with gut microbial enterotypes', *Science*. American Association for the Advancement of Science, 334(6052), pp. 105–108. doi: 10.1126/SCIENCE.1208344/SUPPL_FILE/WU.SOM.PDF.

Wu, Z. L. *et al.* (2016) 'Column bioleaching characteristic of copper and iron from Zijinshan sulfide ores by acid mine drainage', *International Journal of Mineral Processing*. Elsevier, 149, pp. 18–24. doi: 10.1016/j.minpro.2016.01.015.

Xiang, L. *et al.* (2022) 'Antimony transformation and mobilization from stibnite by an antimonite oxidizing bacterium Bosea sp. AS-1', *Journal of Environmental Sciences*. Elsevier, 111, pp. 273–281. doi: 10.1016/J.JES.2021.03.042.

Xingyu, L. *et al.* (2010) 'Bioleaching of chalcocite started at different pH: Response of the microbial community to environmental stress and leaching kinetics',

Hydrometallurgy. Elsevier, 103(1–4), pp. 1–6. doi: 10.1016/J.HYDROMET.2010.02.002.

Xuehong, Z. *et al.* (2006) 'The influence of impurities on the dissolution of Ca- and Sr-bearing barite at room temperature', *Chinese Journal of Geochemistry*. Science in China Press, 25(1), pp. 71–84. doi: 10.1007/BF02894798.

Yahya, A. and Johnson, D. B. (2002) 'Bioleaching of pyrite at low pH and low redox potentials by novel mesophilic Gram-positive bacteria', *Hydrometallurgy*. Elsevier, 63(2), pp. 181–188. doi: 10.1016/S0304-386X(01)00224-9.

Yang, T. *et al.* (2017) *A selective process for extracting antimony from refractory gold ore*, *Hydrometallurgy*. doi: 10.1016/j.hydromet.2017.03.014.

Yin, H. *et al.* (2014) 'Whole-genome sequencing reveals novel insights into sulfur oxidation in the extremophile Acidithiobacillus thiooxidans', *BMC Microbiology*. BioMed Central, 14(1), p. 179. doi: 10.1186/1471-2180-14-179.

You, X. *et al.* (2020) 'Association of plasma antimony concentration with markers of liver function in Chinese adults', *Environmental Chemistry*. CSIRO, 17(4), p. 304. doi: 10.1071/EN19195.

Yu, R. L. *et al.* (2011) 'Effect of EPS on adhesion of Acidithiobacillus ferrooxidans on chalcopyrite and pyrite mineral surfaces', *Transactions of Nonferrous Metals Society of China (English Edition)*, 21(2), pp. 407–412. doi: 10.1016/S1003-6326(11)60729-2.

Zammit, C. M. *et al.* (2011) 'The recovery of nucleic acid from biomining and acid mine drainage microorganisms', *Hydrometallurgy*. Elsevier, 108(1–2), pp. 87–92. doi: 10.1016/J.HYDROMET.2011.03.002.

Zhang, G. *et al.* (2015) 'Catalytic effect of Ag+ on arsenic bioleaching from orpiment (As2S3) in batch tests with Acidithiobacillus ferrooxidans and

Sulfobacillus sibiricus', *Journal of Hazardous Materials*. Elsevier, 283, pp. 117–122. doi: 10.1016/J.JHAZMAT.2014.09.022.

Zhang, G. J., Yang, Q. and Yang, C. (2015) 'Bioleaching of Orpiment (As2S3) in Absence of Fe3+', *Advanced Materials Research*. Trans Tech Publications Ltd, 1130, pp. 363–366. doi: 10.4028/WWW.SCIENTIFIC.NET/AMR.1130.363.

Zhang, J. *et al.* (2007) 'Bioleaching of arsenic from medicinal realgar by pure and mixed cultures', *Process Biochemistry*. Elsevier, 42(9), pp. 1265–1271. doi: 10.1016/J.PROCBIO.2007.05.021.

Zhang, X. *et al.* (2016) 'Comparative Genomics of the Extreme Acidophile Acidithiobacillus thiooxidans Reveals Intraspecific Divergence and Niche Adaptation', *International Journal of Molecular Sciences*. Multidisciplinary Digital Publishing Institute, 17(8), p. 1355. doi: 10.3390/ijms17081355.

Zhang, X. *et al.* (2017) 'Comparative genomics unravels the functional roles of co-occurring acidophilic bacteria in bioleaching heaps', *Frontiers in Microbiology*. Frontiers Media S.A., 8(MAY), p. 790. doi: 10.3389/FMICB.2017.00790/BIBTEX.

Zhang, Y. sheng *et al.* (2008) 'Bioleaching of chalcopyrite by pure and mixed culture', *Transactions of Nonferrous Metals Society of China (English Edition)*. Nonferrous Metals Society of China, 18(6), pp. 1491–1496. doi: 10.1016/S1003-6326(09)60031-5.

Zhang, Z. *et al.* (2000) 'A greedy algorithm for aligning DNA sequences', *Journal of Computational Biology*, pp. 203–214. doi: 10.1089/10665270050081478.

Zhao, H. *et al.* (2019) 'The dissolution and passivation mechanism of chalcopyrite in bioleaching: An overview', *Minerals Engineering*. Elsevier Ltd, pp. 140–154. doi: 10.1016/j.mineng.2019.03.014.

Zhao, K. *et al.* (2017) 'Study on the jarosite mediated by bioleaching of pyrrhotite

using Acidthiobacillus ferrooxidans', *Bioscience Journal* . Universidade Federal de Uberlandia, 33(3), pp. 721–729. doi: 10.14393/BJ-V33N3-33824.

Zhao, X. *et al.* (2013) 'Bioleaching of chalcopyrite by Acidithiobacillus ferrooxidans', *Minerals Engineering*. Pergamon, 53, pp. 184–192. doi: 10.1016/j.mineng.2013.08.008.

Zhou, H.-B. *et al.* (2009) 'Bioleaching of chalcopyrite concentrate by a moderately thermophilic culture in a stirred tank reactor', *Bioresource Technology*, 100(2), pp. 515–520. doi: 10.1016/j.biortech.2008.06.033.

Appendices

Appendix I –Chapter 2 Growth Images Chalcopyrite

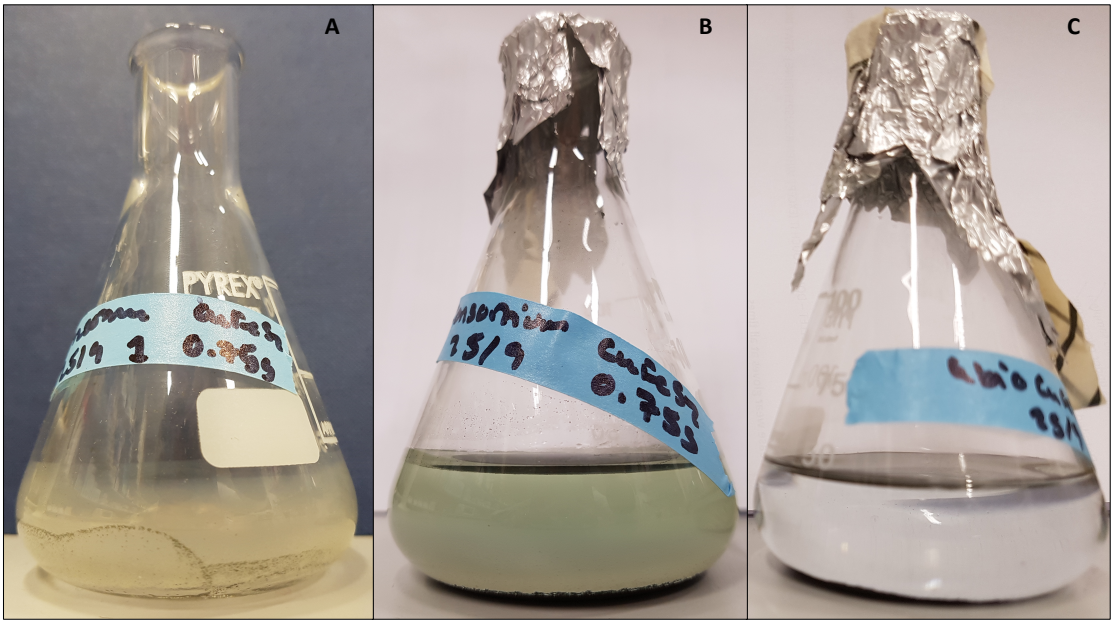

Figure API.1 – Week 4 samples, showing A) yellow/white cloudy residue in biotic sample, B) blue-green medium in biotic sample, and C) clear media in abiotic sample

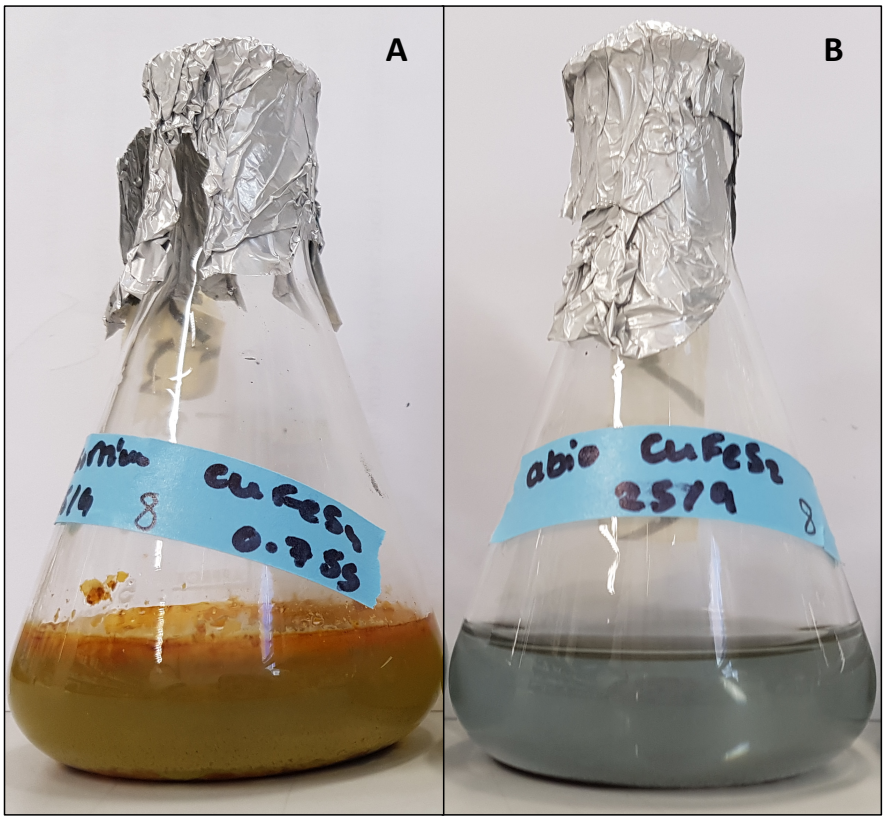

Figure API.2 – Week 12 samples showing medium differences between A) biotic and B) abiotic conditions

Appendix II - Normality Tests and Significance tests of Chapter 2 data

Table API.1 - Shapiro Wilk Normality Testing of Chalcopyrite Ore ICP-OES Values (ppm)

Element	P-Value	Normal?
Fe	<0.01	Not normal
S	<0.01	Not normal
Cu	<0.01	Not normal

Table API.2 - Kruskal Wallis testing of ICP-OES (ppm)

Biotic vs abiotic including all data

Element	P value	Significant?
Fe	<0.01	sf
S	<0.01	sf
Cu	<0.01	sf

Appendix III – ICP-OES Chalcopyrite (ppm)

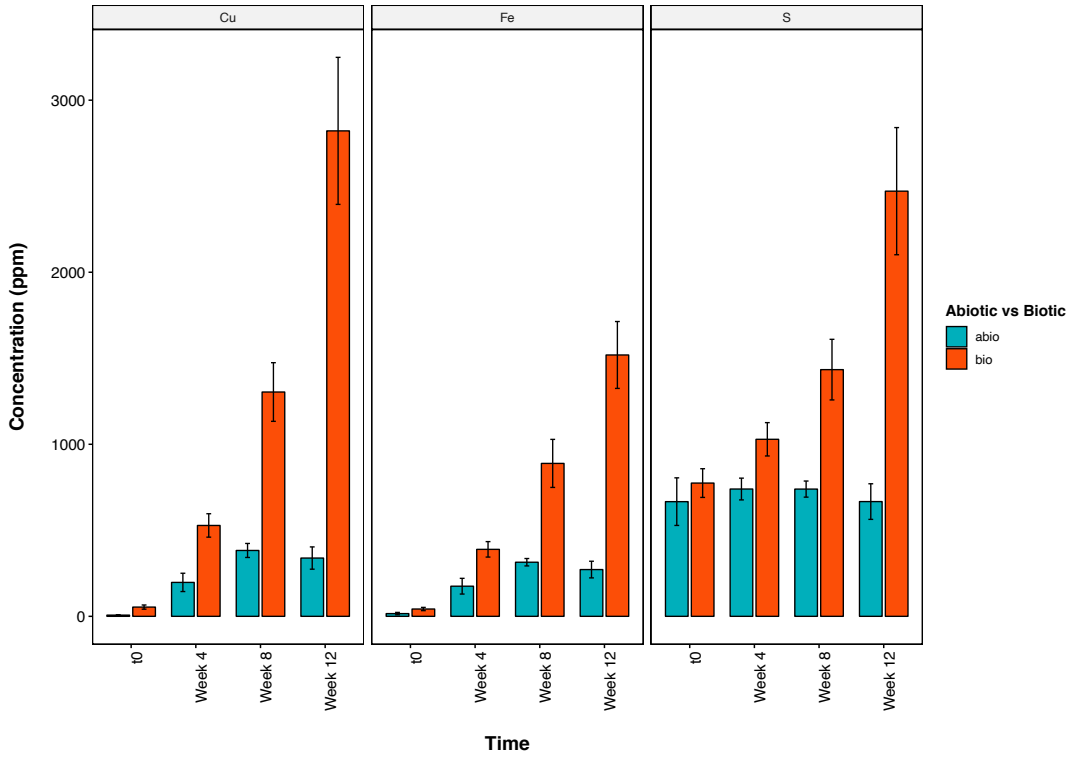

Figure APIII, mean supernatant ICP-OES results (ppm) for copper, iron and sulfur under biotic and abiotic conditions. Error bars show the standard error of the mean.

Appendix IV - Gene similarity scores Blast

Table APIV.1 – sulfur metabolism

Species	Gene	Accession code of comparison	Query Cover %	Identity %
Acidithiobacillus ferrivorans	DSRE-family protein	SMH65574	100	98.72
Acidithiobacillus ferrivorans	rhodanese	ACK78200.1	100	95
Acidithiobacillus ferrivorans	rhodanese	ACK77889.1	99	91.67
Acidithiobacillus ferrivorans	rhodanese	ACK80456.1	100	90.78
Acidithiobacillus ferrivorans	TQO (DoxX)	WP_031568639.1	99	99.38
Acidithiobacillus ferrivorans	TusA	WP_163054051.1	98	97.37
Acidithiobacillus ferrivorans	petII short-chain dehydrogenase	CDQ09795.1	99	93.31
Acidithiobacillus ferrivorans	PetII Ub cyt C reductase subunit	WP_012537361.1	99	95.15
Acidithiobacillus ferrivorans	PetII Ub cyt C reductase subunit b	ACK78596.1	100	92.33
Acidithiobacillus ferrivorans	PetII Ub cyt C reductase subunit C1	WP_014030553.1	99	97.98
Acidithiobacillus ferrivorans	SoxY	WP_081258187.1	99	94.12
Acidithiobacillus ferrivorans	SoxZ	WP_024892985.1	99	90
Acidithiobacillus ferrivorans	SoxB	WP_035192270.1	99	97.91
Acidithiobacillus ferrivorans	hdrB	WP_012537257.1	99	97.54

Acidithiobacillus ferrivorans	hdrC	QFX97247.1	100	96.65
Acidithiobacillus ferrivorans	sor	WP_014029932.1	99	99.04
Acidithiobacillus ferrivorans	Bo3 subunit	ACK80009.1	99	94.31
Acidithiobacillus ferrivorans	Bo3 subunit	ACK77850.1	100	90.52
Acidithiobacillus ferrivorans	Bo3 subunit	ACK80492.1	93	90.91
Acidithiobacillus ferrivorans-related	DSRE-family protein	SMH65574	100	98.08
Acidithiobacillus ferrivorans-related	rhodanese	WP_012537258.1	97	92.59
Acidithiobacillus ferrivorans-related	rhodanese	WP_064219726.1	99	93.62
Acidithiobacillus ferrivorans-related	rhodanese	WP_126604958.1	99	92.19
Acidithiobacillus ferrivorans-related	TusA	WP_163054051.1	98	97.37
Acidithiobacillus ferrivorans-related	sat	WP_163097178.1	99	98.74
Acidithiobacillus ferrivorans-related	petII short-chain dehydrogenase	CDQ09795.1	99	93.68
Acidithiobacillus ferrivorans-related	PetII Ub cyt C reductase subunit	WP_012537361.1	99	95.15
Acidithiobacillus ferrivorans-related	PetII Ub cyt C reductase subunit b	ACK78596.1	100	94.31

Acidithiobacillus ferrivorans-related	PetII Ub cyt C reductase subunit C1	WP_064220210.1	98	89.22
Acidithiobacillus ferrivorans-related	sqr	ACK80058.1	99	87.47
Acidithiobacillus ferrivorans-related	SoxB	WP_024895114.1	99	92.2
Acidithiobacillus ferrivorans-related	SoxY	WP_081258187.1	98	92.94
Acidithiobacillus ferrivorans-related	SoxZ	WP_024892985.1	99	90
Acidithiobacillus ferrivorans-related	SoxB	WP_035192270.1	99	97.57
Acidithiobacillus ferrivorans-related	Bo3 subunit	ACK80492.1	93	90.91
Acidithiobacillus ferrivorans-related	Bo3 subunit	ACK77850.1	100	90.52
Acidithiobacillus ferrivorans-related	Bo3 subunit	ACK80009.1	99	94.03
Acidithiobacillus ferrivorans-related	hdrC	QFX97247.1	100	96.55
Acidithiobacillus ferrivorans-related	hdrB	QFX97290.1	100	95.66
Acidithiobacillus ferrivorans-related	sor	AHZ58326.1	99	97.11
Acidithiobacillus ferrooxidans	TSD1	AFE_0042/ACK78047.1	100	96.67

Acidithiobacillus ferrooxidans	TSD2	AFE_0050/ACK78958.1	100	98.52
Acidithiobacillus ferrooxidans	SQR	BAD99305/AB217915.1	99	99.54
Acidithiobacillus ferrooxidans	SQR	AFE_0267/ACK80058	99	98.67
Acidithiobacillus ferrooxidans	bd subunit II	AFE_0954 /ACK79239.1	100	98.67
Acidithiobacillus ferrooxidans	bd subunit I	AFE_0955/ACK77832.1	97	93.95
Acidithiobacillus ferrooxidans	hdrC	ACK79235.1/AFE_2551	100	98.74
Acidithiobacillus ferrooxidans	hdrB	WP_180830595.1/QLK43761.1	99	100
Acidithiobacillus ferrooxidans	tetH	ACM91726.1	99	98.8
Acidithiobacillus ferrooxidans	sat	WP_163057956.1	99	99.46
Acidithiobacillus ferrooxidans	sdo subunit alpha	WP_163058634.1	99	100
Acidithiobacillus ferrooxidans	petII cyt C4	ACK78424.1	100	99.08
Acidithiobacillus ferrooxidans	petII short-chain dehydrogenase	ACH84551.1	100	100
Acidithiobacillus ferrooxidans	PetII Ub cyt C reductase subunit	ACK79816.1	100	100
Acidithiobacillus ferrooxidans	PetII Ub cyt C reductase subunit b	ACK78596.1	100	99.75
Acidithiobacillus ferrooxidans	PetII Ub cyt C reductase subunit C1	ACK79992.1	100	99.14
Acidithiobacillus ferrooxidans	DSRE-family protein	SMH65574	100	98.72
Acidithiobacillus ferrooxidans	rhodanese	CAC43401.1	100	99.53
Acidithiobacillus ferrooxidans	rhodanese	ACK80456.1	100	98.58

Acidithiobacillus ferrooxidans	rhodanese	ACK77889.1	100	99.08
Acidithiobacillus ferrooxidans	rhodanese	ACK78200.1	100	99.62
Acidithiobacillus ferrooxidans	rhodanese	ACK78494.1	100	96.88
Acidithiobacillus ferrooxidans	rhodanese	ACK78122.1	100	100
Acidithiobacillus ferrooxidans	TusA	WP_163054051.1	98	100
Acidithiobacillus ferrooxidans	Bo3 subunit	ACK79544.1	100	96.88
Acidithiobacillus ferrooxidans	Bo3 subunit	ACK80009.1	100	98.3
Acidithiobacillus ferrooxidans	Bo3 subunit	ACK77850.1	100	96.21
Acidithiobacillus ferrooxidans	Bo3 subunit	ACK80492.1	100	99.15
Acidithiobacillus ferrooxidans	tqo	CBI05577.1	99	99.17
Acidithiobacillus ferrooxidans	tqo(DoxDA)	CBI05581.1	99	98.06
Acidithiobacillus ferrooxidans-related	TSD1	AFE_0042/ACK78047.1	99	98.17
Acidithiobacillus ferrooxidans-related	TSD2	AFE_0050/ACK78958.1	100	98.52
Acidithiobacillus ferrooxidans-related	SQR	BAD99305/AB217915.1	100	96.19
Acidithiobacillus ferrooxidans-related	SQR	AFE_0267/ACK80058	100	98.93
Acidithiobacillus ferrooxidans-related	bd subunit II	WP_113526682	99	100

Acidithiobacillus ferrooxidans-related	bd subunit I	AFE_0955/ACK77832.1	100	98.15
Acidithiobacillus ferrooxidans-related	hdrC	ACK79235.1/AFE_2551	100	97.49
Acidithiobacillus ferrooxidans-related	tetH	ACM91726.1	100	98
Acidithiobacillus ferrooxidans-related	sat	WP_113526832.1	100	98.33
Acidithiobacillus ferrooxidans-related	sdo subunit alpha	WP_113526332.1	100	98.69
Acidithiobacillus ferrooxidans-related	petII short-chain dehydrogenase	ACH84551.1	100	98.33
Acidithiobacillus ferrooxidans-related	DSRE-family protein	SMH65574	100	98.72
Acidithiobacillus ferrooxidans-related	rhodanese	ACK77889.1	100	97.25
Acidithiobacillus ferrooxidans-related	rhodanese	ACK80456.1	100	97.16
Acidithiobacillus ferrooxidans-related	rhodanese	CAC43401.1	100	98.14
Acidithiobacillus ferrooxidans-related	rhodanese	ACK78200.1	100	90.77
Acidithiobacillus ferrooxidans-related	rhodanese	ACK78494.1	100	96.09
Acidithiobacillus ferrooxidans-related	rhodanese	ACK78122.1	100	100

Acidithiobacillus ferrooxidans-related	TusA	WP_113526480.1	98	100
Acidithiobacillus ferrooxidans-related	Bo3 subunit	ACK77850.1	100	97.16
Acidithiobacillus ferrooxidans-related	Bo3 subunit	ACK80009.1	97	98.09
Acidithiobacillus ferrooxidans-related	tqo(DoxDA)	CBI05581.1	99	99.17
Acidithiobacillus ferrooxidans-related	tqo(DoxDA)	CBI05577.1	99	97.5
Acidithiobacillus thiooxidans	SQR	AHA38170.1	99	98.68
Acidithiobacillus thiooxidans	DSRE-family protein	WP_010637276.1	99	100
Acidithiobacillus thiooxidans	sqr1	AHA38169.1	99	99.08
Acidithiobacillus thiooxidans	sqr3	AHA38166.1	99	96.8
Acidithiobacillus thiooxidans	sqr4	AHA38165.1	99	98.6
Acidithiobacillus thiooxidans	sqr5	AHA38170.1	99	99.68
Acidithiobacillus thiooxidans	SoxX	WP_024895117.1	99	99.21
Acidithiobacillus thiooxidans	SoxY	OCX75091.1	99	100
Acidithiobacillus thiooxidans	SoxB	WP_024895114.1	99	99.83
Acidithiobacillus thiooxidans	rhodanese	WP_075323176.1	99	100
Acidithiobacillus thiooxidans	rhodanese	WP_024892993.1	99	100
Acidithiobacillus thiooxidans	rhodanese	WP_142087411.1	99	95.44

Acidithiobacillus thiooxidans	rhodanese	WP_010641189.1	99	99.18
Acidithiobacillus thiooxidans	TQO (DoxX)	WP_024895053.1	99	99.38
Acidithiobacillus thiooxidans	TusA	TQN51362.1	100	100
Acidithiobacillus thiooxidans	teth	QFX96528.1	100	99.6
Acidithiobacillus thiooxidans	SoxA	QFX97266.1	100	100
Acidithiobacillus thiooxidans	SoxZ	WP_175438514.1	100	100
Acidithiobacillus thiooxidans	TQO	WP_010638552.1	99	100
Acidithiobacillus thiooxidans	HdrB	WP_024892968.1	100	100
Acidithiobacillus thiooxidans	HdrC	QFX97247.1	100	100
Acidithiobacillus thiooxidans	Bo3 subunit	ACK80009.1	97	88.66
Acidithiobacillus thiooxidans	Bo3 subunit	ACK80492.1	95	85.84
Ferroplasma acidarmanus	sqr	ARD85677.1	100	99.76
Ferroplasma acidarmanus	sor	WP_009887592.1	99	99.48
Ferroplasma acidarmanus	hdrB	WP_009887778.1	100	98.97
Ferroplasma acidarmanus	fccb	ARD84263.1	100	96.82
Ferroplasma acidarmanus-related	sqr	ARD85677.1	100	99.76
Ferroplasma acidarmanus-related	sor	WP_009887592.1	100	99.02
Ferroplasma acidarmanus-related	hdrB	WP_009887778.1	99	98.97

Ferroplasma acidarmanus-related	fccb	ARD84263.1	100	99.73
Ferroplasma type II	sqr	ARD85677.1	100	92.26
Ferroplasma type II	sor	WP_009887592.1	100	97.87
Ferroplasma type II	hdrB	WP_009887778.1	100	93.13
Gplasma	sqr	EQB68569.1	99	98.51
Leptospirillum	SQR	EES51740.1	99	100
Leptospirillum	SQR	EES53159	99	96
Rhodospirillales	SQR	ABQ35800.1	99	74
Rhodospirillales	TusA	WP_114913215.1	98	100
Rhodospirillales	TQO (DoxX-related)	WP_114912346.1	99	97.78

Table APIV.2– Iron oxidation

Species	Gene	Accession code of comparison	Query Cover%	Identity%
acidithiobacillus ferrivorans	ctat	WP_064218441.1	98	90.82
acidithiobacillus ferrivorans	ctab	OCX77064.1	98	84.27
acidithiobacillus ferrivorans related	Coxb	WP_081919233.1	99	92.26
acidithiobacillus ferrivorans related	Coxa	AEM47198.1	99	92.18
acidithiobacillus ferrivorans related	ctab	OCX75109.1	98	85.64
acidithiobacillus ferrivorans related	ctat	WP_071182563.1	98	90.16
acidithiobacillus ferrooxidans	Cyc1	WP_163059395.1	99	96.61
acidithiobacillus ferrooxidans	Cyc2	WP_163054682.1	99	99.79
acidithiobacillus ferrooxidans	rus	WP_163059407.1	99	99.47

acidithiobacillus ferrooxidans	cup	ACK78265.1	100	93.99
acidithiobacillus ferrooxidans	sdr	ACK78064.1	99	98.85
acidithiobacillus ferrooxidans	coxb	ACK78948.1	100	94.88
acidithiobacillus ferrooxidans	coxc	ACK77876.1	98	93.96
acidithiobacillus ferrooxidans	coxa	ACK79083.1	100	94.58
acidithiobacillus ferrooxidans	coxd	ACK78613.1	100	90.62
acidithiobacillus ferrooxidans	petA	AAF76298	100	99.51
acidithiobacillus ferrooxidans	petB	AAF76299.1	100	98.01
acidithiobacillus ferrooxidans	petC	AAF76300.1	100	95.87
acidithiobacillus ferrooxidans related	rus	WP_113526420.1	99	100
acidithiobacillus ferrooxidans related	Cyc2	WP_151528126.1	99	100
acidithiobacillus ferrooxidans related	Cyc2	WP_113526413.1	99	100
acidithiobacillus ferrooxidans related	Cyc1	WP_126605216.1	99	92.96
acidithiobacillus ferrooxidans related	cup	ACK78265.1	100	99.45
acidithiobacillus ferrooxidans related	coxb	ACK78948.1	100	98.03
acidithiobacillus ferrooxidans related	sdr	ACK78064.1	99	96.95
acidithiobacillus ferrooxidans related	coxc	ACK77876.1	100	97.83
acidithiobacillus ferrooxidans related	coxa	ACK79083.1	100	97.93
acidithiobacillus ferrooxidans related	coxd	ACK78613.1	100	93.75

acidithiobacillus ferrooxidans related	ctat	ACK78336.1	99	96.46
acidithiobacillus ferrooxidans related	ctab	SMH65005.1	99	90
acidithiobacillus ferrooxidans related	petA	AAF76298	100	99.03
acidithiobacillus ferrooxidans related	petB	AAF76299.1	100	100
Ferroplasma acidarmanus	sulfocyanin	WP_009887159.1	99	100
Ferroplasma acidarmanus	cbb3 subunit I/III	WP_009887157.1	98	99.51
Ferroplasma acidarmanus	cbb3 subunit II	WP_009887160.1	100	99.64
Ferroplasma acidarmanus	rieske	ARD84307.1	99	100
Ferroplasma acidarmanus	cytb	WP_081141558.1	99	100
Ferroplasma acidarmanus related	sulfocyanin	WP_009887159.1	99	99.51
Ferroplasma acidarmanus related	rieske	ARD84307.1	100	100
Ferroplasma acidarmanus related	cytb	WP_081141558.1	99	100
Ferroplasma type II	sulfocyanin	EQB71946.1	99	98.01
Ferroplasma type II	cbb3 subunit I/III	WP_009887157.1	100	92.17
Ferroplasma type II	rieske	EQB74440.1	99	94.07
Ferroplasma type II	cytb	EQB74439.1	100	99
Leptospirillum ferrodiazotrophum	CycA1	EES53608.1	100	97.08
Leptospirillum ferrodiazotrophum	Cyt572	EES51436.1	100	94.37
Leptospirillum ferrodiazotrophum	Cyt572	EES53235.1	100	97.69
Leptospirillum ferrodiazotrophum	Cyt579	WP_101494943.1	96	86.03

Leptospirillum ferrodiazotrophum	cbb3	EES51563.1	100	100

Table APIV.3– Nitrogen fixation

Species	Gene	Accession code of comparison	Query cover	Identity%
L. ferrodiazotrophum	NifH	AFD97520.1	100%	98.97%
L. ferrodiazotrophum	NifK	AFD97522.1	100%	99.61%
L. ferrodiazotrophum	NifD	AFD97521.1	100%	100%
L. ferrodiazotrophum	NifE	EES53487.1	100%	99.79%
L. ferrodiazotrophum	NifN	EES53488.1	99%	98.48%
L. ferrodiazotrophum	NifX	EES53489.1	100%	100%
At. ferrooxidans	NifH	WP_009567494.1	99%	100%
At. ferrooxidans	NifD	WP_163054576.1	99%	100%
At. ferrooxidans	NifK	QLK42049.1	100%	99.81%
At. ferrooxidans	NifE	QLK42046.1	100%	100%
At. ferrooxidans	Fer1	WP_012536578.1	99%	100%
At. ferrooxidans	Fer2	WP_163054580.1	98%	100
At. ferrooxidans	NifN	QLK42045.1	100%	98.9%
At. ferrooxidans	NifX	WP_163054933.1	99%	100%
At. ferrooxidans related	NifX	WP_126605245.1	99%	100%
At. ferrooxidans related	NifH	RBM03589.1	100%	99.66%
At. ferrooxidans related	NifD	RBM03588.1	100%	99.39%

At. ferrooxidans related	NifK	WP_126605248.1	99%	99.42%
At. ferrooxidans related	NifE	WP_113525794.1	99%	100%
At. ferrooxidans related	NifN	WP_126605246.1	99%	100%
At. ferrooxidans related	Fer1	WP_113525795.1	99%	100%
At. ferrooxidans related	Fer2	WP_126605247.1	99%	100%
At. ferrivorans	NifN	QLK42045.1	100%	97.13
At. ferrivorans	NifX	WP_035193255.1	99%	98.55%
At. ferrivorans	NifH	WP_163097655.1	99%	99.32%
At. ferrivorans	NifD	WP_035192737.1	99%	99.19%
At. ferrivorans	NifK	QLK42049.1	100%	97.30%
At. ferrivorans	NifE	WP_014029034.1	99%	98.27%
At. ferrivorans-related	NifH	WP_065413759.1	99%	98.65%
At. ferrivorans-related	NifD	WP_012536580.1	99%	98.78%
At. ferrivorans-related	NifK	QLK42049.1	100%	97.88%
At. ferrivorans-related	NifE	WP_163097658.1	100%	99.30%
At. ferrivorans-related	NifX	WP_065413794.1	100%	97.83%
At. ferrivorans-related	NifN	WP_035192725.1	99%	97.86%
At. ferrivorans-related	Fer1	WP_012536577.1	99%	83.33%

Appendix V - Chapter 3 Growth Images Phoukassa Ore

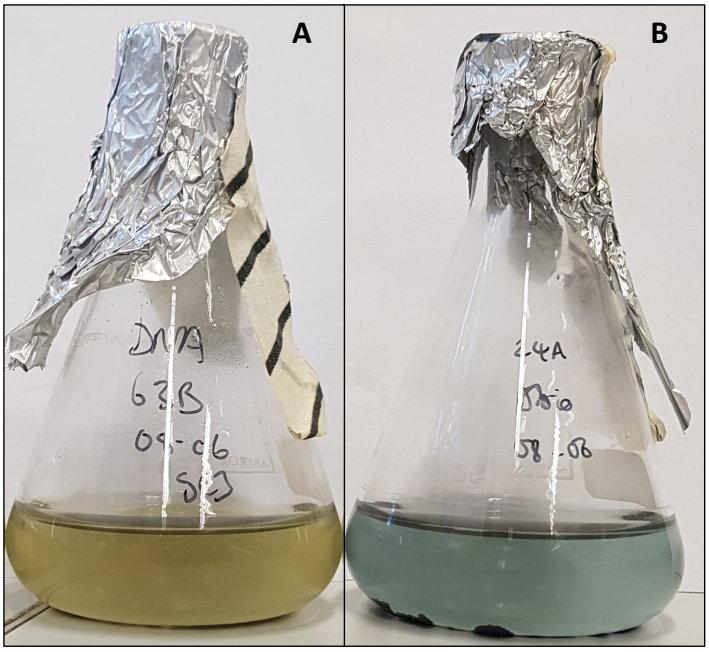

Figure APV – Phoukassa ore experiment, week 16 samples under A) biotic and B) abiotic conditions

Appendix VI - Additional RNA-seq plot Phoukassa Ore

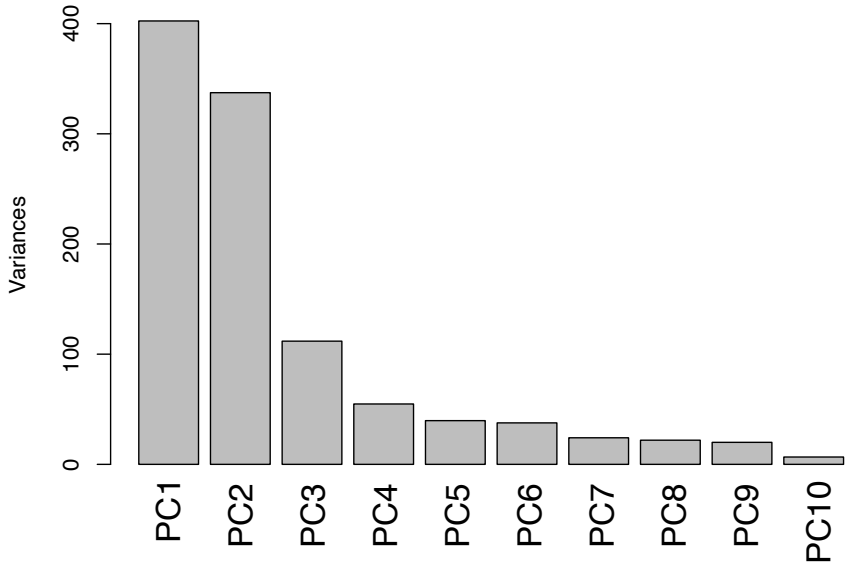

Figure APVI – Principal components responsible for variance in RNA-seq data from the Phoukassa ore.

Appendix VII – Stibnite Background Information

Sample	Location	Type of ore deposit	Host rock	Associated minerals	Mining history	Reference(s)
Stb1	Medas, Portugal	Epithermal, Sb-Au veins in the region formed from hydrothermal mineralizing fluids	Cambrian phyllites and metagraywackes	Sb-Au-quartz veins	Exact location of sample collection unknown. Medas is within the Dúrico Beirão mining district.	(Neiva, Andráš and Ramos, 2008) (Couto and Roger, 2017)
Stb2	Knipe Mine, Scotland	Epithermal, high salinity	Late Caledonian granite	As-Sb-Cu-Pb-Zn-quartz-chert mineralisation	19th Century antimony mining	Sampson & Banks (1988) Smith et al. (2008)-Map
Stb3	Su-Suergiu-Martalai, Sardinia	No information available	Cataclastic carbonaceous black shales and metalimestones	Scheelite, antimonite, arsenopyrite, pyrite, calcite, quartz	Exploitation began 1858, mined intensively during periods of war, closed 1960	(Carmignani *et al.*, 1979) (Cidu *et al.*, 2013)
Stb 4	Bau Mine, Malaysia	There are several deposit types in this mining district	Limestone	Quartz, calcite, pyrite, arsenopyrite, minor Au	Bau mining district saw extraction of 79 thousand tonnes of Sb and 37.3 tonnes of Au between 1820 and 1981, mercury also mined in the area	(Pour, Hashim and Marghany, 2014) (Percival, Radtke and Bagby, 1990) (Breward *et al.*, no date) (Bradshaw, 1972)

Sample	Location	Type of ore deposit	Host rock	Associated minerals	Mining history	Reference(s)
						(Kirwin and Royle, 2019)
Stb5	Les Biards Mine, France	No data	Paragneiss of the Upper Gneiss Unit	Quartz, Pyrite, arsenopyrite, Jamesonite, sphalerite, tetrahedrite, chalcopyrite, (gold), chalcostibite, native antimony	Former Sb mine, c. 1,500t stibnite extracted 1909-1931	Bouchot et al. (2005) (Bellot *et al.*, 2003)
Stb6	Reefton, New Zealand	Mesothermal, Orogenic gold deposit	Greywacke and argillite of lower Palaeozoic Greenland Group	Quartz, auriferous pyrite, arsenopyrite	Historic gold mining occurred 1872-1950. Modern gold mine opened in 2007, currently producing 60,000oz Au per year, with gold recovered at 1.5g/t	Christie & Braithwaite (2003) Craw et al. (2004) Milham & Craw (2009) Milham & Craw (2009b) (Mackenzie, Douglas James; Craw, Dave; Hamish, 2014)

Sample	Location	Type of ore deposit	Host rock	Associated minerals	Mining history	Reference(s)
Stb7	Xikuangshan (XKS) Mine, Hunan Province	Mesothermal	Middle-Upper Devonian carbonate rocks	Quartz and calcite, with rare pyrite and sphalerite. Minor fluorite, barite, chlorite and talc. Trace pyrite, pyrrhotite and sphalerite. Gangue minerals may not be co-genetic	Discovered 1521, originally a tin mine. 172,000 tons Sb produced from 1949-1981.	Hu et al. (1996) Carter & Kiilsgaard (1983) Hu et al. (1996) Fan et al. (2004) Hu & Peng (2018)
Stb8	Xiknangshan XKS Mine, Hunan Province	Information as for Stb7.				
Stb9	Hillgrove, NSW, Australia	Mesothermal	Late Carboniferous sediments, granitoids.	Stibnite-Au-Ag-quartz veins with occasional scheelite, arsenopyrite	Sb and Au intermittently mined in the district since 1877	Ashley et al. (2003) Boyle & Hill (1988)
Stb10	Black Warrior (Silver Prince Mine, Swastika Mine) Mine, AZ, USA	No information available	No information available	Quartz	Ag-Pb-Cu-Au-Zn mine. Discovered 1874, produced 600,000 ounces of silver 1910-15	(Mindat, 2020a) (Guiteras, 1936)

Sample	Location	Type of ore deposit	Host rock	Associated minerals	Mining history	Reference(s)
Stb11	Hampton Mine, Utah, USA	No information available	Predominantly sandstone, some shale	Realgar, arsenates, and sulfate minerals incl: gypsum, epsomite; kaolinite, fluorite. Rare: pyrite, limonite	Discovered 1880, extensively mined during WWI	(Traver, 1949)
Stb12	Bajuz (Baiut) Mine, Romania	Epithermal	Neogene calc-alkaline igneous rocks	No information on specific vein but the metallogenic veins in the region contain	No data	Plotinskaya et al. (2014) Marcoux et al. (2002) Grancea et al. (2002)
Stb13	Red Devil Mine, Alaska, USA	Epithermal	Greywackes and argillaceous rocks	Cinnabar, minor realgar, orpiment and pyrite	Mercury mine 1933-1971, producing 36,000 flasks of mercury.	MacKevett Wemly Gray et al. (1991) Burton and Ball
Stb14	Antimony Peak, San Benito County, California, USA	Epithermal	Tertiary igneous rocks	Quartz, cinnabar, pyrite.	Historical mining in the district – Sb ore mined from 1870-1875, then mercury mining began with intermittent	(Dunning and Cooper Jr, 1989) Bailey and Myers Davidson

Sample	Location	Type of ore deposit	Host rock	Associated minerals	Mining history	Reference(s)
					production of Sb and Hg until the 1950s.	
Stb15	Isle of Pines, Cuba	Epithermal	Greenschist facies, micaceous quartzites and quartz-muscovite schist	Principal: Quartz, arsenopyrite. Minor: sphalerite, galena, sericite, graphite, boulangerite. Rare: pyrite, native gold, tetrahedrite, jamesonite, chlorite, ankerite	No information available	Bortnikov et al. (2010) (Bortnikov *et al.*, 1989)
Stb16	Caspari-Zeche, Arnsberg, Germany	Mesothermal	Carboniferous pyrite-rich black shales and siliceous limestones		Limited information, papers predominantly in German	(Wagner and Boyce, 2003)
Stb17	Boccheggiano, Tuscany, Italy	Epithermal	(Mostly triassic) carbonates	Calcite, fluorite, gypsum, sphalertite, pyrite, native gold, barite, alunite, orpiment, realgar. quartz	Mining of base metals has occurred since 16th C – mostly Cu and pyrite mining	(Morteani, Voropaev and Grinenko, 2017) (Benvenuti *et al.*, 1997) (Dini, 2003)

Sample	Location	Type of ore deposit	Host rock	Associated minerals	Mining history	Reference(s)
Stb18	Echinokawa Mine, Near Saijo, Ehime, Japan	Epithermal	Carboniferous-Permian sedimentary rocks	?	Mined for several hundred years. Mine abandoned in 1957 Almost all stibnite has been removed.	Asaoka Mindat/Geological Survey of Canada
Stb19	Estado de San Luis Potosi, Mexico	Epithermal	Limestone	Chalcedony, calcite, pyrite, quartz, gypsum, anhydrite	Sb deposits in the region discovered 1898, a number of mines have operated in the area since. In the early 20th C, was one of the biggest Sb producers in the world	(Camprubi, 2003) (White and Gonzales, 1946) (Levresse *et al.*, 2012) (Mascunano *et al.*, 2011)
Stb20	Manhattan, Nye County, NV, USA	Epithermal	Limestone	Calcite, quartz, arsenopyrite, pyrite, realgar, orpiment, cinnabar.		(Ferguson, 1921) (Ferguson, 1924)
Stb21	Kremnica, Stredne Slovensko, Slovakia	Epithermal	Diorite porphyry and other volcanic rocks	Quartz, some carbonates, pyrite,	Mined for gold for over a thousand years, 250Kg Au and Ag	(Ševko *et al.*, 2018)

Sample	Location	Type of ore deposit	Host rock	Associated minerals	Mining history	Reference(s)
				marcasite, minor cinnabar, native gold	mined per annum during 15th C, 90-100kg of Au and 120-130kg Ag total produced between 1947-1970, at which point mining ceased	(Majzlan, Števko and Lánczos, 2016) (Koděra and Lexa, 2010)
Stb22	Asturias, Spain	Location not specific enough for research, several deposits in Asturias	NA	NA	NA	
Stb23	Busoh, India	Location incorrect and not specific enough for research	NA	NA	NA	
Stb24	Rawdon, Hants Co., Nova Scotia, Canada	The large number of gold deposits in the region are mesothermal	Unclear which deposit sample was acquired from	Unclear which deposit sample was acquired from	A number of gold mines in this region, Sb-Au deposit mined at West-Gore	(Ryan and Smith, 1998)

Sample	Location	Type of ore deposit	Host rock	Associated minerals	Mining history	Reference(s)
Stb25	Clontibret mine, Co. Monaghan, Ireland	No information available	Greywackes	Quartz, arsenopyrite, pyrite, sphalerite, chalcopyrite, tetrahedrite, Pb-Zn enrichment	Mining occurred during mid 19th Century, WWI, late 1950s. Site cleared and remediated in 1984, no remaining trace of mine	(Hegarty, 2017) (Lusty *et al.*, 2012)
Stb26	San Antonio de Esquilache mine, Puno, Peru	No information available – no specific mine of this name, various mineralisations within the region, none where stibnite/Sb has a notable presence	Local geology is predominantly volcanic	NA	Lead-zinc mines/ Ancient historical silver mines in the region	(Schultze, 2013)
Stb27	Stolica (Stolice) mine, Podrinje, Krupanj, Serbia	Epithermal	Upper/Late Carboniferous Limestone	Arsenopyrite, pyrite, sphalerite, chalcopyrite, tetrahedrite, barite, cinnabar, calcite, realgar, orpiment, dolomite, marcasite quartz	Mine opened 1916, closed 1987 leaving a flotation tailing deposition site, which has latterly been capped.	(Ministry of Mining and Energy (Serbia), 2002) (Vujić, 2014) (Radosavljević *et al.*, 2013) (Jakovljević *et al.*, 2020)

Sample	Location	Type of ore deposit	Host rock	Associated minerals	Mining history	Reference(s)
						(Ranđelović *et al.*, 2020)
Stb28	La Lucette mines, Le Genest, Mayenne, France	No information available	Ordovician to upper Silurian metapelites and sandstones	Quartz-carbonate veins, arsenopyrite, native Au	Produced 42 kt Sb metal and 8 t Au between 1905 and 1939	Pochon Besso0n
Stb29	Sherwood siding, Gwelo, Rhodesia (now Gweru, Zimbabwe)	No information available	No information available	No information available	No information available	
Stb30	Alcacoya mine, San Vicente Prov., Bolivia	No information available	No information available	No information available	No information available	
Stb31	Berndorf, Lower Austria Location assumed by NHM based on historic labelling	No reported Sb/stibnite or related deposits associated with this area	No information available	No information available	No information available	

Sample	Location	Type of ore deposit	Host rock	Associated minerals	Mining history	Reference(s)
Stb32	San Martin mine, Zacatecas, Mexico	Epithermal	Dark grey limestone	Quartz, Late tetrahedite-tennantite, pyrite, native silver. Intermediate sphalerite, chalcopyrite, galena. Early arsenopyrite, bornite, chalcopyrite, pyrrhotite and molybdenite.	Stibnite comparatively rare at this site, mine primarily targeted Cu-Zn-Ag ore	(Rubin and Kyle, 1988) (González-Partida and Camprubí, 2006)
Stb33	Montauto, Grosseto, Toscana (Tuscany), Italy	Epithermal	Dolomitic limestones	Calcite, quartz	Mined from 19th Century until 1960s	Morteani, Voropaev and Grinenko, 2017) (Baroni *et al.*, 2000) (Dessau, 1952) (Mindat, 2020c)
Stb34	Niarbyl trial, Traie Vrish, Isle of Man	No Information available	No Information available	No Information available	A trial made in 1893-4 revealed the stibnite was only a small pocket that had previously been entirely removed in the mid 19th C	(Lamplugh and Geological Survey of Great Britain, 1903)

Appendix VIII – Photographs of stibnite samples analysed in Chapter 2

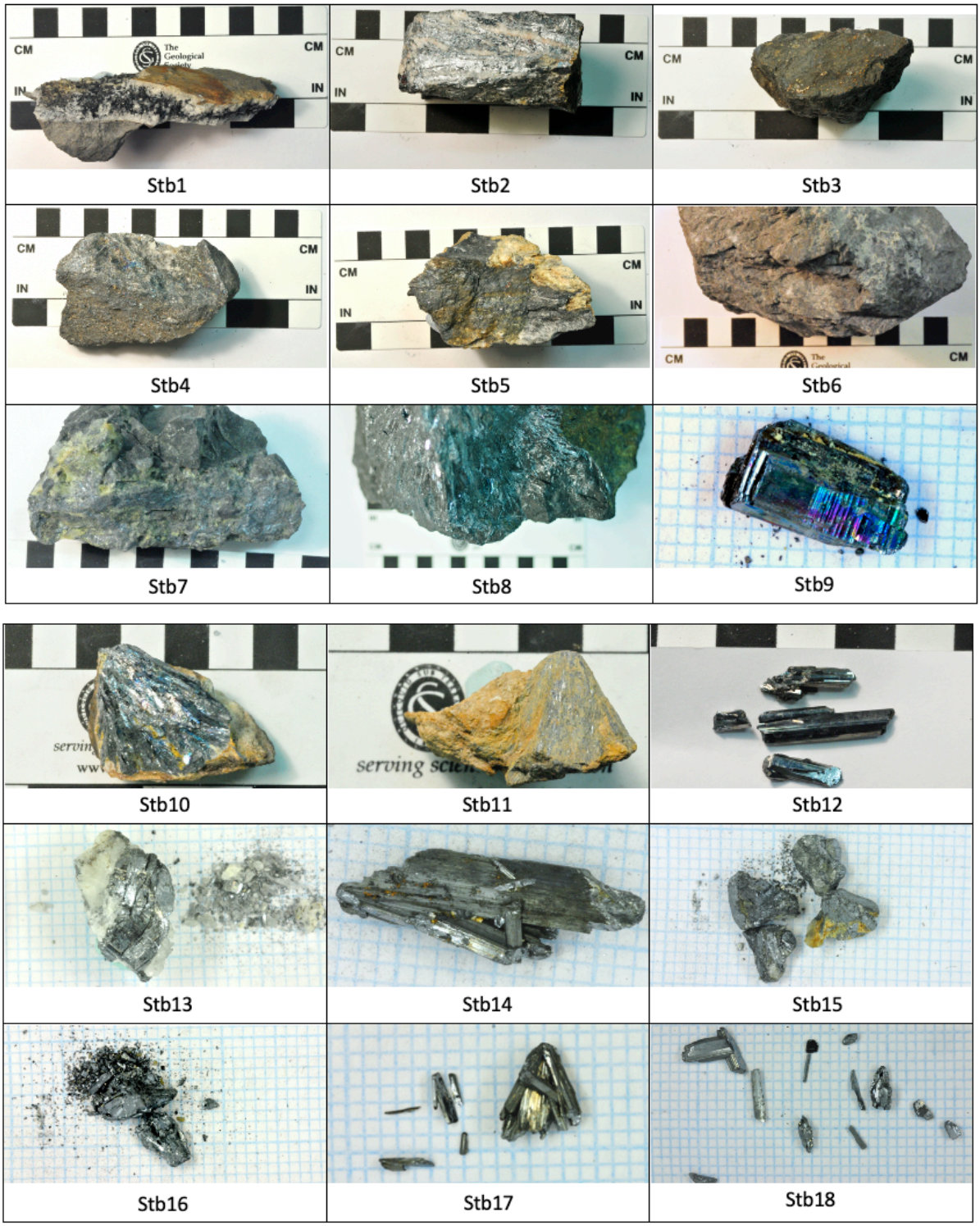

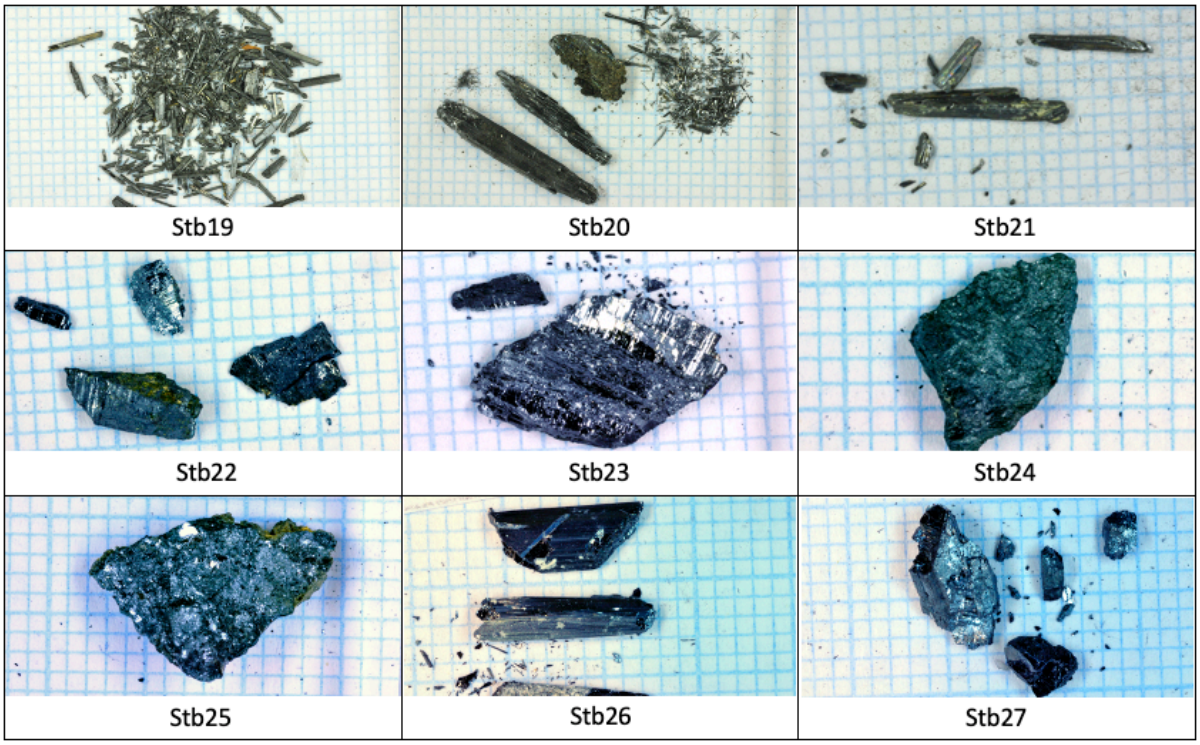
Stb19
Stb20
Stb21
Stb22
Stb23
Stb24
Stb25
Stb26
Stb27

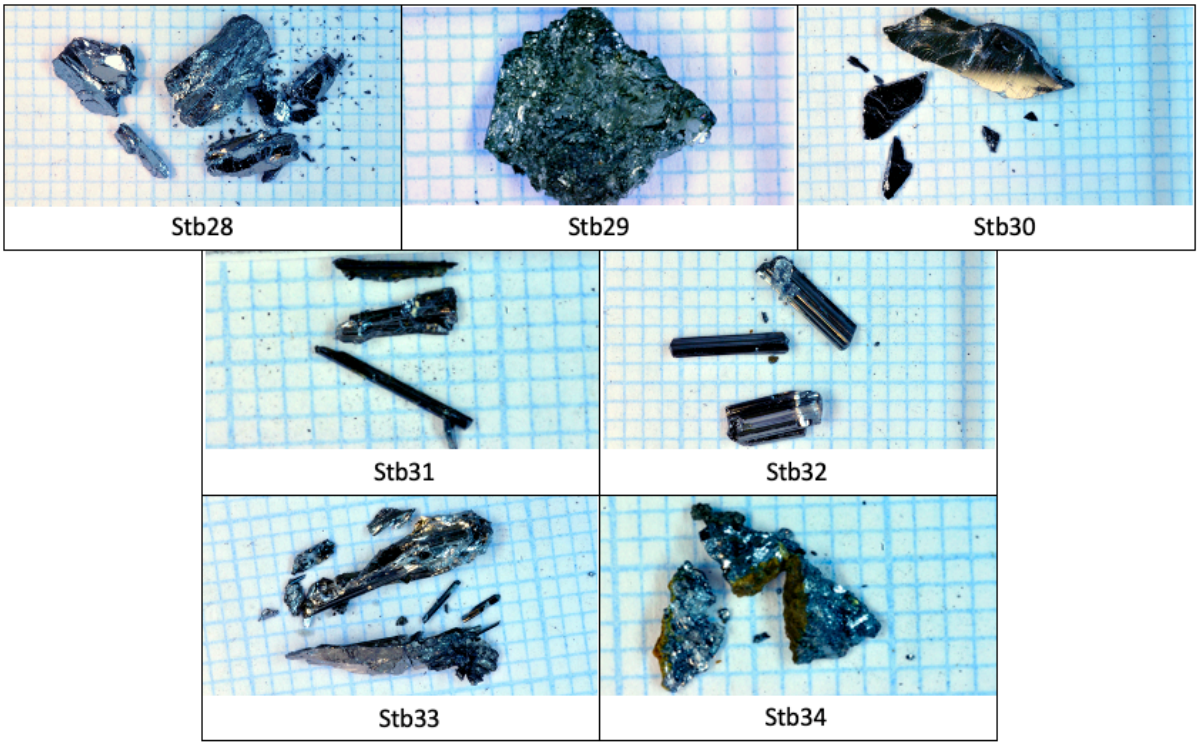
Stb28
Stb29
Stb30
Stb31
Stb32
Stb33
Stb34

Appendix IX – XAS summary of beam energies and scans conducted and XANES standards

Table APIX.1 Summary of μXRF and μXANES scans performed on stibnite samples

Stibnite Sample	Area of Interest	μXRF Map	μXANES Map
1	1	eV 13000 (Pb not covered). 480 x 400 μm. Step size 5 μm.	None
	2	eV 13200 480 x 400 μm. Step size 5 μm.	2 maps - 4μm step size
	3	eV 13200 1140 x 930 μm. Step size 5 μm.	None
7	1	eV 13200 275 x 400 μm. Step size 5 μm.	None
	2	eV 13200 1650 x 2000 μm. Step size 5 μm.	None
	3	eV 13200 760 x 730 μm. Step size 5 μm.	3 maps - 4μm step size
	4	eV 13200 955 x 910 μm. Step size 5 μm.	None
12	1	eV 13200 1490 x 1280 μm. Step size 5 μm. Mercury showing in polishing marks.	None
	2	eV 13200	None

		Longer exposure time of 1sec per point Step size 5 µm.	
	3	eV 11950 to get just above gold edge. Step size 5 µm	None
14	1	eV 13200 480 x 370 µm. Step size 2 µm.	None
	2	eV 13200 510 x 415 µm. Step size 5 µm.	None
	3	eV 13200 810 x 440 µm. Step size 5 µm.	None
	4	eV 13200 950 x 760 µm. Step size 5 µm. Extended out from scan 3	1 map - 4 µm step size
16	1	eV 13200 365 x 295 µm. Step size 5 µm.	None
	2	eV 13200 500 x 300 µm. Step size 5 µm.	None
	3	eV 13200 400 x 260 µm. Step size 5 µm. On a small grain away from main sample body.	None

	4	eV 13200 325 x 350 µm. Step size 5 µm.	3 maps - 4 µm step size
18	1	eV 13200 565 x 425 µm. Step size 5µm.	None
	2	eV 13200 1480 x 890 µm. Step size 5 µm.	None

Standards were prepared for use by grinding 5mg of the standard with 75mg of cellulose, and pressed into a pellet with a hydraulic press. Standards were analysed with the beamline in transmission mode.

Table APIX.2 - standards used in XANES

Standard	**Compound**	**Speciation**	**CAS Number**
1	Sodium selenite pentahydrate	+4	26970-82-1
2	Sodium selenate anhydrous 99.8%	+6	13410-01-0
3	Se sulfide	+4	7488-56-4
4	Se shot 99.99%	0	7782-49-2

Appendix X– Stibnite PXRD patterns

Stb1 diffraction pattern

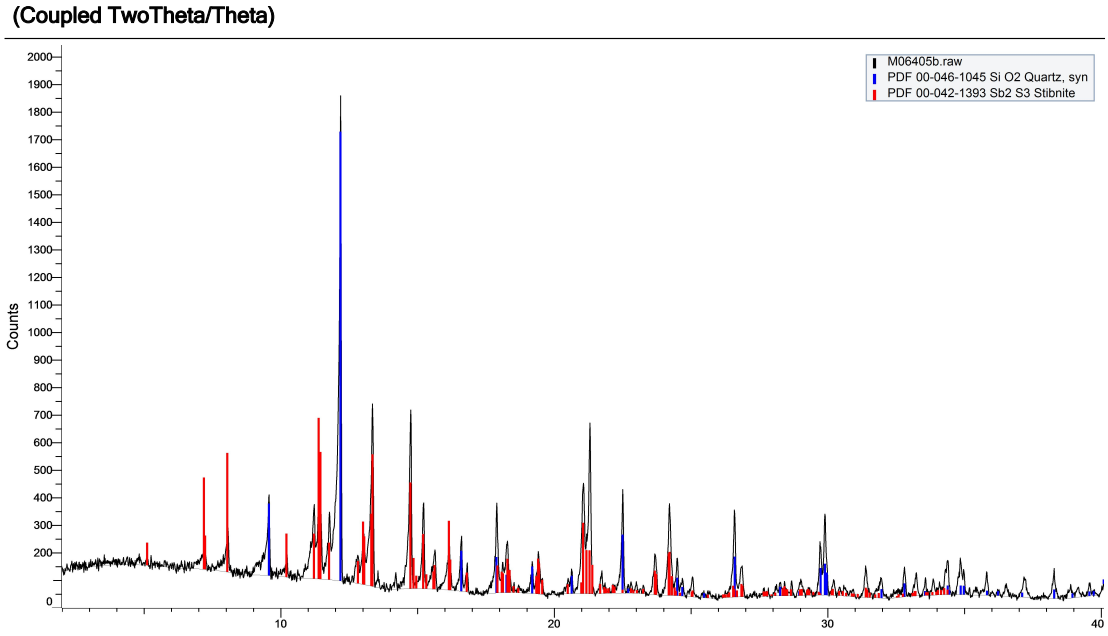

Stb2 diffraction pattern

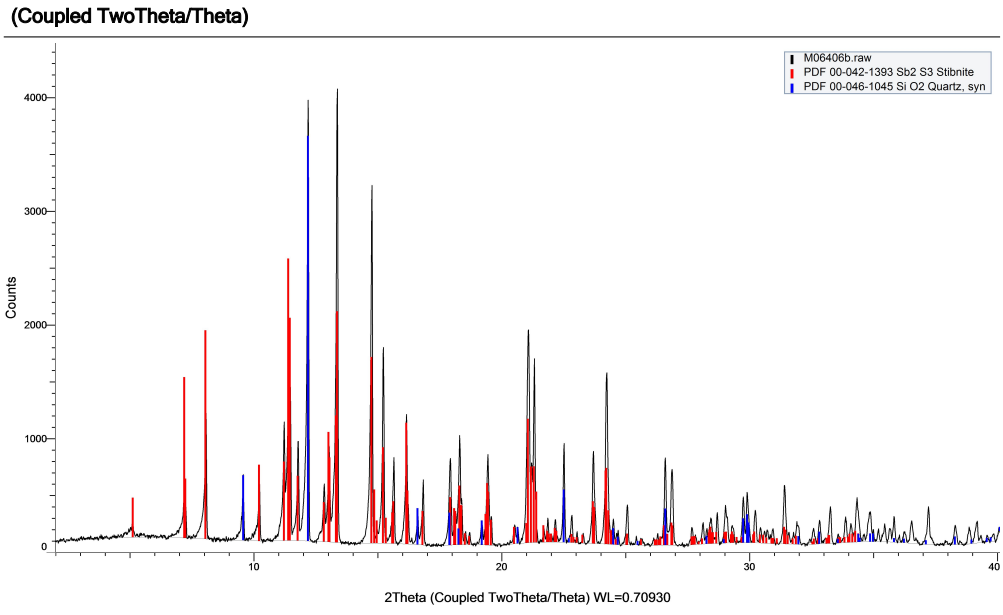

Stb3 diffraction pattern

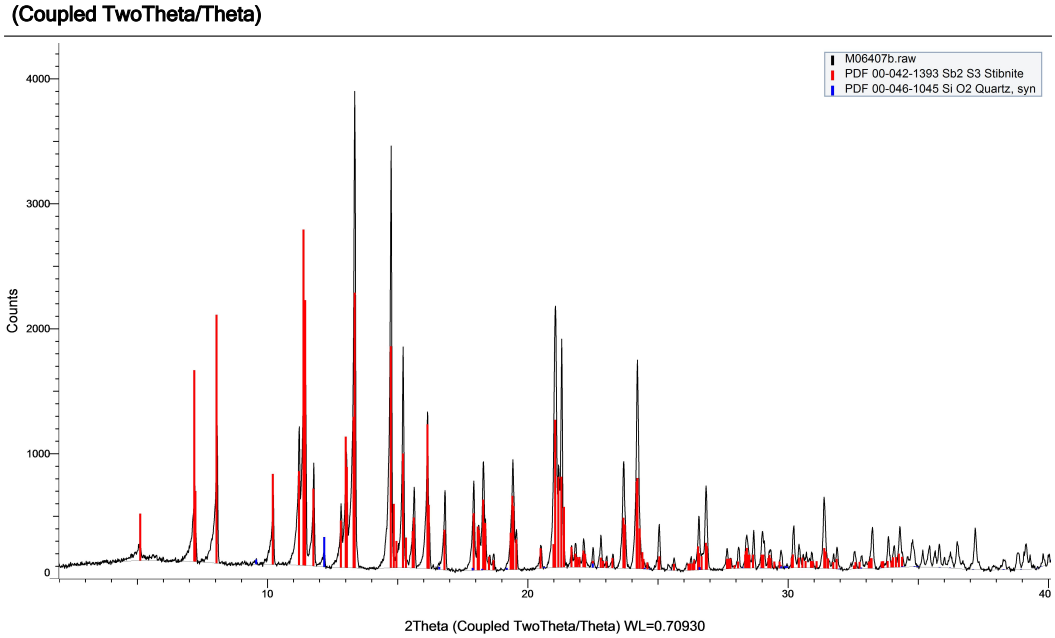

Stb4 diffraction pattern

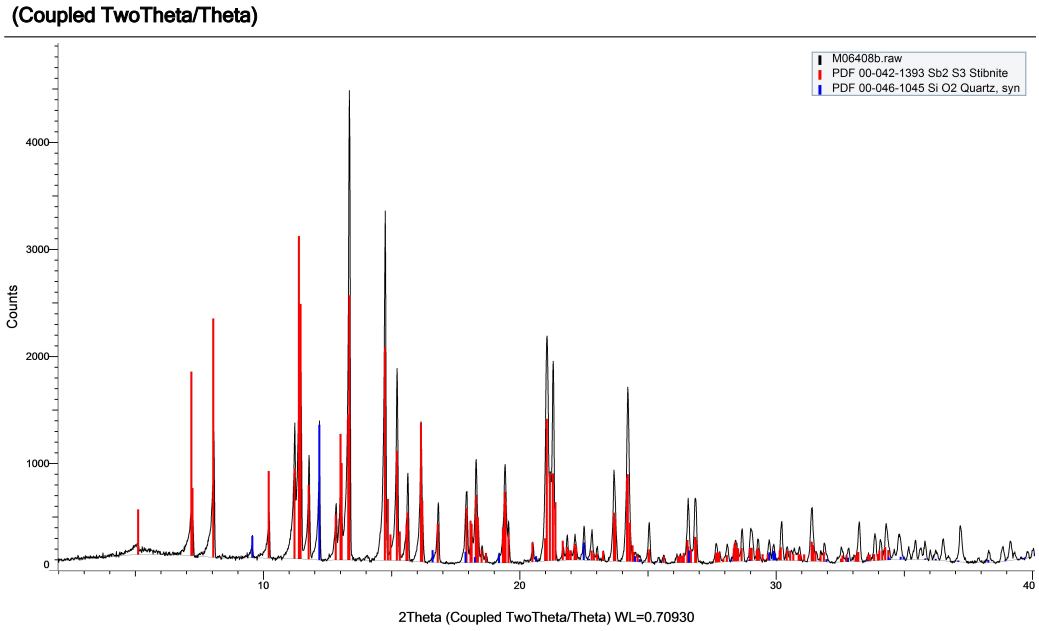

Stb5 diffraction pattern

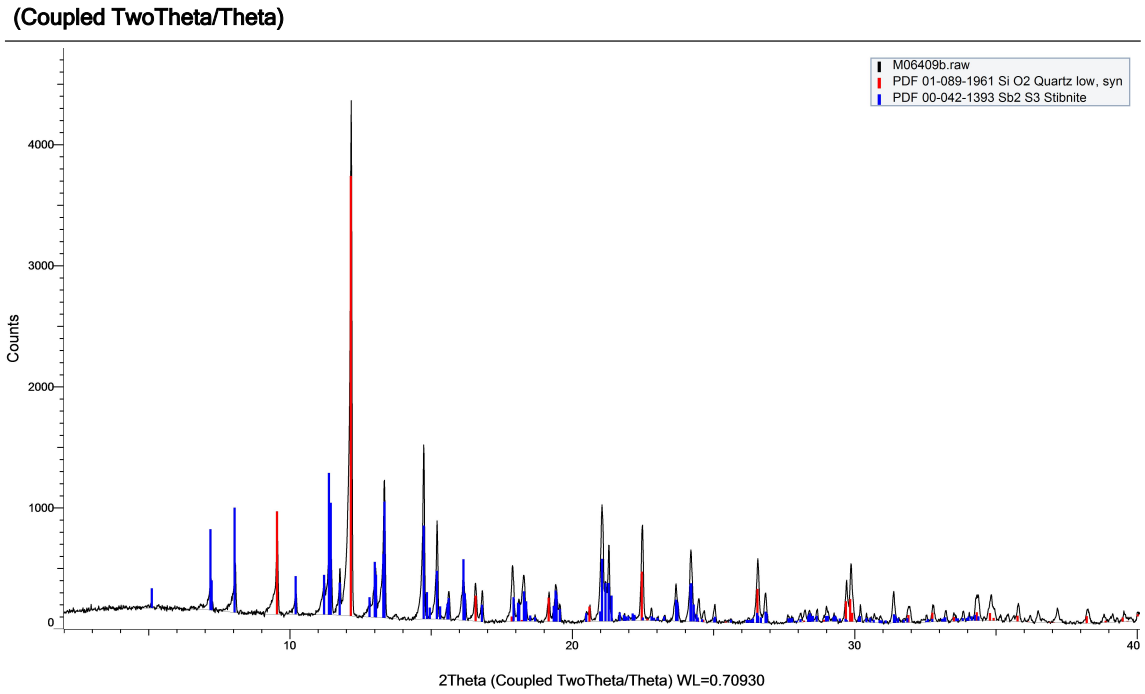

Stb6 diffraction pattern

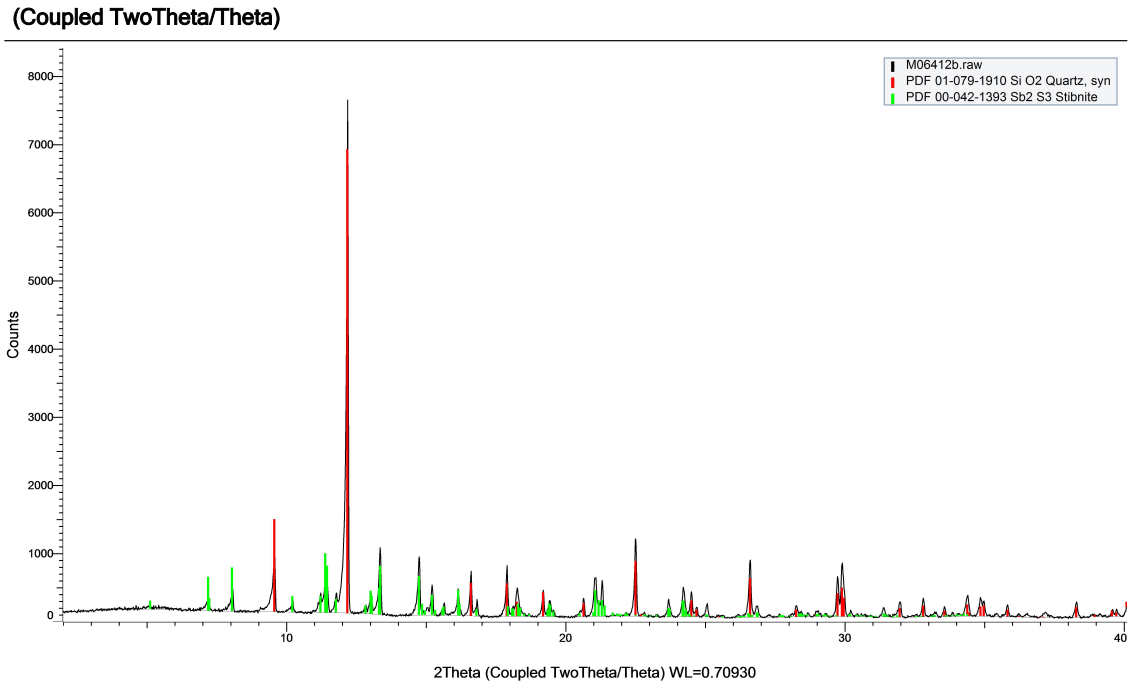

Stb7 diffraction pattern

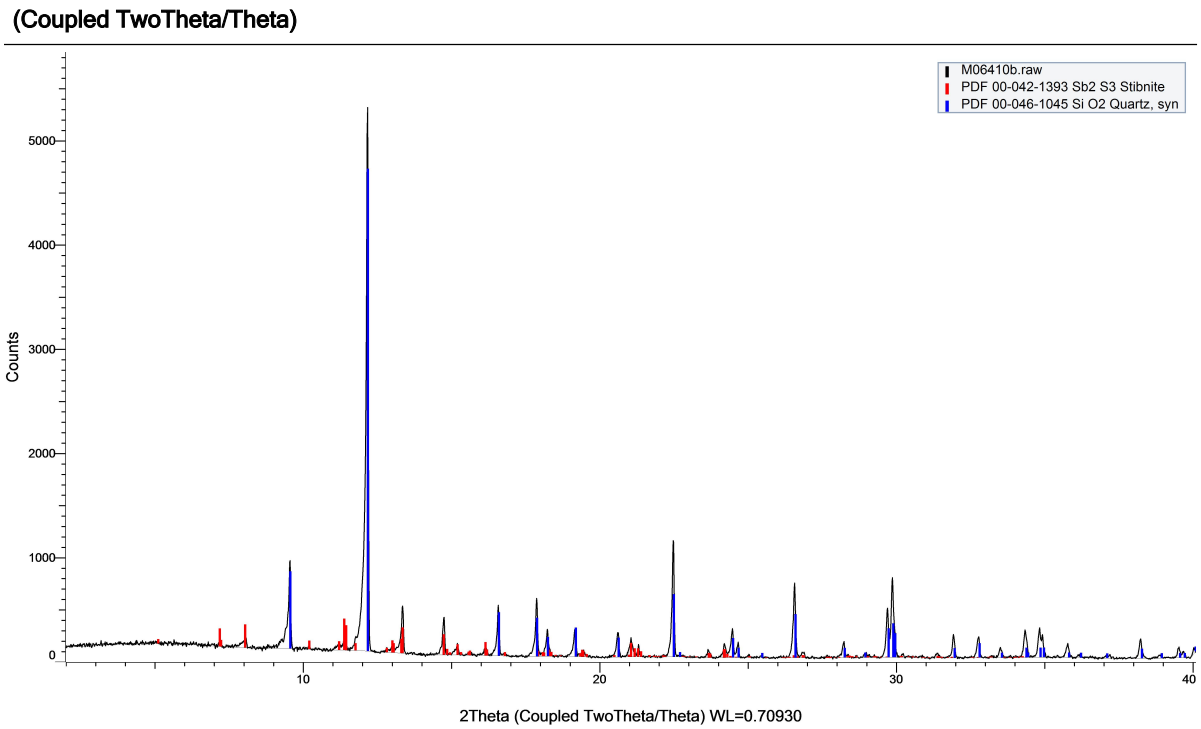

Stb8 diffraction pattern

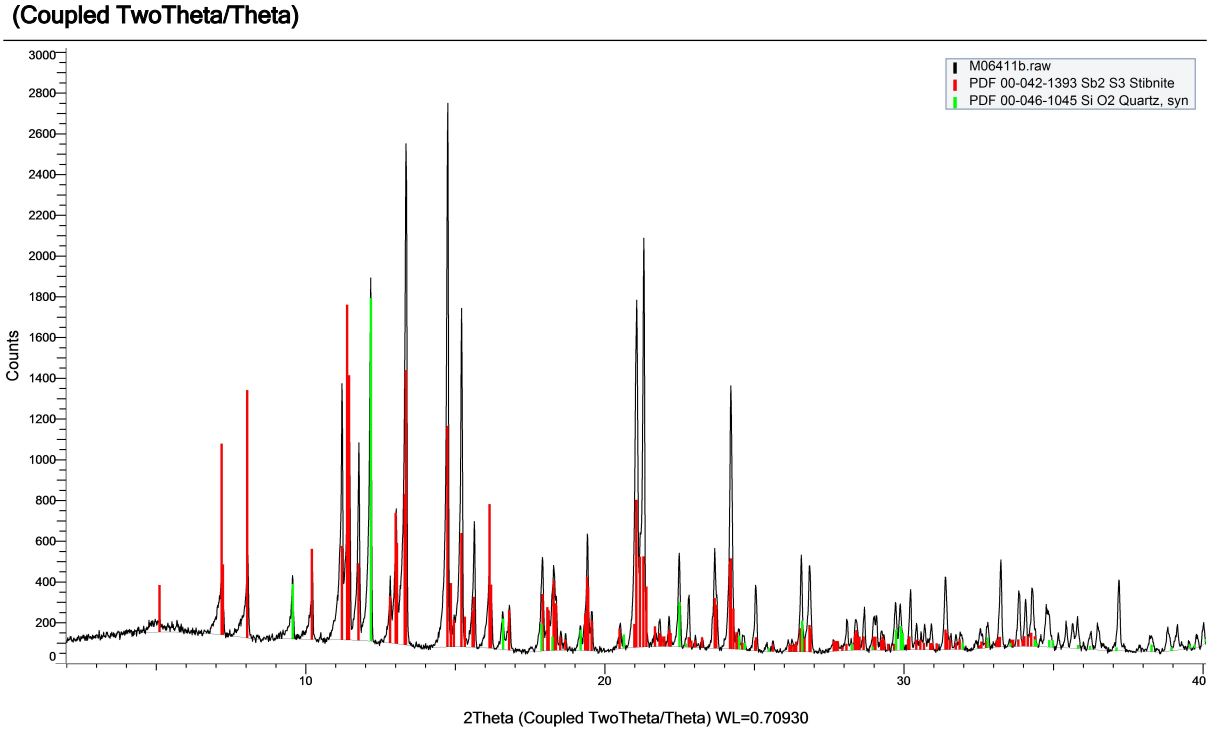

Appendix XI – WDS Maps

Stb6+7

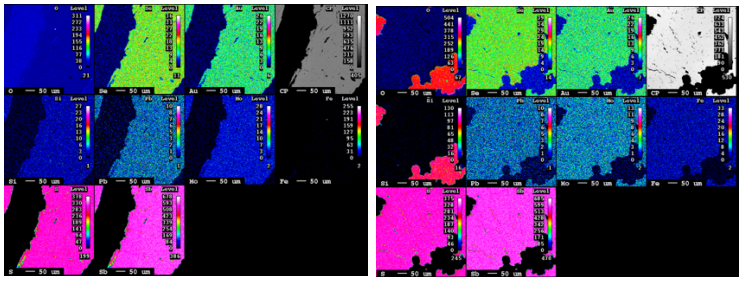

Stb9+12

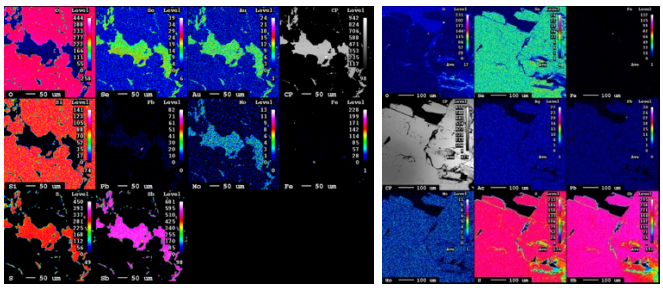

Stb13 +14

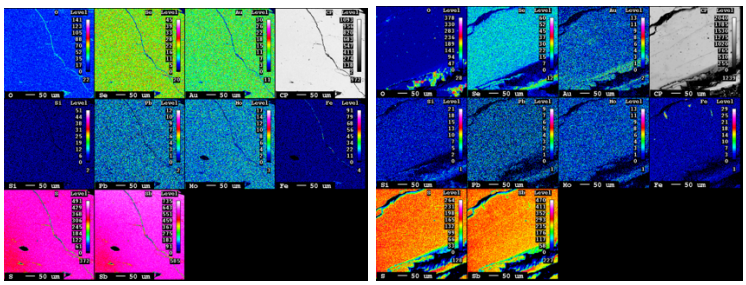

Stb15 + 16

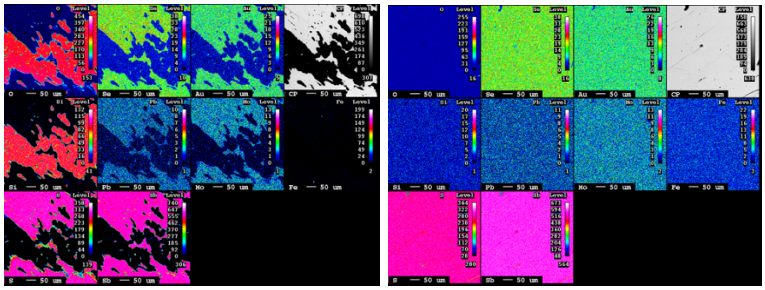

Stb17 + 18

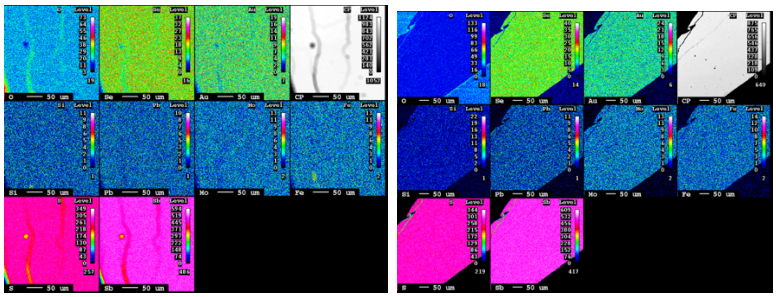

Stb20 + 21

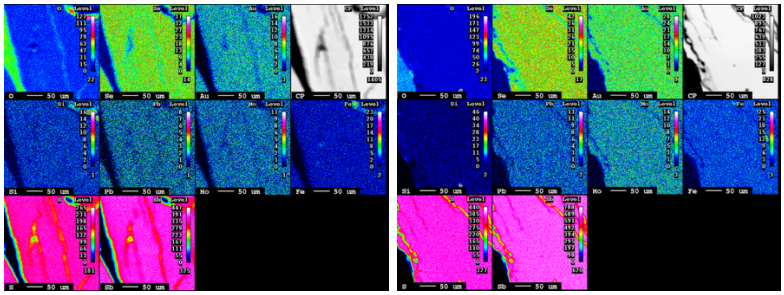

Stb22 + 23

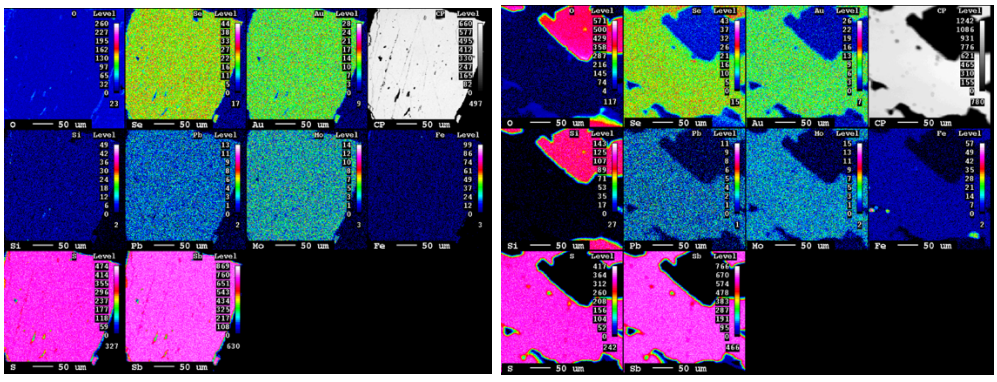

Stb25 + 31

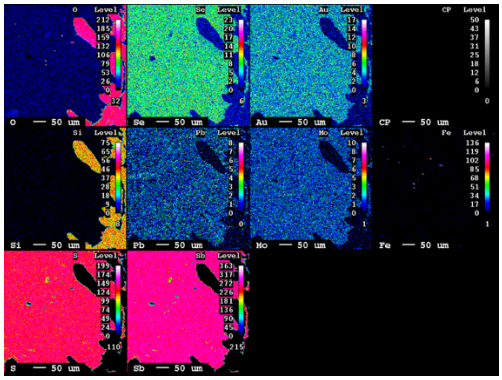

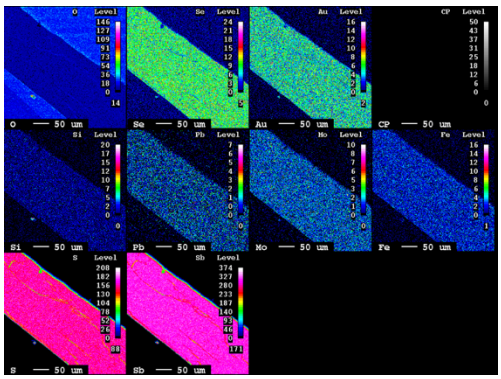

Stb32 + 34

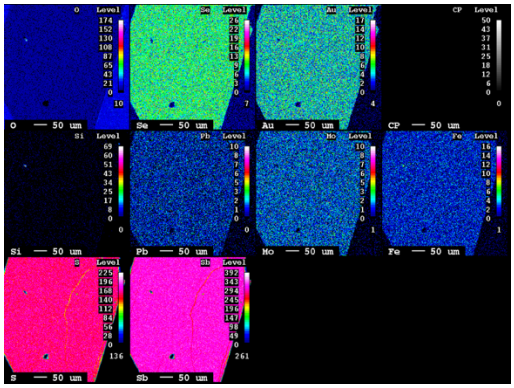

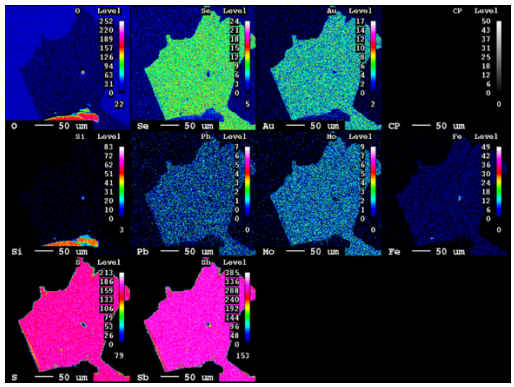

Appendix XII - EPMA X-ray values

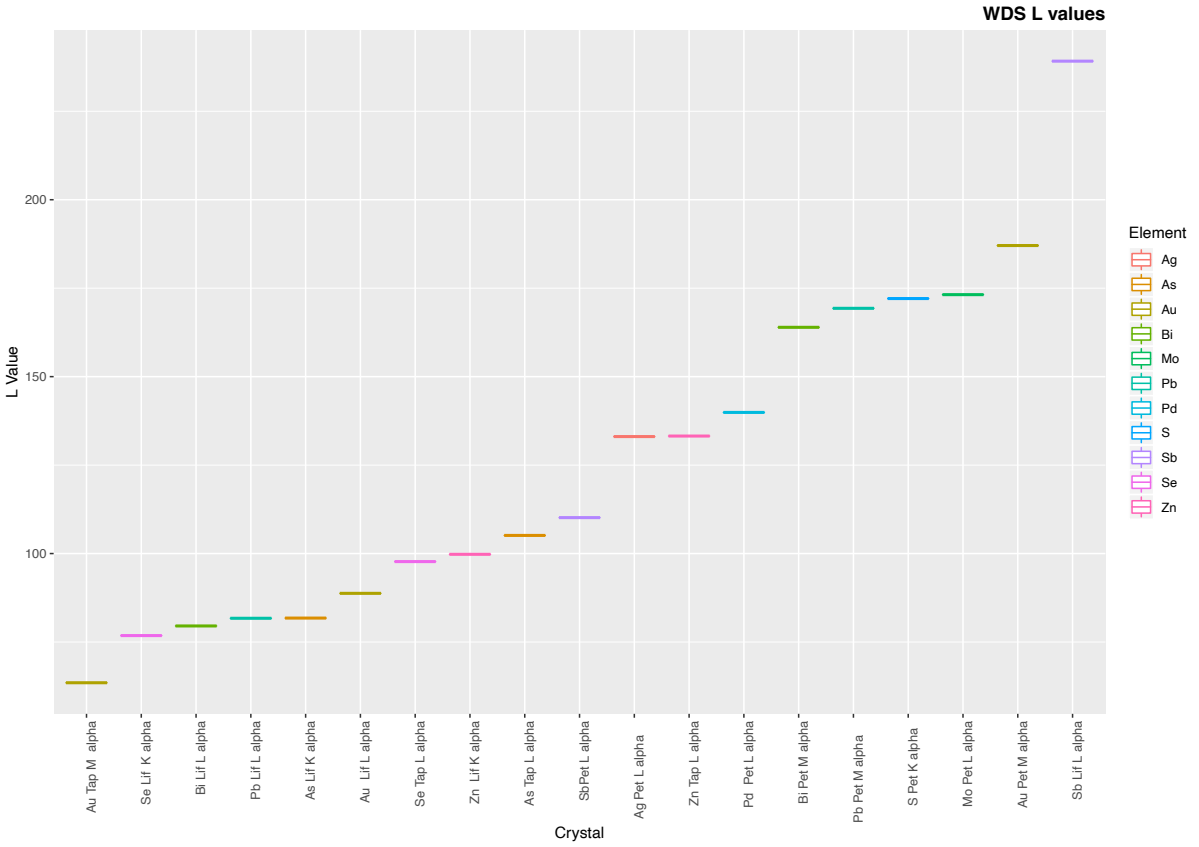
WDS L values
L Value
200
150
100
Au Tap M alpha
Se Lif K alpha
Bi Lif L alpha
Pb Lif L alpha
As Lif K alpha
Au Lif L alpha
Se Tap L alpha
Zn Lif K alpha
As Tap L alpha
SbPet L alpha
Ag Pet L alpha
Zn Tap L alpha
Pd Pet L alpha
Bi Pet M alpha
Pb Pet M alpha
S Pet K alpha
Mo Pet L alpha
Au Pet M alpha
Sb Lif L alpha
Crystal
Element
Ag
As
Au
Bi
Mo
Pb
Pd
S
Sb
Se
Zn